FACULTY OF MARITIME STUDIES

Karlo Bratić

APPLICATION OF SIMULATION MODELLING TO THE ANALYSIS OF THE MARINE SHAFT LINE DYNAMIC RESPONSE

DOCTORAL THESIS

Split, 2025.

POMORSKI FAKULTET U SPLITU

Sveučilište u Splitu University of Split

FACULTY OF MARITIME STUDIES

Karlo Bratić

APPLICATION OF SIMULATION MODELLING TO THE ANALYSIS OF THE MARINE SHAFT LINE DYNAMIC RESPONSE

DOCTORAL THESIS

Supervisors:
Full Prof. Nenad Vulić, Ph.D.
Assist. Prof. Đorđe Dobrota, Ph.D.

Split, 2025.

IMPRESUM/BIBLIOGRAPHICAL DATA

The doctoral thesis is submitted to the University of Split, Faculty of Maritime Studies in fulfilment of the requirements for the degree of Doctor of Philosophy.

Supervisor: Full Tenure Prof. Nenad Vulić, Ph.D.,

University of Split, Faculty of Maritime Studies, Croatia

Co-supervisor: Assist. Prof. Đorđe Dobrota, Ph.D.,

University of Split, Faculty of Maritime Studies, Croatia

The doctoral thesis consists of: 263 pages, including Literature, Lists and Attachments.

Doctoral thesis no.:

This Ph.D. thesis was prepared at the Department of Marine Engineering of the Faculty of Maritime Studies.

DATA ON EVALUATION AND DEFENSE OF THE DISSERTATION

Doctoral dissertation evaluation committee:

1. Assist. Prof. Francisko Lukša, Ph.D., University of Split, Faculty of Maritime Studies, Faculty of Maritime Studies in Split.
2. Assoc. Prof. Andrzej GRZADZIELA, Ph.D., Faculty of Mechanical and Electrical Engineering, Polish Naval Academy, Gdynia, Poland
3. Full Tenure Prof. Nikola Račić, Ph.D., University of Split, Faculty of Maritime Studies, Faculty of Maritime Studies in Split.

Doctoral Dissertation Defence Committee:

1. Assist. Prof. Francisko Lukša, Ph.D., University of Split, Faculty of Maritime Studies, Faculty of Maritime Studies in Split.
2. Assoc. Prof. Andrzej GRZADZIELA, Ph.D., Faculty of Mechanical and Electrical Engineering, Polish Naval Academy, Gdynia, Poland
3. Full Tenure Prof. Nikola Račić, Ph.D., University of Split, Faculty of Maritime Studies, Faculty of Maritime Studies in Split.

Dissertation defended on: , 2025

SUPERVISOR BIOGRAPHY

Nenad Vulić – Born in Split in 1960. Finished the *Split MIOC* (Mathematical and Informational Educational Center) in its first generation in 1979. Earned his degree in General Mechanical Engineering from the *Faculty of Electrical Engineering, Mechanical Engineering, and Naval Architecture in Split* in 1983. Completed master's degree study in the postgraduate program *"Theory of Structures - Structural Strength"* at the *Faculty of Mechanical Engineering and Naval Architecture in Zagreb* in 1989, with MSc thesis on *"Numerical Calculation of Linear Systems."* Obtained the Ph.D. from the same faculty in 1995 with doctoral dissertation on *"Numerical Modelling of Crack Propagation Arrest Procedures."*

After completing his graduate studies, he briefly worked at *Brodosplit* as the engineer in the *Machinery Outfitting* department. He then moved to what is now the *Croatian Register of Shipping (CRS)* in Split, where he remained for 31 years, holding positions as the expert and senior expert in mechanical engineering. In 1994, he became the *Head of the Department of Mechanical Engineering and Materials*, and in 2011, he was appointed *Assistant Director for Research and Development*. At the CRS, he primarily worked on ship propulsion systems and their components, performing calculations and supervising tests of their static and dynamic response. He prepared technical rules and regulations, approved technical documentation for ship machinery, and conducted type approvals. He specialized in technical calculations for engines, transmissions, shafts, gears, as well as marine shafting alignment, and vibration analysis. He participated in the work of the *International Association of Classification Societies (IACS)* and the *European Association of Classification Societies (EurACS R&D)*.

Concurrently, he built the academic career at the *University of Split* as the external collaborator at the *Faculty of Electrical Engineering, Mechanical Engineering, and Naval Architecture in Split*, advancing from assistant lecturer (1988) to full tenure professor (2013). He lectured courses in *Strength of Materials I & II, Technical Mechanics, Quality Management Systems*, and *Machine Elements*. He participated in multiple scientific research projects at the faculty, publishing academic and professional papers regularly linked to practical industrial applications.

In 2015, he transferred to the *Faculty of Maritime Studies in Split*, of the same university where he lectures courses in *Ship Propulsion Systems, Modelling and Simulation of Marine Systems,* *Mechanics of Maritime Structures*, *Vibrations of Ship Machinery* and *Marine Machine Elements*. He actively collaborates with machinery design and production companies and other interested industrial partners.

CO-SUPERVISOR BIOGRAPHY

Đorđe Dobrota was born on January 15, 1963, in Split. He completed his primary education in Omiš and graduated from the Maritime High School in Split, specializing in marine engineering. After graduating from the Maritime High School, he sailed on the ships of the shipping company JADROPLOV d.d. Split from 1984 to 1988, serving as an engine apprentice and officer. In 1991, he continued his education by enrolling at the Maritime Faculty in Dubrovnik, studying in Split. He graduated in 1994, earning the title BSc in maritime transport and ship's engineering. From 1988 to 2002, he held various positions at the shipping company JADROPLOV d.d. Split, including Assistant Head of the General Services Department, Head of the Quality Department, and Marine Superintendent.

From September 2003 to April 2004, he worked at Hipermarketi Coop d.o.o., Zagreb, as Maintenance Manager.

At the *Faculty of Maritime Studies, University of Split*, he defended his master's thesis in 2008, earning the professional title of Master of Maritime Transport, specializing in Marine Engineering. He enrolled in the postgraduate doctoral study "*Mechanical Engineering*" at the *Faculty of Electrical Engineering, Mechanical Engineering, and Naval Architecture in Spli*t and .in January 2018, he obtained Ph.D with doctoral dissertation on " *Modeling the distribution of prior in failure analysis of marine hydraulic equipment* ".

He built the academic career at the Faculty of Maritime Studies, University of Split advancing from external assistant (2009), assistant (2010) assistant lecturer (2011), lecturer (2016) to assistant professor (2019) where he lectures courses in *Technical Mechanics II, Failure Diagnostics, Marine Hydraulics and Pneumatics, Mechanisms in Ship Machinery* and *Risk Management.* He participated in three scientific research projects at the faculty, publishing academic and professional papers regularly linked to practical marine engineering applications.

ACKNOWLEDGMENT

I would like to express my sincere appreciation to all those who made the completion of this doctoral dissertation possible. I am deeply grateful to my family, and above all to my parents, for their unwavering support, unconditional love, and endless patience through the many challenges I have faced in recent years.

To my mentor and co-mentor for their exceptional professional and scientific guidance, their unfaltering support and immeasurable patience, I expressed my profound gratitude. Beyond their expertise, they extended genuine empathy and stood by me throughout my personal and academic growth, often embodying the roles of reliable advisor and true confidant.

I thank my colleagues and friends, past and present, for their encouragement and companionship, whether intentional or unspoken, that sustained me throughout this experience. To the one who kept the *compass needle* steady and true, guiding me when the path was uncertain, I offer my heartfelt thanks.

Last but not least, I am deeply grateful to my office colleague and, above all, my true friend, Igor Pavlović. Time and again, he has proven to be the *best man*, offering an immense source of psychological support, both in my professional life and personal struggles. His presence and guidance were essential in helping me maintain my integrity and composure throughout this journey. I sincerely hope that one day I will be able to offer him the same support and friendship he has so generously given me.

ABSTRACT

Various types of vibration may occur in ship propulsion systems during operation. Torsional vibration in main propulsion shafting are often identified as the most hazardous and most important to deal with. Vibration calculations are conducted during the design phase of newly constructed ships and are experimentally validated during sea trials. Torsional vibration analysis (TVA) of marine propulsion systems with Diesel engines involves determination of critical speeds and evaluation of additional torsional stresses within the shaft line across the full operating range of the propulsion engine. These calculations are typically performed using software tools employing analytical, numerical, or simulation modelling methods. This study explores the application of simulation modelling software in the torsional vibration calculation (TVC) of propulsion systems. The research aims to verify and validate the results obtained, while also assessing the accuracy, advantages, and limitations of the employed method. Several simulation models were developed using SimulationX software to account for the varying characteristics of different propulsion systems. These models consider both normal firing and misfire operating conditions. Specifics on the preparation of input data are discussed, with particular attention given on damping and excitation. The calculation of tangential forces, cylinder pressures, and torques from the Fourier coefficients of tangential forces was necessary to prepare the excitation input data, requiring application of specialized program for this purpose. Damping within the engine cylinders, as well as propeller damping in the system, is modelled using dynamic magnification elements previously developed for this application. Obtained simulation results are verified by comparing with those of well-known and field-proven GTORSI program that uses the analytical approach. Furthermore, the outcomes from both methods are validated by comparison with measurements performed on the actual newly built ships. Statistical analysis using mean squared deviation (MSD) aimed to validate the consistency and accuracy of the applied method. Results showed satisfactory agreement in terms of verification and validation across the entire engine operating range. In addition, results indicate that they are inherently influenced by the chosen modelling approach within the software. This research demonstrates that simulation modelling can be effectively and reliably applied in TVA of ship propulsion systems. However, it requires particular attention in the preparation of input data, especially excitation data in misfiring operating conditions. Future research will explore branched four-stroke engine-based systems with nonlinear behaviour.

***Keywords**:* marine shaft line, torsional stress amplitudes, simulation modelling, marine Diesel engine, normal and misfiring conditions

CONTENTS

1. INTRODUCTION

1.1. Topic of the research and motivation

The marine shaft line is the fundamental component of propulsion system in every ship, because it converts the prime mover power into the thrust required for navigation, thereby directly influencing the safety and functionality of the vessel. With the advent of mechanical engines, the dynamic response of the marine shaft line became critical concern due to the damaging effects of vibrations, particularly torsional vibrations. This has necessitated the development of methods for their calculation and measurement. The majority of modern merchant ships are equipped with marine Diesel engine propulsion systems, specifically slow-speed, two-stroke Diesel engines. These engines are characterized by high power output per cylinder, which generates significant excitation forces that induce vibrations within the shaft line.

In recent decades, however, the shipping industry, driven by economic and environmental concerns, has undergone significant technological transformations. These include design optimizations, retrofitting with advanced technologies, the application of dual-fuel systems, exhaust gas cleaning systems, and the introduction of slow steaming operations. These changes have introduced new complexities in the design and operation of marine propulsion systems, further accentuating the need for accurate vibration analysis. In addition, the demand for constructing increasingly larger ships, based on assumptions of continuous global trade growth, underscores the importance of reliable mathematical and simulation models. These models are crucial not only for design purposes but also for verifying compliance with project specifications, regulatory requirements and standards.

The design of the marine shaft line is typically initiated during the early stages of the propulsion system's design phase. At this point the designer has only limited information available, primarily the main particulars of the ship, such as its intended purpose, general size, service speed and fuel oil consumption requirements related to the propulsion system power. Based on these initial parameters, the designer's task is to develop the shaft line design that aligns with the ship's purpose, complies with classification society rules and requirements, and exhibits satisfactory dynamic response. The digital revolution in computer science has advanced engineering across all branches, including propulsion system design and vibration analysis, where contemporary TVC programs commonly use analytical, numerical, or simulation modelling methods. Until recently, dedicated engineering specialists were required for conduction of these calculations, based upon proper implementation of dedicated the software. However, modern engineers are expected to have extensive theoretical and practical knowledge to solve the wide variety of technical problems. Strong theoretical engineer's background provides precise understanding of the underlying physical principles, while accurate solutions often involve the use of modern software tools for efficient analysis and design.

TVC software tools can provide high accuracy, speed, and ease of use, facilitating complex simulations and ensuring compliance with classification rules and regulations, as well as branch, national and/or standards. These tools allow engineers to model various operating conditions, which helps in preventing vibrations that would damage the propulsion system. Additionally, these tools often enhance productivity by automating processes and integrating with other engineering software, resulting in streamlined and efficient workflow. However, despite these advantages, the use of such tools comes with potential drawbacks. They can be expensive, and there is often a steep learning curve associated with their use, requiring substantial expertise to interpret results accurately. Furthermore, their user-friendly interfaces can sometimes lead to oversimplification, particularly in more complex projects, which may compromise the quality of the analysis. Excessive reliance on these tools may also cause engineers to overlook errors, especially in non-standard designs. Although these tools offer numerous advantages, their use without a thorough understanding of their benefits and limitations can lead to unreliable results. Over-reliance on simulation tools without careful validation against alternative models or experimental data could result in catastrophic failures and compromise the safety of the ship.

Although recent literature presents the application of simulation modelling methods, a comprehensive analysis detailing the implementation process and a systematic evaluation of their advantages and limitations remain insufficiently addressed. This presents a scientific challenge, forming the core research objective to systematically and rigorously investigate the application of simulation modelling method for TVA of marine shaft lines.

1.2. Research objectives and hypothesis

The aim of this research is to enhance the safety, reliability, and functionality of newly built ships and ships in service that undergo conversion by improving their propulsion shafting systems concept and design through modern simulation modelling tools. In practice, simulation modelling means replacement of the actual real existing or future system by its model behaving as much as possible as the real system and the analysis of the model on the computer. The purpose of this research (its particular task) is to provide and demonstrate the approach and procedure for applying simulation modelling in the analysis of marine shaft line dynamic response using scientific based numerical calculation methods. This approach involves data preparation, TVC and result interpretation, comparing them against the acceptance criteria specified within the classification rules. The research specifically seeks to examine the strengths and limitations of current state-of-the-art simulation modelling techniques and propose the most effective procedure for modelling the dynamic torsional system. Therefore, the research results must always undergo verification and validation steps. Verification means performance of the calculation by another different method. Validation means experimental check out of the calculation results by comparing the verified results with the ones measured on-board. Classification society rules prescribe the acceptance criteria that the validated results shall meet. In relation to the chosen problem and research topic, the objectives of this dissertation are outlined as follows:

- Apply simulation-based tool to develop equivalent numerical calculation models of different ship propulsion systems and conduct TVA for each case study.
- Provide description of input data preparation process, interpret calculation results, identify influential parameters and evaluate accuracy of system´s response.
- Verify and validate calculated results by comparing them to results obtained using alternative method and available measurement data.
- To develop conceptual framework for implementing numerical simulation modelling for the analysis of marine shaft line dynamic response.

This dissertation aims to demonstrate the method for implementing TVA using simulation modelling tools, based on the case studies investigated. From the addressed problem and research subject, scientific hypothesis may be formulated as follows:

“By applying numerical simulation modelling approach to steady-state torsional vibrations analyses of marine shafting systems, it is possible to identify and choose the best approach that will be able to provide the most accurate results, based on verification through analytical methods and validation with available on-board measurement data.”

The proposed hypothesis leads to additional supporting hypotheses:

AH1: Developed procedure for implementation of simulation modelling software will contribute to its application for TVC of ship propulsion systems.

AH2: Obtained results will enhance existing practices in the design and analysis of ship machinery systems and will be presented effectively for marine engineering applications.

1.3. Literature review and state-of-the-art

This literature review is dedicated to the presentation and analysis of recent research concerning steady-state torsional vibrations in marine propulsion shaft line systems. Scientific and technical contributions have been examined, particularly those related to contemporary methods for the calculation, measurement, and mitigation of torsional vibrations. Among various vibration phenomena, torsional vibrations have been the most extensively explored in the literature, due to their classification as particularly hazardous within propulsion shafting systems. In most studies, TVA is conducted to evaluate and enhance system responses or to investigate the behaviour of individual components. For these purposes, dedicated software packages employing analytical, numerical, or simulation-based modelling approaches are commonly utilized.

Historically, torsional vibration problems were frequently associated with mechanical engines used for ship propulsion [1]. Since the 1950s, the issue of shaft line torsional vibrations has been subjected to more rigorous investigation, as evidenced by well-known publications by Nestorides and Wilson that introduced systematic and methodological calculation approaches [2, 3]. Eshleman in [4], conducted comprehensive study which provided an explanation of torsional vibrations in machinery systems through illustrative examples involving design, development, fault diagnosis, and troubleshooting procedures Furthermore, a detailed exposition was offered on the physical behaviour of torsional vibrations in shafting systems, encompassing torsional excitation mechanisms.

To acquire deeper insights into the subject, investigations by Vulić et al. and Savolainen et el. have been conducted into shaft alignment calculations, comparative analyses of crankshaft calculation methods, and the design and verification of crankshaft fatigue strength [5, 6, 7]. Mendes et al. [8] emphasized the importance of TVA in the structural dimensioning of crankshafts. The software used for TVA was developed in MATLAB, applying a mathematical model to a six-cylinder diesel engine, which was experimentally validated using measured torsional vibration amplitudes.

Wachel and Szenasi [9] addressed the requirements for TVA in rotating machinery, covering both steady-state and transient conditions. While these studies encompass various facets of torsional vibrations, specific attention to their occurrence in marine propulsion systems is often lacking. Nonetheless, certain works have drawn upon manufacturer experiences to address vibrations in typical marine propulsion setups. Bryndum and Jacobsen [10, 11] conducted studies which offer descriptions and examples of mitigation strategies, along with discussions on the coupling effects between propeller-induced torsional vibrations and axial vibrations within the shaft system, engine, and hull structures. Margaronis [12] highlighted practical considerations, including the link between inadequate maintenance and the emergence of torsional vibrations in propulsion systems.

Batrak [13] addressed and summarized key issues associated with the calculation of torsional vibrations in propulsion systems. A historical overview of torsional vibrations in marine propulsion systems was provided, along with fundamental mathematical expressions, calculation methodologies, and an algorithm for method selection.

Hesterman and Stone [14, 15, 16] presented chronological and comprehensive review of research on secondary inertia effects in the torsional vibrations of reciprocating engines. To evaluate the nonlinear characteristics of such systems, a frequency-domain model incorporating inertial effects from reciprocating mechanism components was developed. The model's results demonstrated strong agreement with experimental data and established a foundation for the subsequent investigation of time-domain modelling approaches.

In mechanical systems, the damping force is characterized as a nonlinear function of the system's velocity. Batrak noted [13] that torsional behaviour may be ambiguously interpreted by marine shaft designers, primarily because the accuracy of the damping data used in calculations is typically validated through on-board measurements. Vulić et al. [17] presented methodology for the definition of damping, using examples derived from various modern software tools to facilitate the conversion of damping values. Furthermore, engine excitation was classified into three distinct forms, and a corresponding software tool was made available to enable conversion between these excitation categories.

Tienhaara and Mikonaho [18] utilized finite element models of turbocharged Wärtsilä 8L46 and 9L46 engines to assess the feasibility and effectiveness of employing a tuned mass damper. This method is typically adopted when substantial modifications to the engine's dynamic characteristics or firing order are not feasible.

Holm [19] performed a comparative analysis of two torsional vibration measurement methods, focusing on vibration behaviour observed on the camshaft of a large, medium-speed diesel engine. Schramm [20] explored countermeasures against torsional vibrations in the drivetrain of electric motors, wherein a model for overall damping behaviour was developed and validated using simulation environments and experimental setups.

Vulić et al. [21] presented the methodology and calculation results for steady-state torsional vibration responses, utilizing the TVA module within the SimulationX software. The propulsion systems examined consisted of slow-speed, two-stroke marine diesel engines equipped with fixed-pitch propellers. For validation purposes, two computer programs were employed to perform TVC, with the outcomes verified against available on-board measurement data. Vulić et al. [22] evaluated practical software tool for TVA, with emphasis placed on its modelling capabilities for elastic and damping properties, as well as its effectiveness in addressing damping and cylinder excitation loads in various forms. Vulić et al. [23] further explored the capabilities of SimulationX for simulating torsional vibrations in marine shafting systems, along with formulations for modelling steady-state propeller loads.

Rimstad [24] demonstrated a comprehensive TVA of slow-rotating propulsion systems using two software tools: Nauticus Torsional Vibration by DNV GL for frequency-domain simulation, and Simpack Multi-Body Simulation software for time-domain analysis. Gunnarsson and Sigurðsson [25] thoroughly examined calculation methods currently employed by classification societies for determining the diameter of ship propulsion shafts. The shaft behaviour was modelled using the Nauticus Machinery simulation software, resulting in the development of an improved methodology for calculating the minimum required shaft diameter.

Murawski and Charchalis [26] introduced an estimation method for calculating the natural torsional vibration modes of marine propulsion systems was introduced. Two estimation approaches were developed and validated against detailed finite element method (FEM) calculations and on-board measurement data. Additionally, Murawski et al. [27, 28, 29] demonstrated torsional vibration calculations through the use of simplified approaches and specialized FEM software tailored to various ship propulsion configurations. Murawski and Dereszewski [30] investigated commercial measuring device based on instantaneous angular velocity to enable continuous monitoring of torsional vibrations. This methodology incorporated measurements at both the free and power output ends of the engine crankshaft and was designed for integration into ship condition management systems.

Senjanović et al. [31] presented a simplified calculation methodology for propulsion system vibrations, proposing two analytical procedures, was presented. One procedure involves two-degree-of-freedom model encompassing propeller and crankshaft masses, while another based on multi-degree-of-freedom model combining these components. Senjanović et al. [32] further examined the shaft system reduction to two- and three-mass models using finite element formulations, while also comparing the analytical results with numerical simulations and on-board measurement data.

The calculation of torsional vibrations in propulsion systems operating under ice conditions presents a notable challenge for numerical simulation. Batrak et al. [33, 34] investigated the unsteady torsional vibration response arising from propeller-ice interactions, utilizing simulation software to evaluate dynamic behaviours. Current research efforts by Zambon et al. as well as by Burella et al. [35, 36, 37], have combined experimental measurements with numerical analyses to elucidate the relationship between ice-induced propeller loads and varying sea ice conditions.

Despite the growing reliance on simulation tools, implementation steps for these software packages are frequently underemphasized in both academic and industrial contexts. Such oversight may lead to suboptimal or ineffective utilization, thereby limiting the potential benefits of these technologies. However, recent advancements have considerably expanded the availability of modern numerical and simulation modelling tools, many of which are now accessible as commercial software products. These tools offer substantial opportunities for enhancing the accuracy and efficiency of analyses in engineering and scientific disciplines.

The increased accessibility of advanced software packages presents significant potential for modelling complex systems and optimizing their performance. Nonetheless, the effective use of these tools necessitates a comprehensive understanding of their functionalities and best practices. In the absence of proper implementation, the full capabilities of such tools may not be realized, potentially resulting in diminished analytical effectiveness. Owing to the fact that simulation modelling software continues to play an integral role in both research and industry, addressing implementation challenges has become essential. Timely and focused research in this area is required to bridge the gap between theoretical potential and practical application, thereby enhancing methodological robustness, improving result reliability, and fostering innovation.

In conclusion, the necessity for research into the practical implementation of simulation software is underscored by the accelerated development and adoption of advanced modelling tools. Such research is imperative to ensure that these tools are fully leveraged, contributing to more precise analyses, improved decision-making processes, and technological and scientific advancements.

1.4. Research methodology and structure of doctoral thesis

For this doctoral dissertation, the range of scientific methods is employed in conjunction with available and relevant scientific literature and technical documentation. The analysis method, synthesis method, compilation and comparison methods, statistical method and simulation modelling methods are used in the process of conducting the research and preparing this dissertation. Information, knowledge, and data obtained from literature and other sources using the aforementioned methods were cited to support observations, requirements, conclusions, and insights in a scientifically grounded manner.

The dissertation is organized and structured into eight chapters. This introductory Chapter 1, explaining the topic, motivation, research objectives, hypothesis, literature review and research methodology is followed by Chapter 2, outlining the research problem by classifying vibration types and examining their effects on system performance. This chapter presents a comparison of marine propulsion system configurations, highlighting their operational characteristics and limitations. The focus narrows to the marine shaft line, examining its response to operational loads and compliance with stress limits set by classification rules and regulations, as well as technical standards. The chapter concludes with the review of torsional vibration measurement techniques for assessing dynamic behaviour.

The Chapter 3 focuses on vibration analysis using longitudinal vibration models, which effectively capture various vibration phenomena. Torsional vibrations are addressed by adapting the longitudinal vibration model to rotational mechanics, A solid theoretical foundation is established, as ship propulsion systems comprise multiple single-degree-of-freedom (DOF) elements, requiring multi-DOF system analysis.

Torsional vibration analysis (TVA) of the ship propulsion system is typically conducted using the lumped parameter modelling approach. In this model, the system is represented as a torsional lumped mass model, with concentrated masses interconnected by torsional springs. As outlined in Chapter 4, this approach facilitates the effective dynamic behaviour analysis of the shaft line under variable excitations. Accurate input data is essential for reliable results, and this section emphasizes the preparation of verified data, including mass moments of inertia, stiffness, damping characteristics, and excitation forces. The chapter also discusses various methodologies used in TVA, including analytical, numerical, simulation modelling, and experimental methods, focusing on their applications, advantages, and limitations within ship propulsion systems.

Chapter 5 focuses on the modelling and simulation of engine excitation in combustion engine, specifically within the context of marine propulsion systems. It outlines the use of various SimulationX elements to model engine dynamics, which include reciprocating and rotating masses, crank stiffness, and damping. The chapter also discusses the integration of excitation forces and torques through application of additional elements. The challenges associated with preparing and entering engine excitation data, such as cylinder pressure and crank torque, are addressed. Additionally, the chapter details the preparation of engine and propeller loading components using VBA programs, highlighting the process of acquiring and inputting vibration data, and the modelling of engine performance under various load conditions, including normal, misfiring, and idling states. Overall, the chapter reflects the procedure of input data preparation. It also emphasizes the importance of data accuracy and model integration for simulating engine excitation and evaluating system performance.

Chapter 6 focuses on the structure, evaluation, and validation of simulation models developed to analyse torsional vibration amplitudes in marine propulsion systems. The models, created using SimulationX software, are designed to represent various properties of marine propulsion systems and are evaluated under both normal and misfiring operating conditions. Each model is verified and validated against reference data, including results from the GTORSI program and experimental on-board measurements. A detailed comparison of simulation results, including natural frequencies, torsional stress, and critical speed, is provided in tabular and graphical forms. The chapter also describes the methodology for developing simulation models, which involve interconnecting various SimulationX elements to accurately represent system properties like inertia, stiffness, and damping. Finally, the chapter presents case studies with four distinct ship propulsion systems, each featuring a two-stroke marine Diesel engine, and highlights the distinctive features of each system.

To further demonstrate the potential and capacity for implementation the simulation modelling concept using SimulationX software, a case study of the marine propulsion system featuring 4-stroke Diesel engine, nonlinearly elastic highly-flexible coupling, and branched shafting configuration has been selected and presented.

Application of SimulationX software to model and analyse the dynamic response of marine shaft lines, focusing on TVA under normal and misfiring conditions is thoroughly discussed in Chapter 7. The simulation results were verified and validated against reference data, with findings showing strong alignment, though some challenges were encountered in modelling engine excitation and misfire. Overall, the study confirms that simulation modelling can effectively support the analysis and design of marine propulsion systems.

The results of the research, the scientific contributions, and the advantages of the proposed methodology are thoroughly analysed in the conclusion, presented in Chapter 8. Additionally, the limitations of the proposed methodology and potential directions for future research are presented and discussed in detail.

2. DESCRIPTION OF THE RESEARCH TOPIC

This chapter introduces research problem by outlining vibration types and their effects on system performance. It explores ship propulsion systems by comparing different configurations and their operational characteristics and limitations. Focus is then given on the marine shaft line, by examining its response to operation loads, shaft control calculations, and compliance with stress limits defined by technical standards. Methods for torsional vibration measurement are presented, emphasizing techniques for assessing the dynamic behaviour of the system.

2.1. Vibrations of ship propulsion systems

The marine shaft line, as a mechanical system, may be analysed on the model of the equivalent behaviour consisting of mass, stiffness, and damping elements. The shaft line is designed to efficiently transmit the propulsion engine's power to the ship's propeller, maintaining a specific rotational speed. Definition from [38] states that: "*Vibrations are mechanical oscillations about the equilibrium point where oscillations may be periodic or random.*" When the shaft line rotates at constant speed, its elastic line, which is a curved shape formed by the centres of all cross-sections, settles into a specific position in space called the dynamic equilibrium position. To maintain constant rotational speed all rotational moments fitted on the shaft line must be balanced within the tolerances prescribed by the classification rules. During operation, the shaft line vibrates around its dynamic equilibrium position due to excitation forces from various sources and other causes. Vibrations that can occur within the propulsion system include axial, lateral (whirling included) and torsional vibrations. They are generated from the dynamic interactions among rotating components and fluid forces. Although, torsional vibrations are widely considered the most critical due to their potential to cause severe damage to the shaft line [39, 40]. Evaluation of critical speeds for all vibration types to ensure structural integrity and safe operation is required.

2.1.1. Torsional vibration

Torsional vibration refers to small-amplitude angular displacements around reference axis through the shaft line centre, causing the shaft line to twist alternately in both directions. This results in linearly distributed tangential stresses within the shaft line cross-sections, causing cyclic changes in angular acceleration, thus leading to rotational velocity fluctuations. The restoring moment arises from the torsion of the elastic member or the unbalanced moment [41]. Note that the torque is considered here as external generalized force to the system and moment of torsion as internal generalized force.

In propulsion systems, torsional vibrations mainly originate from the pulsating torque generated by the Diesel engine and the propeller operation in the non-uniform wake field [31]. Unlike steam and gas turbines, which maintain constant torque at steady loads, in Diesel engine propulsion systems, the torque fluctuates throughout the combustion process [42]. These vibrations impose significant risks to the shaft line, especially in direct Diesel engine propulsion systems [31, 43]. The response of the marine shaft line can be expressed by the system of ordinary differential equations concisely formulated in matrix form as:

$$\mathbf{J}\ddot{\boldsymbol{\varphi}}(t)+\mathbf{C}\dot{\boldsymbol{\varphi}}(t)+\mathbf{K}\boldsymbol{\varphi}(t)=\mathbf{m_t}(t) \tag{1}$$

where **J, C, K** are inertia, damping and stiffness matrices, $\boldsymbol{\varphi}, \dot{\boldsymbol{\varphi}}, \ddot{\boldsymbol{\varphi}}$ are vectors of angular displacements, velocity and acceleration, and $\mathbf{m_t}$ is vector of time dependent excitation torques.

Marine shaft line components will vibrate when excited by variable torque, generated in the engine's cylinders, thereby results resulting in torsional vibration stress within the components [44]. Currently, conventional TVA includes free vibration calculations and steady-state vibration calculations induced by harmonic excitation [13]. After the defining preliminary dimensions of the shaft line (diameters and lengths), it is crucial to conduct TVC to determine its steady-state response due to torsional vibrations as soon as possible. This response is contained within calculation results of angular displacements of individual cross-sections, torsional moments, and resulting shear stresses due to torsion for forced steady-state torsional vibrations. Tangential stresses due to torsion in each shaft are determined from the angular displacement:

$$\tau_t=\frac{M_t}{W_p}=\frac{16k_t\theta}{\pi d^3} \tag{2}$$

where

W_p – the polar moment of resistance of the circular cross-section,

M_t – harmonic excitation torque, and k_t is the torsional rigidity of the shaft.

The stress amplitudes from torsional vibrations must be verified against allowable stress limits, defined by classification societies for both continuous and transient operation [45]. Calculation results must be validated through onboard measurements performed during sea trial, with the maximum deviation of 5%. If this condition is not met, the calculations shall be revised. In the case of series of newly built ships the validation measurements shall be performed on the first newbuilding in this series.

2.1.2. Axial vibration

Axial (longitudinal) vibration is characterized by small-amplitude displacements along the shaft line axis, causing the shaft line elements to alternately elongate and contract. This results in tensile and compressive stresses across shaft line cross-sections. These vibrations are typically caused by fluctuating thrust forces from the propeller, radial forces acting on the cranks of the crankshaft, and pressure variations within the propulsion system [46]. Thrust bearing transmits these forces to the ship's structure, spreading vibrations throughout the hull [47].

The response of the marine shaft line components can be described as:

$$\mathbf{M}\ddot{\mathbf{x}}(t)+\mathbf{C}\dot{\mathbf{x}}(t)+\mathbf{K}\mathbf{x}(t)=\mathbf{f}(t) \tag{3}$$

where **M, C, K** mass, damping and stiffness matrices, $\boldsymbol{x}, \dot{\boldsymbol{x}}, \ddot{\boldsymbol{x}}$ are vectors of displacement, velocity and acceleration, and **f** is excitation forces vector.

Natural frequency calculation is essential to avoid resonance, however more detailed analysis is necessary if the resonance is possible near the maximum operating speed. In practice, axial vibrations are often measured at the crankshaft's free end and compared against manufacturer limits. While they rarely causing severe damage to the shaft line, these vibrations can increase risk of crankshaft failure and affect the ship's superstructure [47]. To reduce vibration amplitudes, modern Diesel engines are equipped with the axial vibration damper. The potential damper malfunction must be analysed to prevent excessive vibrations in the case of its failure [45].

2.1.3. Lateral vibration

Lateral vibration, also called flexural, bending, or transverse vibration, is characterized by the shaft perpendicular motion to its longitudinal axis. This causes the shaft line to alternately bends in both directions, leading to normal bending stresses distributed linearly across its cross sections [47]. Lateral vibrations are primarily caused by factors such as the propeller's weight, variable forces, shaft misalignment, imbalances in shaft segments, and hull deformations. The response of the marine shaft line to lateral vibration is expressed identically to equation (3), but in the horizontal or vertical plane. Although lateral stress amplitudes are often considered negligible when compared to torsional stresses [47, 48], lateral vibrations are evaluated through calculations to assess excitation frequencies that influence critical speeds [45].

Whirling vibrations mostly related to the gyroscopic effect of the rotating propeller trying to preserve its axis of rotation. They result from the combination of lateral vibration motions occurring in perpendicular planes that pass through the shaft's neutral position [44]. The propeller shaft bends due to weight of the propeller, its buoyancy, and the hydrodynamic forces acting on the propeller. Ship propeller with propeller shaft undergoes compound motion initiating certain deflection and inclination angle. This motion is called whirling. In propulsion systems with heavy propellers, gyroscopic effects significantly influence whirling vibrations especially at higher rotational speeds. These propellers, characterized by substantial mass and high polar and diametric moments of inertia, generate gyroscopic moments during rotation [48]. Negative gyroscopic moment mitigates shaft deflection, while the positive moment amplifies it.

2.1.4. Coupled vibrations

In mechanical systems, vibrations propagate through physical connections and are influenced by the medium and interaction type. In vibration systems, elastic components like springs can enable energy transfer between modes, particularly when systems have similar or identical natural frequencies, leading to resonance and mode coupling. Dynamic interactions along the shaft line can lead to both lateral-torsional and axial-torsional vibration coupling.

Lateral-torsional coupling refers to interaction between lateral and torsional vibrations, amplifying amplitudes and increasing stress on bearings and couplings, which can lead to misalignment and fatigue failure. Axial-torsional coupling occurs when axial and torsional vibrations interact. Propeller rotation generates oscillating thrust and torque, linking longitudinal and torsional motions. Torsional vibrations induce cyclic shaft contraction and extension, driving axial vibrations along the shaft. Recent studies highlight improved understanding of multi-mode interactions, their impact on fatigue, energy efficiency and modelling methods [49, 50, 51, 52]. In this research, coupled vibrations are only briefly referred to, since the validation results indicate strong agreement without inclusion of vibration coupling phenomenon.

Next section will discuss operational characteristics of ship propulsion systems and its components. The following sections delve deeper into the mechanical behaviour and performance of the marine shaft line under various loading conditions. These sections explore key concepts such as stress distribution, fatigue limits, and vibration control, which are essential for assessing the structural integrity and operational reliability of the propulsion system. This detailed examination provides the foundation for evaluating design choices and compliance with classification rules and technical standards.

2.2. Ship propulsion system and its components

Ship propulsion system is designed to generate, convert and transmit energy, thus enabling ship to achieve and maintain speed and direction. Properly designed propulsion system must achieve the contracted fuel oil consumption and speed while ensuring efficient and reliable operation. The marine shaft line serves as the essential link that transmits power from the prime mover to the propeller, making its design crucial for the overall system efficiency and reliability. Diesel engine based marine propulsion systems vary in their configuration based on the power transmission mode [53], but the basic categorization involves direct and indirect configuration.

In direct configuration, power from the propulsion engine is transmitted directly to the propeller via the shaft line, ensuring that the engine and propeller operate at the same rotational speed. This setup often employs large two-stroke slow-speed Diesel engines, which allow the ship to be operated by adjusting the engine's speed and direction. This configuration generally comprises fewer components compared to alternative designs, which minimizes energy losses and simplifies maintenance procedures. However, its performance is limited to very low speeds.

In indirect configurations, power from the engine is transmitted to the propeller through intermediary devices like couplings and gearboxes. The gearbox reduces engine revolutions, enabling efficient propeller operation at lower speeds. This setup simplifies reversing and accommodates additional machinery, such as shaft generator, though added energy conversion steps lower overall efficiency. Notable variant is the electrical propulsion system, which, despite being relatively novel, is now widely adopted in the shipping industry. Regardless of the configuration, basic components of ship propulsion system include:

- propeller,
- shaft line,
- gearbox and reversing clutches (if necessary),
- prime mover (e.g. propulsion Diesel engine).

Rotating propeller generates thrust force, which is transmitted as internal axial force through the entire shaft line to the thrust bearing, thereby enabling the movement of the ship. The primary components of the propeller are hub and blades. The hub is the central part of the propeller where the blades attach. Propellers may vary in number of blades. Although the increased number of blades generally reduces hydrodynamic efficiency, it also distributes the load more evenly, reducing stress on each individual blade.

The shaft line, shown in Figure 1, provides means for transmitting rotational motion and torque from the engine to the propeller, allowing it to rotate at the same or different speed than the engine. It consists of propeller shaft and one or more intermediate shafts, interconnected by flanges or detachable couplings. The propeller shaft is placed in stern tube and supported on stern tube bearings. It serves as a structural component, supporting the weight and forces of the propeller. The intermediate shaft, supported by independent radial bearings, connects the propeller shaft either to the thrust shaft or directly to the engine crankshaft. Multiple intermediate shafts are used if propulsion engine is located far away from the propeller. In the thrust bearing, positioned along the shaft line or within the gearbox, the thrust is transferred to the ship's hull.

Typical propulsion system configuration, shown in Figure 1, includes single-acting, reversible, low-speed, two-stroke Diesel engine, turbocharged, and directly coupled via the shaft line to the large-diameter, fixed-pitch, solid propeller.

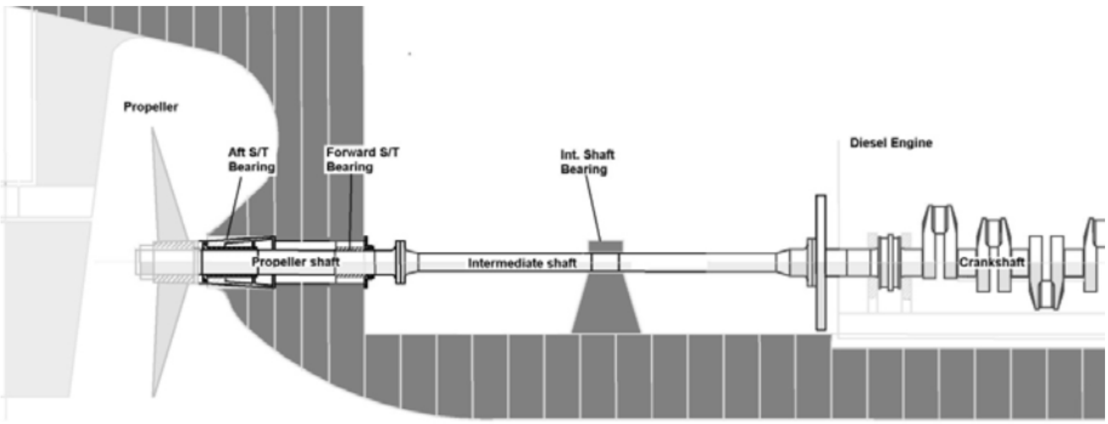

Figure 1. Typical shaft line arrangement [54]

This configuration is important as most commercial ships rely on such Diesel engine propulsion systems [42, 53], due to their high-power output and thermal efficiency, reliability and ease of maintenance, as well as the ability to operate on heavy fuel oil. The following sections will cover marine shaft line design and calculations, highlighting compliance with relevant classification rules and technical standards.

2.3. Marine shaft line

Marine shaft line represents assembly of interconnected shafts, often varying in diameter, designed to transmit rotational motion and torque from the propulsion engine to the propeller. During operation, shaft line components are subjected to various types of loads, which can be either static or dynamic, depending on their time-dependence. The external forces, acting as operating loads, induce internal forces within shaft line cross-sections, which are described and quantified by normal σ and shear τ stresses. Stresses actually do not exist in reality, because they are only the proper means to describe internal forces in the shaft cross section taking into account the spatial orientation of that cross section [55]. As stresses (originating from the external and internal forces) and strains (originating from displacements) are interrelated by means of Hooke's law, the resulting stresses, deformations, and displacements at specific points arise from the applied loading.

2.3.1. Mechanical response and control calculations

Mechanical response characterizes behaviour of the system under mechanical loads and is typically defined in terms of stress, strain and displacement [56]. Machine elements shall be designed to maintain integrity and functionality under different operating conditions, accounting for both static and dynamic loads.

The static response of the shaft line describes the behaviour of the system when at rest or in steady-state conditions. It involves static load increase from zero to some specific level, which then remains constant, or changes gradually [57]. The dynamic response of the shaft line describes the behaviour of the system under dynamic loads, which vary over time in magnitude, direction, and orientation. These loads can exhibit non-stationary time patterns, where stress varies unpredictably over time or stationary time patterns, characterized by periodic stress variations, shown in Figure 2. From left to right illustrated loads represent the general case, steady (unidirectional) and alternating. These variations are typically described as harmonic (sinusoidal) function, or a sum of harmonic functions. These harmonic dynamic loads are result of internal forces generated by external loads and are characterized by their time dependence and expressed in terms of stress.

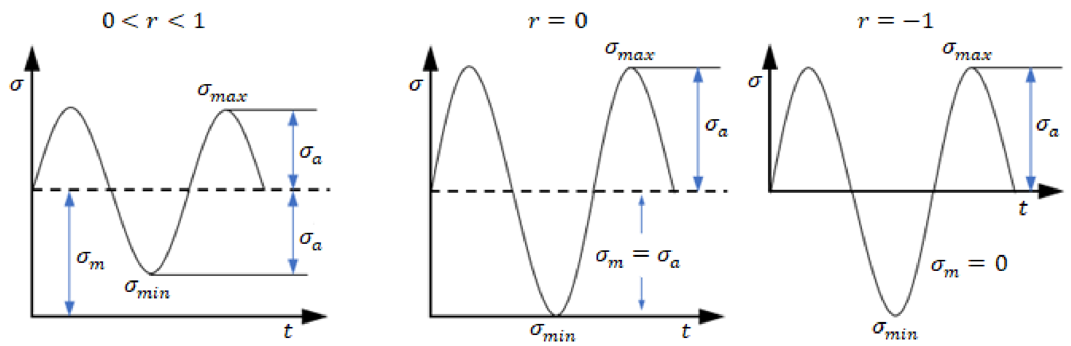

Figure 2. Stresses under harmonic load [57]

Denotation is consistent in all load cases, with maximum stress σ_{max} and minimum stress σ_{min}, mean stress σ_m represents static component, while amplitude stress σ_a represents dynamic component, and r is coefficient of cycle asymmetry. These terms are defined as follows:

$$\sigma_m = \frac{\sigma_{\max} + \sigma_{\min}}{2} \tag{4}$$

$$\sigma_a = \frac{\sigma_{\max} - \sigma_{\min}}{2} \tag{5}$$

$$r = \frac{\sigma_{\min}}{\sigma_{\max}} \tag{6}$$

Material strength is influenced by the magnitude and variability of maximum and minimum stresses in each loading cycle, along with their interrelation [57] Although maximum stresses may remain below the material's ultimate or yield strength, repeated stress cycles can lead to fatigue failure. Distinguishing between high-cycle and low-cycle fatigue is essential for the effective design and evaluation of shaft line behaviour under varying stress conditions, especially with vibratory stresses.

Purpose of control calculations, is to evaluate strength of the shaft due to the bending, torsion, and axial loads. These calculations are performed once the shaft design is fully defined, including all diameters, transitions, slots, and the positions of components. Due to the complex loading conditions, stress analysis is performed using certain strength theory, such as the Huber-Mises-Hencky (HMH) theory, which is suitable for ductile materials as they are more or less only materials used in shaft construction [56]. Calculations may be performed using either simplified or detailed approach, with key difference being that in detailed method individual safety coefficients for bending, axial load, and torsion are calculated separately [57].

In simplified approach, the equivalent stress at a specific section of the shaft is compared with the allowable normal stress for the uniaxial stress state. The equivalent stress is calculated by summing the nominal normal stresses due to bending and axial loads, along with the nominal shear stresses due to torsion. Each stress is then adjusted by the appropriate effective stress concentration factor.

In detailed approach safety coefficients are combined into a single safety coefficient, which is compared with the minimum required safety coefficient according to specified scheme illustrated in Figure 3. According to [57], detailed shaft strength calculations are conducted based on the requirements of standards DIN 743 [58] or guidelines from classification societies, such as DNV [59], which adapt the core provisions of DIN 743 to marine shaft systems.

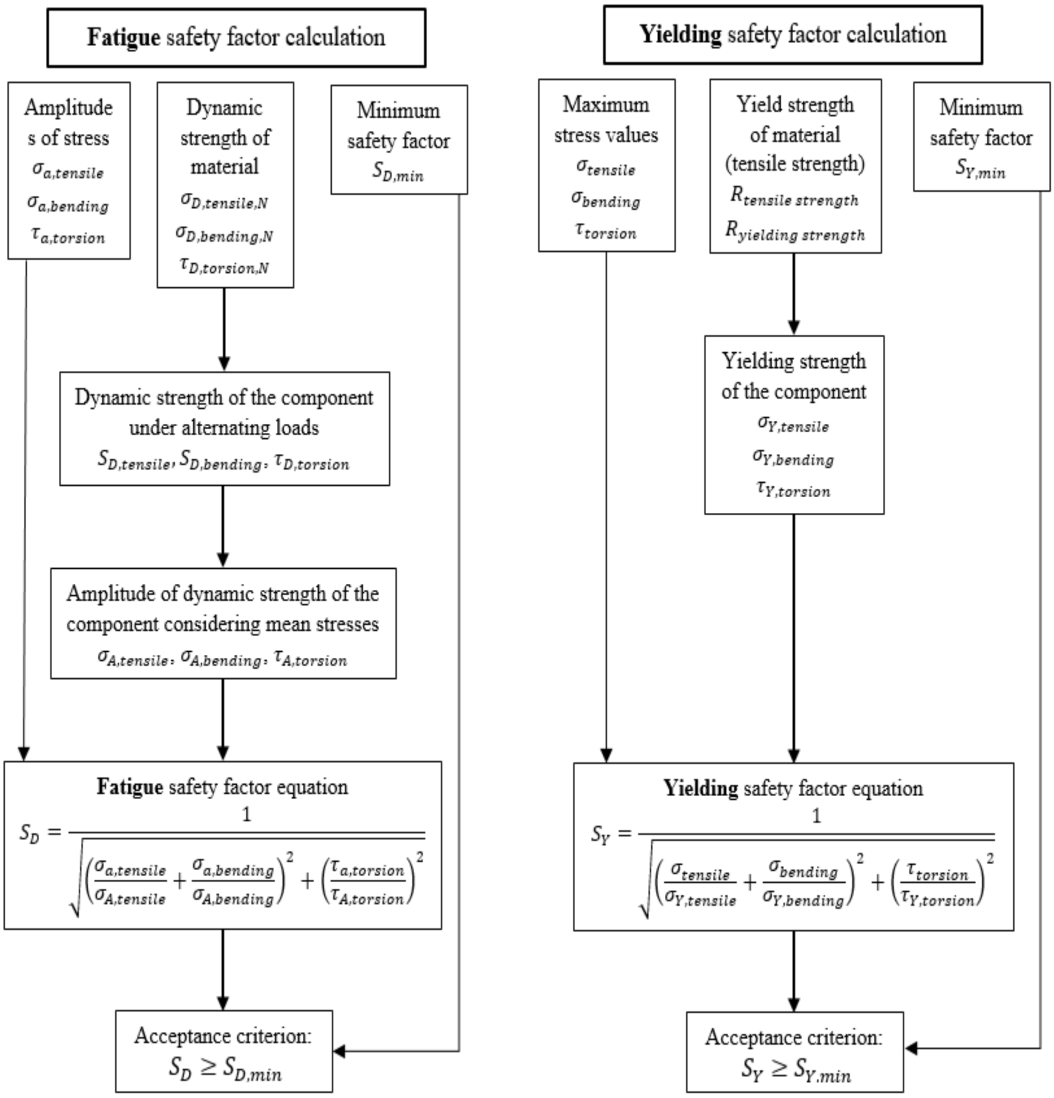

Figure 3. Calculation scheme for the safety factor for shafts [58]

The choice between simplified and detailed methods for shaft strength analysis depends on the required precision. The next section will cover design characteristics of the marine shaft line, focusing on key considerations such as structural form, dimensions, material type, and operational load, i.e. the four pillars of describing mechanical or marine engineering components.

2.3.2. Design characteristics

In any mechanical design, including ship machinery design, information on functions, specifications, and evaluation criteria is crucial [60]. Generally, new ships are ordered based on their size, speed, and cargo type, with the ship's speed contracted for a specific design point and fuel oil consumption [61]. The initial step is to select appropriate propeller based on the hull form, that will ensure that the ship achieves contracted speed. The subsequent step involves definition of marine shaft line preliminary dimensions, followed by vibration calculations in the later stages. Marine shaft line design process is realized through multiple steps that often require iterative adjustments, schematically shown in Figure. 4.

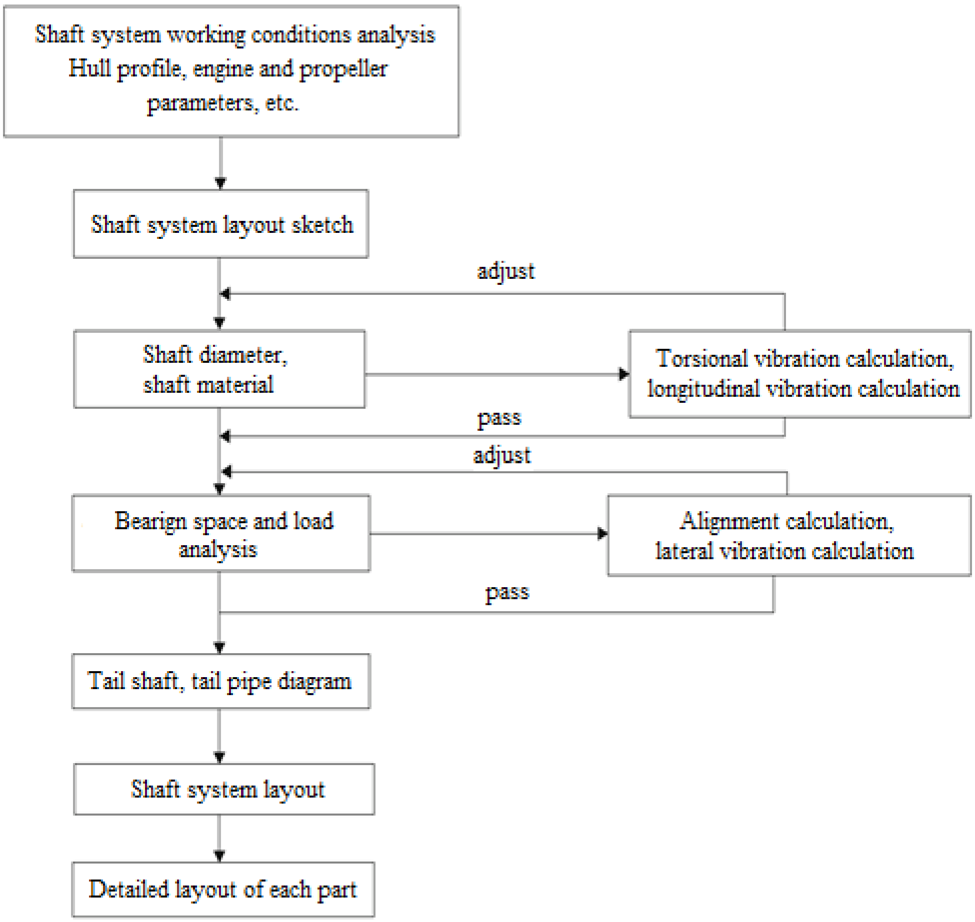

Figure 4. Main shaft line design steps [53]

Design requirements for marine shaft line are outlined in IACS UR document [62], which covers shafts that are not integral part of the propulsion engine itself but are driven by the engine or other prime mover. Accordingly, this relates to propeller, intermediate and thrust shaft for which minimum dimensioning requirements are based on engine rated power, rotational speed at rated power and the mechanical properties of the selected material, expressed in formula:

$$d \geq F \cdot k_d \cdot \sqrt[3]{\frac{P}{n_0} \cdot \frac{1}{1-\frac{d_o^4}{d_i^4}} \cdot \frac{560}{\sigma_B + 160}} \tag{7}$$

where

d - minimum required diameter, mm

F - factor for type of propulsion installation,

k_d - factor for the particular shaft design features,

P - rated power transmitted through the shaft, kW

n_o - rotational speed of the shaft at rated power, rpm

d_o - outside diameter of shaft, d_i is inner diameter of shaft bore, mm

σ_B - specified minimum tensile strength of the shaft material, N/mm^2.

As detailed in [25], the prescribed formula (7) is based on empirical data and is considered to consists of three key parts: fractions under the cubed square root, corresponding to load, inertia, and material properties. Factors F and k serve as multipliers for adjusting the data results and the units of measurement. Material selection primarily involves carbon, carbon-manganese, and alloy steels, which are defined by minimum tensile strength requirements. This indicates that the material factor in the formula relates to ultimate strength rather than yield strength. Actually, material fatigue strength is more closely related to its ultimate tensile strength than to its yield strength, since fatigue failure involves a different mechanism than yielding, which represents a complete failure of the component. Consequently, essential propulsion shaft design criteria are based on the fatigue and endurance limits for the dynamic load of the system.

According to [63], one of initial steps in the engine selection is to specify the maximum continuous rating load (MCR), that meets the ship's requirements for power and speed. This must ensure sufficient thrust to move ship through the water while counteracting resistances. Initial estimates for the specific design point are based on the required propeller power and rotational speed. Therefore, operational load is considered as the propulsion engine's MCR power transmitted through the shaft line. Engine manufacturers specify MCR as the upper limit of the engine's sustained operational capacity. However, in practice, engines are frequently operated at reduced power level known as the continuous service rating (CSR). This adjustment mitigates increased fuel consumption, reduced power reserves, and accelerated engine wear at MCR. Despite this operational preference, MCR remains essential for compliance calculations within the rules and regulations established by classification societies.

2.3.3. Applicable technical standards

Classification societies have essential role in the shipping industry by integrating diverse technical standards and regulatory guidelines into unified framework. They establish and ensure that merchant marine ships comply with comprehensive set of technical standards for the design, construction, and maintenance. Consequently, for ships that comply with prescribed rules, designated classification society issues certificate of class and conducts regular surveys to ensure ongoing compliance with the class requirements.

The International Association of Classification Societies (IACS) represents technical body that provides platform for sharing research and development of maritime safety standards. IACS through Unified Requirements (UR) defines minimum common technical standards for ship construction, classification, and life-cycle compliance. It consists of twelve-member societies which incorporate these requirements into their regulations and practices, and if considered necessary may incorporate more stringent requirements [64].

In shipping industry, technical standards are closely integrated with guidelines and standards set by international organizations, government bodies, and industry groups such as International Organization for Standardization (ISO) and International Electrotechnical Commission (IEC), etc. For example, ISO standards define the quality criteria for steel used in ship construction, while classification societies ensure its proper application and inspection. Similarly, IEC standards prescribe electrical safety measures for maritime systems, and classification societies verify compliance through certification and audits.

To enhance safe and reliable operation of ships, additional standards that address vibration analysis, machinery performance, and system design can complement rules of classification societies. To name a few examples, torsional vibrations in internal combustion engines are addressed in [65], while balancing rotating machinery is covered in [66]. Methods for calculating shaft strength, which is crucial for TVA, are outlined in [58], while methodologies for TVA are provided in [67]. The integration of diverse technical standards by classification societies ensures unified framework for overall ship safety, including critical aspects such as vibration analysis. These standards play key role in mitigating vibrations and ensuring reliable propulsion system performance. This research adopts the IACS member Croatian Register of Shipping (CRS) rules for ship classification as the reference for technical standards, supplemented by essential URs and VDI guidelines [45, 67, 68].

2.3.4. Permissible stress limits

Components of the marine shaft line must comply with certain fatigue criteria outlined in [62]. Low-cycle fatigue, involving fewer than 10^4 cycles, encompasses the full load range, while high-cycle fatigue involves over 10^7 cycles, addressing permissible torsional vibration stresses during continuous operation. For this purpose, fatigue factors k_d for low-cycle used in equation (7) and C_k for high-cycle are included, to account different design features such as geometric stress concentration, notch sensitivity, etc.

The TVA for ship propulsion systems involves calculating critical speeds and evaluating additional torsional stresses within the shaft line, both normal firing and misfiring conditions.

These additional stresses can ultimately result in fatigue failure, so it is necessary that TVA covers entire operating range of propulsion engine, as shown in Figure 5. Misfiring condition is defined as compression without fuel injection and is particularly significant as it may induce peak torsional vibration stresses and occur in any cylinder. Variable torque from the engine induces vibration stresses within the shaft line components.

According to [62], alternating torsional stress amplitude is defined as the difference between maximum and minimum stress measured on the shaft during a repetitive cycle under relevant conditions.

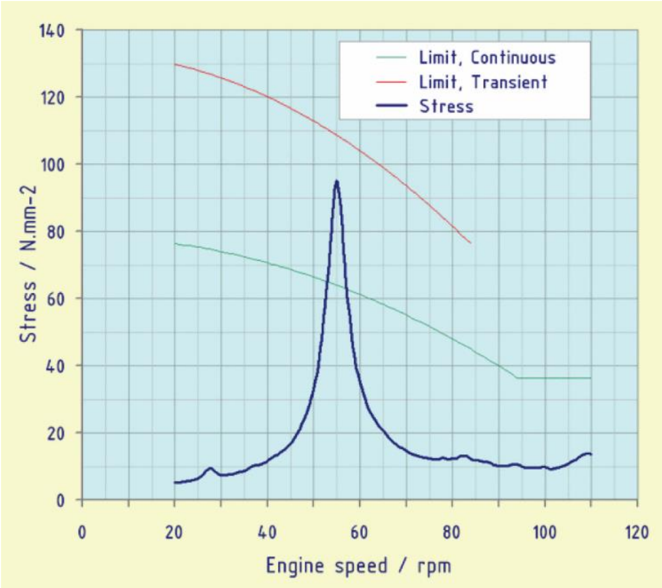

Figure 5. Torsional vibration stress response for intermediate shaft with stress limits [44]

The allowable alternating torsional vibration stresses for continuous operation τ_c shall remain within the limits defined by the following equations:

$$\begin{aligned} \pm\tau_c &= \frac{\sigma_B + 160}{18} \cdot C_k \cdot C_D \cdot \left(3 - 2 \cdot \lambda^2\right) \quad for \quad \lambda < 0,9 \\ \pm\tau_c &= \frac{\sigma_B + 160}{18} \cdot C_k \cdot C_D \cdot 1.38 \quad for \quad 0,9 < \lambda < 1,05 \end{aligned} \tag{8}$$

Where

C_k - factor for the particular shaft design,

C_D - size factor,

n - shaft speed under consideration in rpm,

n_0 - shaft speed at rated power in rpm,

λ - speed ratio of n to n_0.

When stresses exceed the limits set by the classification society, as shown in Figure 5, the corresponding operating range must be restricted and passed rapidly with stable engine operation at each end, thus ensuring that permissible stress amplitude τ_t due to steady-state torsional vibration remains within the limits defined as:

$$\pm\tau_t = 1.7\frac{\tau_c}{\sqrt{C_k}} \tag{9}$$

In summary, the vibration limits established by classification societies are crucial for ensuring the safety and reliability of marine propulsion systems, preventing issues such as fatigue failure. Adhering to these standards not only minimizes the risk of mechanical failure but also contributes to overall performance and safety of ships.

2.4. Vibration measurements

A properly designed machine typically generates low vibration levels. However, over time vibration amplitudes increase due to wear, misalignment, imbalance, and increased clearances. These factors potentially lead to failure, as they increase the risk of resonance and impose dynamic stress on bearings. Purpose of vibration measurements is to assess the condition the system. In any vibration measurement, initial step is to establish vibration profile by quantifying key parameters such as displacement, velocity and acceleration, along with frequency for both forced and resonant vibrations. Next step is to identify the source of vibration, namely whether it originates from internal, from drive system itself, or external factors, such as foundation or ship structure. Since vibrations arise from periodic forces and torques at specific frequencies, identifying the excitation frequency is crucial for diagnosing their cause. Measurement techniques can vary depending on vibration type [67], thus axial and lateral vibrations are measured with accelerometers or displacement sensors, while torsional vibrations are detected using rotational sensors or strain gauges.

To ensure accurate results, measurement system must include sensors, recording equipment, and data processing capable of delivering distortion-free data within the specified range [69]. For transmitting output signals rotary transmitters (slip rings) and co-rotating transmitters (telemetry systems) are used. Slip rings enable power and signal transmission between stationary and rotating structures, while co-rotating transmitters send signals digitally or via frequency modulation.

This section provides a brief overview of torsional vibration measurement techniques and practical considerations. The aim of torsional vibration measurements is to determine quantities such as angular velocity, angular acceleration and torque. It is important to highlight that angular displacement cannot be measured directly, yet are calculated by integrating angular velocity or acceleration. Angular velocity measurement is commonly used in rotating machinery with revolutions per minute (rpm) being the standard unit. It is typically measured by generating a pulse train or sine wave, where the frequency corresponds to angular velocity [70]. These methods provide relative measurements, as they assess motion between two bodies with respect to the base of the measured object. Measurement technologies based on this principle include incremental encoder, electrodynamic torsional vibration transmitter, or laser transmitter [67].

Incremental encoder, shown in Figure 6, rotates with the object that is being measured. It consists of segments such as transparent disk with engraved angles or gear wheel with teeth, that are equally spaced for angular increment $\Delta\varphi$. Stationary optical or electrical transducer detects the passing segments, using relative measurement principle. When rotation speed is constant and unaffected by torsional vibration, the transducer signal is periodic with the fundamental frequency, but the presence of torsional vibration modulates this frequency.

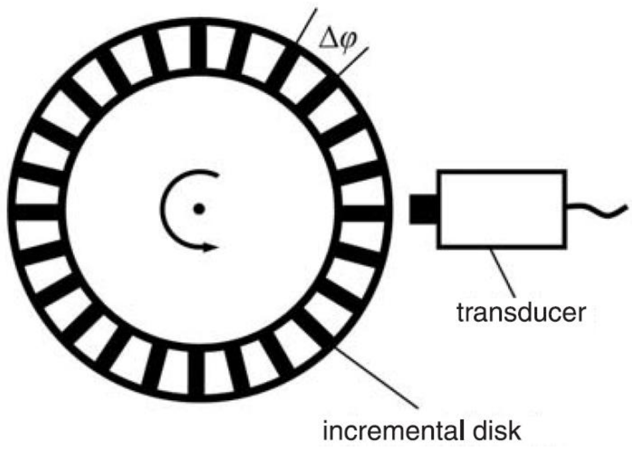

Figure 6. Basic design of the incremental encoder [67]

Electrodynamic torsional vibration sensors, often of the seismic type shown in Figure 7, are typically mounted centrally at the free end of the driveline. During torsional vibrations, a seismic mass within the housing oscillates relative to it due to the shaft's torsional flexibility. This motion, proportional to the shaft's angular deflection, generates the electrodynamic voltage corresponding to the angular vibration velocity of the transducer and the shaft. A voltage is electrodynamically induced by the relative motion of the rotating seismic mass, making the transducer output proportional to the angular vibration velocity of both the transducer and the shaft. The signal must be transmitted from the rotating to the stationary component using slip rings or telemetry.

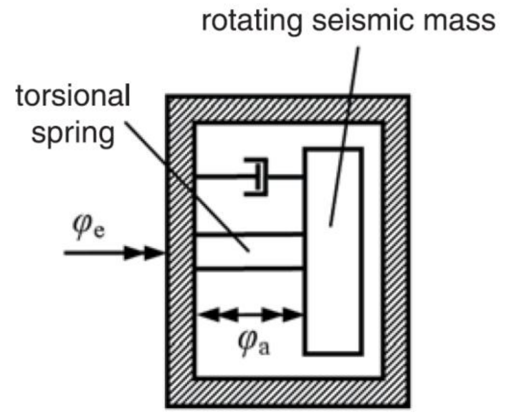

Figure 7. Seismic transducer for torsional vibrations [67]

Laser sensors measure vibration velocities using the optical Doppler effect, detecting only the speed component along the laser beam's direction. The measuring instrument captures the light reflected from the target, with the frequency shift between the emitted and reflected laser light proportional to their relative velocity. Thereby it is based on relative measurement principle, so the equipment should be mounted with minimal vibration.

For measuring angular acceleration vibrations, two piezoelectric accelerometers can be mounted tangentially and symmetrically in housing attached to the driveline, as shown in Figure 8. Operating principle is based on the piezoelectric property of quartz crystals or specialized ceramics, which generate the electric charge proportional to acceleration under dynamic pressure or shear of the inertial mass. Their signals are transmitted via telemetry or slip rings, while radial acceleration minimally affects tangential measurements.

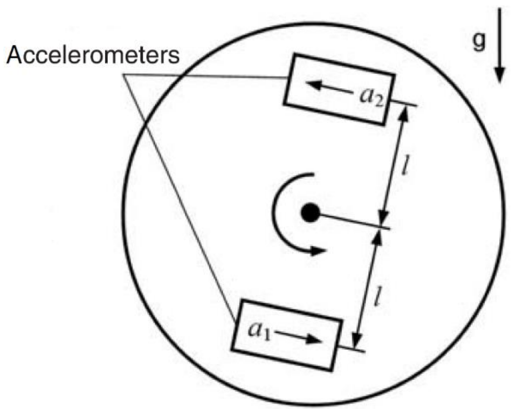

Figure 8. Angular accelerometer [67]

Torque is measured using strain gauges, commonly made from constantan wire as shown in Figure 9, or semiconductor foil. They are tangentially bonded to shafts to measure elongations caused by shear deformation, which correlates with shear strain and torque [71].

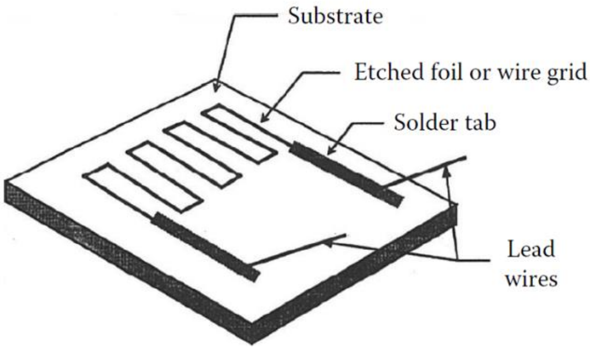

Figure 9. Construction of wire or foil strain gauge [67]

For constantan wire strain gauges, elongation reduces the wire's cross-sectional area, leading to proportional change in its electrical resistance. Semiconductor strain gauges, on the other hand, rely on the piezoresistive effect, where crystalline deformation during elongation alters the material's electrical resistance. In both cases, the resistance change is measured using Wheatstone bridge circuit [72]. When combined with the applied excitation voltage, the circuit generates bridge voltage directly proportional to the torsional deformation and torque experienced by the shaft.

In general, torsional vibration measurements can be challenging due to sensor sensitivity, signal noise, calibration accuracy, and environmental effects, which introduce uncertainties under real-world conditions. According to [67], metrological issues include inability of direct measurement of certain quantities of interest, such as torque and torsional stress. Also, issue of accessibility to critical points on the driveline, thus further complicating measurements. Accurate comparison between measurements and calculations, along with necessary adjustments, requires significant expertise. In many cases, vibration excitation cannot be directly measured but must be inferred indirectly by analysing the system's response to the excitation. Conclusions regarding vibration excitation are often drawn using calculation models. Despite these challenges, accurate vibration measurements provide empirical basis which is essential for assessing dynamic behaviour and validating theoretical models.

In next chapter, focus will be to provide fundamental theoretical framework of vibration analysis, which are crucial for interpreting and predicting system responses under dynamic conditions.

3. FUNDAMENTALS OF VIBRATION THEORY

Vibrations, while advantageous in certain technological processes across various industries, are typically considered detrimental in practical applications, as they can induce structural damage, accelerate wear, and disrupt machinery performance. Vibrations are mechanical oscillations with small amplitudes, whereas oscillations describe any periodic motion, regardless of amplitude [73]. Study of mechanical vibrations is fundamental to vibration theory and crucial in engineering, where small-amplitude periodic motion often occurs. Across literature vibration definitions mainly differ in level of detail, with simple definition from [41] describing vibration as: *"Any motion that repeats after a time interval."* A fuller definition from [74] adds that: *"Vibration is periodic motion along a straight line, circle, or curve, where a particle or body returns to its initial position and phase after completing one period."*

Vibrations are primarily classified as either free or forced, both of which occur in damped or undamped form. Free vibrations occur when system is displaced from its equilibrium position and allowed to vibrate at its natural frequency, with no external force acting on it. Forced vibrations occur when the external force continuously acts on a system and makes it vibrate at the same frequency. Also, vibration can be classified according to other characteristics, such as: the nature of the physical process (mechanical, electrical, or acoustical), the form of differential equation (linear or nonlinear), the predictability of excitation (deterministic or random), and the degrees-of-freedom (discrete or continuous). In vibration analysis, system components are considered as rigid bodies with positions defined by coordinates. Degrees-of-freedom (DOF) refer to the minimum number of independent coordinates needed to uniquely specify the position of every component in the vibrating system.

This chapter primarily focuses on vibration analysis through longitudinal vibration models, as they simply and effectively represent many vibration phenomena. Torsional vibrations are addressed by translating the mathematical model for longitudinal vibrations into the context of rotational mechanics. A comprehensive theoretical background is essential, as the ship propulsion system consists of numerous single-DOF elements, requiring analysis as the vibration system with multiple DOF. The dynamics of longitudinal single DOF vibrating system is presented in following sections, for both free and forced vibrations. The focus is then expanded to systems with two or more DOF, for both free and forced vibrations, analysing their more complex interactions and responses. The same approach is applied in the analysis of torsional vibration systems addressed at the end of the chapter, highlighting characteristics and challenges regarding rotational dynamics, particularly in the context of ship propulsion system. Given the extensive literature on vibration theory, this chapter is structured around key sources [41, 73, 75, 76, 77, 78], which are not cited individually throughout the text.

3.1. Single degree-of-freedom System

During vibration motion, kinetic energy of the system is continuously converted into potential energy and vice versa. In real systems, vibration motion eventually disappears due to damping which causes energy dissipation during each vibration cycle. In vibration analysis, the dynamic behaviour of mechanical systems under specific input conditions is evaluated using physical and mathematical models. To identify key system characteristics and derive the governing equations of motion vibration systems are typically represented as inertial elements connected by elastic and damping elements.

The inertial element stores system's kinetic energy and is typically represented as weight with mass or, for rotational motion as disc with mass moment of inertia. The elastic element stores potential energy, often represented as linear spring generating restorative force proportional to its extension:

$$F_s = kx \tag{10}$$

Where

F_s - the spring force,

k - the spring stiffness constant, and

x –elongation of the spring (equivalent to mass displacement).

The real springs are nonlinear and follow expression (10) only to certain level of extension, after which the behaviour of the spring deviates from linearity, so often in practical problems spring behaviour is linearized.

Damping causes energy loss during each vibration cycle, which results in gradual decrease of the vibration amplitude. It occurs due to internal or external friction and is represented by the damping element. Internal friction arises from the relative movement of material particles during deformation. External friction can be dry, viscous, or generally fluid resistance. Frictional forces between dry surfaces depend on material type, surface roughness, and sliding speed, whereas for lubricated surfaces, it depends on the lubricant's viscosity and the relative sliding speed [73]. Damping force is generally expressed as:

$$F_c = c\dot{x}_{rel}^{n} \tag{11}$$

where

c - damping factor,

x_{rel} - relative speed of contact surfaces, and

n - the exponent: $n = 0$ for dry friction,

$n = 1$ for viscous friction, and

$n = 2$ for fluid resistance.

To simplify mathematical analysis, viscous friction is commonly assumed and represented with viscous damping element, consisting of piston and cylinder filled with oil.

Vibrating system with single DOF, as shown in Figure 10, typically consists of cart that represents inertial element with mass m. It is connected to the frictionless surface by spring with stiffness constant k and damper with damping coefficient c. According to the free-body diagram, the spring force $F_s = kx$, the damping force $F_c = c\dot{x}$, the inertia force $F_i = m\ddot{x}$, and the active disturbance or excitation force is $F(t)$ act on cart, causing it to slide.

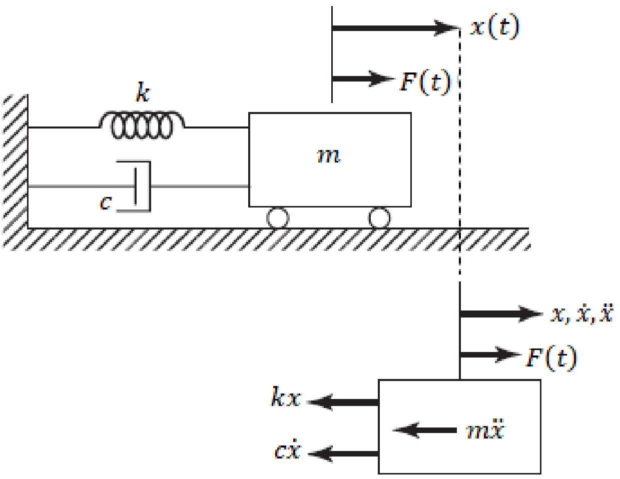

Figure 10. Linear vibration system with single DOF

The excitation force is assumed to act according to harmonic law:

$$F(t) = F_0 \sin(\Omega t - \varphi) \tag{12}$$

where

F_0 - amplitude of the excitation force,

Ω - circular frequency of excitation force, and

φ - initial phase.

Then, the governing equation of motion can be expressed as:

$$m\,\ddot{x}+c\,\dot{x}+k\,x=F(t) \tag{13}$$

Vibration analysis investigates the dynamic response of mechanical systems, which is characterized through governing equations formulated from mathematical models. In the following sections the dynamics of free and forced vibrations in both damped and undamped systems is introduced.

3.1.1. Free undamped vibration

If the viscous damper and excitation force are removed from the system in Figure 10, it consists only of inertial and elastic elements, allowing it to experience free vibrations described by the following differential equation of motion:

$$m\ddot{x}+kx=0 \tag{14}$$

which can also be expressed in the form as:

$$\ddot{x}+\omega_n^2 x=0 \tag{15}$$

where ω_n denotes the natural circular frequency of free undamped vibrations, shown as:

$$\omega_n=\sqrt{\frac{k}{m}} \tag{16}$$

Natural circular frequency is the intrinsic property of the system and it depends solely on the parameters of the system, namely spring constant *k* and mass *m*. At this point, it is important to make distinction between natural circular frequency ω_n and common frequency f_n, which represents the number of cycles per unit time, expressed as:

$$f_n=\frac{\omega_n}{2\pi}=\frac{1}{T_n} \tag{17}$$

where time required to complete one cycle is defined as period T_n, expressed as:

$$T_n=\frac{2\pi}{\omega_n} \tag{18}$$

The general solution of equation (13) can be assumed in the form:

$$x=C_1\cos\omega_n t+C_2\sin\omega_n t \tag{19}$$

First and second derivatives of (19) with respect to time yield the velocity and acceleration:

$$\dot{x}=-C_1\omega_n\sin\omega_n t+C_2\omega_n\cos\omega_n t \tag{20}$$

$$\ddot{x} = -\omega_n^2 \left(C_1 \cos \omega_n t + C_2 \sin \omega_n t \right) = -\omega_n^2 x \tag{21}$$

By defining the initial conditions for initial time, as well as the initial displacement and velocity, and substituting them into equations (19) and (20), the integration constants C_1 and C_2 are determined:

$$\begin{aligned} C_1 &= x_0 \\ C_2 &= \frac{\dot{x}_0}{\omega_n} \end{aligned} \tag{22}$$

By substituting integration constants into expression (19), the general solution of the differential equation (15) with the included initial conditions is obtained:

$$x = x_0 \cos \omega_n t + \frac{\dot{x}_0}{\omega_n} \sin \omega_n t \tag{23}$$

or written as:

$$x = \sqrt{x_0^2 + \left(\frac{\dot{x}_0}{\omega_n} \right)^2} \sin\left(\omega_n t + \varphi \right) \tag{24}$$

where φ is initial phase determined using the relationships between the integration constants:

$$\varphi = \tan \frac{\dot{x}_0}{\omega_n x_0} \tag{25}$$

To summarize, free undamped vibrations describe the natural vibration motion of the system without any energy loss, governed by its mass and stiffness properties. The next section explores free damped vibrations, where energy loss due to damping forces affects behaviour of the vibrating system.

3.1.2. Free damped vibration

By removing the excitation force from the system in Figure 10, the system experiences free damped vibrations, described by the following differential equation of motion:

$$m\ddot{x} + c\dot{x} + kx = 0 \tag{26}$$

The general solution of (26) is homogeneous equation is assumed in the form:

$$x = C\, e^{rt} \tag{27}$$

By substituting the first and second derivatives of function (27) with respect to time into differential equation (26), the following expression is obtained:

$$Ce^{rt}\left(mr^2+cr+k\right)=0 \tag{28}$$

From this step, the characteristic equation is expressed as:

$$mr^2+cr+k=0 \tag{29}$$

For which the roots are as follows:

$$r_{1,2}=\frac{-c\pm\sqrt{c^2-4mk}}{2m} \tag{30}$$

Accordingly, the general solution of (26) is written as:

$$x=C_1e^{r_1t}+C_2e^{r_2t} \tag{31}$$

For which the nature of the solution depends on the discriminant:

$$D=c^2-4mk \tag{32}$$

The existence and nature of the solution is directly conditioned by the discriminant and properties of the quadratic function. The next sections will examine the different cases of damped vibrations: underdamped, overdamped, and critically damped, each characterized by distinct behaviour and response characteristics.

3.1.2.1. Critically damped systems

In the case of critical damped system, the discriminant *D* is equal to zero, so the magnitude of critical damping is:

$$c_c=2\sqrt{mk} \tag{33}$$

From expression (30), the roots of the characteristic equation are obtained, and are real and equal as shown:

$$r_1=r_2=-\frac{c_c}{2m}=-\omega_n \tag{34}$$

Thus, in accordance with expression (31) the solution of equation (26) is expressed in the form:

$$x=e^{-\omega_nt}\cdot\left(C_1+C_2t\right) \tag{35}$$

Determining the integration constants for the initial conditions and substituting them along with initial conditions into expression (35), the general solution to the differential equation is expressed as:

$$x=e^{-\omega_nt}\cdot\left[x_0+\left(\dot{x}_0+\omega_nx_0\right)t\right] \tag{36}$$

In critically damped system, the roots of the characteristic equation are real and equal, leading to quick stabilization without vibration. The next sections will explore underdamped and overdamped systems, where damping conditions produce different dynamic responses.

3.1.2.2. Underdamped systems

In the case of underdamped system, the viscous damping coefficient *c* is less than the critical damping value. Whether the system is considered overdamped, critically damped, or underdamped is indicated by the damping factor expressed as:

$$\zeta = \frac{c}{c_c} \tag{37}$$

Damping factor ζ is introduced to describe the ratio of damping coefficient to the critical damping value. In the case of critical damping the value of damping factor is equal to one, while for overdamped systems it exceeds one, and is less than one for underdamped systems. The motion, i.e. the response of the system for all three damping cases is shown in Figure 11.

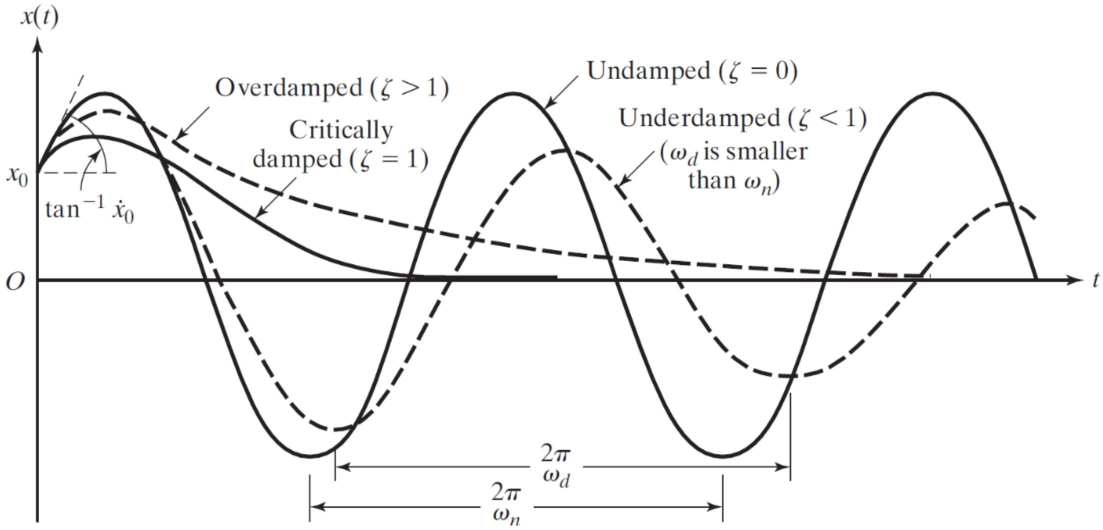

Figure 11. Comparison of motions with different types of damping [41]

In undamped systems, the discriminant is negative according to equation (32), thereby the roots of the characteristic equation (30) are determined as:

$$r_{1,2} = -\frac{c}{2m} \pm \sqrt{\left(\frac{c}{2m}\right)^2 - \frac{k}{m}} = -\zeta\omega_n \pm i\omega_{nc} \tag{38}$$

where ω_{nc} is the natural angular frequency of free damped vibrations, expressed as:

$$\omega_{nc} = \omega_n\sqrt{1-\zeta^2} \tag{39}$$

According to expression (31), general solution of the differential equation (26), is formed as:

$$x = e^{-\zeta\omega_n t} C \sin\left(\omega_{nc} t + \varphi\right) \tag{40}$$

In underdamped vibration systems, the displacements of the vibrational motion decrease exponentially, as shown in Figure 12. This amplitude decrease during single vibration cycle is defined by time instants t_1 and t_2 and corresponding displacements x_1 and x_2.

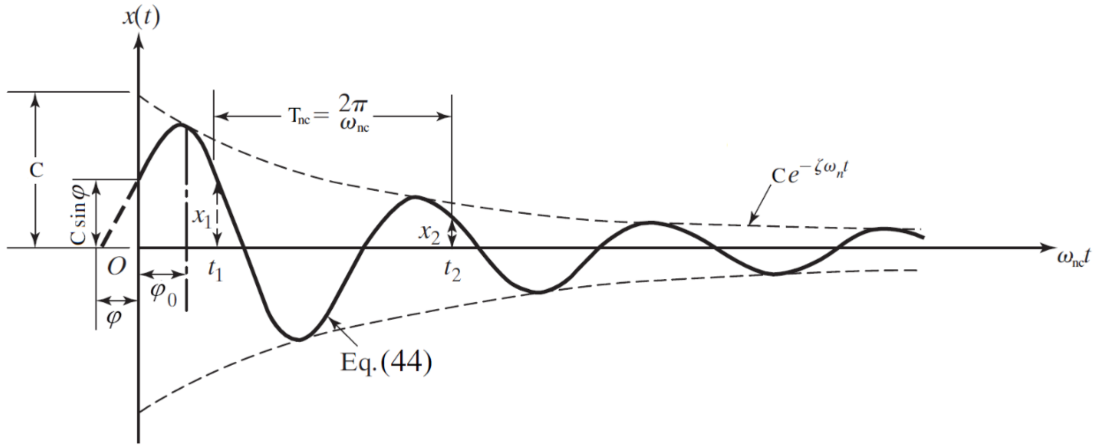

Figure 12. Time variation of the displacement x in underdamped vibration system [41]

Their ratio provides the effective measure for describing damping magnitude, expressed as:

$$\frac{x_1}{x_2} = e^{\zeta\omega_n T_{nc}} \tag{41}$$

As this ratio has exponential form, it is conventionally expressed through its natural logarithm:

$$\Lambda = \ln\frac{x_1}{x_2} = \zeta\omega_n T_{nc} = \frac{2\pi\zeta}{\sqrt{1-\zeta^2}} \tag{42}$$

where Λ is logarithmic decrement indicating the rate of vibration damping and can be used to determine damping factor. In underdamped systems the amplitude of vibration motion exponentially decreases, however in overdamped system, the system exhibits different dynamic response.

3.1.2.3. Overdamped systems

In the case of overdamped vibration system, the viscous damping coefficient *c* is greater than the critical damping value. This can be expressed by the damping factor ζ, which is greater than one, indicating that the discriminant is positive according to equation (36). Consequently, the roots of the characteristic equation (34) are real and different, expressed as:

$$r_{1,2} = -\frac{c}{2m} \pm \sqrt{\left(\frac{c}{2m}\right)^2 - \frac{k}{m}} = \omega_n(-\zeta \pm \sqrt{\zeta^2 - 1}) \tag{43}$$

According to (31), the general solution of the differential equation in (26), can be expressed:

$$x = e^{-\zeta\omega_n t}\left(C_1 e^{\omega_{nc} t} + C_2 e^{-\omega_{nc} t}\right) \tag{44}$$

Initial phase angle and integration constant are determined from the initial conditions. By substituting integration constants into (43), the general solution is obtained:

$$x = Ce^{-\zeta\omega_n t} \cdot \sinh\left(\sqrt{\zeta^2 - 1} \cdot \omega_n t + \varphi\right) \tag{45}$$

In overdamped systems, the damping factor exceeds one, resulting in the non-vibratory response with real and distinct roots. The system gradually returns to equilibrium without vibrating, but at slower rate compared to critically damped systems. This concludes the discussion on free damped and undamped vibrations. The next chapter will focus on forced vibrations, where the behaviour of the system is influenced by external forces.

3.2. Forced vibration

Forced vibrations occur when system is subjected to external periodic force. This results in vibrations that are influenced by both the system's natural characteristics and the applied excitation frequency. In contrast to free vibrations, where the system's motion is determined solely by its initial conditions, forced vibrations involve excitation that acts as continuous input that drives the system's behaviour. The following sections will first explore undamped systems, where the motion is solely governed by harmonic excitation, and then discuss damped systems, where the amplitude and phase of the resulting vibrations are affected by damping forces.

3.2.1. Undamped systems

Single DOF undamped system subjected to harmonic excitation force exhibit dynamic response that can be described by differential equation (13), in this case expressed in form:

$$m\ddot{x} + kx = F_0 \sin\left(\Omega t - \varphi\right) \tag{46}$$

Solution to this equation consists of the general homogenous and the particular solution:

$$x(t) = x_h(t) + x_p(t) \tag{47}$$

The general solution of this differential equation with included initial conditions is:

$$x(t) = x_0 \cos\omega_n t + \frac{v_0}{\omega_n}\sin\omega_n t + X\sin\Omega t \tag{48}$$

The general homogenous part in (47) consists of first two terms in (48) that describe vibrations at the natural frequency. The particular solution expressed in the third term represents vibrations at the excitation frequency. Vibrations at the natural frequency decay over time, leaving only the forced vibrations at the excitation frequency. Thus, the former vibrations are known as transient vibrations, and the latter as steady-state vibrations, for which the amplitude is expressed as:

$$X = \frac{F_0}{k - m\Omega^2} = \frac{\dfrac{F_0}{k}}{1 - \dfrac{m}{k}\Omega^2} = \frac{x_{st}}{1-\eta^2} \tag{49}$$

where

$x_{st} = F_0/k$ - static displacement of mass subjected to the constant force F_0.

$\eta = \dfrac{\Omega}{\omega_n}$ - dimensionless ratio of the excitation frequency Ω to the system's natural frequency ω_n.

The amplitude of steady-state vibrations depends upon the value of η, so as the excitation frequency approaches natural frequency $\eta=1$, the amplitude tends toward infinity. However, in real systems friction prevents the amplitude from increasing infinitely, instead it gradually approaches some finite value. The ratio of dynamic to static amplitude, also referred as magnification factor, is expressed as:

$$M=\frac{X}{x_{st}}=\frac{1}{1-\eta^2} \tag{50}$$

In undamped systems, the vibrations eventually settle into a steady-state vibration at the excitation frequency, with resonance occurring as the excitation frequency approaches the natural frequency of the system. The next section will explore forced damped systems, where the presence of damping forces alters the system's response to harmonic excitation.

3.2.2. Damped systems

In the case of damped system subjected to harmonic excitation force *F(t)*, the motion of mechanical system with single DOF, shown in Figure 10, is described by differential equation (13). It has general solution as in (47), where x_h is the general solution of the homogeneous part, which for underdamped system, can be expressed as in (40).

The second part of the general solution x_p is expressed as:

$$x_p(t)=\frac{x_{st}}{\sqrt{\left[1-\left(\frac{\Omega}{\omega_n}\right)^2\right]^2}}\sin(\Omega t-\gamma) \tag{51}$$

This solution represents the response of mechanical system to harmonic excitation force, specifically the steady state forced vibrations of the observed system. By taking into consideration $\omega_n = k/m$, $x_{st} = F_0/k$, $\zeta = c/c_c = c/\sqrt{2mk}$ then equation (47) can be expressed as:

$$x_p(t)=X\sin(\Omega t-\gamma) \tag{52}$$

where

$$X=\frac{F_0}{\sqrt{\left(1-\eta^2\right)^2+\left(2\zeta\eta\right)^2}} \tag{53}$$

and

$$\gamma = \text{arc tan}\frac{2\zeta\eta}{1-\eta^2} \tag{54}$$

The complete general solution is then:

$$x(t) = e^{-\zeta\omega_n t}C\sin(\omega_{nc}+\varphi) + X\sin(\Omega t-\gamma) \tag{55}$$

The character of transient vibrations depends on η, indicating that if $\Omega > \omega_n$, the system during transient phase vibrates at its natural frequency, with additional beats at the excitation frequency. Conversely, when $\Omega < \omega_n$, the vibrations at the excitation frequency are more pronounced. Once the vibrations stabilize, the system vibrates at the excitation frequency, with amplitude that depends upon damping. This amplitude can be expressed by dimensionless magnification factor:

$$M = \frac{X}{x_{st}} = \frac{1}{\sqrt{(1-\eta^2)^2+(2\zeta\eta)^2}} \tag{56}$$

This factor, shown in Figure 13, represents the ratio of the amplitude X to the static displacement x_{st}, thus quantifying the extent of amplitude increase due to the excitation frequency relative to the static response. In systems with low damping, resonance effectively occurs when $\Omega=\omega_n$, causing the vibration amplitude to theoretically become infinitely large in the absence of damping. As damping increases, peak amplitudes occur at progressively lower ratios of Ω/ω_n. In the sub resonant region $\zeta<1$, reducing stiffness k leads to the increase in amplitude X, as it lowers the natural frequency. Conversely, in the super resonant region $\zeta>1$, a decrease in stiffness reduces the vibration amplitude.

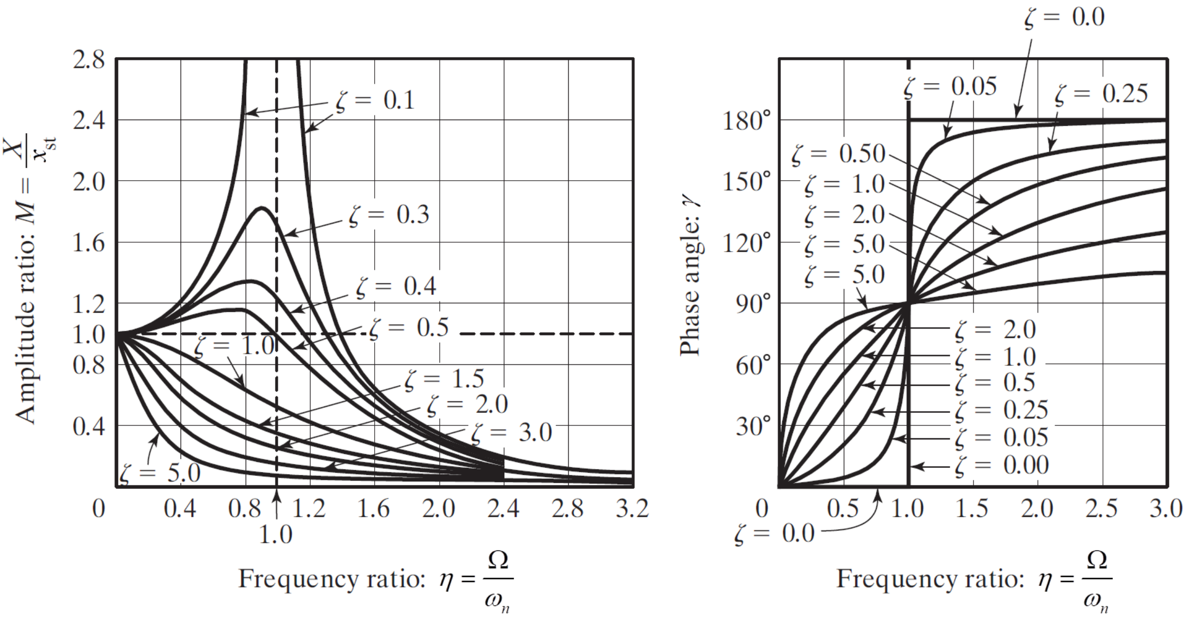

Figure 13. Dependency of amplitude ratio and phase angle on frequency ratio for different damping factors [41]

In damped vibration systems, vibrations typically have phase lag in relation to the excitation, characterized by phase shift γ, whose dependency on frequency ratio is shown in Figure 13.

In damped systems, the presence of damping forces alters the system's response to harmonic excitation, affecting both the amplitude and phase of vibrations. Together, the analysis of free and forced damped and undamped vibrations provides a comprehensive understanding of how systems behave under various conditions of excitation and damping. The next chapter will focus on the vibration of two DOF, where the interactions between multiple masses and springs lead to more complex dynamic behaviour.

3.3. Two degree-of-freedom System

To determine position or describe motion of systems with two DOF, two independent generalized displacements are required. The number of DOF of the system depends upon the number of masses in the system and the number of possible types of motion of each mass. Thus, there are two equations of motion, resulting in two natural frequencies of the system. An example under consideration, shown in Figure 14, represents viscously damped two DOF system with accompanying free-body diagram.

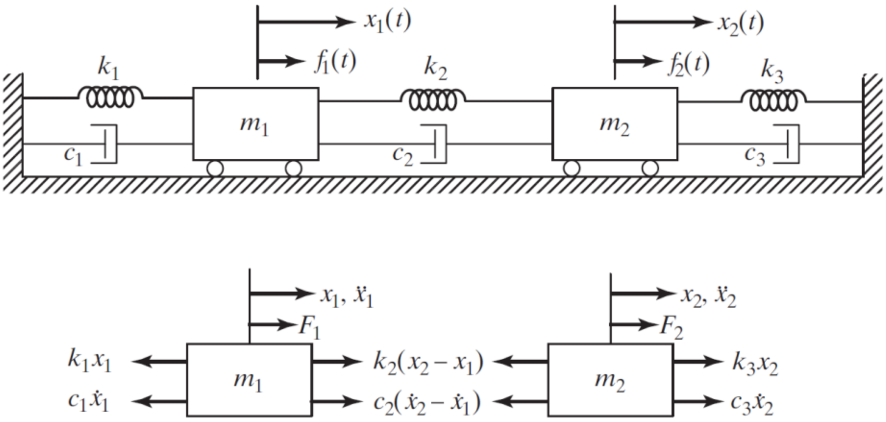

Figure 14. Linear vibration system with two DOF [41]

The system consists of the masses m_1 and m_2 upon which the external forces $F_1(t)$ and $F_2(t)$ act, displacing them from the respective equilibrium positions. The motion of the system is described by the coordinates x_1 and x_2, which define the positions of the masses m_1 and m_2 at any time t, and the equations of motion for such system are:

$$\begin{aligned} m_1\ddot{x}_1 + (c_1+c_2)\dot{x}_1 - c_2\dot{x}_2 + (k_1+k_2)x_1 - k_2x_2 &= f_1(t), \\ m_2\ddot{x}_2 + (c_2+c_3)\dot{x}_2 - c_2\dot{x}_1 + (k_2+k_3)x_2 - k_2x_1 &= f_2(t). \end{aligned} \tag{57}$$

Where

$c_{1\text{-}3}$ - damping coefficients, and

$k_{1\text{-}3}$ - spring constants.

These equations represent a system of two coupled ordinary differential equations of second-order, indicating that the motion of the mass m_1 influence the motion of the mass m_2, and vice versa. Expressions in (57) can be rewritten in matrix form as:

$$\mathbf{M}\ddot{\mathbf{x}}(t) + \mathbf{C}\dot{\mathbf{x}}(t) + \mathbf{K}\mathbf{x}(t) = \mathbf{f}(t) \tag{58}$$

Where matrices **M**, **C**, and **K** represent the mass, damping, and stiffness, of the system. They are square and symmetric matrices containing the following elements:

$$\mathbf{M} = \begin{bmatrix} m_1 & 0 \\ 0 & m_2 \end{bmatrix}, \tag{59}$$

$$\mathbf{C} = \begin{bmatrix} c_1 + c_2 & -c_2 \\ -c_2 & c_2 + c_3 \end{bmatrix}, \tag{60}$$

$$\mathbf{K} = \begin{bmatrix} k_1 + k_2 & -k_2 \\ -k_2 & k_2 + k_3 \end{bmatrix}. \tag{61}$$

The displacement **x** and excitation force **f** vectors are single column matrices with elements:

$$\mathbf{x} = \begin{Bmatrix} x_1 \\ x_2 \end{Bmatrix}, \quad \mathbf{f} = \begin{Bmatrix} f_1 \\ f_2 \end{Bmatrix}. \tag{62}$$

In brief, systems with two DOF are described by coupled equations of motion, providing insight into their dynamic behaviour. The next section discusses free vibrations in two DOF systems.

3.3.1. Free vibration

Undamped two DOF system, shown in Figure 15, have two natural frequencies and corresponding modes of vibration, with distinct amplitude ratios in each mode.

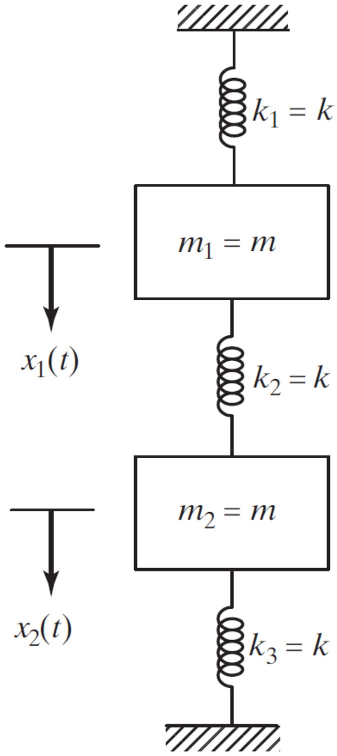

Figure 15. Two DOF undamped system [41]

The system's motion is governed solely by its initial conditions and natural characteristics in the absence of external forces. Considering that no excitation forces act upon the free undamped system illustrated in Figure 15, the equations of motion are as follows:

$$\begin{aligned} m_1\ddot{x}_1 + (k_1 + k_2)x_1 - k_2x_2 &= 0, \\ m_2\ddot{x}_2 + (k_2 + k_3)x_2 - k_2x_1 &= 0. \end{aligned} \tag{63}$$

Their solution is given by:

$$\begin{aligned} x_1 &= X_1 \sin(\Omega t - \varphi_1), \\ x_2 &= X_2 \sin(\Omega t - \varphi_2). \end{aligned} \tag{64}$$

These solutions, when substituted into the two equations of motion, yield the equal number of homogeneous linear algebraic equations, where the unknowns are the amplitudes X_1 and X_2. The amplitudes will be non-zero if the determinant of the coefficients of the algebraic equations is equal to zero, that is:

$$\left|\mathbf{K} - \omega^2\mathbf{M}\right| = 0 \tag{65}$$

In its expanded form, the expression (65) for the determinant becomes:

$$m_1 m_2 \omega^4 - \left[(k_1 + k_2) m_2 + (k_2 + k_3) m_1 \right] \omega^2 + \left[(k_1 + k_2)(k_2 + k_3) - k_2^2 \right] = 0 \tag{66}$$

The above equation is called the characteristic or frequency equation and always has two positive real solutions:

$$\omega_{1,2} = \sqrt{\frac{k_1 + k_2}{2m_1} + \frac{k_2 + k_3}{2m_2} \pm \sqrt{\left(\frac{k_1 + k_2}{2m_1}\right)^2 \cdot \left(\frac{k_2 + k_3}{2m_2}\right)^2 - \frac{k_1 k_2 + k_2 k_3 + k_1 k_3}{m_1 m_2}}} \tag{67}$$

Each natural frequency is associated with specific amplitude ratio, referred to as the natural, principal, or normal mode of vibration [41]. Two DOF system exhibits two distinct natural frequencies ω_1 and ω_2, corresponding to the two unique natural modes of vibration. The frequency at which the system vibrates is dictated by the initial conditions. Notably, orthogonality is the fundamental characteristic of these natural vibration modes. The equations of motion are homogeneous, so the amplitude ratios can be determined and expressed as:

$$\frac{X_2}{X_1} = \frac{-m_1 \omega^2 + k_1 + k_2}{k_2} = \frac{k_2}{-m_2 \omega^2 + k_2 + k_3} \tag{68}$$

By defining the masses $m_{1,2}=m$ and stiffnesses $k_{1\text{-}3}=k$ for the system in Figure 15, the natural frequencies $\omega_{1,2}$ can be determined, for which the corresponding modes of vibration show distinct characteristics, as shown in Figure 16.

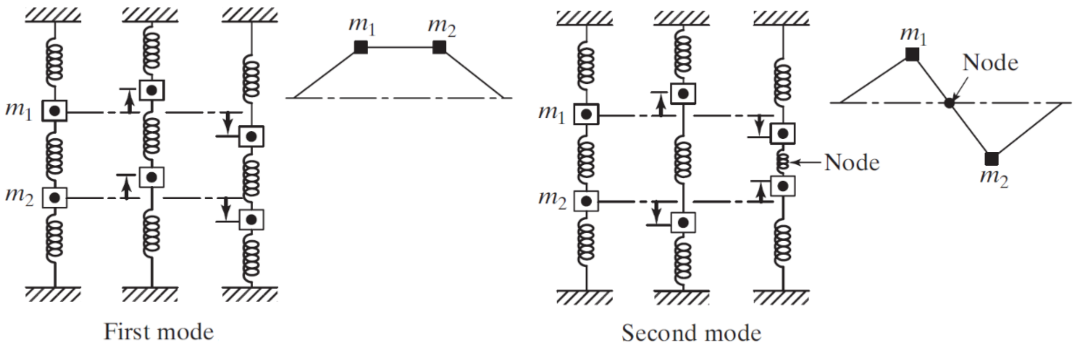

Figure 16. Modes of vibration [41]

The first natural frequency corresponds to the first mode of vibration $X_2/X_1=1$, characterized by in-phase motion of the masses. In this case, both masses exhibit identical amplitudes, maintaining the length of the middle spring constant. The second natural frequency corresponds to the first mode of vibration $X_2/X_1=-1$, characterized by out-of-phase motion of the masses. In this case, masses have equal-magnitude displacements in opposite directions. Also, stationary point, called node, forms between the masses, thus giving the appearance of two independent subsystems with a single mass each.

The analysis of free vibrations in two DOF systems reveals their fundamental frequencies and modes, which are critical for understanding their dynamic responses. The following sections will explore the effects of external excitation forces, focusing on forced vibrations and their influence on system behaviour.

3.3.2. Forced vibration

For two DOF systems subjected to harmonic excitation, the equations of motion are influenced by the frequencies of the excitation forces. For the system in Figure 10, exposed to forced vibration, equations in (57) can be expressed in expanded matrix form as:

$$\begin{bmatrix} m_1 & 0 \\ 0 & m_2 \end{bmatrix}\begin{Bmatrix} \ddot{x}_1 \\ \ddot{x}_2 \end{Bmatrix}+\begin{bmatrix} c_1+c_2 & -c_2 \\ -c_2 & c_2+c_3 \end{bmatrix}\begin{Bmatrix} \dot{x}_1 \\ \dot{x}_2 \end{Bmatrix}+\begin{bmatrix} k_1+k_2 & -k_2 \\ -k_2 & k_2+k_3 \end{bmatrix}\begin{Bmatrix} x_1 \\ x_2 \end{Bmatrix}=\begin{Bmatrix} f_1(t) \\ f_2(t) \end{Bmatrix} \tag{69}$$

Here, harmonic excitation forces are expressed as:

$$\begin{aligned} f_1(t) &= f_{c1}\cos\Omega t + f_{s1}\sin\Omega t \\ f_2(t) &= f_{c2}\cos\Omega t + f_{s2}\sin\Omega t \end{aligned} \tag{70}$$

Where $F_{c1,2}$ and $F_{s1,2}$ represent the sine and cosine components of the vector of external excitation forces acting on each mass. For the general case of harmonic excitation, expression (69) can be written in concise matrix form as:

$$\mathbf{M}\begin{Bmatrix} \ddot{x}_1 \\ \ddot{x}_2 \end{Bmatrix}+\mathbf{C}\begin{Bmatrix} \dot{x}_1 \\ \dot{x}_2 \end{Bmatrix}+\mathbf{K}\begin{Bmatrix} x_1 \\ x_2 \end{Bmatrix}=\begin{Bmatrix} f_{c1} \\ f_{c2} \end{Bmatrix}\cos\Omega t+\begin{Bmatrix} f_{s1} \\ f_{s2} \end{Bmatrix}\sin\Omega t \tag{71}$$

or in symbolic form, respectively, as:

$$\mathbf{M}\ddot{\mathbf{x}}+\mathbf{C}\dot{\mathbf{x}}+\mathbf{K}\mathbf{x}=\mathbf{f}_c\cos\Omega t+\mathbf{f}_s\sin\Omega t \tag{72}$$

This symbolic representation of the equation of motion generally applies to vibration system with *n* DOF, subjected to harmonic excitation with circular frequency Ω. The particular solutions to the equation of motion, i.e. the displacements of individual masses, are assumed as follows:

$$\begin{aligned} x_1(t) &= X_{c1}\cos\Omega t + X_{s1}\sin\Omega t \\ x_2(t) &= X_{c2}\cos\Omega t + X_{s2}\sin\Omega t \end{aligned} \tag{73}$$

By determining the velocity and acceleration from equations (73) and substituting them into equation (74), a system of linear equations is obtained, which can then be solved to calculate the displacement amplitudes. This is expressed in concise matrix form:

$$\begin{bmatrix} \mathbf{K}-\Omega^2\mathbf{M} & \Omega\mathbf{C} \\ -\Omega\mathbf{C} & \mathbf{K}-\Omega^2\mathbf{M} \end{bmatrix} \begin{Bmatrix} \mathbf{x}_{c1} \\ \mathbf{x}_{s1} \end{Bmatrix} = \begin{Bmatrix} \mathbf{f}_c \\ \mathbf{f}_s \end{Bmatrix} \tag{74}$$

Or in expanded matrix form as:

$$\begin{bmatrix} k_1-\Omega^2 m_1 & k_2 & \Omega c_1 & \Omega c_2 \\ k_2 & k_3-\Omega^2 m_2 & \Omega c_2 & \Omega c_3 \\ -\Omega c_1 & -\Omega c_2 & k_1-\Omega^2 m_1 & k_2 \\ -\Omega c_2 & -\Omega c_3 & k_2 & k_3-\Omega^2 m_2 \end{bmatrix} \begin{Bmatrix} x_{c1} \\ x_{c2} \\ x_{s1} \\ x_{s2} \end{Bmatrix} = \begin{Bmatrix} f_{c1} \\ f_{c2} \\ f_{s1} \\ f_{s2} \end{Bmatrix} \tag{75}$$

To summarize, the equations of motion for two DOF systems subjected to harmonic excitation are governed by the excitation frequencies, which influence the system's response. The following section examines systems with n DOF, where the complex interactions between masses and springs are further analysed.

3.3.3. Systems with *n* degrees-of-freedom

System with n DOF generalize the analysis of two DOF systems to more complex scenarios, where the equations of motion become more intricate. However, the process for determining natural frequencies and responses to external forces remains similar, as demonstrated for the vibrating system shown in Figure 17.

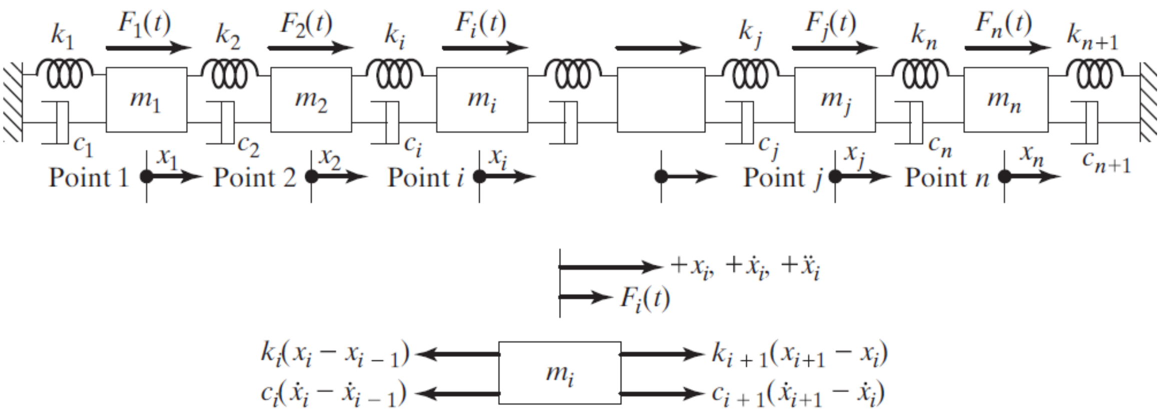

Figure 17. Longitudinal vibration system with finite number of DOF [41]

System with n DOF is characterized by n independent coordinates, thus exhibiting n natural frequencies. By applying Newton's second law, the corresponding set of n equations of motion:

$$\begin{gathered}
m_1\ddot{x}_1+\left(c_1+c_2\right)\dot{x}_1-c_2\dot{x}_2+\left(k_1+k_2\right)x_1-k_2x_2=f_1\left(t\right),\\
m_2\ddot{x}_2-c_2\dot{x}_1+\left(c_2+c_3\right)\dot{x}_2-c_3\dot{x}_3-k_2x_1+\left(k_2+k_3\right)x_2-k_3x_3=f_2\left(t\right),\\
\vdots\\
m_n\ddot{x}_n-c_n\dot{x}_{n-1}+\left(c_n+c_{n+1}\right)\dot{x}_n-k_nx_{n-1}+\left(k_n+k_{n+1}\right)x_n=f_n\left(t\right).
\end{gathered}\tag{76}$$

Equations in the expression (80) can be rewritten in matrix from as in (62), with each matrix defined by:

$$\mathbf{M}=\begin{bmatrix} m_1 & 0 & 0 & \cdots & 0\\ 0 & m_2 & 0 & \cdots & 0\\ 0 & 0 & m_3 & \cdots & 0\\ \vdots & & & & \vdots\\ 0 & 0 & 0 & 0 & m_n \end{bmatrix},\tag{77}$$

$$\mathbf{C}=\begin{bmatrix} \left(c_1+c_2\right) & -c_2 & 0 & \cdots & 0\\ -c_2 & \left(c_2+c_3\right) & -c_3 & \cdots & 0\\ 0 & -c_3 & \left(c_3+c_4\right) & \cdots & 0\\ \vdots & & & & \vdots\\ 0 & 0 & 0 & -c_n & \left(c_n+c_{n+1}\right) \end{bmatrix},\tag{78}$$

$$\mathbf{K}=\begin{bmatrix} \left(k_1+k_2\right) & -k_2 & 0 & \cdots & 0\\ -k_2 & \left(k_2+k_3\right) & -k_3 & \cdots & 0\\ 0 & -k_3 & \left(k_3+k_4\right) & \cdots & 0\\ \vdots & & & & \vdots\\ 0 & 0 & 0 & -k_n & \left(k_n+k_{n+1}\right) \end{bmatrix}.\tag{79}$$

The displacement, velocity, acceleration, and force vectors, respectively, are expressed by:

$$\mathbf{x}=\begin{Bmatrix} x_1\left(t\right)\\ x_2\left(t\right)\\ \vdots\\ x_{n(t)} \end{Bmatrix},\quad \dot{\mathbf{x}}=\begin{Bmatrix} \dot{x}_1\left(t\right)\\ \dot{x}_2\left(t\right)\\ \vdots\\ \dot{x}_{n(t)} \end{Bmatrix},\quad \ddot{\mathbf{x}}=\begin{Bmatrix} \ddot{x}_1\left(t\right)\\ \ddot{x}_2\left(t\right)\\ \vdots\\ \ddot{x}_{n(t)} \end{Bmatrix},\quad \mathbf{f}=\begin{Bmatrix} f_1\left(t\right)\\ f_2\left(t\right)\\ \vdots\\ f_{n(t)} \end{Bmatrix}\tag{80}$$

It is worth noting that the equations of motion for systems with n DOF can be alternatively expressed in two different ways. First, by using the influence coefficients, where each matrix represents a specific set of coefficients. Second, by employing generalized displacements, which represent linear or angular displacements from equilibrium. In accordance with the principles of analytical mechanics, when external forces are applied, the system configuration adjusts, with each change in the generalized virtual displacements corresponding to the virtual work done by the associated generalized force. Owing to the fact that influence coefficients and generalized displacements are fundamental concepts, they will not be further explored in this research.

Investigation of systems with n DOF provides insights into complex mechanical vibrations, where multiple masses mutually interact under various conditions. This chapter has covered the fundamental principles of vibration analysis of systems with two and more DOF, emphasizing both free and forced vibrations. The following chapter will explore torsional vibrations, examining systems from single to n DOF, with the example for the ship propulsion system as the torsional vibration system with n DOF.

3.4. Torsional vibrations

In this section, the analysis of torsional vibration systems with single, two and n DOF is presented. The analysis follows same procedure used in the analysis of longitudinal vibrations, with corresponding modifications to certain terms, such as:

- The masses m are to be replaced with mass moments of inertia J around the longitudinal axis of rotation.
- Damping, within dampers, is to be substituted with torsional damping c_t.
- The spring stiffness k is to be replaced with torsional stiffness k_t.
- The components of excitation forces F are to be replaced with components of excitation moments M_t.
- The components of linear displacements x are to be replaced with components of angular displacements θ.

Symbols for the natural frequencies of free undamped vibrations ω_n and for the angular frequency of external excitation moments Ω , as well as their ratio η, remain unchanged. The next section will focus on undamped and damped torsional vibration systems with single DOF.

3.4.1. Single degree-of-freedom Systems

Torsional vibration system with a single DOF, shown in Figure 18, is represented by a rigid disk vibrating around its longitudinal axis. The disk is fixed at one end of the elastic shaft, while the other end of the shaft is clamped.

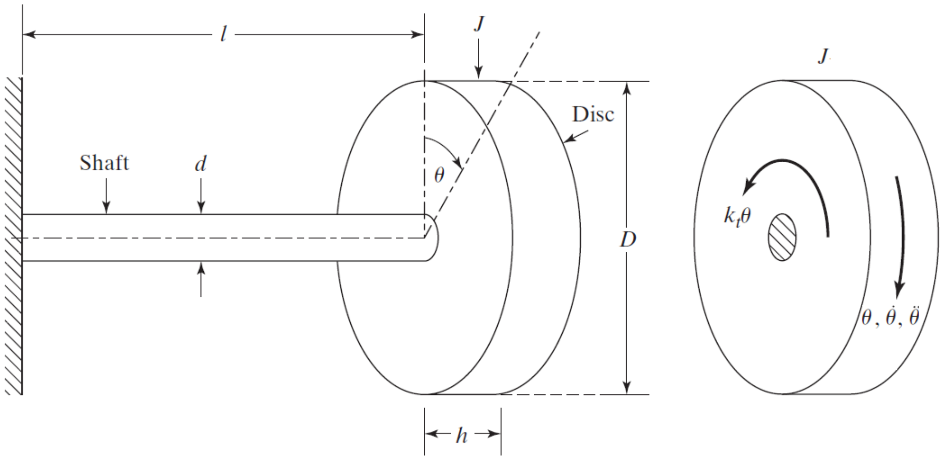

Figure 18. Undamped single DOF torsional vibration system

When considering free vibration of the undamped torsional system, the equation of the angular motion of the disc about its axis can be derived by using Newton's second law:

$$J_0\ddot{\theta} + k_t\theta = 0 \tag{81}$$

For which the general solution can be expressed as:

$$\theta(t) = C_1 \cos \omega_n t + C_2 \sin \omega_n t \tag{82}$$

The expressions presented for linear vibrations with viscous damping can be applied for the case of viscously damped torsional vibrations, so the equation of motion can be stated as:

$$J_0\ddot{\theta} + c_t\dot{\theta} + k_t\theta = 0 \tag{83}$$

This equation applies to a single DOF torsional system with viscous damping shown in Figure 19, for which the solution is identical to that of linear vibrations, so it is not presented here.

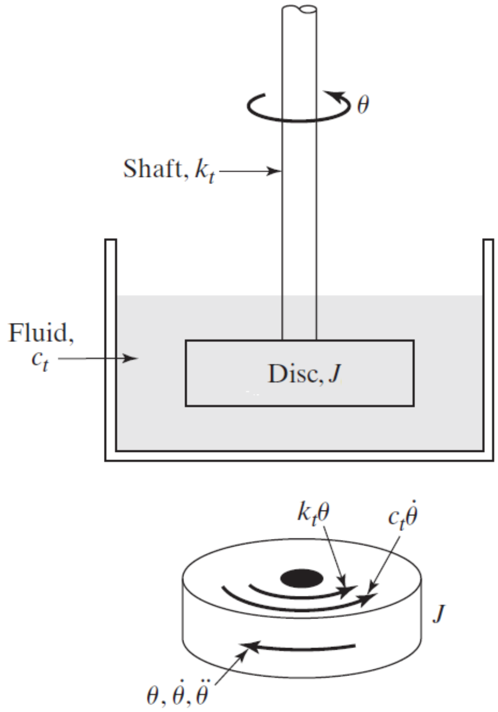

Figure 19. Single DOF torsional vibration system with viscous damper [41]

The frequency of damped vibration is identical to the expression (41), while the damping factor is expressed as:

$$\zeta = \frac{c_t}{c_{tc}} = \frac{c_t}{2J_0\omega} = \frac{c_t}{2\sqrt{k_t J_0}} \tag{84}$$

By introducing the harmonic excitation torque into the system:

$$M_t(t) = M \sin \Omega t \tag{85}$$

the equation of motion can be expressed as:

$$J_0\ddot{\theta} + c_t\dot{\theta} + k_t\theta = M_t(t) \tag{86}$$

For torsional system analogous equations apply as for the longitudinal vibration system, so it is unnecessary to derive them separately. Instead, only essential calculation expressions for the response in the most general case, where Θ denotes amplitude and for phase angle γ expression (54) applies, are presented:

$$\theta(t) = \theta_h(t) + \theta_p(t) \tag{87}$$

$$\theta_h(t) = e^{-\zeta\omega_n t}\left(\theta_0 \cos\omega_{nc}t + \frac{\dot{\theta}_0}{\omega_{nc}}\sin\omega_{nc}t\right) \tag{88}$$

$$\theta_p(t) = \Theta \frac{1}{\sqrt{\left(1-\eta^2\right)^2 + \left(2\zeta\eta\right)^2}} \sin\left(\Omega t - \gamma\right) \tag{89}$$

The equations and principles outlined demonstrate the parallels between torsional and longitudinal vibration systems, allowing for the application of analogous methods to analyse their behaviour under various conditions. In the next section, the focus is on undamped torsional systems with two degrees of freedom.

3.4.2. Two degrees-of-freedom

Undamped torsional system with two degrees of freedom is shown in Figure 20. To determine equations of motion analogous approach is applied as for the longitudinal vibration. So, for the general case the response calculation expressions for torsional system are as follows:

$$\begin{aligned} J_1\ddot{\theta}_1 + \left(k_{t,1} + k_{t,2}\right)\theta_1 - k_{t,2}\theta_2 &= M_{t,1}(t), \\ J_2\ddot{\theta}_2 + \left(k_{t,2} + k_{t,3}\right)\theta_2 - k_{t,2}\theta_1 &= M_{t,2}(t). \end{aligned} \tag{90}$$

Presented system exhibits two natural frequencies, determined as in (66) with certain term modifications. The vibration frequency depends on the initial conditions.

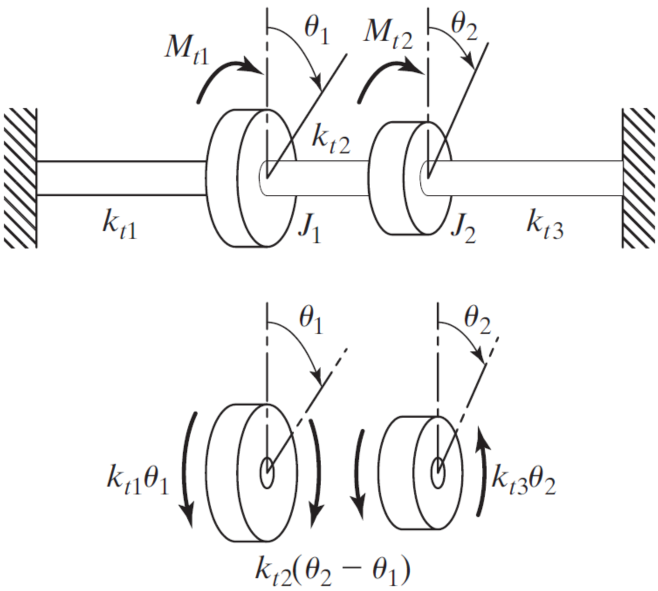

Figure 20. Two-degree-of freedom torsional vibration system [41]

As in the previous section, the parallel between torsional and longitudinal vibration systems is demonstrated, allowing for the application of analogous methods to analyse their behaviour. The following section will present transition to the analysis of systems with *n* degrees of freedom. using the ship propulsion system as a representative example to illustrate the modelling and analytical techniques involved.

3.4.3. Systems with *n* degrees of freedom

A system with *n* concentrated masses has *n* degrees of freedom, thus exhibits *n* natural frequencies. Its torsional vibrations can therefore be characterized by the *n* independent general displacements, specifically the angular displacements.

For such systems, the analysis involves determining the natural frequencies, associated vibration modes, and the dynamic response under external excitations. This provides critical insights into the behaviour of torsional vibrations and the system's stability, which can be analysed similarly as the system with two degrees of freedom. By applying Newton's second law, the resulting set of *n* equations of motion is as follows:

$$\begin{gathered} J_1\ddot{\theta}_1+\left(c_{t,1}+c_{t,2}\right)\dot{\theta}_1-c_{t,2}\dot{\theta}_2+\left(k_{t,1}+k_{t,2}\right)\theta_1-k_{t,2}\theta_2=M_{t,1}\left(t\right), \\ J_2\ddot{\theta}_2-c_{t,2}\dot{\theta}_1+\left(c_{t,2}+c_{t,3}\right)\dot{\theta}_2-c_{t,3}\dot{\theta}_3-k_{t,2}\theta_1+\left(k_{t,2}+k_{t,3}\right)\theta_2-k_{t,3}\theta_3=M_{t,2}\left(t\right), \\ \vdots \\ J_n\ddot{\theta}_n-c_{t,n}\dot{\theta}_{n-1}+\left(c_{t,n}+c_{t,n+1}\right)\dot{\theta}_n-k_{t,n}\theta_{n-1}+\left(k_{t,n}+k_{t,n+1}\right)\theta_n=M_{t,n}\left(t\right). \end{gathered} \tag{91}$$

In systems with *n* degrees of freedom, there are *n* complementary equations of as in (89), that can be rewritten as in (56), with certain term modifications:

$$\mathbf{J}\ddot{\boldsymbol{\theta}}\left(t\right)+\mathbf{C_t}\dot{\boldsymbol{\theta}}\left(t\right)+\mathbf{K}\boldsymbol{\theta}\left(t\right)=\mathbf{m_t}\left(t\right) \tag{92}$$

For such systems, the analysis involves determining the natural frequencies, associated vibration modes, and the dynamic response under external excitations. This provides critical insights into the behaviour of torsional vibrations and the system's stability.

Since the same approach applies for torsional vibration system with *n* degrees of freedom as presented in case of longitudinal vibrations, the ship propulsion system will serve as the example. The next section focuses on outlining physical model and the mathematical modelling techniques used to characterize such a complex system.

3.4.3.1. Ship propulsion system as torsional vibration system with n degrees of freedom

When analysing any physical structure, the initial step is to represent it with mathematical model that accurately reflects its dynamic behaviour. Vibration systems are commonly described as discrete systems, typically by the lumped parameter modelling approach. This approach simplifies transformation of physical model into mathematical model suitable for TVA. Representative model should have sufficient DOF to determine the modes that significantly respond to the exciting force or motion. Ship propulsion system is effectively represented as torsional vibration system with *n* DOF, typically described with one DOF per node, the angular displacement respectively. An exemplary propulsion system, shown in Figure 21, includes six-cylinder Diesel engine directly connected to the propeller via intermediate and propeller shaft.

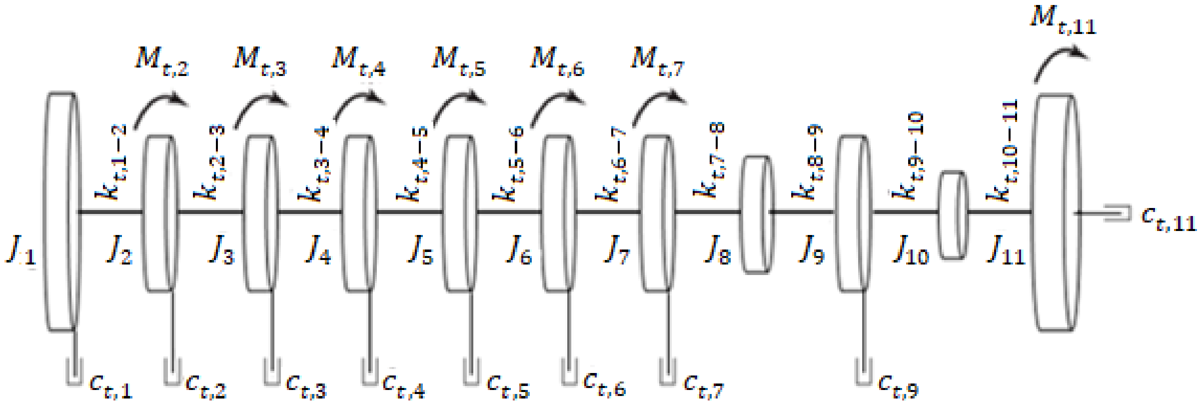

Figure 21. Ship propulsion system as torsional system with n degrees of freedom

Represented lumped mass model consists concentrated masses, massless shafts, concentrated dampers and periodic excitation forces. Concentrated masses are represented with rotating discs and described by mass moments of inertia about the axis of rotation. Shafts represent the stiffness and, in some cases, relative damping of individual system components. Concentrated dampers describe absolute damping at specific masses, while periodic excitation forces represent external loads from the engine and propeller. In given example, concentrated masses refer to designated propulsion system components as follows:

- tuning wheel (J_1),
- cylinders 1–6 ($J_{2\text{-}7}$),
- camshaft drive(J_8),
- turning wheel (J_9),
- flange (J_{10}),
- propeller (J_{11}).

Thereby, the exemplary torsional vibration system consists of n=*11* inertial elements, each defined with single angular displacement, so the system has *n* degrees of freedom. Its dynamic behaviour is described with *n* linear differential equations as expressed in (91), that can be compactly formulated as in (92), but for sake of clarity matrices are presented in expanded form:

$$\mathbf{J} = \begin{bmatrix} J_1 & 0 & 0 & \cdots & 0 \\ 0 & J_2 & 0 & \cdots & 0 \\ 0 & 0 & J_3 & \cdots & 0 \\ \vdots & & & & \vdots \\ 0 & 0 & 0 & 0 & J_{11} \end{bmatrix}, \tag{93}$$

The inertia matrix in the presented case is diagonal matrix representing rotational masses of the system as equivalent mass moments of inertia. It accounts for the distribution of shaft masses, which are divided and concentrated at their respective endpoints.

$$\mathbf{C_t} = \begin{bmatrix} c_{t,1} & 0 & 0 & \cdots & 0 \\ 0 & c_{t,2} & 0 & \cdots & 0 \\ 0 & 0 & c_{t,3} & \cdots & 0 \\ \vdots & & & & \vdots \\ 0 & 0 & 0 & 0 & c_{t,11} \end{bmatrix}, \tag{94}$$

The damping matrix is diagonal matrix representing all damping within the system. In the observed case, dissipated energy is permanently taken away through engine foundation or ship construction.

$$\mathbf{K_t} = \begin{bmatrix} k_{t,1} & -k_{t,2} & 0 & 0 & \cdots & 0 \\ -k_{t,2} & \left(k_{t,2}+k_{t,3}\right) & -k_{t,3} & 0 & \cdots & 0 \\ 0 & -k_{t,3} & \left(k_{t,3}+k_{t,4}\right) & -k_{t,4} & 0 & 0 \\ \vdots & & & & & \vdots \\ 0 & 0 & 0 & -k_{t,9} & \left(k_{t,9}+k_{t,10}\right) & -k_{t,10} \\ 0 & 0 & 0 & \cdots & -k_{t,10} & k_{t,10} \end{bmatrix} \tag{95}$$

The stiffness matrix is tridiagonal matrix and it represents the elasticity of the system, contained within the shaft line. The angular displacement, velocity, acceleration, and excitation torque vectors, are expressed as:

$$\boldsymbol{\theta} = \begin{Bmatrix} \theta_1(t) \\ \theta_2(t) \\ \vdots \\ \theta_{11}(t) \end{Bmatrix}, \quad \dot{\boldsymbol{\theta}} = \begin{Bmatrix} \dot{\theta}_1(t) \\ \dot{\theta}_2(t) \\ \vdots \\ \dot{\theta}_{11}(t) \end{Bmatrix}, \quad \ddot{\boldsymbol{\theta}} = \begin{Bmatrix} \ddot{\theta}_1(t) \\ \ddot{\theta}_2(t) \\ \vdots \\ \ddot{\theta}_{11}(t) \end{Bmatrix}, \quad \mathbf{m_t} = \begin{Bmatrix} 0 \\ m_{t,2}(t) \\ \vdots \\ m_{t,11}(t) \end{Bmatrix} \tag{96}$$

The given example represents appropriate TVA physical and analytical model, with external loads represented as applied torques generated in engine cylinders and the propeller, which result with angular displacements within the shaft line sections. As torsional vibrations propagate along the shaft line, they create dynamic interactions between interconnected components, leading to variations in the angular displacement amplitudes of the masses. These interactions result in additional vibratory stress within the shaft line, emphasizing the necessity of torsional vibration calculation and analysis to ensure compliance with the classification rules and regulations.

This chapter provides a fundamental overview of vibration analysis, covering longitudinal and torsional vibration systems with single, two, and multiple degrees of freedom, using the real ship propulsion system as the example. It highlights the importance of systematically organizing key system parameters to accurately characterize dynamic behaviour. The practical application of theoretical principles is demonstrated, laying the foundation for further exploration of modelling methodologies. The next chapter will expand on this by presenting a framework for modelling torsional vibration systems, discussing lumped-mass modelling, data preparation, and various modelling techniques, including analytical, numerical, experimental, and simulation-based methods.

4. MATERIAL AND METHODS FOR TORSIONAL VIBRATION ANALYSIS

In Diesel engine propulsion systems, two primary types of vibrations are significant: vibrations transmitted by the engine to its foundation and torsional vibrations within the shaft line. In the early design phase, it is essential to assess the shaft line's steady-state torsional vibration response to variable torque excitations from the engine and propeller. This response depends on the system properties and excitation, and can be analysed manually or with computer software. The former option (manual analysis) is no more in use at all. The latter option is faster and more efficient for complex structures and therefore commonly applied.

4.1. Modelling methodology for TVA

In general, modelling methodology includes definition of the system, assumption formulation, derivation of mathematical models, and result validation. The two most important parameters in any vibration system are its mass and its stiffness. A common modelling approach it to lump all the different contributions to mass and stiffness together, called the lumped parameter modelling approach. This approach simplifies representation of the system by concentrating components at single points, which enables the description of its behaviour with idealized mathematical models.

As propulsion system components primarily perform rotational motion, the system as whole can be classified as rotating machinery, thus represented as torsional lumped mass model. Propulsion system is modelled as mechanical system that consists of concentrated masses interconnected by torsional springs with constant stiffness, with absolute viscous damping on certain masses and relative damping between two adjacent masses. Forces in the engine cylinders and forces on the ship propeller excite torsional vibrations in the system model. It is common that entire mechanical system, including the engine, is assumed to be detached from the variable loads transmitted by the ship's structure [47].

The general arrangement drawing prepared by the shipyard provides essential information for developing the equivalent lumped-mass model, also known as a mass-elastic model, of the propulsion system. To demonstrate TVA modelling methodology, the propulsion system's shaft line arrangement is presented in Figure 22. The propulsion system under consideration consists of 7 cylinder two-stroke slow-speed marine Diesel engine directly connected via intermediate and propeller shaft to the solid 4-bladed propeller [21].

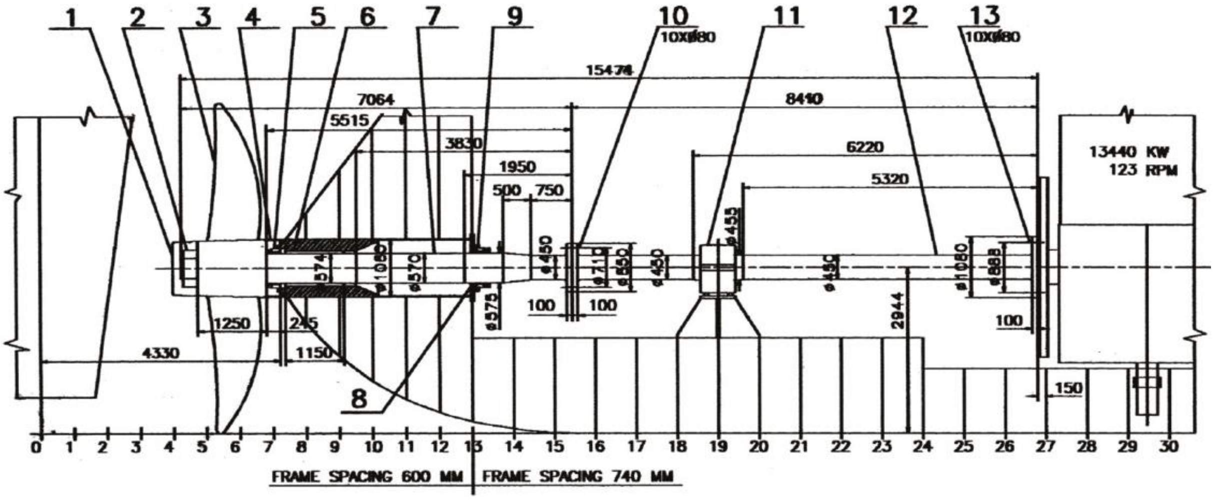

Figure 22. Propulsion system shaft line arrangement [21]

In the shaft line general arrangement drawing, the propeller is positioned on the left hand side and the propulsion engine on the right. However, in the equivalent torsional lumped-mass model, shown in Figure 23, elements are arranged reversely compared to the general arrangement drawing. The equivalent mass-elastic model is created using GTORSI program, developed by MAN Energy Solutions, Copenhagen [79]. In general, torsional lumped-mass models provide the effective means for accurate analysis of the shaft line's dynamic behaviour under variable excitations. Model is comprised of different elements that represent inertia, stiffness, damping and excitation within the system.

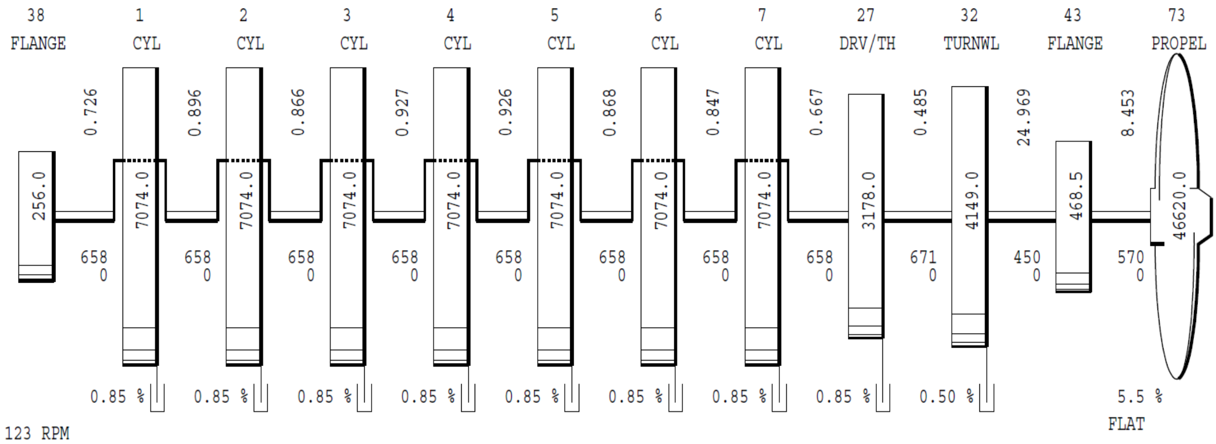

Figure 23. Equivalent torsional lumped mass for torsional vibration calculation

The exemplary model is comprised of twelve inertial elements, with associated damping, and eleven elastic shafts. Additionally, this modelling approach encompasses all numerical values of the system's properties. Ensuring the reliability of these models requires meticulous preparation of input data, such as dimensions, material properties, and operating conditions. The following section focuses on the process of data preparation required to accurately build and describe models for TVA.

4.2. Data preparation

The accuracy of any calculation is fundamentally dependent upon the correctness of input data. Ensuring both verified and validated input data is a prerequisite for obtaining of reliable results. Data preparation for TVC involves gathering precise details of inertial moments of actual masses, the stiffness and damping characteristics of shaft line components, along with excitation forces and moments generated by the propulsion engine and the propeller. While mass moments of inertia and stiffness can be unambiguously defined, the same is not the case with damping and engine excitation [17].

4.2.1. Mass moments of inertia

For rotating machinery, inertial elements are commonly represented by discs, modelled as rigid bodies defined by their mass moment of inertia about the longitudinal axis. This physical quantity refers to resistance of rigid body to changes in its angular velocity or rotational direction. It is equal to the sum (integral) of the product of the masses *dm* of the individual particles (elements of masses) of a body and the square of their distances (radii *r*) from the axis, expressed as:

$$J_0 = \int_m r^2 \mathrm{d}m \tag{97}$$

For homogeneous solid cylinder or disc with mass *m* and diameter *D*, mass moment of inertia is defined as:

$$J_0 = \frac{1}{8} m D^2 \tag{98}$$

A comprehensive understanding of the mass moment of inertia is essential for accurately modelling the dynamic behaviour of rotating components. Following the characterization of inertial properties, the torsional stiffness of the propulsion shaft must be considered as a critical parameter influencing the system's vibrational response.

4.2.2. Stiffness

In the TVA model of a propulsion system, the massless elastic shaft represents the system's stiffness and, if applicable, its relative damping. The shafts are modelled as straight torsional springs, actually straight elastic rods with a circular cross-section. These shafts exhibit elastic behaviour by twisting along their length when subjected to torque and follow a linear relationship between the applied torque and angular displacement.

The torsional rigidity of the shaft, denoted as k_t is commonly expressed by the formula:

$$k_t = \frac{G\,I_p}{l} \tag{99}$$

where

G - shear modulus of the material,

l - length of the shaft,

$I_p = \dfrac{\pi d^4}{32}$ - polar moment of inertia of the shaft's circular cross-section. (100)

The torsional rigidity of the shaft provides a fundamental measure of its resistance to angular deformation under applied torque, directly affecting the vibrational behaviour of the propulsion system. In addition to torsional stiffness, damping mechanisms are to be evaluated, because they govern dissipation of vibrational energy within the propulsion system.

4.2.3. Damping

Damping refers to the energy dissipation effect that reduces the vibratory amplitude of any oscillating system. Although, the total damping value has negligible impact on the stress level outside this range, the damping effect must be considered within the approximate range of the main resonance [29]. Estimation of torsional damping imposes challenging task for marine shafting designers, as the accuracy of the damping data used in calculations is required to be validated later through results by onboard measurements [13]. Main damping types for TVC of the marine shaft line include viscous, fluid, internal and structural damping [17].

Viscous damping originates from energy dissipation that occurs in the lubricating fluid between system components in relative motion. The damping force is directly proportional to the relative velocity of these components. It can be categorized as absolute, occurring between moving component and stationary environment, or relative, occurring between two components in relative motion. Fluid damping is caused by dynamic interaction of the propeller and surrounding water. Internal or material damping results from the dissipation of mechanical energy within the material of the shaft line, material of flexible couplings and torsional vibration dampers (TVDs). Structural damping is caused by relative friction between contacting surfaces of shaft line components.

Simplified analytical approach is considered applicable only with linear viscous damping, so other damping models are effectively remodelled into equivalent viscous damping [13]. Typically, fluid damping is represented as absolute viscous damping, while relative viscous damping models internal and structural damping. As a result, damping can be defined in various forms and as such entered into modern TVC programs. This issue is thoroughly identified and presented in [17], providing expressions for three important TVC programs, of which two are part of this research. The GTORSI program, developed by MAN Diesel & Turbo in Copenhagen, includes damping definitions as follows [79]:

- absolute torsional damping expressed as percentage of critical damping ρ_{θ},
- physical damping (between the actual and previous inertia) b_{θ},
- percentage of modal damping with respect to stiffness ρ_{inner},
- resulting physical damping b.

The SimulationX program, developed by ITI GmbH in Dresden [80], is designed for the physical simulation of technical systems. In this program, damping is defined as linear viscous damping b, and can be expressed using various approaches as outlined below:

- viscous damping torque T_D,
- estimation damping approach with factor B,
- relative damping ψ,
- Lehr’s damping factor D.

It is important to note that the engine damping data in TVC is typically obtained from the engine manufacturer. However, if the damping data for specific engine is unavailable and cannot be obtained from the manufacturer, default values can be used as given in [13].

During propulsion system design phase, selection of shaft line material is cost-effective and favourable option to initially mitigate torsional vibrations. Other methods include application of tuning and turning wheels, installed on each side of the engine, or torsional vibration damper (TVD), with steel spring type dampers being commonly applied in direct propulsion system configurations.

Accurate estimation of damping effects is essential in marine shaft line design, requiring precise estimation methods and careful material selection to effectively mitigate torsional vibrations. The following section focuses on the unique phenomenon of propeller damping, which arises from the interaction between the propeller's vibratory motion and the surrounding water.

4.2.3.1. Propeller damping

Rotating marine propeller entrains certain amount of water. Thereby, as it vibrates, the water around the blades also participates in the vibratory motion. Because of this, portion of energy in the shaft line is dissipated in the water, thus reducing the torsional vibration amplitudes of the propulsion system. The damping effects of the propeller and entrained water is collectively referred to as propeller damping, which can be modelled using the concept of equivalent absolute viscous damping. According to [13], determination of propeller damping remains ambiguous step, as no single definitive solution is available. Therefore, it is typically estimated using various formulas and recommendations, such as Archer’s, Frahm’s, Ker Wilson’s, and Dien-Schwanecke’s formulas, as well as the guidelines provided by MAN Diesel & Turbo. The latter approach, adopted in this research, follows the engine manufacturer's recommendation to set propeller damping at 5% of the critical damping.

Propeller damping significantly contributes to the reduction of torsional vibration amplitudes by dissipating energy into the surrounding water, so it is critical factor in TVA. With the damping characteristics defined, the next section examines excitation forces as primary drivers of torsional vibrations in ship propulsion systems.

4.2.4 Excitation

Excitation sources impose disturbance that initiates and sustains vibrations, which in ship propulsion systems are dominantly generated by the propulsion engine and the propeller. Engine excitations vary periodically during operation cycle of the engine and induce high variable torque at the crankshaft. They thus contribute as main excitation factor in stress amplitudes calculations. Propeller excitation originate from the non-homogeneous water flow across the entire surface of the propeller's interaction area. This non-uniformity arises from uneven inflow in the propeller operating region, often pronounced in ships with a single-screw propeller, potentially influencing the magnitude of resonant stresses.

Engine excitations can be categorized as primary and secondary [81]. The primary excitations involve forces and moments originating from the combustion pressure and the inertia forces of the rotating and reciprocating masses [10]. Variable combustion gas pressure acts over the piston, thereby generating variable combustion gas forces and inertia forces in the crankshaft and connecting rod mechanism. Both forces consist of radial and tangential components, with the tangential components producing the cylinder torque [31]. As stated in [44], the constant part of the tangential force adds to ship propulsion, while the variable part induces torsional vibrations in the shaft line.

Secondary excitations result from the forced vibratory response within ship sub-structures, whose vibration characteristics are largely independent of the rest of the ship's structure [81]. Ship sub-structures can reach or approach resonance conditions, thus can significantly amplify dynamic reaction forces at their interface with the rest of the ship. Primary excitations can be predetermined and as such stated along with engine specification. However, this is not the case with secondary excitations, so they are calculated during ship propulsion system design phase [10]. Secondary excitations will not be further discussed, as they are not evaluated within this research.

According to [42], excitations in internal combustion engines may be systematically presented using flow diagram in Figure 24. As stated in [44], total engine excitation arises from the combined effect of all cylinders, with the phase angle between them determined by the firing order. The firing order refers to specific sequence in which the fuel is ignited within the engine's cylinders. According to [82], firing order and firing conditions can influence the intensity of torsional vibratory stresses in the marine shaft line.

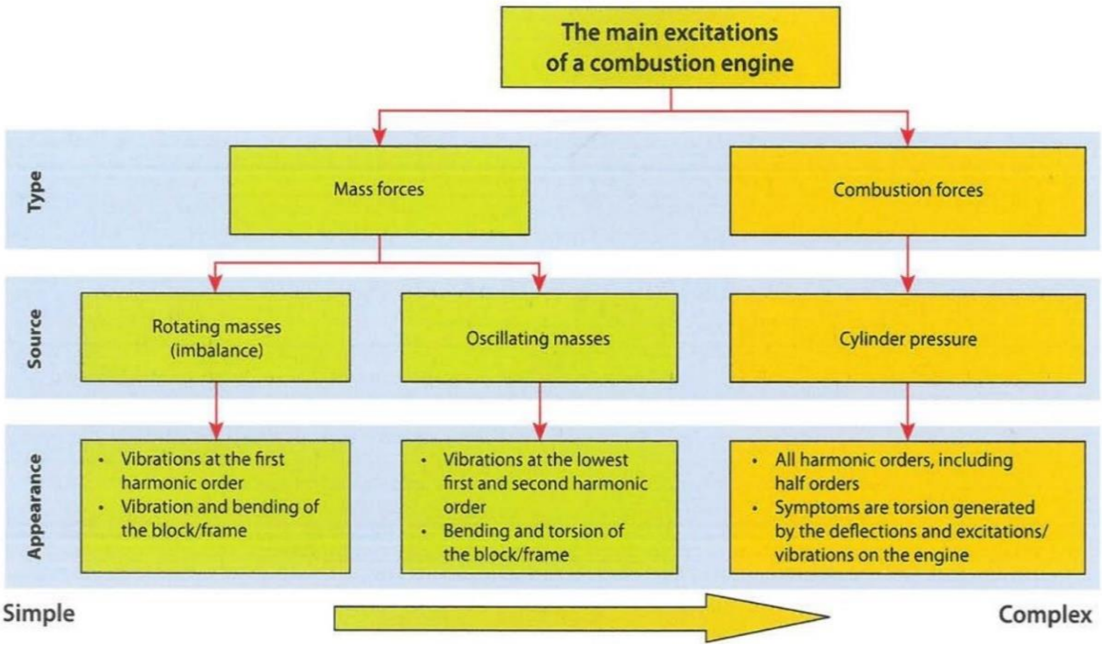

Figure 24. Main excitations of internal combustion engine [42]

Reciprocating internal combustion engines operate under normal and misfiring conditions. Under normal firing conditions, combustion occurs in all cylinders, so each cylinder contributes to the total engine power output. In misfiring condition, combustion process does not occur in one of engine's cylinders, thereby it is not contributing to the total engine power output. The remaining active cylinders operate under increased load to compensate for the reduced power output, resulting in higher cylinder torque and, consequently, increased excitation moments.

The excitation torque is comprised of individual harmonic excitations, each characterized by distinct frequency which is the multiple of the engine's rotational frequency [10]. This multiple is referred as order, with the first-order excitation corresponding to the fundamental frequency, the second-order excitation to twice the fundamental frequency, and so forth. Similarly, the system's dynamic response is composed of multiple individual harmonic responses, each associated with specific resonance condition. According to [44], the main resonance, often termed as system's main critical speed, occurs when the system vibrates in phase with the n-*th* order excitation, where *n* equals the number of cylinders for two-stroke engines, and *n* equals half the number of cylinders for four-stroke engine (one fuel oil injection in two crankshaft revolutions).

Excitation moments caused by forces in the engine cylinders, as well as those acting on the ship's propeller, are typically periodic but non-harmonic functions. Using trigonometric approximations with Fourier coefficients, they are decomposed into their harmonic components for excitation frequencies Ω, 2Ω, 3Ω, etc. In practice, sufficiently accurate calculation is achieved with 24 components. Data on excitation in Diesel engine cylinders is provided by the engine manufacturer in one of the following forms:

- Measured cylinder pressure as a function of the crank angle, within a range of ±180° for two-stroke engines or ±360° for four-stroke engines.
- Tangential forces on the crankpin as a function of the crank angle, derived from cylinder gas pressures.
- Tangential forces on the crankpin expressed via Fourier coefficients, namely the trigonometric approximation coefficients for harmonics 1, 2, 3, … for two-stroke engines, or 0.5, 1.0, 1.5, 2.0, 2.5, … for four-stroke engines).

In this research, engine excitation data is prepared using Microsoft Excel workbooks implementing programs written in Visual Basic for Applications (VBA) code. The theoretical background for both programs, including kinematic and dynamic equations of crankshaft/connecting rod mechanism, is presented in Appendix A. Harmonic analysis involves calculating Fourier coefficients from known cylinder pressure or crank tangential force (crank torque) data. Engine excitation harmonic synthesis involves calculation of cylinder pressures and crank torques from tangential coefficients.

The following chapter explores methodologies employed in TVA, including analytical, numerical, simulation modelling, and experimental methods, emphasizing their applications, advantages, and limitations in the context of ship propulsion systems

4.3. Modelling methods

Different modelling methods can be employed to predict and analyse the torsional vibrations in ship propulsion systems. These methods range from theoretical to practical approaches, each offering advantages and limits depending on the complexity of the system, the required accuracy, and the available data. This section will explore the primary modelling methods used in vibration analysis, which include analytical, numerical, simulation modelling, and experimental methods.

4.3.1. Analytical methods

Analytical methods involve manipulating formulas and equations using algebra, trigonometry, calculus, and similar mathematical rules to find solution for specific variable. These methods offer analytical solutions, while presuming certain assumptions regarding boundary conditions and material properties. Analytical methods in vibration analysis are applied to create mathematical models that describe the system's behaviour under vibratory forces, offering insights into natural frequencies, resonance, mode shapes, and stress distribution. Several methods of determining the natural frequencies and mode shapes of discrete systems are outlined in [41], such as the methods of Dunkerley, Rayleigh, Holzer tabulation, Jacobi, etc.

In this research, the natural frequencies (eigenvalues) and the natural modes (eigenvectors) of the investigated propulsion systems are verified using dedicated computer program. The program, written in VBA code, is intended for the calculation of eigenvalues (natural frequencies) and eigenvectors (natural vibration modes) using Jacobi method, and is presented in Appendix A. The Jacobi method is an iterative algorithm commonly used for solving homogenous systems of linear equations, particularly advantageous for large systems where direct methods (such as Gauss method) are inefficient. Jacobi method operates by decomposing the complex set of equations into simpler components, facilitating the approximation of solutions. By leveraging matrix properties, the Jacobi method efficiently determines all eigenvalues and eigenvectors simultaneously. However, Gauss method is basically the row reduction algorithm for solving linear equations systems. It can be efficiently applied to determine the cosines and sines of the displacement amplitudes in case of n DOF torsional vibration of systems under harmonic excitation.

Analytical solutions are particularly valuable for understanding system's behaviour as its parameters vary, making them particularly advantageous in the early stages of design by facilitating the selection of parameter values to achieve desired response characteristics. However, as the complexity of the system increases, e.g. in case of nonlinearities or multiple interacting components, the accuracy and applicability of purely analytical methods may decrease. When obtaining the analytical solution is challenging, the system's response can be determined using the appropriate numerical integration method. Despite these limitations, analytical methods remain a fundamental tool in vibration analysis, as they can be employed in conjunction with other techniques to validate numerical models and simulations. Moreover, analytical methods are essential for understanding the basic principles of torsional vibration and for deriving the theoretical frameworks upon which more complex models are built.

4.3.2. Numerical methods

Numerical approach is applied when the differential equation governing the free or forced vibration of a system cannot be integrated in closed form. Numerical integration methods and their fundamental characteristics are thoroughly discussed in [41]. They satisfy governing differential equations at discrete time intervals, assuming specific variations in displacement, velocity, and acceleration within each interval. In general, numerical methods rely on extensive algebraic operations to approximate the solution for the variable.

Numerical methods have become increasingly important in TVA of propulsion systems, particularly for complex systems that cannot be easily described by analytical equations. These methods involve discretizing the system into small, manageable components and solving the resulting set of equations using computational numerical techniques. The most common numerical methods employed in vibration analysis include the finite element method (FEM), because it allows for the modelling of complex geometries, material properties, and boundary conditions. By dividing the system into smaller elements, FEM approximates the system's behaviour by solving for the unknown variables at discrete points. This method is particularly effective for analysing systems with intricate details, such as varying cross-sectional shapes, nonlinear damping effects, and non-uniform material properties.

Although numerical methods require significant computational resources and expertise, they enable engineers to deal with large-scale systems with numerous interacting components, provide high level of accuracy, and can be adapted to different stages of the design and operational phases.

4.3.3. Simulation modelling methods

The application of simulation modelling methods in TVA enables virtual representation of the propulsion system, allowing it to be subjected to simulated dynamic conditions. Simulation enables experimentation on digital representation of the system, conducted through simulation software that provides dynamic platform for real-time analysis of computer models during execution. Simulation modelling is computer-based method which combines numerical techniques, namely algorithms and equations, with time or frequency domain simulations to model the response of the system and its components to various excitations, including engine-induced vibrations and external forces [83].

Specialized simulation software packages, such as MATLAB/Simulink, SimulationX, ANSYS, and AVL EXCITE, provide dynamic environment for real-time analysis, allowing users to visualize the propagation of torsional vibrations and assess the impact of design modifications. Simulation software tools can be used to perform sensitivity analyses, optimize damping strategies, and validate compliance with classification society standards.

The advantages of simulation modelling methods include their capacity to represent system's behaviour across wide range of operating conditions and the ability to analyse the model in real time during execution. This ability provides critical insights into potential failure modes and helps engineers optimize the system design for better reliability and performance. While simulation models require accurate input data and comprehensive understanding of the system's dynamics, they offer valuable predictive capabilities that can reduce the need for costly physical tests and improve overall system design.

4.3.4. Experimental methods

Experimental methods in TVA involve conducting physical tests on ship propulsion systems or scaled models to directly measure the response of the system to torsional excitations. These methods provide empirical data that can be used to validate theoretical and numerical models, ensuring that the predictions align with real-world behaviour. Common experimental techniques include vibration testing, strain gauge measurements, and modal analysis, all of which allow for the measurement of stresses, displacements, and frequencies.

Vibration testing involves subjecting the propulsion system to controlled excitations and measuring the resulting vibrations using accelerometers or displacement transducers. Modal analysis, on the other hand, involves identifying the natural frequencies and mode shapes of the system, which can be compared with the excitation frequencies to detect resonance conditions. Strain gauges are used to measure the stress and strain in specific locations of the system, providing data for assessing torsional stresses. Torsional vibration measurements, conducted during sea trials, typically involve strain gauges as measurement method. These measurements are mandatory under regulations to confirm the validity of torsional calculations [45]. They include description of the instrumentation setup, details of the measurement system and positions, and the calculation procedure for additional torsional stresses.

The primary advantage of experimental methods is their ability to provide direct, real-world measurements of the system's response. Thus, they are particularly useful for validating numerical and simulation models. However, experimental methods can be time-consuming and costly, requiring specialized equipment and facilities. Despite these challenges, experimental methods remain the essential component of vibration analysis, particularly for fine-tuning system designs and confirming theoretical predictions.

The following chapter outlines the simulation modelling methodology, focusing on software selection and periodic steady-state simulations. It will cover the computation steps, methods, and techniques for modelling in SimulationX, including basic and TVA-specific structures. The chapter will address the development of ship propulsion system models, engine excitation modelling, and various cylinder elements. Finally, it will discuss the preparation and entry of input data, particularly for loading components in TVC within SimulationX.

5. APPLIED SIMULATION MODELLING METHODOLOGY

This chapter presents the simulation modelling methodology applied in this research, covering software selection, simulation approaches, and integration of engine and propulsion system components. It includes discussions on periodic steady-state simulations, model structure, engine excitation modelling, and input data preparation, with each subchapter detailing the techniques and tools used to evaluate system performance.

5.1. Software selection

This research examines the application of simulation modelling in the analysis of marine shaft line dynamic response. The SimulationX software is selected as the most suitable tool due to its robustness, availability, and advanced simulation capabilities. Also, the software selection is reinforced by its, somewhat outdated, approvals from certain IACS classification societies for implementation in the ship classification process [84, 85]. Given its advanced simulation capabilities, it is widely used in multiphysics applications across various industries [86]. Also, it is designed for the modelling, analysis, and optimization of complex, dynamic, and nonlinear technical systems. Originally developed by the former ITI, and later part of the ESI Group (Dresden), the software incorporates simulation-based approach for calculating torsional vibrations.

According to [87], this software offers advanced modelling tools that enable users to represent complex physical and technological relationships with compound elements. Its intuitive interface allows for interactive model definition using prebuilt components, streamlining the design process by integrating diverse sub-models within a unified simulation environment. Additionally, it features universal data interfaces, component object model (COM) programming, and co-simulation modules facilitate seamless data usage, computer-aided design (CAD) integration, and connection to computer-aided engineering (CAE) tools. The software platform supports rapid model creation with validated library elements and offers advanced users powerful TypeDesigner tool for custom element development. The use of the object-oriented Modelica language enhances development efficiency and safety.

To handle the complexity of model descriptions, various analytical and numerical methods are employed in SimulationX. The differential-algebraic equations (DAE) system is optimized through global symbolic analysis, simplifying it for efficient processing by high-performance solvers. The default backward differentiation formula (BDF) method is used to ensure reliable performance for stiff systems common in heterogeneous models, while adjustable precision is applied to address nonlinearities and discontinuities, ensuring accurate simulations.

The software supports various analysis tasks, with transient and periodic steady-state simulations in both time and frequency domains being particularly relevant for vibration analysis. This research focuses on the dynamic response of the marine shaft line due to steady-state torsional vibrations, excluding transient vibrations as they are temporary, non-repetitive, and diminish as the system stabilizes. To analyse this, the SimulationX *Periodic Steady-State Simulation* option has been employed, calculating the periodic limit cycles of both nonlinear and linear systems as a function of the preselected reference quantity, such as the mean angular velocity of a rotating mass. This approach is extended with a linearly time-dependent term to account for the steadily increasing angles of rotating masses in the vibration analysis of freely rotating powertrains. The computed results include various frequency-domain quantities, such as amplitudes, fluctuation coefficients, excitations, and phases, displayed also in form of real and imaginary parts. For each case, the sum curve, mean value, and spectral components (orders) may also be presented.

The following section provides the theoretical background, including basic terminology and computational expressions, for the steady-state simulation option used in this research.

5.2. Periodic steady state simulation

The periodic steady state simulation requires definition of system properties, which include reference quantity, period variable, period, orders, and compensation parameter. It is designed as parametric analysis, thus is suitable for investigation of the system´s periodic solution based on a user-defined reference quantity. This quantity can be system parameter or mean value of a state variable, which varies across user-defined interval. In control systems, the frequency and amplitude of the signal source are suitable reference parameters. In powertrain applications, the reference parameter is often the mean angular velocity of a rotating mass. If state variable is used for reference quantity, its mean value changes during steady-state simulation, requiring the compensation parameter. Actually, this parameter is harmonic balance algorithm that adjusts the mean value of reference quantity, thus keeping it within its defined range. If this parameter serves as the reference value, no compensation parameter is needed.

The time-domain approach for steady-state simulation includes the term that grows or decreases linearly with time, thus allowing for the simulation of freely rotating powertrains. The user must assign one variable with nonzero time-linear component as the period variable, and define its period length. This value represents the change in the period variable over one vibration period. The crankshaft angle serves as the period variable in powertrain application, which in case of two stroke engine is changing by 2π over one excitation period.

Fundamental order represents the quantity that determines the denotation of the spectral component with fundamental frequency of the periodical signal component. The period duration of the lowest spectral component is determined by the user-defined period length of the period variable. This component is assigned to the fundamental order, while the second spectral component corresponds to twice the fundamental order, and so on, up to the user-defined maximum order. The number of spectral components used in the harmonic balance solver is calculated by dividing the maximum order by the fundamental order. In powertrain with internal combustion engines, one full period of the oscillation typically corresponds to one or two turns of the crankshaft, depending of the engine cycle (two stroke or four stroke).

5.2.1. Computation steps

The steady-state behaviour of the system examined through available periodic steady-state analysis, includes the period vector, period variable, and period computation. Additionally, the analysis incorporates harmonic balance, parametric analysis, reference quantities, and compensation parameters. In this context, dynamic system such as a powertrain is represented by differential-algebraic equation (DAE) system:

$$f\left(x(t),\dot{x}(t)\right)=0 \tag{101}$$

where $x(t)$ is the time-dependent vector of state variables, $\dot{x}(t)$ is the corresponding vector of time-derivatives. Computation of the user-selected result quantities $y(t)$ is expressed as:

$$y(t)=g\left(x(t),\dot{x}(t)\right) \tag{102}$$

Model is considered valid when the number of state variables n matches the number of equations in (101), thereby for valid models $x(t)$ and function f have equal number of components.

In most powertrain applications the vector $x(t)$ of state variables is composed of the angles and the angular velocities of the rotational masses. Newton´s law of motion is constituted in (101) together with the equations representing the angular velocities as time-derivatives of the angles of the rotational masses. During steady-state simulation, the system's solutions $x(t)$ are computed and represented as a composition expressed as:

$$x(t) = x_P(t/T) + \hat{x}[0] + \tilde{x}(t) \tag{103}$$

Here, uniform linear motion is described by the first member on the right side, the second is constant member, while the third member is unbiased periodical component. Thereby, the periodical motion is approximated by the finite sum of harmonic components:

$$\tilde{x}(t) := \sum_{k=1}^{N} \hat{x}_R[k]\cos(\omega k t) - \hat{x}_I[k]\sin(\omega k t) \tag{104}$$

Here, the symbol := means defined to be equal to, while the subscripts *R* and *I* refer to the real and imaginary part of the complex amplitudes, expressed as:

$$\underline{\hat{x}}[k] := \hat{x}_R[k] + j\hat{x}_I[k] \tag{105}$$

This can be represented in a concise form as:

$$\tilde{x}(t) = \sum_{k=1}^{N} \mathrm{Re}\left(\underline{\hat{x}}[k]e^{jk\omega t}\right) \tag{106}$$

The quantities in stated equations include:

x_P - constant period vector with dimension of the steady state variables,

T - period duration of the vibration,

ω - phase velocity of the vibration,

$\underline{\hat{x}}[k]$ - complex amplitude of the *k-th* spectral component,

$\hat{x}[0]$ - constant signal component (also denoted as mean value),

$\hat{x}_R[k]$ - real part,

$\underline{\hat{x}_I}[k]$ - imaginary part of $\underline{\hat{x}}[k]$, and

N - the number of spectral components for the representation of $\tilde{x}(t)$.

The result quantities denoted with *y* are similarly decomposed into their mean value and complex spectral components, which are subsequently transformed into different representations.

Internal combustion engine generates angle-dependent torque that excites vibrations throughout the freely rotating powertrain, which are investigated for nonzero mean engine speed, Thereby, within one vibration period, the rotational mass angle increases by the mean angular velocity multiplied by the duration of period. In the context of the periodic steady state, this motion is considered within the formulation of the period vector x_p, whose components correspond to the angular positions of the rotational mass and represent the angle covered within one vibration period.

During the setup of the steady-state simulation, the state variable is chosen along with the corresponding period vector component for that variable. For powertrain application, the excitation wave repeats after one or two crankshaft rotations, thus the crankshaft angle provides suitable period variable. The remaining period vector components are determined separately in the initial step of the simulation, referred to as period computation. After the period computation, next task involves computation of the spectral components, the mean value, and the phase velocity, in accordance with the expressions (103) and (104). The system of equations (101) must be satisfied at least for the mean value $\hat{f}\left[0\right]$ and the first N spectral components on the right-hand side.

The algorithm for this computation is referred to as *harmonic balance*, which is designed as a parametric analysis. Therefore, the periodic steady state is determined based on a reference quantity x_{ref} which varies across the user-defined range. The system has one more variable than equations because the phase velocity ω is unknown. To ensure the unique solution, the mean value of the period variable is always set to zero.

Depending on whether the parameter or the variable is selected as the reference quantity, two different equation systems can be configurated. If the parameter is chosen, the differential-algebraic system (101) remains a parametric system, where for each parameter value of x_{ref} the number of equations matches the number of variables. Alternatively, if the mean value of a state variable is chosen as the reference quantity, the relation acts as the additional equation in the harmonic balance. To maintain consistency between the number of variables and equations, one system parameter, denoted as *compensation parameter*, must be set free as a variable in order to modify the differential-algebraic system (101) accordingly.

In conclusion, the periodic steady-state simulation offers a robust framework for analysing system dynamics by decomposing periodic signals into spectral components. Using harmonic balance and parametric analysis, it is essential for evaluating steady-state performance in powertrain applications. The following chapter will discuss the methods used in periodic steady-state simulations, focusing on adjusting algorithm parameters for period computation and harmonic balance. It will cover techniques like curve tracing, step size control, and oversampling, comparing nonlinear and linear methods for different systems.

5.2.2. Methods

The method involves adjusting key algorithm parameters for period computation and harmonic balance, with default settings appropriate for most applications, rarely requiring modifications. Higher spectral components often exhibit smaller resonance peaks than lower-order, but still remain important for steady state analysis of the system. To maintain accuracy across all spectral orders, relative measures are used to determine error tolerance and point density along the solution curve. For computing the numerical error and step size, all components where the difference between the maximum and minimum computed values exceeds one are multiplied by the scaling factor *1/(*max-min*)*. For step size control, the reference quantity is scaled by the factor *1/|Stop-Start|* if the start and stop values do not coincide.

Curve tracing algorithm is used for the computation of the solution curve. This ensures fine tracking of resonance peaks and enables computation of nonlinear frequency responses with turning points. The relative step is measured tangentially to the solution curve, composed of the reference quantity and all spectral components of state variable as shown in Figure 25, rather than strictly along the reference quantity.

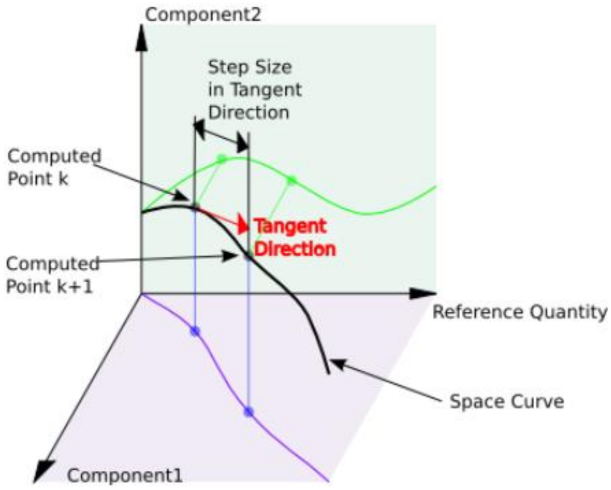

Figure 25. Step size tangential to the solution curve [80]

This approach is crucial for tracking curves with turning points, as shown in Figure 26. Frequency responses of nonlinear systems may have turning points in which the tangent direction of the curve is perpendicular to the direction of the reference quantity. In such points the step size in direction of the reference quantity is zero. The step size is also controlled by the curvature of the solution curve and the convergence of the Newton-algorithm.

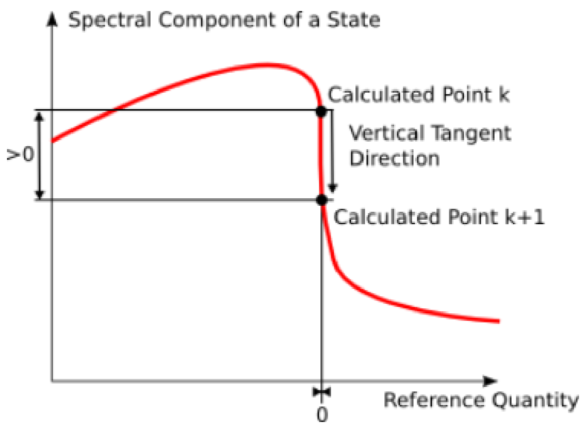

Figure 26. Frequency response of nonlinear system [80]

The relative tolerance defines the precision of computed spectra. Since the exact solution is unknown, the numerical error cannot be determined precisely. Instead, the length of the predicted Newton step is used as the estimate of the remaining error. In addition to remaining error of Newton iteration, the Fast Fourier Transformation (FFT) introduces a sampling error which contributes to overall error in spectral results. This error can only be reduced through oversampling. In the linear method, relative tolerance is irrelevant since only one Newton step is performed, regardless of numerical error.

During harmonic balance, nonlinear functions are evaluated in the time domain. For the balance of the frequency-domain residuals function values are transformed via Fast Fourier Transformation (FFT) into frequency domain. The *Oversampling* determines the number of time-domain samples used for discrete Fourier transformation. If N represents the number of spectral components for the harmonic balance, then at least double number of N points are used in the time domain for oversampling.

Methods to determine harmonic balance include one of the following algorithms:

– **Nonlinear method** (Newton, Generalized Minimal Residual Method (GMRES), Jacobi-Preconditioned) – applies the harmonic Newton algorithm iteratively to the system if equations, until the relative approximation error falls below the user-defined tolerance. The approximation error is estimated by the length of the predicted Newton step, so the FFT contributes to the overall error. Therefore, oversampling must be high enough to minimize sampling errors.

– **Linear method** – executes a single step of the harmonic Newton algorithm at each point of the solution curve, making it faster than the nonlinear method. However, this method cannot control approximation error, as only one Newton step is performed. It is suitable for systems where constant and time-linear components dominate over oscillatory behaviour, such as powertrains with rigidly modelled connecting rods. This method is exact for linear systems with excitation source whose frequency is the reference quantity, and phase is the period variable.

In conclusion, the methods ensure accurate periodic steady-state solutions through curve tracing, step size control, and oversampling, with the choice of nonlinear or linear methods tailored to different system dynamics. This chapter will explore the various modelling approaches in SimulationX, including physical object-oriented, signal-oriented, and equation-based methods. It will also cover the application of these methods to develop and customize models for different simulation tasks.

5.3. Modelling in SimulationX

SimulationX offers various modelling approaches that can be seamlessly combined within single simulation, including physical object-oriented, signal-oriented, along with equation and algorithm-based approach.

Physical object-oriented modelling, also termed as network modelling, provides natural representation of physical behaviour in simulation models. This approach, whose concept is shown in Figure 27, is employed across all physical domains and libraries. Models are formed of elements interconnected by connections, which intersect or branch in nodes. Elements represent objects found within software libraries, whereas connections are created by interconnection of elements.

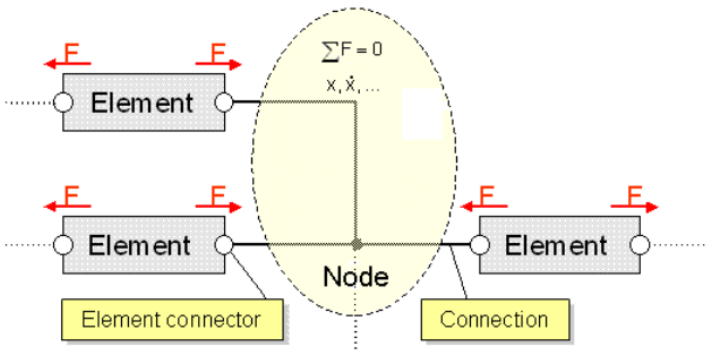

Figure 27. Physical network modelling [80]

In network models, physical relationships are expressed through potential and flow quantities. These quantities exist within the connection and remain the same for all element connectors linked to it. Examples of these quantities include displacements, speeds, and accelerations in mechanics, pressures in fluid mechanics, voltages in electronics and temperatures in thermal models. Balance equations must be satisfied, i.e. forces or torques at mechanical connections must sum to zero, just as currents must be in balance in electrical systems. Signal structure modelling differs from physical network models, as it represents information processing systems, such as control systems. In these models, elements generate output data from provided input data, following the well-defined information flow and causality.

The Modelica object-oriented modelling language is used in SimulationX for equations and algorithms [87]. This enables direct text-based representation of physical relationships through differential or algebraic equations. This approach is particularly useful for customizing SimulationX and developing user-specific elements beyond the standard libraries.

5.3.1. Basic model structure

Basic simulation model structure, shown in Figure 28. consists of elements and connections. Elements have connectors that link through connections, which can branch arbitrarily and connect multiple elements. Connectors include mechanical (linear and rotary), hydraulic, electrical, and signal interfaces. Each connector has its unique name relative to its corresponding element, and only connectors of the same type can be linked.

SimulationX offers comprehensive set of element libraries for various physical domains and applications, developed and maintained by ESI Group. These include: SimulationX libraries, Modelica Standard libraries and user-defined element type libraries. This software integrates the Modelica language as a model development and programming interface for user-defined elements.

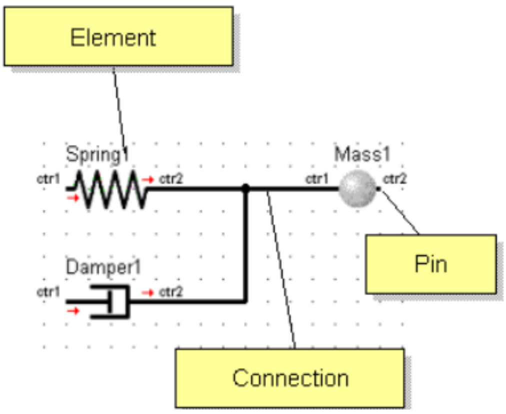

Figure 28. Basic model structure in SimulationX [80]

Parameters can be defined as mathematical functions instead of solely numerical values. Each parameter can also be linked to logical conditions defined in brackets. Any variable in the model, including result variables, can be used as the input for parameters. Each model element calculates several result variables based on its functionality and complexity. All active result variables from all model elements are provided at each output time step. The solution algorithm assumes that parameters remain constant, unless the elements are specifically designed to handle variable parameters.

5.3.2. Model structure for TVA

The available Torsional Vibration Analysis (TVA) package enables the steady-state analysis of torsional powertrain models, with the focus on marine and stationary drive systems that include internal combustion engines, transmission elements, and machines. This package is divided into three sub-packages: basic elements, engines, and machines. It seamlessly integrates with components from other SimulationX libraries, such as *Mechanics*, *Signal Blocks*, and *Power Transmission*. Also, user can develop and customize models for specific simulation tasks. The model structure, shown in Figure 29, follows the left-to-right layout, with the engine on the left and the load component on the right. This layout defines main rotation axis of the system as well as the coordinate system of connectors.

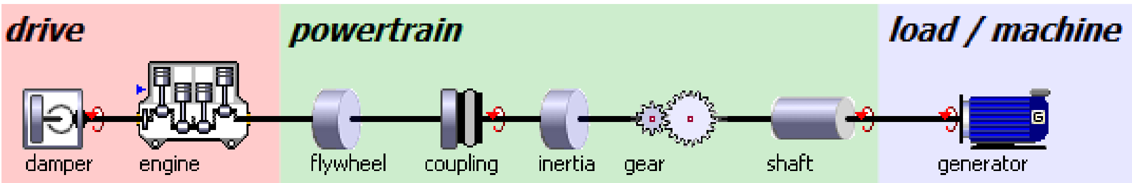

Figure 29. Modelling principle with TVA package [80]

In this research, the TVA model structure is applied to the developed models of the ship propulsion system. This is illustrated for two modelling structures, shown in Figures 30 and 31, respectively, for the direct propulsion system configuration equipped with the 6-cylinder two-stroke Diesel engine. The main difference between the modelling structures is in the number of elements used to represent combustion engine and marine shaft line components.

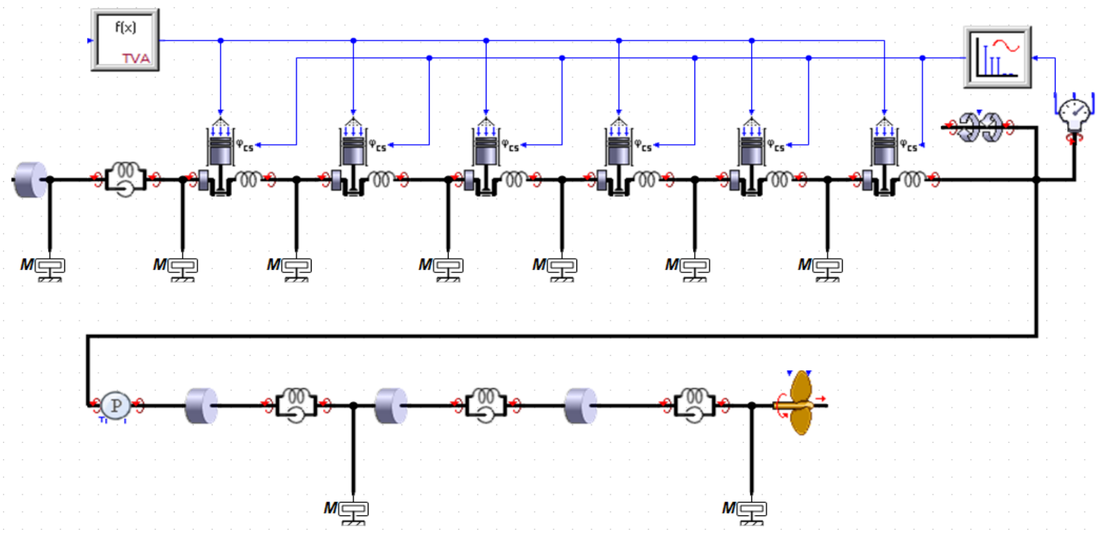

Figure 30. Expanded modelling structure of ship propulsion system

The expanded model consists of the upper part, which primarily represents the combustion engine, and the lower part, which represents the marine shaft line. In the compact modelling structure shown in Figure 31, the same propulsion system is composed of fewer elements, and its horizontal layout offers the clearer and more streamlined overview.

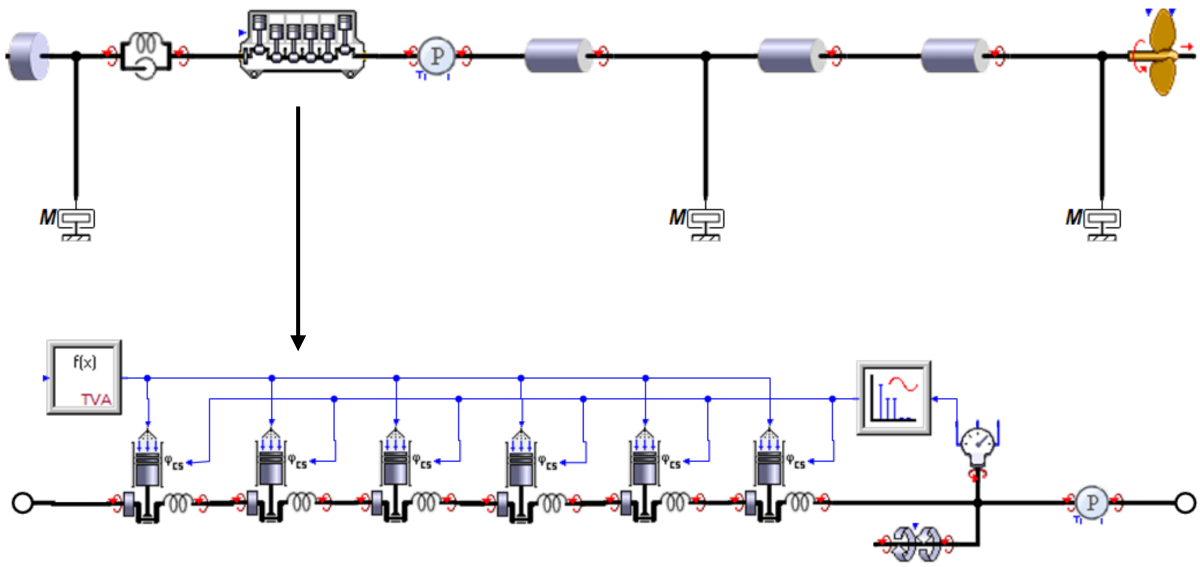

Figure 31. Compact modelling structure of ship propulsion system with open engine element

Representation of engine element as open compound serves as basis for expanded modelling structured used to develop simulation models in this research.

The available TVA shaft element accounts for all properties (mass, stiffness and damping) relevant for the vibration calculation and can calculate both torsional stress and stress limits for the specified shaft line component, as shown in Figure 32. Torsional stress (amplitude sum in red) calculation is based on cross-section geometry and internal torque T_i, which remains constant if the element is defined as rigid, or is represented by the sum of spring torque and damping torque if the element is defined as elastic.

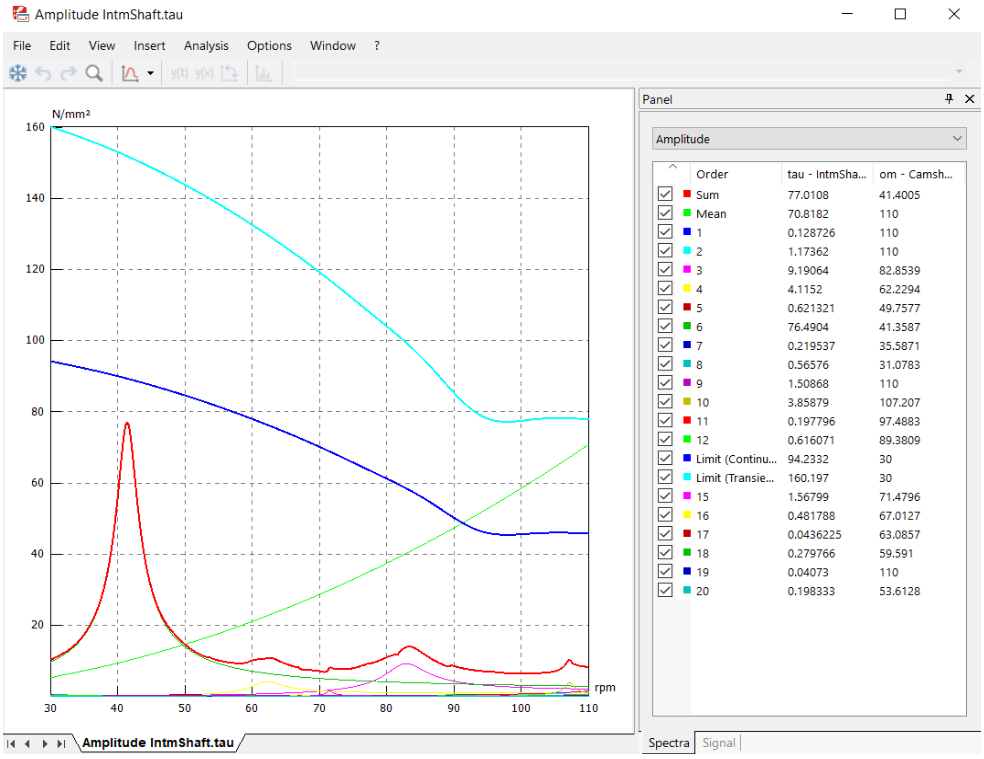

Figure 32. Torsional stress within intermediate shaft with included stress limits

Allowable stress limits for continuous (dark blue) and transient (light blue) operations are determined based on the formulations presented in equations (8) and (9). In the steady-state simulation results window, the mean stress limit values are automatically displayed as supplementary curves above the amplitude curve. Stress limits can also be computed through individual approaches or given values for the stress limits (e.g. the allowable torsional stress amplitudes in the crankshaft for which the engine has been type approved), in which case it is also possible to enter analytical expressions.

Both modelling structures are examined, as the objective of this research is to conduct the comprehensive investigation of the simulation modelling application to the TVA of marine shaft lines. Nevertheless, the expanded modelling structure is applied within the developed ship propulsion system models, because the individual elements provide and include broader capabilities regarding engine excitation simulation. Additionally, single element representation of the engine in SimulationX is limited only to configurations with even number of cylinder and cannot account for possible internal components such as engine distribution mechanism or additional absolute damping elements that may be needed. Also, both modelling structures are suitable for complete TVA investigation of the marine shaft line, but the compact modelling structure can be more convenient as it provides clearer overview of the system.

To conclude, SimulationX TVA package integrates physical, signal, and algorithm-based modelling approaches for comprehensive simulations across multiple domains, thus offering flexible framework for analysing torsional vibrations in powertrain systems in general. Next chapter presents detail description of SimulationX elements used in developing ship propulsion system models.

5.4. Elements used in developed models

In this research models of ship propulsion systems were developed using the elements presented in Table 1., where for each element associated connectors along with abbreviations for input and output connectors are displayed. Due to their unambiguous display by default, both mechanical (black lines) and signal (blue lines) connections are not tabularly represented.

The rotary mechanical connection enables both graphical and functional interconnection of rotary mechanics elements. It plays the crucial role in simulation by carrying rotation angle, speed, and angular acceleration while ensuring torque balance. Initial values for angle and velocity must be chosen for consistent solver initialization. The computed motion quantities are available as result variables for display and further processing.

Signal connections (blue lines) transmit values unidirectionally from signal outputs to inputs within model objects. They enable interconnection between *Signal block* elements and other library components for reading or setting quantities. They are commonly used for control system modelling, where the physically-oriented model represents the controlled system. Quantities in the controlled system are measured as signals and fed back to control system. This approach avoids complex translation into the signal-oriented model. These connections can branch, thus allowing one signal output to connect to multiple inputs, yet the signal input can only connect to one output at a time.

Table 1. Elements used for developing marine propulsion systems models

Name	Element symbol
Cylinder with elastic crank	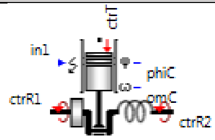
Dynamic magnifier	
External torque	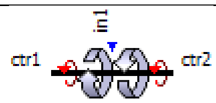
Force excitation	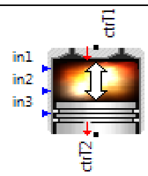
Function *f(x)*	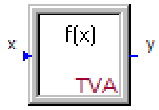
Inertia	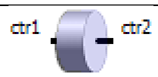
LTI order filter	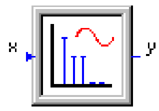
Marine propeller	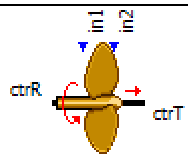
Power and Torque Sensor	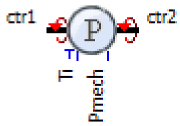
Shaft	
Sensor	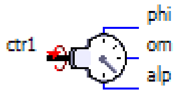
Spring-damper	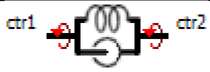
Torque excitation	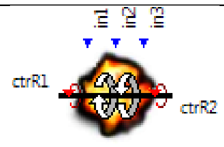
TVA inline cylinder	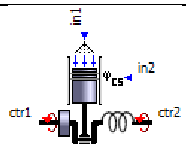

Certain abbreviations are included in the element symbols, where *ctr*$_R$ denotes to rotational system while *ctr*$_1$ and *ctr*$_2$ denote to rotational mechanical connectors. Similarly, *ctr*$_T$ denotes to translational system while *ctr*$_{T1}$ and *ctr*$_{T2}$ denote linear mechanical connectors. Signal input x and output y relate to function element. Small blue triangles, denoted as *in*$_1$, *in*$_2$ and *in*$_3$, refer to signal inputs such as crank angle, crank speed, control value, mean load torque, etc. Angle is denoted as *phi*, rotational speed as *om* and angular acceleration as *alp*.

Function f(x) element enables signal creation or modification based on the user-defined rule. The parameter F denotes the function $f(x)$ which defines the transformation, in which arbitrary expressions with numbers, variables, and functions are allowed. The input signal x is referenced as *self.x* within the expression. The computed output y is available as the result variable and output pin for further processing. This element can function as the signal source (with no input) or the sink (with no output).

Inertia element is used to model rotary inertias in real or simplified systems, such as flywheel inertia in the powertrain with one or more internal combustion engines. When referring to rotating mass the key parameter J is defined as mass moment of inertia. In general, it can be defined numerically or through functional expressions, but it must remain constant. From the physical perspective, inertias relate to one coordinate or set of motion quantities, while from the modelling perspective, they represent capacities relative to the reference system.

Power and Torque Sensor is used for analysis of power flow between two mechanical elements in the rotational system. It acts as the rotational constraint with no angle or speed difference, ensuring both connectors have equal speeds, thus allowing internal torque T_i and mechanical power P_e to be calculated and provided as output signal.

Sensor element measures angle, rotational speed, and angular acceleration at the rotary connection These quantities represent output signals for use in simulation models, thus enabling modelling of motion feedback, e.g. angle-dependent torque in combustion engine, or signal processing structures.

Spring-damper element is used to describe elasticity and/or damping between two rotating components. It is characterized by the parallel action of the spring and damper, as indicated by the symbol of the element. Implementing this element, user can define the element’s behaviour as pure spring or pure damper, and spring-damper in parallel. The available parameters depend on the selected configuration, with elasticity defined by the stiffness parameter k, which can be constant or numerically specified variable, through analytical expressions, or reference formulations. Damping, however, cannot be set directly and must be determined using available approaches:

1. **Viscous damping** uses the damping torque T_d, which is proportional to the speed difference between the connectors:

$$T_d = b \cdot d\omega \tag{107}$$

where b - the damping constant, applied consistently in both time-domain and steady-state simulations, in which all harmonics are equally damped.

2. **Estimation approach** is suitable when only stiffness is known, so the damping constant b is approximated using damping approach factor B, expressed as:

$$b = B \cdot \sqrt{k} \tag{108}$$

The approach factor B can be chosen provided guidelines:

– B = 0.005 ... 0.01 for damping in metallic materials (e.g., shafts),

– B = 0.1 ... 0.25 for damping in highly elastic materials (e.g., rubber elements),

– B = 0.05 ... 0.15 for structural and contact damping.

3. **Relative damping** ψ is defined as the ratio of energy loss per period (represented by the area enclosed by the angle-torque curve) to the maximum elastic deformation energy (reversible spring deformation). This is expressed as the work ratio between the damper and the spring, given by the following expression:

$$\psi = \frac{W_D}{W_S} \tag{109}$$

Consequently, this is dimensionless quantity which, if deviation amplitude does not change, holds the torque constant over the excitation frequency for certain damping phenomena (e.g. Coulomb friction damping). If relative damping is assumed constant, the equivalent damping coefficient for the dominant excitation frequency ω can be derived as follows:

$$b = \frac{k\psi}{2\pi\omega} \tag{110}$$

This frequency-dependent damping is considered in steady-state simulations, but due to inherent nonlinearity, the output results are only approximations.

4. **Lehr's damping** represents nonlinear, frequency-dependent damping parameter in the normalized differential equation of the damped harmonic oscillator. It directly relates to relative damping by expression:

$$D = \frac{\psi}{4\pi} \tag{111}$$

Similar to relative damping, Lehr's damping allows defining the equivalent speed-dependent damping constant, which varies with excitation frequency. Due to nonlinear effects, simulations provide only approximate solutions.

There are some propeller elements available within SimulationX libraries, basically differing in modelling capabilities and extent of input data entry. The basic structure, as shown in Figure 33, remains the same for available propeller elements. Both load and damping torque elements are connected to the rotor inertia element. The load element represents the external load torque T_{load} exerted by the propeller on the propulsion system, specifically the propulsion engine. The damping element represents the damping torque T_d, which accounts for energy losses due to damping as the propeller interacts with the surrounding water.

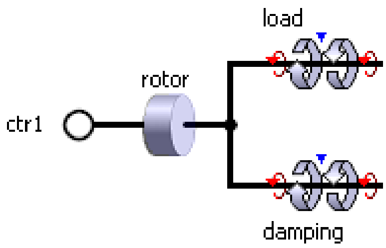

Figure 33. The structure of propeller element [80]

In this research, ship propeller is represented by the *Marine propeller* element, designed for transient and steady-state TVA of propulsion systems. Developed in collaboration with the famous IACS classification society from the past, *Germanischer Lloyd (GL),* it adheres to classification society standards, safety regulations and applicable technical requirements [88, 89, 90]. This element accounts for inertia, blade excitation, load effects, and damping, while also enabling ice impact calculations and analysis. Although ice impact analysis is not part of this research, this element is selected because of the extent of input data entry capabilities. The propeller element connects to rotational powertrains, i.e. ship propulsion system at ctr_R point. Additional feature, not part of this research, is translational connector ctr_T through which generated jet of the propeller can be modelled when necessary.

Marine propeller element parameters may be entered for various input data. The rotor inertia parameter can include rotor inertia in air J_r or total inertia J_{rw} which is the rotor inertia in air plus water inertia. The total inertia is computed using internal approach by Schwanecke [80]. The standard propeller design parameters are also incorporated: rotor diameter d, hub diameter d_H, number of blades n, nominal $p_{0.7n}$ and adjustable $p_{0.7}$ blade pitch at 70% rotor radius, as well as area ratio A_e/A_o used in Schwanecke's water inertia and damping calculations. Also, it accounts for the density ρ of propeller's operating medium. In general, the nominal power P_n and nominal speed ω_n are load parameters used to define the mean load torque:

$$T_n = \frac{P_n}{\omega_n} \tag{112}$$

The mean load torque is defined for the nominal operating point as it is specified in usual propeller data sheets. Different options are available for mean load torque specification and calculation:

- propeller curve at nominal point,
- normalized combinator curve,
- combinator curve,
- propeller map,
- custom parameterization.

Among the listed options, this study specifically utilized two options. Firstly, the combinator curve with direct input of mean load torque as the function of the current mean rotor speed ω_m. Secondly, the propeller curve at the nominal point, where mean load torque is expressed as:

$$T_{load} = T_n \cdot \left(\omega_m / \omega_n\right)^2 \tag{113}$$

Although not utilized in this research, the selected element incorporates oscillating load torque, enabling sinusoidal oscillations with up to two harmonic orders and adjustable phase shifts. Damping only affects oscillatory torque components, which for steady state analysis can be applied using predefined approaches or user-defined damping factors.

The *Special Signal Blocks* category, within the SimulationX element library, includes elements that model Linear Time Invariant (LTI) subsystems, whose key property is suitability for frequency-domain analysis. In general, they do not conform to delay-differential-algebraic equations, thus their full functionality is available only in periodic steady-state simulations. In this research, the LTI element type *LTIOrderFilter* is used to apply user-defined complex multipliers to spectral components. Its application is to filter out vibrations in the angle signal, preserving only components corresponding to uniform circular motion. During time-domain simulation, the input signal is simply scaled by the transfer function's zero-frequency value, amplifying the mean value component. Given the vector c of real filter coefficients, the spectral components $\underline{\hat{x}}[k]$ of the input signal are mapped to those of the output signal $\underline{\hat{y}}[k]$, as follows:

- The period y_p and mean value component $\hat{y}[0]$ of the output signal are determined by the corresponding components of the input signal:

$$y_p = c[1]x_p \tag{114}$$

$$\hat{y}[0] = c[1]\hat{x}[0] + c[2]x_p\frac{\omega}{2\pi} \tag{115}$$

- The complex amplitude $\underline{\hat{y}}[k]$ of the output signal for $k = 1,\ldots$ is computed from the corresponding input amplitude:

$$\underline{\hat{y}}[k] = \left(c[2k+1] + jc[2k+2]\cdot\underline{\hat{x}}[k]\right) \tag{116}$$

Here, the unspecified coefficients in c default to zero. In periodic steady-state simulations, the output signal y is computed in the frequency domain, while in time-domain simulations, it is obtained by multiplying the input signal by $c[1]$.

The *user-developed dynamic magnification* element describes absolute frequency-dependent damping, for which theoretical background along with expressions are extracted from [22]. This standalone *SimulationX* element is comprised of multiple basic elements illustrated in Figure 34. This element is used to model damping by applying the dynamic magnification factor. Input data regarding the reference inertia J_{ref} and dynamic magnification factor M are required for the application of this element.

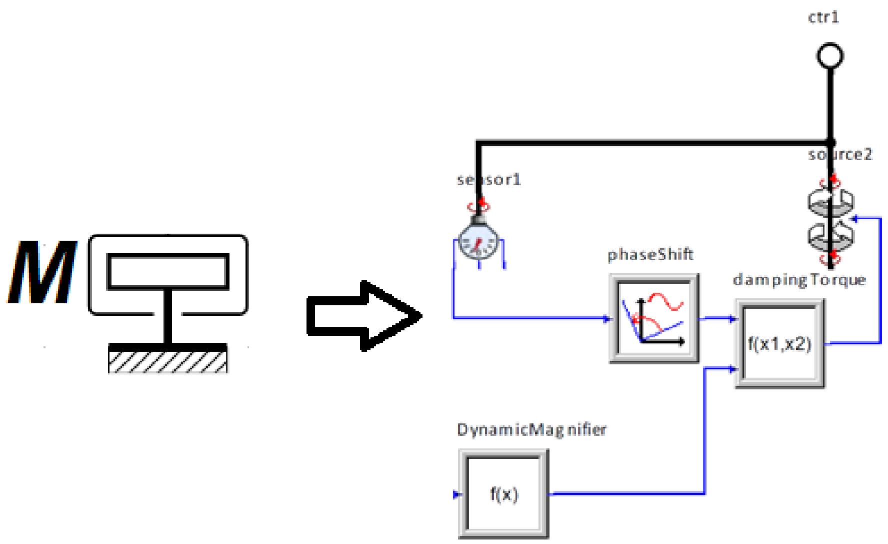

Figure 34. Schematic layout of absolute damping element in closed and open form

Absolute damping effect refer to energy loss between the element and the environment, which is represented using this user-developed element. This element is linked to the simulation model by ctr_1 mechanical connection, which extends to the sensor element (label *sensor*1) and the torque element (label *source*2). Angular acceleration is fed as signal output from the sensor element to the *LTIMultJ* element (*phaseShift* label) which had crucial part in modelling of material damping. This element, of the LTI system type, multiplies the spectral components at positive frequencies with the imaginary unit $j = \sqrt{1}$, while blocking the mean value and period component of the input signal. During periodic steady state simulation, the output signal y is computed in the frequency domain. This signal along with signal from element *function block* element (label *DynamicMagnifier*) is to *function block* element (label *dampingTorque*). This element is used to compute the output signal depending on two input signals, which serves as input torque signal in_1 for the external torque element (label *source*2).

The damping can be expressed by complex mass in the frequency domain, proportional to acceleration. The torque for frequency-independent damping follows formulation as in (107). However, the torque for frequency-dependent damping is derived from the dynamic magnification factor M, expressed as:

$$M = \frac{\omega \cdot J}{b(\omega)} \rightarrow b(\omega) = \frac{\omega \cdot J}{M} \tag{117}$$

By using complex properties, the torque for frequency-dependent damping is determined as:

$$T_E = -\omega^2 \cdot \left(J - j \cdot \frac{J}{M} \right) \cdot \varphi(j\omega) + k \cdot \varphi(j\omega) \tag{118}$$

The derived equation (118) is directly implemented in the user defined compound element. This research primarily investigates direct propulsion configurations, typically equipped with two-stroke engines. According to [22], in such systems, each lumped mass model component has its damping represented by the dynamic magnification factor. This factor must be linked to the moment of inertia, justifying the creation of the user-developed element used in this study.

All in all, the key elements implemented to develop models of ship propulsion system have been presented and discussed in detail. These elements enable detailed simulation and analysis of system dynamics, including damping, load effects, and power transmission. The next section will cover the modelling of engine excitation, focusing on internal combustion engine cylinders and elements from various SimulationX libraries. It will explore how cylinder excitation through pressure and torque will be modelled and integrated with additional elements for the comprehensive engine simulation.

5.5. Modelling of engine excitation

Elements for modelling the combustion engine cylinders cover both inline and V-engine types and are contained within three SimulationX libraries. In the *Power transmission (*1*D)* library, two elements of mechanical cylinders termed as *Cylinder with Rigid Crank* and *Cylinder with Elastic Crank* are available. This study focuses exclusively on the latter element, which is essential because the remaining cylinder elements are structurally based upon this element. The excitation cannot be modelled within this element, so it is defined using additional separate elements. In the both *TVA* and *ITI External* element library, two elements are available for modelling engine cylinder excitation through cylinder pressure and crank torque.

5.5.1. Element Cylinder with Elastic Crank

The element *Cylinder with Elastic Crank* is used to model the mechanical aspects of combustion engine cylinder, accounting for internal and external forces and movements. It includes the rigid piston rod and considers the rotating inertia of the crank and piston rod at ctr_{R1}, as well as the reciprocating mass of the piston and piston rod at ctr_T. The crank's rotational stiffness and damping are modelled at ctr_{R2}. Crank losses are represented by the absolute damper, accounting for speed-dependent torque losses. The element allows for connections:

– $ctr_{R1,\ R2}$ – for additional cylinders, springs, inertias, or powertrain structures (e.g., excitation torques).
– ctr_T – for translational structures, including force elements for modelling translational excitations, such as cylinder pressure forces.

The element features the signal input connector in_1 and two signal output connectors (φ_C and ω_C). By default, in_1 transmits the phase angle, while the crank angle and speed are available as result variables. Key parameters of the element include:

- cylinder geometry,
- effective crank diameters,
- rotating mass and initial motion quantities,
- reciprocating mass,
- model of crank behaviour (rigid or elastic),

- crank stiffness k_C and damping b_C,
- losses.

Cylinder geometry is defined by the connecting rod ratio λ, which represents the ratio of crank radius to rod length. It is determined using either the crank radius r_C or the total piston stroke s, which when eccentricity is zero equals to the double crank radius. The phase angle ψ allows modelling of different crank (consequently also piston) positions at the same initial crank angle. In 4-stroke engines, ψ ranges up to 720° or 4π, while in 2-stroke engines it ranges up to 360° or 2π. In addition, the eccentricity e_x parameter illustrated in Figure 35, accounts for crank mechanisms with eccentrically pivoted pistons.

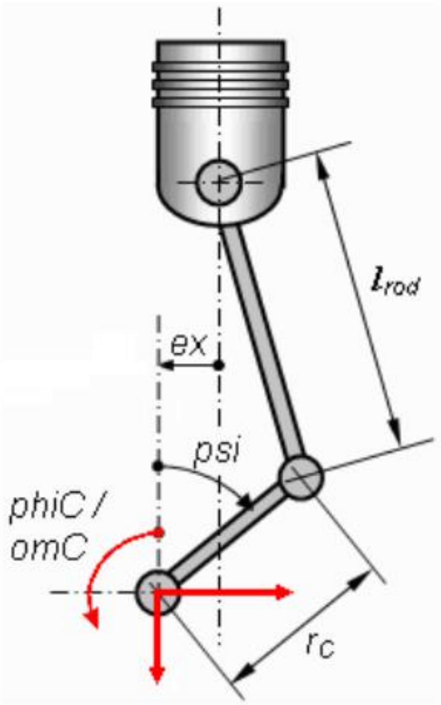

Figure 35. Geometry and coordinates of the cylinder model [80]

Here, r_C is the crank radius, l_{rod} is the length of the connecting rod, ψ (psi) is the phase angle, φ_C (phiC) is the crank angle and ω_C (omC) is the crank speed. The torsional stress τ_C is computed using the effective inner d_i and outer d_o diameters of the crankshaft, along with the internal torque of the crank T_{iC}, using the following expression:

$$\tau_C = \frac{T_{iC}}{W_p} = \frac{T_{iC}}{\frac{\pi}{16} \cdot \left(\frac{d_o^4 - d_i^4}{d_o} \right)} \tag{119}$$

Within the element. the rotating mass refer to the crank inertia J_C, W_p is the polar moment of resistance of the circular cross-section, while the initial motion values include initial phase angle φ_{C0} and initial velocity ω_{C0}.

The reciprocating mass m_{osc} includes the piston mass and the part of the connecting rod mass, with two models available for computing the acceleration forces for m_{osc}, as follows:

1. **Physical model** – accounts for all interactions between the oscillating mass and the rotating crank.
2. **Crank angle approach (non-reactive) model** – accounts for acceleration forces as external forces dependent on the crank angle φ_C, without considering interactions between piston accelerations and the crank. The acceleration forces are computed as:

$$F_{aP} = m_{osc} \cdot \frac{s}{2} \cdot \omega_C^2 \cdot \left[\cos\left(\varphi_C\right) + \lambda \cdot \cos\left(2\varphi_C\right)\right] \tag{120}$$

Where s is piston stroke length, while the initial values of m_{Osc} depend on the initial angle and speed values. The connecting is modelled as rigid without backlash, while the losses are represented by damping which includes absolute damping parameter b_{Cabs} used for consideration of absolute losses at the crank or oscillation damping with or without mean value damping. Different power components can be observed as change of potential energy and the relative power loss (due to crank damping), as absolute power loss (from speed-dependent torque loss at the crank) or as change of kinetic energy (computed for the masses). Obtained results include inertia and mass-related values such as acceleration forces and torques, accelerations, speeds, piston displacement, and crank angle. This element can be integrated with various excitation models to simulate complete inline cylinder systems, as shown in Figure 36.

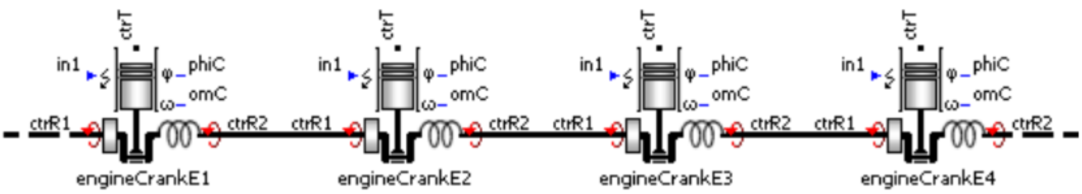

Figure 36. Sample structure of the multi-cylinder in-line engine with elastic crankshaft [80]

However, this element does not offer option for defining the excitation, therefore it must be modelled using additional elements, namely the *ForceExcitation* and the *TorqueExcitation* elements. The *Force Excitation* element is used to model the characteristic excitation force of combustion engine cylinders. The cylinder force is computed using by predefined cylinder pressure, i.e. pressure in the combustion chamber, or cylinder force characteristic which can be set in several different ways. Connectors are located at the top and bottom of the element, allowing it to connect to mechanical cylinder models at the ctr_{T2} connector and to the environment (e.g., cylinder head) at the ctr_{T1} connector. The *Torque Excitation* element is used to model the excitation torque at combustion engine cylinder crank. In this element, connectors are located horizontally, thus allowing it to connect to mechanical cylinder models at the ctr_{R2} connector and to the environment (e.g., crankcase) at the ctr_{R1} connector.

Both force and torque excitation depend on the crank angle, control parameter and optionally on the crank speed. Also, in both elements input parameters can be provided directly or via signal input pins (in_1, in_2, in_3). These inputs define excitation characteristics through curves, maps, or harmonic components. Cylinder pressures are converted to torques and vice versa using geometry parameters, with ignition typically starting near the top dead centre. Key parameters for both elements include crank motion quantities, phase angle and geometry.

Crank motion quantities refer to the crank angle φ_C and crank speed ω_C, measured at the cylinder crank or the flywheel, and used as default references at input signals (φ_C as in_1, ω_C as in_2). Phase angle define the crank's position relative to the crankshaft, while geometry parameters include cylinder bore, piston stroke and connecting rod ration. The latter two parameters are only required for excitation torque calculation, as the influence excitation torque from tangential pressure.

Depending on the excitation model, either tangential pressures and excitation torques or cylinder forces and pressures are provided for multiple load states. The control parameter (denoted as *con*) determines the actual load state and interpolates between them to compute the effective mean pressure, force, or torque. By default, all control parameters reference signal pin in_3 and can be selected as follows:

- $con=inj$ – normalized injection (0% = drag load, 100% = full load),
- $con=p_m$ – mean pressure (e.g., cylinder, effective, or indicated pressure),
- $con=F_{em}$, T_{em} – mean excitation force or torque,
- $con=\omega_C$ – speed-controlled load changes,
- $con=control$ – custom-defined load states.

Depending on the kind of the control parameter, the corresponding control values of the load states have to be defined for the force or pressure excitation curves and the excitation torque or tangential pressure, respectively. Several excitation database options are available:

- **Internal Approach** scales internal excitation characteristics by maximum cylinder pressure.
- **Curves for Two Load States** defines excitation via two curves, interpolated by control parameter. The resulting excitation is the function of the crank angle and the control value.
- **Family of curves and Map-Based Models** uses characteristic maps with input signals to define excitation. The *Family of Curves* interpolates between curves based on the control parameter, while option *2D-Maps* represent load states as the function of crank angle and control parameter. Option *3D-Maps* extend this by incorporating crank speed.
- **Harmonic Components for Two Load States** defines excitation characteristics using Fourier coefficients instead of characteristic curves.
- **Harmonic Component Maps** – allows Fourier-based excitation maps, dependent on crank angle and speed, or control value.
- **Parameters** approach allows direct input of constant values or expressions.

Excitation can be disabled via Boolean parameter, which beneficial for simulating cylinder with open valve or misfiring conditions. Disabling excitation in SimulationX engine cylinder models has also shown to be essential in order to obtain correct frequencies in the calculations of natural frequencies and mode shapes (i.e. eigenvalues and eigenvectors). Misfiring cylinder condition is simulated by applying the compression only load state for cylinder force/pressure or excitation torque/tangential pressure, thus requiring additional parameter to be defined as misfiring load state.

5.5.2. ITI cylinder elements

The *ITI External* library includes two elements for modelling cylinder, namely the *Cylinder (Pressure Excitation, Elastic Crank)* and *Cylinder (Torque Excitation, Elastic Crank)*. These elements have been shown very important to understand behaviour and functioning of *TVAcylinder* elements. Both elements represent the in-line combustion engine cylinder with the elastic crank, the rigid connecting rod, and are used to calculate the displacements and forces. These elements also include the excitation related to cylinder force or crank torque, with similar substructures based upon excitation torque or pressure data, respectively. The substructure of cylinder element with pressure excitation is shown in Figure 37, while the substructure of cylinder element with torque excitation is shown in Figure 38.

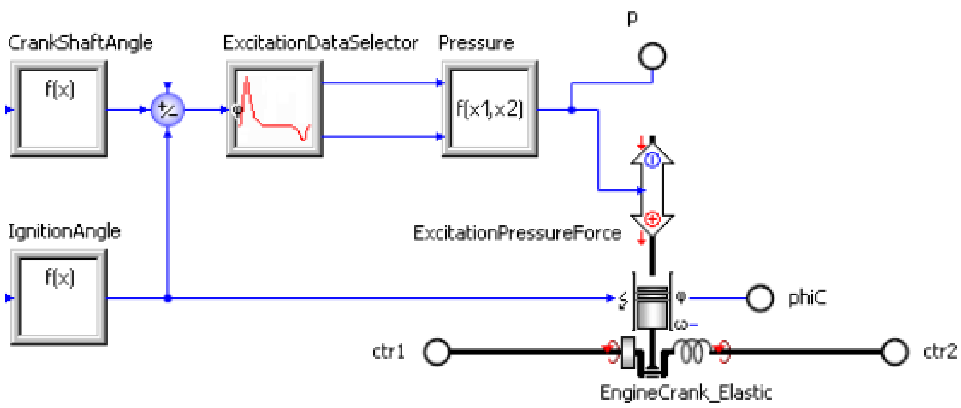

Figure 37. Model structure of ITI cylinder element with pressure excitation [80]

Their substructures differ in function definition and type of excitation element connected to the cylinder. Therefore, the substructure of these elements reveals that they are essentially identical to the element Cylinder with Elastic Crank connected to either *ForceExcitation* and the *TorqueExcitation* elements.

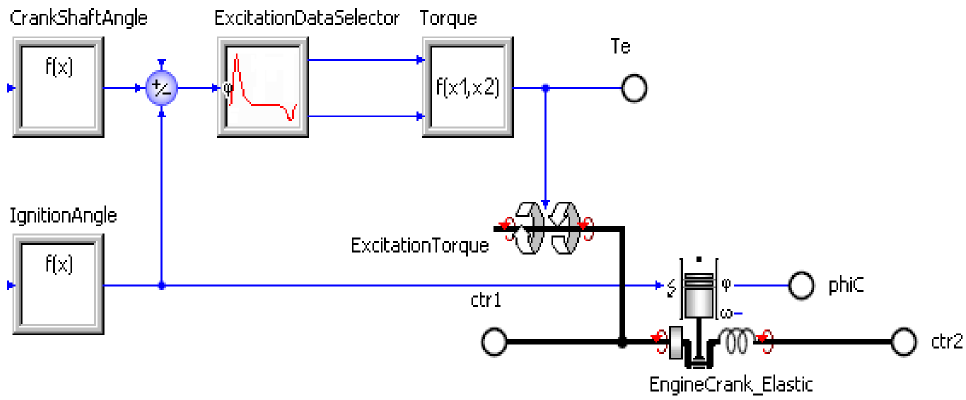

Figure 38. Model structure of ITI cylinder element with torque excitation [80]

To avoid excessiveness and redundancy within the scope of this research, the application of the available ITI cylinder elements has been investigated but is not represented within this result, because they produce identical results as the ones obtained with the *Cylinder with Elastic Crank* connected to elements modelling force or torque excitation.

However, the availability of their substructures proven to be crucial for this entire research as it enables free excitation modelling, thus providing the insight for comprehensive practical understanding of theoretical background incorporated within *Harmonic Synthesis* element. This element represents the signal block used to compute periodic signal described by its harmonic components, thereby representing vibrations at discrete frequencies. Various methods can be used to describe the output signal. The enumeration of computation methods, frequency, and period input results in 16 distinct variants, as outlined in Table 2. which details the computation approaches, required coefficients, and their utilization. Parameterization includes defining the reference value, constants, coefficients, computation method, frequency and period input, as well as the fundamental frequency and period.

Table 2. Computation variants and required input data [80]

Computation variants	**Required inputs (apart from constant *c*)**
$R_i \cdot \cos(X - \varphi_{0i})$	R_i, φ_{0i}, f_i or p_i
$A_i \cdot \cos(X) + B_i \sin(X)$	A_i, B_i, f_i or p_i
$R_i \cdot \cos(X - \varphi_{0i})$	f_0 or *per*, R_i, φ_{0i}, O_i
$A_i \cdot \cos(X) + B_i \sin(X)$	f_0 or *per*, A_i, B_i, O_i
$R_i \cdot \cos(X + \varphi_{0i})$	R_i, φ_{0i}, f_i or p_i
$A_i \cdot \cos(X) - B_i \sin(X)$	A_i, B_i, f_i or p_i
$R_i \cdot \cos(X + \varphi_{0i})$	f_0 or *per*, R_i, φ_{0i}, O_i
$A_i \cdot \cos(X) - B_i \sin(X)$	f_0 or *per*, A_i, B_i, O_i
$R_i \cdot \sin(X - \varphi_{0i})$	R_i, φ_{0i}, f_i or p_i
$A_i \cdot \sin(X) - B_i \cos(X)$	A_i, B_i, f_i or p_i
$R_i \cdot \sin(X - \varphi_{0i})$	f_0 or *per*, R_i, φ_{0i}, O_i
$A_i \cdot \sin(X) - B_i \cos(X)$	f_0 or *per*, A_i, B_i, O_i
$R_i \cdot \sin(X + \varphi_{0i})$	R_i, φ_{0i}, f_i or p_i
$A_i \cdot \sin(X) + B_i \cos(X)$	A_i, B_i, f_i or p_i
$R_i \cdot \sin(X + \varphi_{0i})$	f_0 or *per*, R_i, φ_{0i}, O_i
$A_i \cdot \sin(X) + B_i \cos(X)$	f_0 or *per*, A_i, B_i, O_i

Here A_i and B_i are coefficients of the *i-th* component, f_i is i^{th} fundamental frequency, p_i is i^{th} period, *per* is fundamental period, O_i is order, R_i magnitude (amplitude of the harmonic *i*) and φ_{0i} phase (phase position of the harmonic *i*).

This signal block computes the output variable *y* based on the specified computation variant and input parameters in which *c* is constant. There are several computation relations, shown in Table 3, in respect to reference variable.

Table 3. Calculation basis for magnitude, phase input and Fourier transformations [80]

If reference variable is the simulation time: $X = 2\pi \cdot f_i t$	
Fourier transformation	**Consideration of magnitude and phase**
$y = c + \sum_{i=1}^{n} \left[A_i \cos\left(2\pi \cdot f_i t\right) + B_i \sin\left(2\pi \cdot f_i t\right) \right]$	$y = c + \sum_{i=1}^{n} R_i \cos\left(2\pi \cdot f_i t - \varphi_{0i}\right)$
$y = c + \sum_{i=1}^{n} \left[A_i \cos\left(2\pi \cdot f_i t\right) - B_i \sin\left(2\pi \cdot f_i t\right) \right]$	$y = c + \sum_{i=1}^{n} R_i \cos\left(2\pi \cdot f_i t + \varphi_{0i}\right)$
$y = c + \sum_{i=1}^{n} \left[A_i \sin\left(2\pi \cdot f_i t\right) - B_i \cos\left(2\pi \cdot f_i t\right) \right]$	$y = c + \sum_{i=1}^{n} R_i \sin\left(2\pi \cdot f_i t - \varphi_{0i}\right)$
$y = c + \sum_{i=1}^{n} \left[A_i \sin\left(2\pi \cdot f_i t\right) + B_i \cos\left(2\pi \cdot f_i t\right) \right]$	$y = c + \sum_{i=1}^{n} R_i \sin\left(2\pi \cdot f_i t + \varphi_{0i}\right)$
If reference variable is connected to the signal input *x*: $X = \frac{2\pi}{p_i} \cdot x$	
Fourier transformation	**Consideration of magnitude and phase**
$y = c + \sum_{i=1}^{n} \left[A_i \cos\left(\frac{2\pi}{p_i} \cdot x\right) + B_i \sin\left(\frac{2\pi}{p_i} \cdot x\right) \right]$	$y = c + \sum_{i=1}^{n} R_i \cos\left(\frac{2\pi}{p_i} \cdot x - \varphi_{0i}\right)$
$y = c + \sum_{i=1}^{n} \left[A_i \cos\left(\frac{2\pi}{p_i} \cdot x\right) - B_i \sin\left(\frac{2\pi}{p_i} \cdot x\right) \right]$	$y = c + \sum_{i=1}^{n} R_i \cos\left(\frac{2\pi}{p_i} \cdot x + \varphi_{0i}\right)$
$y = c + \sum_{i=1}^{n} \left[A_i \sin\left(\frac{2\pi}{p_i} \cdot x\right) - B_i \cos\left(\frac{2\pi}{p_i} \cdot x\right) \right]$	$y = c + \sum_{i=1}^{n} R_i \sin\left(\frac{2\pi}{p_i} \cdot x - \varphi_{0i}\right)$
$y = c + \sum_{i=1}^{n} \left[A_i \sin\left(\frac{2\pi}{p_i} \cdot x\right) + B_i \cos\left(\frac{2\pi}{p_i} \cdot x\right) \right]$	$y = c + \sum_{i=1}^{n} R_i \sin\left(\frac{2\pi}{p_i} \cdot x + \varphi_{0i}\right)$

Table 4. presents conversion relations between orders, frequencies, coefficient, as well as magnitudes and phases.

Table 4. Conversion relation of frequency to order and coefficients to magnitude/phase [80]

Relation in change between…	Reference variable: simulation time *t*	Reference variable: input *x*
Frequency $\rightarrow$ Order	$f_i = f_0 \cdot O_i$	$p_i = per / O_i$
Coefficient $\downarrow$ Magnitude/phase	$A_i = R_i \cdot \cos(\varphi_{0i})$ $B_i = R_i \cdot \sin(\varphi_{0i})$	
	$R_i = \sqrt{A_i^2 + B_i^2}$ $\varphi_{0i} = \arctan\left(\frac{B_i}{A_i}\right)$	

When entering the parameters in this block, the user should take care whether the given phase angles correspond to the respective harmonic or the fundamental frequency. In brief, engine excitation modelling enables detailed dynamic analysis through pressure and torque inputs.

5.5.3. TVA inline cylinder

The TVA package includes elements for modelling the combustion engine cylinders, covering both inline and V-engine types. The TVA inline cylinder element incorporates the crank element derived from the *Cylinder with Elastic Crank* element. Its geometry, stiffness, and damping parameters remain consistent with this element. The model accounts for both rotating and reciprocating masses, with crank stiffness and damping represented by the internal spring-damper system. The element structure is illustrated in Figure 39, highlighting its role as the component in inline engine models.

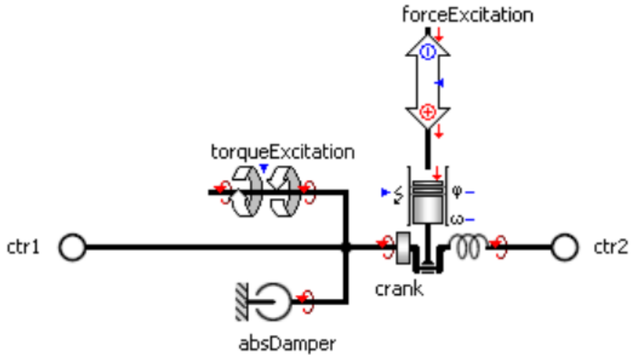

Figure 39. Model structure of TVA inline cylinder [80]

On the inertia side, the crank connects to the substructure at the ctr_1 connector, while on the spring-damper side, it connects at the ctr_2 connector. An absolute damper, linked to the inertia, models speed-dependent energy losses. The excitation torque is provided by *torqueExcitation* element and acts on the inertia side, whereas the excitation forces is provided from *forceExcitation* element and acts on the piston side. Within this element, excitation forces or torques are introduced and selected during parametrization in the properties dialog tab, whose description is applicable to all cylinder elements available in the SimulationX libraries.

In general, engine cylinders are expected to operate under either normal or misfiring conditions. In the TVA excitation models, these conditions are represented by the normalized injection and misfiring parameters. In the natural frequency analysis, the forces or torques act as the spring between the piston or crankshaft and the environment, so they have adverse effect to the results unless the excitation in these has been turned off during the calculation of natural frequencies. The normalized injection parameter controls the excitation by defining the actual load state. Based on this value, the model interpolates between the provided torque or pressure curves. The misfiring parameter, on the other hand, identifies the misfiring cylinder, which is then excited by the drag load curve, what also showed to be completely wrong and produced disastrous calculation results in the actual cases of misfiring cylinders. This curve can either be defined internally or computed by extrapolation to zero. The force excitation is calculated based on the cylinder pressure in the combustion chamber and the cylinder bore, which determines the pressure area. The torque excitation, acting on the crank, is computed using torque curves. For each excitation model, two curves are required to represent two load states (pressures or torques). Also, by using the normalized injection parameter, the interpolation is performed to obtain the correct pressure or torque. Additionally, the Boolean parameter (set as true or false) is used as switch to allow for the excitation to be on or off. When set to true, the excitation forces or torques are active; when set to false, the force and torque are zero. It is important to note that when the excitation is off, this represents the cylinder with open valves, meaning no compression or expansion occurs.

In TVA inline cylinder element, excitation can be set as either *Cylinder Pressure Excitation* or *Crank Torque Excitation*, for which the excitation data entered either as T*wo Curves for 2 Load States* or *Two Parameters*. In first case, two pressure or two torque curves ($p_{CylCurve1}$, $p_{CylCurve2}$ or $T_{eCurve1}$, $T_{eCurve2}$) are defined for two load states. In the second case, the pressure and torque parameters (p_{Cyl1}, p_{Cyl2} or T_{e1}, T_{e2}.) are defined for two load states. For both cases the injection parameters (inj_1, inj_2) specify the load states for which the parameters are provided. In second option, the values can be constant numbers, analytical expressions, or reference expressions. This will not be discussed further, because it has not been utilized in this research.

The crankshaft angle φ_{CS} is usually measured at the flywheel side of the engine model and whose default value is reference to the input signal. Together with the firing angle ψ, the curves will be evaluated. In the case of two curves for 2 load states the computation base of the excitation, namely of the pressures and torques for the given load states (p_{Cyl1x}, p_{Cyl2x}, T_{e1x}, T_{e2x}) are as follows:

$$p_{Cyl1x} = p_{CylCurve1}\left(\varphi_{CS} - \psi\right) \tag{121}$$

$$p_{Cyl2x} = p_{CylCurve2}\left(\varphi_{CS} - \psi\right) \tag{122}$$

$$T_{e1x} = T_{eCurve1}\left(\varphi_{CS} - \psi\right) \tag{123}$$

$$T_{e2x} = T_{eCurve2}\left(\varphi_{CS} - \psi\right) \tag{124}$$

If cylinder operates in normal firing conditions, the resulting cylinder pressure p_{Cyl} is determined by interpolating the injection parameter *inj* using the following expression:

$$p_{Cyl} = \frac{\left(inj - inj_1\right)\cdot\left(p_{Cylx2} - p_{Cylx1}\right)}{\left(inj_2 - inj_1\right)} + p_{Cylx1} \tag{125}$$

Resulting excitation torque *Te* is determined as:

$$T_e = \frac{\left(inj - inj_1\right)\cdot\left(T_{ex2} - T_{ex1}\right)}{\left(inj_2 - inj_1\right)} + T_{ex1} \tag{126}$$

Resulting excitation force F_e is computed using cylinder bore d_{cyl} by following expression:

$$F_e = \frac{\pi \cdot d_{cyl}^2 \cdot p_{Cyl}}{4} \tag{127}$$

In the case of the misfiring cylinder, no interpolation is performed, and the excitation force is defined as in (127), with resulting cylinder pressure and torque equal to p_{Cyl1x} and T_{Cyl1x}.

In brief, modelling of engine excitation in combustion cylinders involves integrating various elements to simulate the complex dynamics of pressure and torque excitation. The next section discusses the process of entering loading components into SimulationX, focusing on the preparation and integration of engine and propeller excitation data for simulation. It outlines the methods used to incorporate technical specifications and vibration data for system evaluation.

5.6. Preparation and entry of input data

In this research, several simulation models were developed to evaluate the proposed hypothesis and to achieve the objectives of this dissertation. During the verification and validation of the developed models, the preparation and entry of input data, particularly the engine excitation data, proved to be a challenging step that could lead to significant errors in the obtained results. Generally, the technical specifications of the propulsion system components were obtained directly from the shipyard. In the case of engine specifications or certain elements, such as the elastic coupling, the technical specifications were obtained directly from the manufacturer.

In SimulationX input of technical specifications, i.e. the geometric characteristics of the shaft line components and the propeller, represents the straightforward and simple process that does not require preparation but only careful attention when specifying physical units. However, the same is not the case with input of engine excitation data. Although engine excitation data can be requested and obtained from the engine manufacturer in the form of harmonic components, their preparation and entry in the SimulationX cylinder elements proven to be somewhat ambiguous and demanding task.

This research investigates available options within the cylinder elements that allow for the input of engine excitation in the form of cylinder pressure, crank torque, or as harmonic components expressed as excitation torque and tangential pressure. For this purpose, several VBA programs that were developed long ago by the Croatian Register of Shipping R&D staff, were employed, with the theoretical background for each provided in Appendix A. The program *S06HarmSynth* was used to determine the combustion gas pressures in cylinder and the crank torque for two load states, namely full and drag load. To conduct harmonic analysis of engine parameters the program *S02CrankL* was used. Propeller loading which accounts for losses due to friction between cylinder and cylinder liner was determined using the program *S06PropLaw*. Calculations of free vibrations were also conducted using the *S06ViBra* program to verify the simulated analysis of natural frequencies.

5.6.1. Loading components for TVC in the SimulationX

In the SimulationX, the input of prepared loading (engine and propeller) components for TVC are exemplified for the case of container ship propulsion system. The ship features direct configuration of propulsion system equipped with main engine MAN B&W 12K98ME-C Mark 7, with nominal power of 72240 kW at 104 rpm, directly coupled with solid six bladed propeller. The propeller loading is defined using two options of the propeller element, namely the *Propeller curve at nominal point* and *Combinator curve*. The first option is the straightforward process that does not require data preparation, whereas the second option necessitates data preparation. In this case, the data is prepared using the CRS *S06PropLaw* program, as shown in Figure 40.

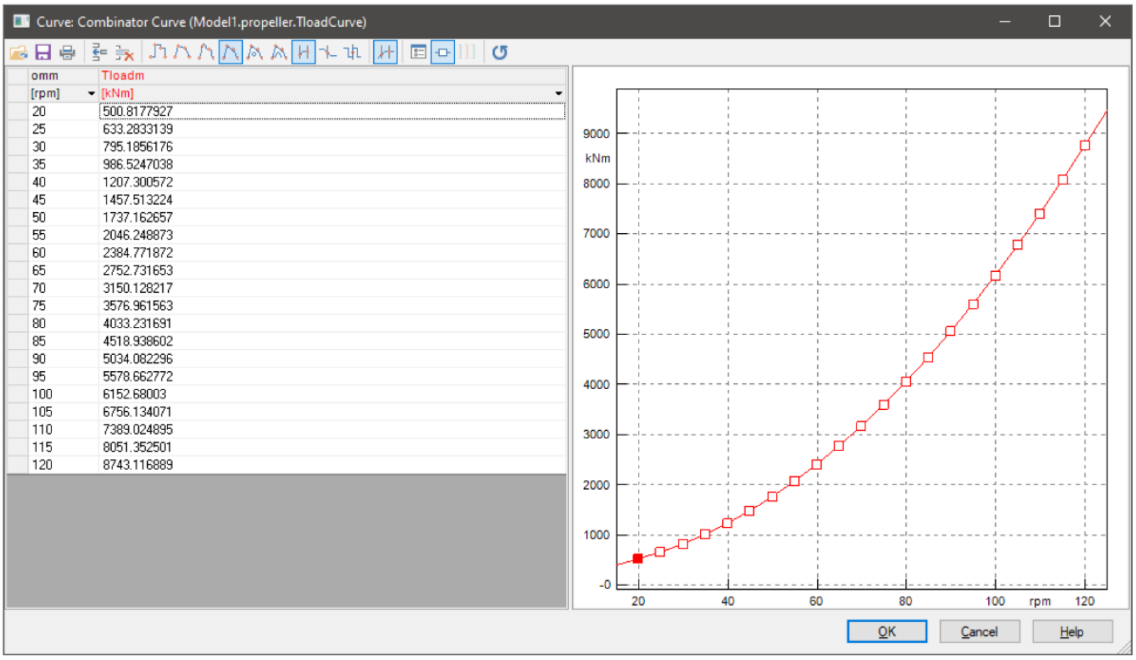

Figure 40. Prepared loading components for the propeller

Vibration data for the specific engine, shown in Figure 41, are provided directly from the manufacturer´s extranet service platform Nexus as harmonic components of tangential pressure termed T243795 for normal firing state and Tm43795 for misfiring state.

VIBRATION DATA / HARMONIC COMPONENTS

NAVIGATION : HOME / INFO

STANDARD RATING >>

ME-C : NOX - MODE : UPRATED

ENGINE TYPE	MK -	BORE [m]	STROKE [m]	CYLD [m]	POWER [kW]	MCR [r/min]	Pe [bar]	Pi [bar]	PD [bar]	PMAX [bar]	Tangential Normal	Radial Normal	Tangential Misfir	Radial Misfir
K98ME-C	7	0.98	2.4	1.75	6020	104	19.2	20.2	1	150	T243795	R243796	Tm43795	Rm43796

Figure 41. Acquisition of vibration data for engine MAN B&W 12K98ME-C Mark 7 [91]

The engine's MCR is calculated by multiplying the power per cylinder by the total number of cylinders. Indicated P_i and effective P_e pressures are given, allowing the drag pressure to be determined as their difference, and mechanical efficiency as their ratio. To enter acquired vibration data in SimulationX, the engine loading components are prepared in the form of cylinder pressure, crank torque and harmonic components expressed as excitation pressure and torque or tangential pressure. In SimulationX, the engine loading data must be prepared for the three load states, namely normal, misfiring and idling, of which the last is defined through drag load curve.

Using available entry options in TVA cylinder model element, engine loading data can be entered in form of cylinder pressure, as shown in Figure 42.

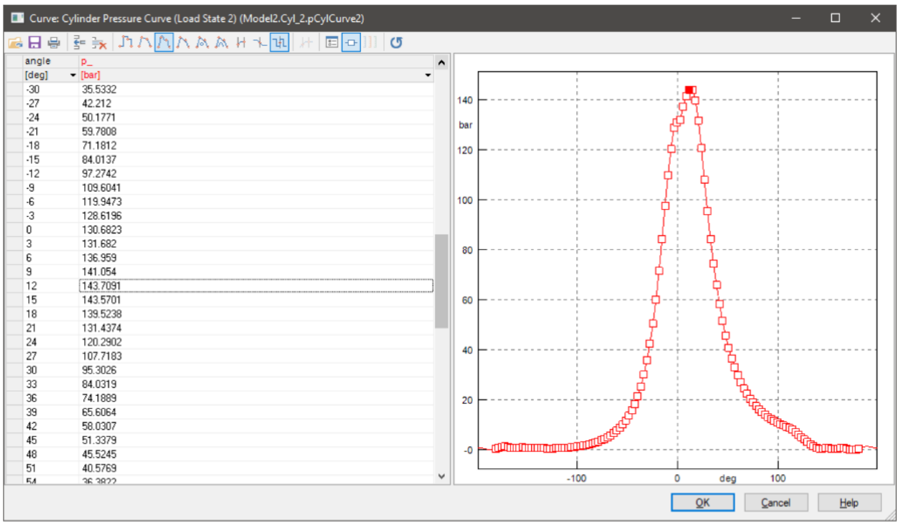

a) Normal firing

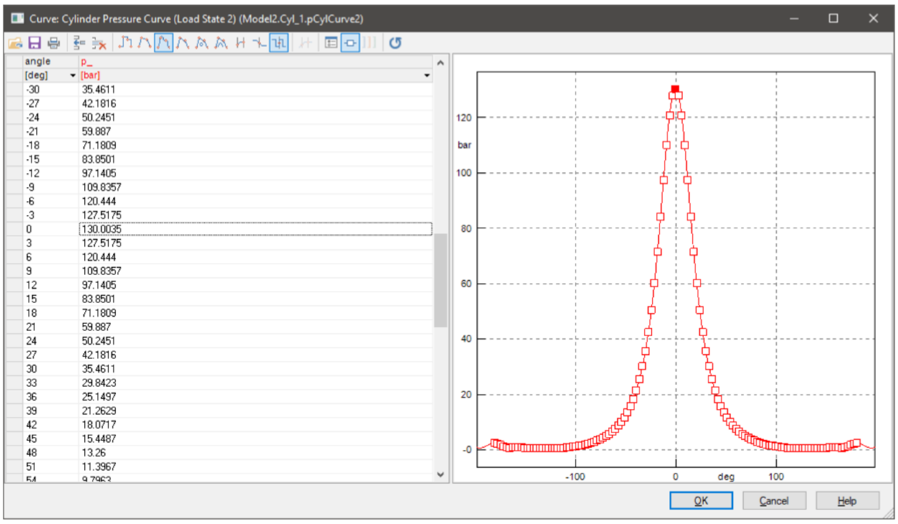

b) Misfire

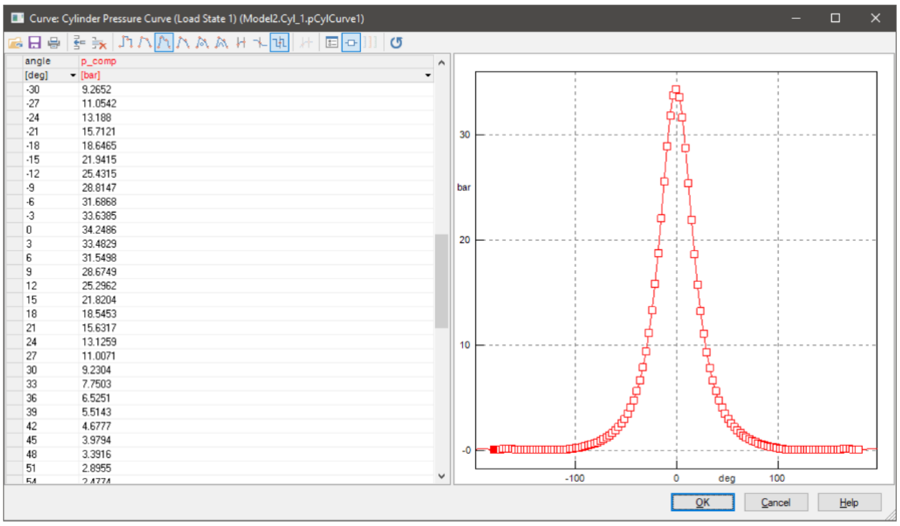

c) Drag load

Figure 42. Cylinder pressure excitation in TVA cylinder element for different load states

In TVA cylinder model elements, the engine loading data can also be entered in form of crank torque, as shown in Figure 43.

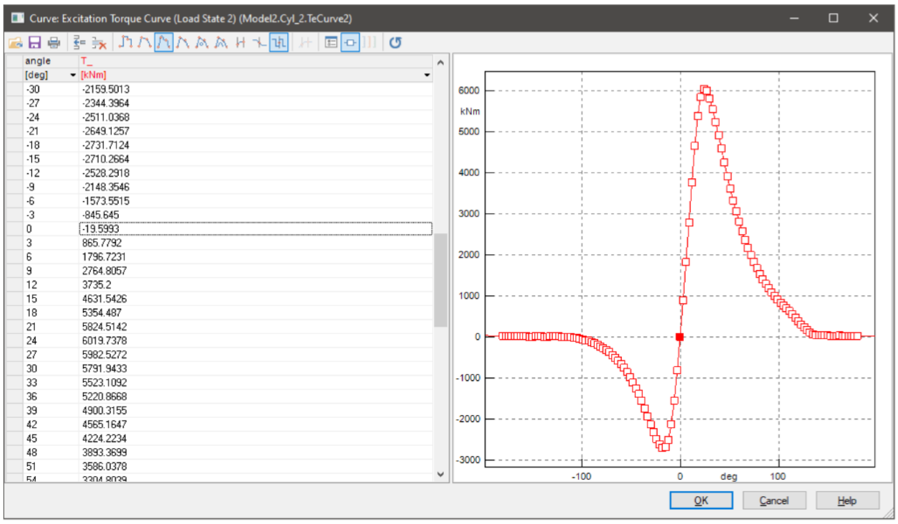

a) Normal firing

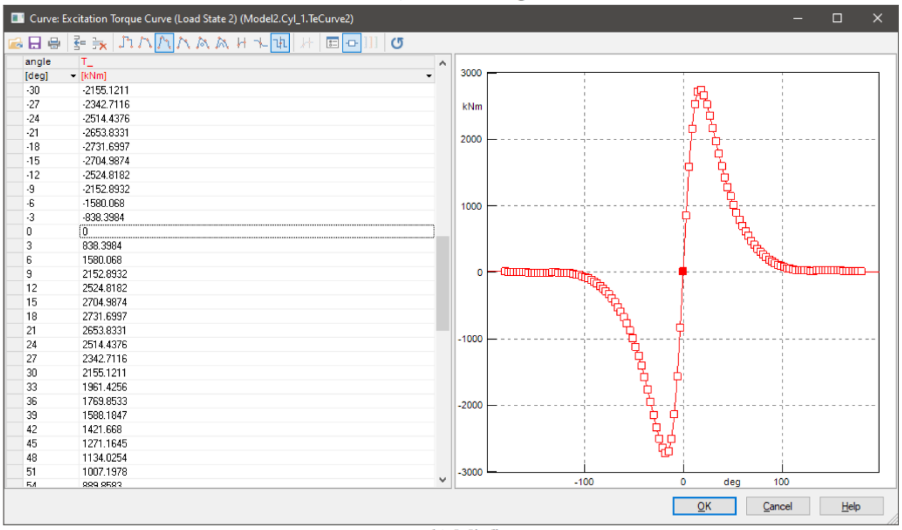

b) Misfire

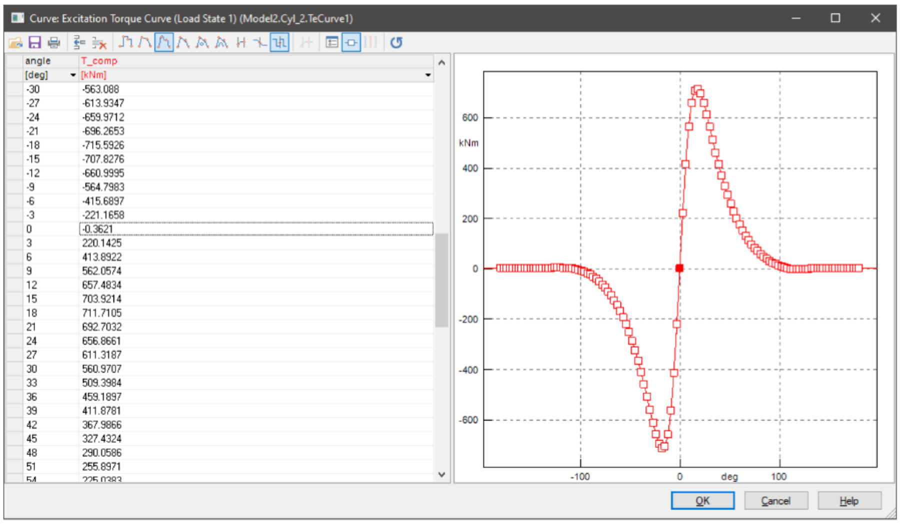

c) Drag load

Figure 43. Crank torque excitation in TVA cylinder element for different load states

Preparation and input of engine loading data in form of harmonic components, expressed as excitation torque, is shown in Figure 44.

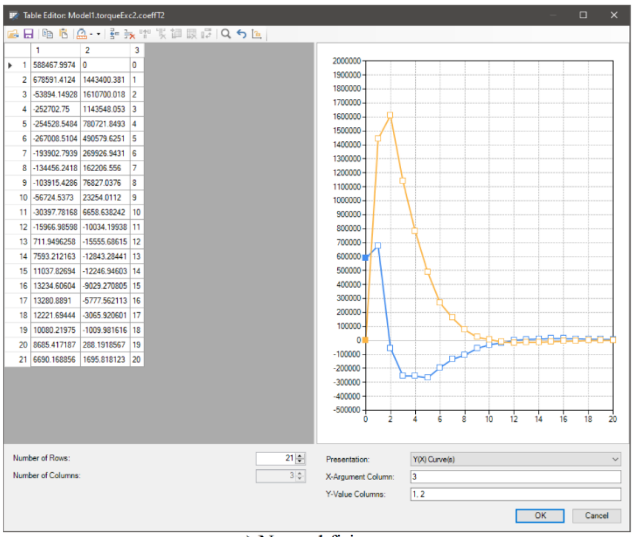

a) Normal firing

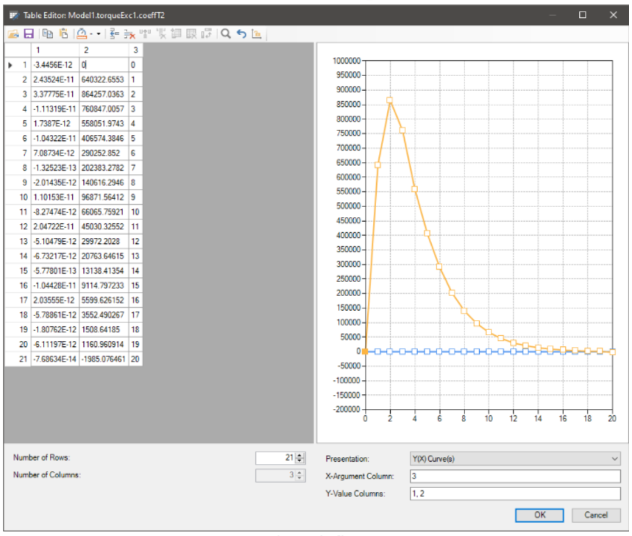

b) Misfire

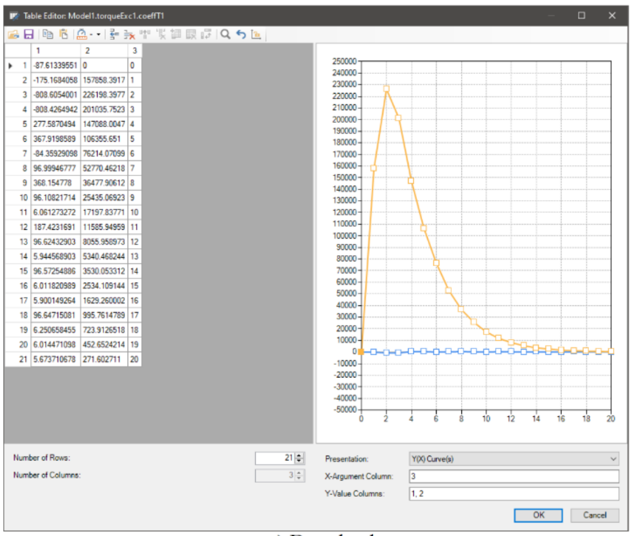

c) Drag load

Figure 44. Harmonic components expressed as excitation torque for different load states

Engine loading data prepared in the form of harmonic components can also be expressed as cylinder pressure, which is not presented, or as tangential pressure as illustrated in Figure 45.

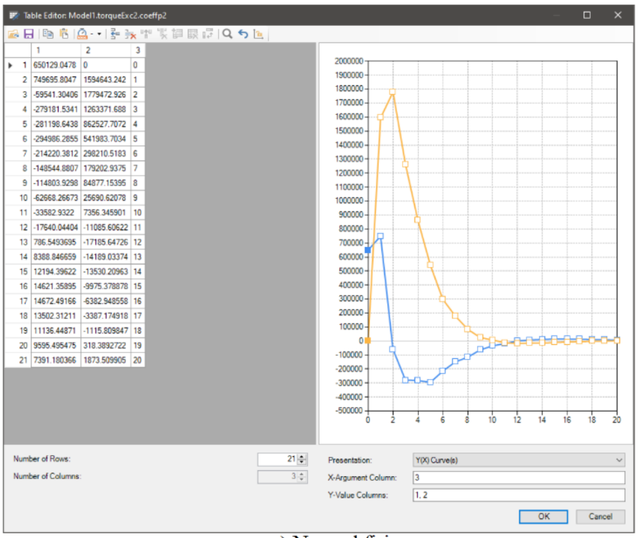

a) Normal firing

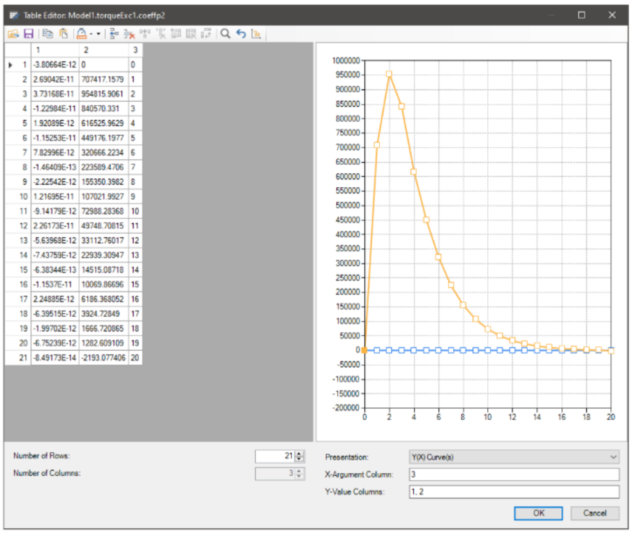

b) Misfire

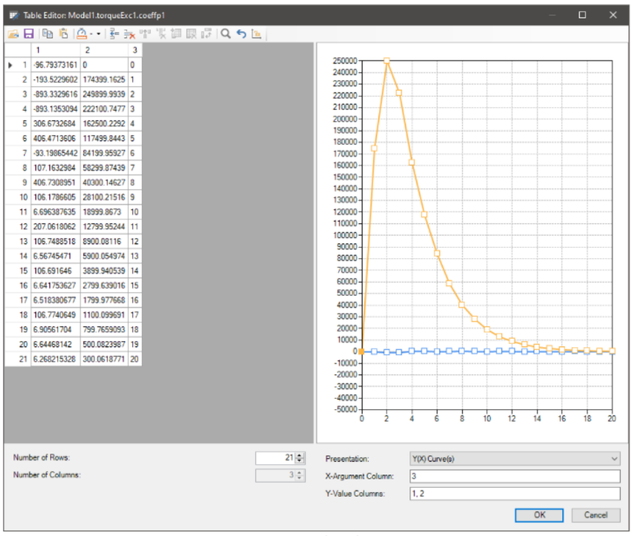

c) Drag load

Figure 45. Harmonic components expressed as tangential pressure for different load states

The essential step in the preparation of engine loading data in the case of harmonic components involves proper adjusting of physical quantities according to the International System of Units (SI). The option for entering engine load in form of harmonic components expressed as tangential pressure (defined the force acting on the crank pin of the crankshaft in tangential direction per unit area of the piston) is crucial for verification of prepared data, because engine manufacturers typically provide excitation data in the form of harmonics expressed in form of tangential pressure. Additionally, the engine loading is tested in the form of harmonic components expressed as pressure excitation, but this is omitted from the illustrations to avoid redundancy.

In the following chapter, the developed simulation models for ship propulsion systems are presented in detail. These models represent various case studies, each with the unique configuration and set of parameters. The following subsections describe the structure, result evaluations for each of the simulation models. A comparative analysis of the simulation results, including verification and validation, is also provided to demonstrate the accuracy and reliability of the models.

6. SIMULATION MODELS AND RESULTS

This chapter presents the structure of developed simulation models of ship propulsion systems, that have been chosen as the basis for the entire doctoral research, along with the comprehensive evaluation of the obtained simulation results. Simulation models are created using several options available in the SimulationX software, of which all cover both normal and misfiring operating conditions. For each option, the obtained simulation results are mutually compared, verified, and validated using other relevant sources. The comparison graphs of total torsional stress amplitude are presented for the simulation model which provides results that are the best match in terms of verification and validation.

6.1. Simulation model structure

In this research, simulation modelling method is applied to conduct TVA of ship propulsion systems. For this purpose, different simulation models are developed to represent properties and characteristics of ship propulsion systems. Developed models physically represent the direct propulsion system configuration, maintain the same modelling structure in each case. Presented modelling structure is provided in expanded form, meaning that each engine cylinder, along with its appropriate excitation, is represented as the single unit using designated element. This form is used to account for engines with odd number of cylinders. Although the real ship propulsion systems in direct configuration are characterized by their straight-line form, for illustration purposes the developed simulation models are compactly structured with shaft line placed below the engine cylinders.

These models are basically structured by appropriately interconnecting selected SimulationX element types, needed for accurate representation of properties of the system, such as inertia, stiffness and damping, as well as the excitation sources. In general, in ship propulsion systems the combustion engine is used to generate necessary power to move the ship, while the propeller represents the load on the propulsion system. When analysing propulsion system as vibration system, the combustion engine represents main source of vibration, especially torsional vibration, while the propeller acts as the element with dominant mass moment of inertia and damping, though it can also produce torsional excitation by its blades. For the sake of consistency and due to extensive number of elements in certain models, only the simplest modelling structure is illustrated, as it does not require additional elements for modelling the engine excitation.

In developed simulation models, the dynamic response of the marine shaft line is only accounted for torsional vibrations, meaning that the following TVA does not consider the influence of the ship structure vibration, namely the vibration from the hull, neither the coupling effects of torsional vibration with axial or lateral vibration.

6.2. Evaluation, verification and validation of simulation results

The evaluation of simulation results obtained through developed SimulationX models for TVA of ship propulsion systems is performed through tabular comparison. Each developed simulation model is investigated for normal and misfiring operating conditions, with obtained results for each condition represented in two tables.

In general, first table contains colour coded rows, with the first row set as blue and containing the reference data, i.e. verification data, which represents calculation results obtained using some other software tool. In this research, the GTORSI program was used for this purpose, except in the 12 cylinder case where shipyard TVC results were also available and set as reference.

Fourteen simulation models, placed across green rows in tables, were developed for each case of real ship propulsion system examined within this research. The SimulationX is powerful software with many different simulation capabilities. In this research, seven simulation models were developed to examine the SimulationX capabilities for TVA of ship propulsion system for both normal and misfiring operating conditions. However, to incorporate additional propeller loading evaluation, it was necessary to develop additional seven model from the initial simulation models, resulting in total of fourteen models per investigated propulsion system. The last row is in white colour and it contains validation results obtained experimentally by performing on board measurements of torsional vibration during sea trails.

In the middle columns, results related to the initial three natural frequencies are contained. Total torsional stress expressed in terms of maximum amplitudes is contained in the following columns on the right side. Critical speed is determined for several points along the shaft line, which are selected and determined as suitable and sufficient for evaluation of maximum torsional stress amplitude. These points refer to different shaft line component, namely stress on the crank at the last cylinder, thrust shaft, intermediate shaft and propeller shaft. In the 12 cylinder case, the shipyard TVC are provided in terms angular displacement of the first engine cylinder and the propeller shaft, thereby such observation stress points are covered using SimulationX and incorporated for that case. For each simulation model, the obtained results incorporate values of critical speed and torsional stress (or angular displacements). In the last column on the right side, these values are statistically evaluated as average squared deviations. This provides the average value of the squared deviations about the arithmetic mean for the set of selected values.

The verification step is integrated within the first table by comparing obtained simulation results against the reference, i.e. the verification results. The GTORSI program is selected for this purpose, as it is numerously proven in practice. This can be supported with recent research [24], in which the authors used the TVC program *Nauticus Torsional Vibrations, Version 12.3.89*, developed by DNV GL, which is obviously only an upgraded version of GTORSI program MAN Diesel & Turbo. In the case with the shipyard TVC results, the GTORSI results are verified along with SimulationX results. In addition to verification process, complete TVA reports from both programs are presented in the Appendix C and D.

The validation step is also integrated within the first table by comparing obtained simulation results against the result from on board measurements, i.e. the validation results. Regardless of the construction date difference among the investigated ship propulsion system, torsional vibration measurements during sea trials were conducted using the strain gauge method. This method involves application of strain gauges along with appropriate instrumentation data for recording and transmitting signal. Purpose of this onboard vibration testing is to validate calculation results for the first newly built ships in series. The vibration test reports contain necessary ship data, conditions during measurements, instrumentation data, description of measurement method, block diagram and measuring position, as well as measurement results and analysis. Experimental measurement results are given in form of graph, so the tool *Graph Grabber 2.0*, developed by Quintessa, was used to extract values of data points from the available graph image in each case.

As this research incorporates the extensive number of simulation models, as well as number of simulation result, single table would be too large to include all evaluation data. Therefore, second table, added below the first one, contains the relative values defined as ratio of simulation value to the reference value and expressed in percentages.

The evaluation, verification and validation steps of obtained results are conducted for both normal and misfiring operating conditions and represent numerical analysis of amplitude values. However, TVC determines values for discrete time intervals, which are collected and graphically represented. Graphical comparisons are represented for the best matching SimulationX model in each case, thus providing the graphical analysis of the obtained result along the complete operating range of the engine.

The following section will cover investigated simulation models along with numerical and graphical representation of the obtain simulation results. Basic description of examined ship propulsion systems is also provided.

6.3. Simulation models

For this research four simulation models of ship propulsion systems are developed and analysed as case studies. Each case features direct configuration in which marine two-stroke Diesel engine is used as propulsion engine. Although similar in many aspects, each propulsion system includes distinctive features, with the number of engine cylinders varying in each case. In all simulation models the excitation is the consequence of gas forces in the engine cylinders and the inertia forces due to reciprocating motion of masses within these cylinders. The selection of case studies is also based upon the availability of verification and validation data. The structure of each simulation model, along with the comparison of results and graphs, is presented in the following sections.

6.3.1. Model 5S50 - propulsion system of 24533 GT bulk carrier

Simulation model *5S50*, shown in Figure 46, represents propulsion system of bulk carrier and her gross tonnage (GT) is 24533. It consists of one two-stroke slow-speed five-cylinders inline marine Diesel engine MAN B&W 5S50MC with MCR of 7150 kW at 127 rpm. Also, the system contains intermediate (diameter 325 mm) and propeller shaft (diameter 423 mm), and the solid fixed pitch 4-bladed propeller (diameter 5400 mm, mean pitch 4039 mm and area ratio 0.572). The propulsion shafting model for TVA discretized the actual system into 10 concentrated masses, each represented by its mass moments of inertia, connected by shafts represented by means of torsional springs. Absolute damping at certain masses is expressed in terms of dynamic magnifiers, while relative damping occurring between shaft line masses is expressed within spring-damper elements.

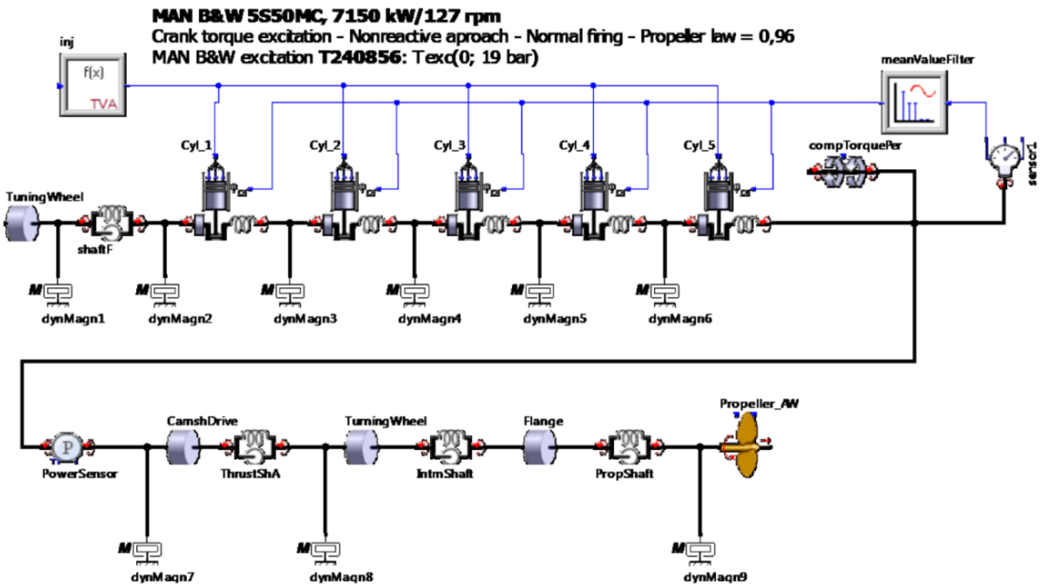

Figure 46. Structure of simulation model 5S50

Evaluation, verification and validation of natural frequencies and torsional stress amplitudes of the model *5S50* under normal firing conditions are shown in Figure 47.

SimulationX evaluation of TVA — **MAN B&W 5S50MC, 7150 kW/127 rpm, comparison of results**

Excitation S06HarmSynt — Propeller law torque load factor: default = 1,00 otherwise = *

Normal firing

Compare results at critical speeds

case	program	system	excitation	natural frequencies n1 [rpm]	n2 [rpm]	n3 [rpm]	critical speed [rpm]	total tors. stress max. amplitude: tors. stress cylinder 5 [MPa]	tors. stress thrust shaft [MPa]	tors. stress inter. shaft [MPa]	tors. stress propeller shaft [MPa]	notes	average squ. deviation [%]
1	GTORSI, v3.6.4	5S50MC	tang. press. coeff. T240856	**310,6**	**1587,0**	**3222,2**	**61,9**	**27,0**	**28,9**	**118,7**	**65,6**	**reference**	
2	SimX, v3.8	5x TVAcyl, cyl. press. nonreact.	exc T240856 pCyl(0 19 bar)	310,6	1587,0	3222,1	61,7	24,7	26,5	108,7	60,0		3,4
3	SimX, v3.8	5x TVAcyl, crnk. torq. nonreact.	exc T240856 Texc(0 19 bar)	310,6	1587,0	3222,1	62,1	25,4	27,2	112,0	61,9		2,3
4	SimX, v3.8	5x TVAcyl, cyl. press. nonreact.*0,96	exc T240856 pCyl(0 19 bar)	310,6	1587,0	3222,1	61,8	26,2	28,0	115,2	63,6		1,2
5	SimX, v3.8	5x TVAcyl, crnk. torq. nonreact. *0,96	exc T240856 Texc(0 19 bar)	310,6	1587,0	3222,1	62,1	26,9	28,9	118,9	65,7	best match	0,1
6	SimX, v3.8	5x ForceExc, nonreact.	exc T240856 pCyl(0 19 bar)	310,6	1587,0	3222,1	61,8	26,6	28,4	116,8	64,5		0,6
7	SimX, v3.8	5x ForceExc HarmComp, nonreact.	exc T240856 HC_pCyl(0 19 bar)	310,6	1587,0	3222,1	61,7	26,6	28,5	116,9	64,5		0,6
8	SimX, v3.8	5x ForceExc, nonreact. *0,96	exc T240856 pCyl(0 19 bar)	310,6	1587,0	3222,1	61,8	28,1	30,1	123,8	68,3		1,7
9	SimX, v3.8	5x ForceExc HarmComp, nonreact. *0,96	exc T240856 HC_pCyl(0 19 bar)	310,6	1587,0	3222,1	61,8	28,2	30,1	123,8	68,4		1,7
10	SimX, v3.8	5x TorquExc, nonreact.	exc T240856 Texc(0 19 bar)	310,6	1587,0	3222,1	62,2	27,1	29,1	119,7	66,1	2nd match	0,3
11	SimX, v3.8	5x TorquExc HarmComp, nonreact.	exc T240856 pTan(0 19 bar)	310,6	1587,0	3222,1	62,2	27,3	29,3	120,4	66,5	3rd match	0,5
12	SimX, v3.8	5x TorquExc HarmComp, nonreact.	exc T240856 Texc(0 19 bar)	310,6	1587,0	3222,1	62,2	27,3	29,3	120,4	66,5	3rd match	0,5
13	SimX, v3.8	5x TorquExc, nonreact. *0,96	exc T240856 Texc(0 19 bar)	310,6	1587,0	3222,1	62,1	28,8	30,9	127,0	70,2		2,7
14	SimX, v3.8	5x TorquExc HarmComp, nonreact. *0,96	exc T240856 pTan(0 19 bar)	310,6	1587,0	3222,1	62,1	28,9	31,0	127,8	70,6		3,0
15	SimX, v3.8	5x TorquExc HarmComp, nonreact. *0,96	exc T240856 Texc(0 19 bar)	310,6	1587,0	3222,1	62,1	28,9	31,0	127,8	70,6		3,0
16	BIS Validation	Result of Sea Trial, norm. firing					62,8			109,5		intm. shaft, GphGrabb.	3,9

Relative values [%]

case	program	system	excitation	n1	n2	n3	critical speed	tors. stress cylinder 5	tors. stress thrust shaft	tors. stress inter. shaft	tors. stress propeller shaft	notes
1	GTORSI, v3.6.4	5S50MC	tang. press. coeff. T240856	0,0%	0,0%	0,0%	0,0%	0,0%	0,0%	0,0%	0,0%	reference
2	SimX, v3.8	5x TVAcyl, cyl. press. nonreact.	exc T240856 pCyl(0 19 bar)	0,0%	0,0%	0,0%	-0,4%	-8,3%	-8,4%	-8,4%	-8,5%	
4	SimX, v3.8	5x TVAcyl, cyl. press. nonreact.*0,96	exc T240856 pCyl(0 19 bar)	0,0%	0,0%	0,0%	-0,2%	-2,9%	-3,0%	-3,0%	-3,0%	
3	SimX, v3.8	5x TVAcyl, crnk. torq. nonreact.	exc T240856 Texc(0 19 bar)	0,0%	0,0%	0,0%	0,3%	-5,9%	-5,8%	-5,6%	-5,7%	
5	SimX, v3.8	5x TVAcyl, crnk. torq. nonreact. *0,96	exc T240856 Texc(0 19 bar)	0,0%	0,0%	0,0%	0,4%	-0,2%	-0,1%	0,2%	0,1%	best match
6	SimX, v3.8	5x ForceExc, nonreact.	exc T240856 pCyl(0 19 bar)	0,0%	0,0%	0,0%	-0,1%	-1,5%	-1,6%	-1,6%	-1,7%	
8	SimX, v3.8	5x ForceExc, nonreact. *0,96	exc T240856 pCyl(0 19 bar)	0,0%	0,0%	0,0%	-0,2%	4,3%	4,2%	4,3%	4,2%	
9	SimX, v3.8	5x ForceExc HarmComp, nonreact. *0,96	exc T240856 HC_pCyl(0 19 bar)	0,0%	0,0%	0,0%	-0,2%	4,4%	4,3%	4,3%	4,2%	
10	SimX, v3.8	5x TorquExc, nonreact.	exc T240856 Texc(0 19 bar)	0,0%	0,0%	0,0%	0,4%	0,5%	0,7%	0,9%	0,8%	2nd match
13	SimX, v3.8	5x TorquExc, nonreact. *0,96	exc T240856 Texc(0 19 bar)	0,0%	0,0%	0,0%	0,3%	6,6%	6,8%	7,0%	7,0%	
11	SimX, v3.8	5x TorquExc HarmComp, nonreact.	exc T240856 pTan(0 19 bar)	0,0%	0,0%	0,0%	0,4%	1,1%	1,3%	1,4%	1,4%	3rd match
14	SimX, v3.8	5x TorquExc HarmComp, nonreact. *0,96	exc T240856 pTan(0 19 bar)	0,0%	0,0%	0,0%	0,3%	7,2%	7,4%	7,6%	7,6%	
12	SimX, v3.8	5x TorquExc HarmComp, nonreact.	exc T240856 Texc(0 19 bar)	0,0%	0,0%	0,0%	0,4%	1,1%	1,3%	1,4%	1,4%	3rd match
15	SimX, v3.8	5x TorquExc HarmComp, nonreact. *0,96	exc T240856 Texc(0 19 bar)	0,0%	0,0%	0,0%	0,3%	7,2%	7,4%	7,6%	7,6%	
16	BIS Validation	Result of Sea Trial, norm. firing					1,5%			-7,8%		intm. shaft, GphGrabb.

Figure 47. Comparison of simulation results for model 5S50 under normal firing conditions

For model *5S50* under normal firing conditions across the complete engine operating range, the torsional stress in the intermediate shaft is presented graphically in Figure 48. This includes the best-case simulation results from Figure 47. along with verification and validation data.

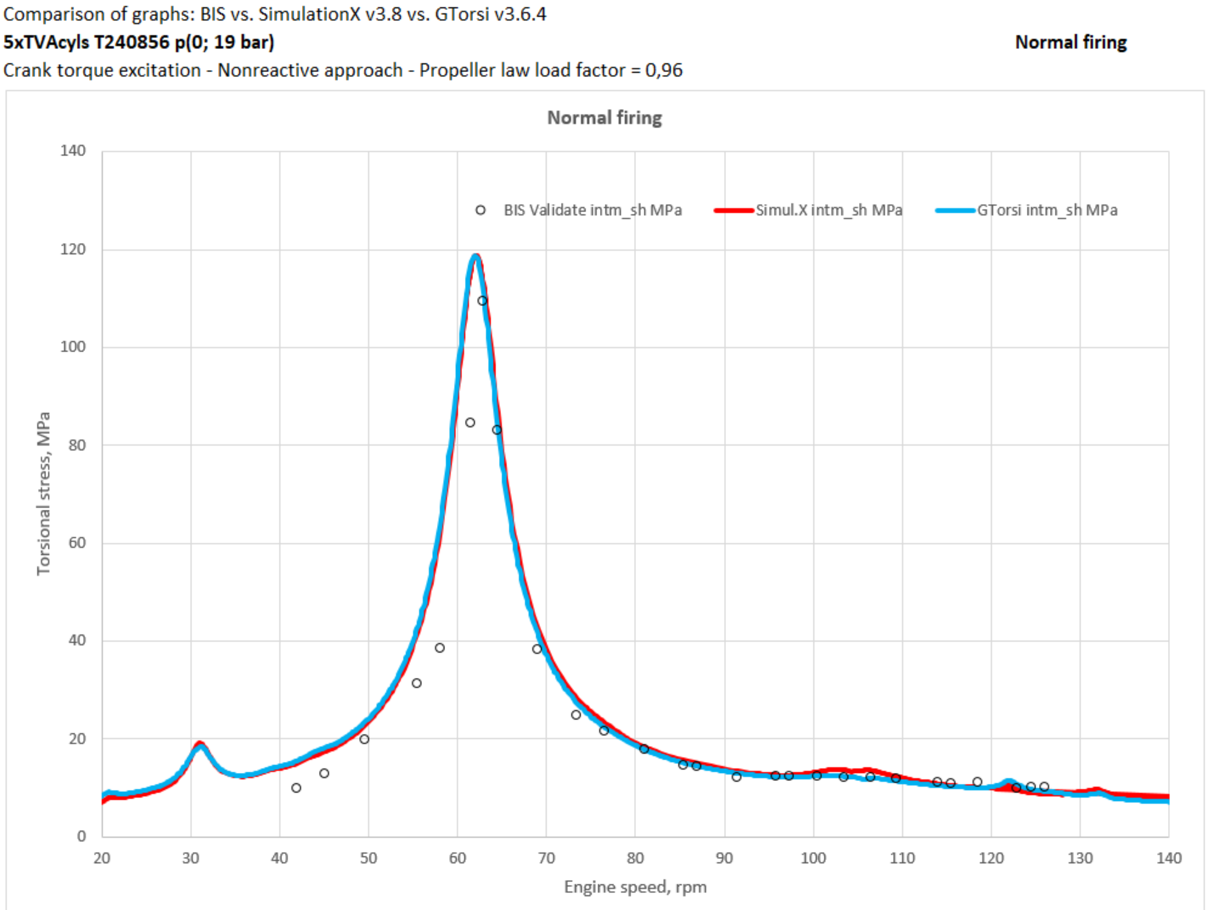

Figure 48. Graphical comparison of torsional stress results in the intermediate shaft for model 5S50 under normal firing conditions

The torsional stress in thrust shaft and propeller shaft for model *5S50*, under normal firing conditions across the complete engine operating range, is presented graphically in Figure 49, for the best-case simulation results from Figure 47, together with verification and validation data.

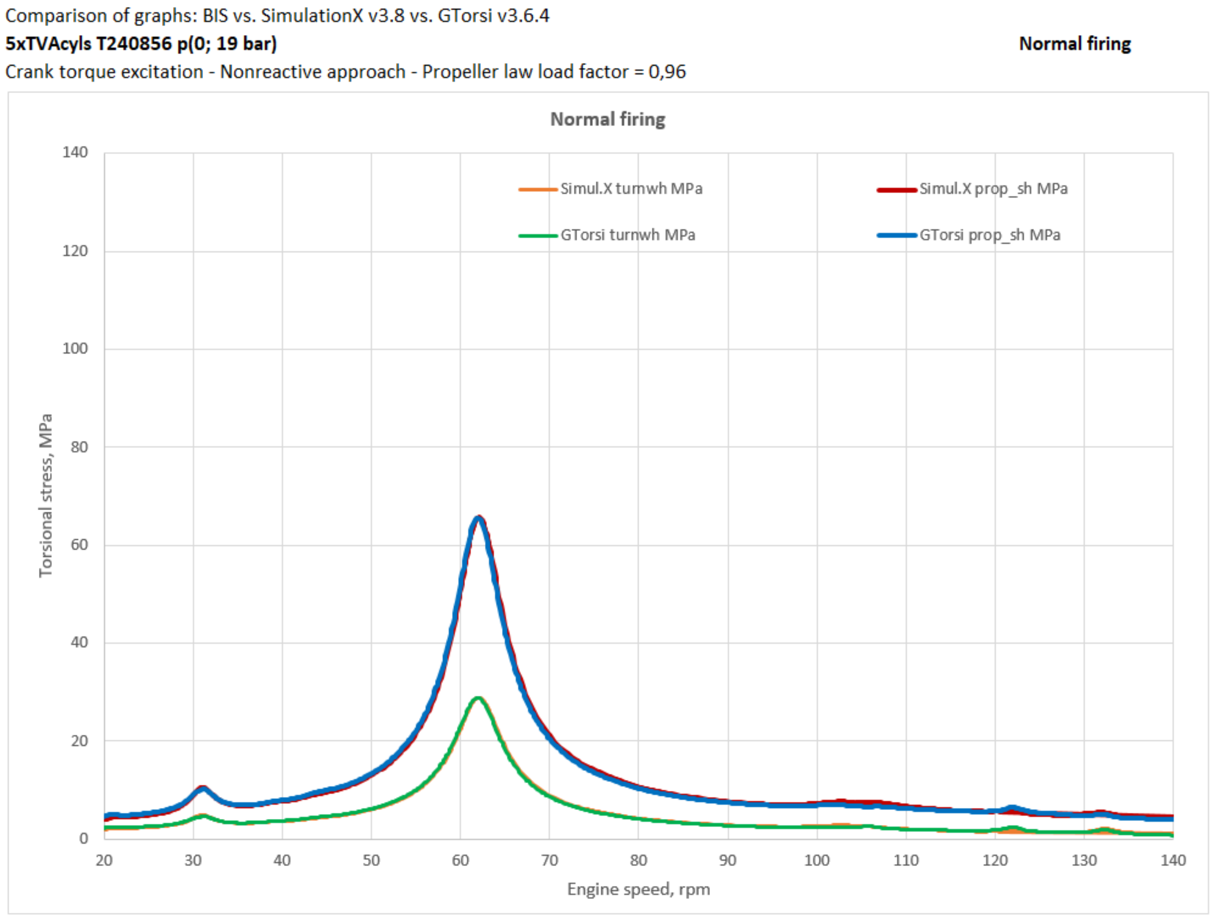

Figure 49. Graphical comparison of torsional stress results in thrust shaft and propeller shaft for model 5S50 under normal firing conditions

Simulation results for natural frequencies and torsional stress amplitudes of the model *5S50* under misfiring conditions are evaluated, verified and validated as shown in Figure 50.

SimulationX evaluation of TVA — **MAN B&W 5S50MC, 7150 kW/127 rpm, comparison of results**

Excitation S06HarmSynt — Propeller law torque load factor: default = 1,00 otherwise = *

Misfiring cylinder 5				natural frequencies			tors. stress max. ampl.					tors. stress max. ampl.						
case	*program*	*system*	*excitation*	*n1*	*n2*	*n3*	*critical speed 1*	*tors. stress cylinder 5*	*tors. stress thrust shaft*	*tors. stress inter. shaft*	*tors. stress propeller shaft*	*critical speed 2*	*tors. stress cylinder 5*	*tors. stress thrust shaft*	*tors. stress inter. shaft*	*tors. stress propeller shaft*	*notes*	*average squ. deviation*
				[rpm]	[rpm]	[rpm]	[rpm]	[MPa]	[MPa]	[MPa]	[MPa]	[rpm]	[MPa]	[MPa]	[MPa]	[MPa]		[%]
1	GTORSI, v3.6.4	5S50MC	tang. press. coeff. Tm40856	**310,6**	**1587,0**	**3222,2**	**62,0**	**27,1**	**30,4**	**124,9**	**68,9**	**104,4**	**17,2**	**14,5**	**60,6**	**33,5**	**reference**	
2	SimX, v3.8	5x TVAcyl, cyl. press. nonreact.	exc T2/Tm40856 pCyl(0 19 bar)	310,6	1587,0	3222,1	61,8	27,6	29,5	120,9	66,7	103,3	13,5	14,3	60,4	33,4	2nd match	2,2
3	SimX, v3.8	5x TVAcyl, crnk. torq. nonreact.	exc T2/Tm40856 Texc(0 19 bar)	310,6	1587,0	3222,1	62,2	28,3	30,2	124,3	68,7	104,3	14,2	14,6	62,4	34,5	best match	1,9
4	SimX, v3.8	5x TVAcyl, cyl. press. nonreact.*0,96	exc T2/Tm40856 pCyl(0 19 bar)	310,6	1587,0	3222,1	61,8	29,3	31,2	128,2	70,8	102,8	13,1	13,9	60,2	33,3		2,6
5	SimX, v3.8	5x TVAcyl, crnk. torq. nonreact. *0,96	exc T2/Tm40856 Texc(0 19 bar)	310,6	1587,0	3222,1	62,2	30,2	32,3	132,7	73,3	104,3	14,4	14,9	63,7	35,2		2,4
6	SimX, v3.8	5x ForceExc, nonreact.	exc T2/Tm40856 pCyl(0 19 bar)	310,6	1587,0	3222,1	61,8	29,5	31,5	129,2	71,3	103,0	14,1	15,0	63,4	35,0	3rd match	2,3
7	SimX, v3.8	5x ForceExc HarmComp, nonreact.	exc T2/Tm40856 pCyl(0 19 bar)	310,6	1587,0	3222,1	61,8	30,0	32,0	131,1	72,4	103,0	16,2	16,5	67,3	37,2		2,6
8	SimX, v3.8	5x ForceExc, nonreact. *0,96	exc T2/Tm40856 pCyl(0 19 bar)	310,6	1587,0	3222,1	61,8	31,3	33,4	137,0	75,7	103,0	13,7	14,7	63,3	35,0		3,1
9	SimX, v3.8	5x ForceExc HarmComp, nonreact. *0,96	exc T2/Tm40856 pCyl(0 19 bar)	310,6	1587,0	3222,1	61,8	31,4	33,5	137,5	75,9	103,0	14,0	14,6	63,4	35,1		3,1
10	SimX, v3.8	5x TorquExc, nonreact.	exc T2/Tm40856: Texc(0 19 bar)	310,6	1587,0	3222,1	62,2	30,2	32,3	132,6	73,2	104,1	14,9	15,2	65,5	36,2		2,4
11	SimX, v3.8	5x TorquExc HarmComp, nonreact.	exc T2/Tm40856 pTan(0 19 bar)	310,6	1587,0	3222,1	62,1	30,3	32,4	133,3	73,6	104,1	14,9	15,2	65,6	36,3		2,5
12	SimX, v3.8	5x TorquExc HarmComp, nonreact.	exc T2/Tm40856 Texc(0 19 bar)	310,6	1587,0	3222,1	62,1	30,3	32,4	133,3	73,6	104,1	14,9	15,2	65,6	36,3		2,5
13	SimX, v3.8	5x TorquExc, nonreact. *0,96	exc T2/Tm40856 Texc(0 19 bar)	310,6	1587,0	3222,1	62,2	32,2	34,4	141,5	78,2	104,1	15,3	15,5	66,9	37,0		3,6
14	SimX, v3.8	5x TorquExc HarmComp, nonreact. *0,96	exc T2/Tm40856 pTan(0 19 bar)	310,6	1587,0	3222,1	62,2	32,4	34,6	142,3	78,6	104,1	15,2	15,5	67,1	37,1		3,7
15	SimX, v3.8	5x TorquExc HarmComp, nonreact. *0,96	exc T2/Tm40856 Texc(0 19 bar)	310,6	1587,0	3222,1	62,2	32,4	34,6	142,3	78,6	104,1	15,2	15,5	67,1	37,1		3,7

Relative values [%]																	
case	*program*	*system*	*excitation*	*n1*	*n2*	*n3*	*critical speed 1*	*tors. stress cylinder 5*	*tors. stress thrust shaft*	*tors. stress inter. shaft*	*tors. stress propeller shaft*	*critical speed 2*	*tors. stress cylinder 5*	*tors. stress thrust shaft*	*tors. stress inter. shaft*	*tors. stress propeller shaft*	*notes*
1	GTORSI, v3.6.4	5S50MC	tang. press. coeff. Tm40856														reference
2	SimX, v3.8	5x TVAcyl, cyl. press. nonreact.	exc T2/Tm40856 pCyl(0 19 bar)	0,0%	0,0%	0,0%	-0,2%	1,9%	-3,1%	-3,2%	-3,2%	-1,1%	-21,5%	-1,5%	-0,2%	-0,4%	2nd match
4	SimX, v3.8	5x TVAcyl, cyl. press. nonreact.*0,96	exc T2/Tm40856 pCyl(0 19 bar)	0,0%	0,0%	0,0%	-0,4%	7,9%	2,7%	2,6%	2,6%	-1,6%	-23,9%	-4,0%	-0,7%	-0,7%	
3	SimX, v3.8	5x TVAcyl, crnk. torq. nonreact.	exc T2/Tm40856 Texc(0 19 bar)	0,0%	0,0%	0,0%	0,3%	4,3%	-0,5%	-0,4%	-0,4%	-0,1%	-17,6%	0,4%	3,0%	3,0%	best match
5	SimX, v3.8	5x TVAcyl, crnk. torq. nonreact. *0,96	exc T2/Tm40856 Texc(0 19 bar)	0,0%	0,0%	0,0%	0,3%	11,3%	6,2%	6,3%	6,3%	-0,1%	-16,3%	2,5%	5,2%	5,1%	
6	SimX, v3.8	5x ForceExc, nonreact.	exc T2/Tm40856 pCyl(0 19 bar)	0,0%	0,0%	0,0%	-0,3%	8,8%	3,6%	3,4%	3,5%	-1,3%	-18,4%	3,4%	4,7%	4,5%	3rd match
8	SimX, v3.8	5x ForceExc, nonreact. *0,96	exc T2/Tm40856 pCyl(0 19 bar)	0,0%	0,0%	0,0%	-0,3%	15,3%	9,9%	9,8%	9,8%	-1,3%	-20,2%	1,3%	4,6%	4,5%	
7	SimX, v3.8	5x ForceExc HarmComp, nonreact.	exc T2/Tm40856 pCyl(0 19 bar)	0,0%	0,0%	0,0%	-0,3%	10,7%	5,2%	5,0%	5,0%	-1,3%	-6,0%	13,5%	11,2%	11,1%	
9	SimX, v3.8	5x ForceExc HarmComp, nonreact. *0,96	exc T2/Tm40856 pCyl(0 19 bar)	0,0%	0,0%	0,0%	-0,3%	15,7%	10,3%	10,1%	10,1%	-1,3%	-18,6%	0,8%	4,8%	4,7%	
10	SimX, v3.8	5x TorquExc, nonreact.	exc T2/Tm40856: Texc(0 19 bar)	0,0%	0,0%	0,0%	0,3%	11,1%	6,1%	6,2%	6,2%	-0,3%	-13,4%	4,7%	8,2%	8,1%	
13	SimX, v3.8	5x TorquExc, nonreact. *0,96	exc T2/Tm40856 Texc(0 19 bar)	0,0%	0,0%	0,0%	0,3%	18,6%	13,3%	13,4%	13,4%	-0,3%	-11,5%	6,9%	10,5%	10,5%	
11	SimX, v3.8	5x TorquExc HarmComp, nonreact.	exc T2/Tm40856 pTan(0 19 bar)	0,0%	0,0%	0,0%	0,2%	11,8%	6,7%	6,8%	6,8%	-0,3%	-13,5%	4,7%	8,4%	8,3%	
14	SimX, v3.8	5x TorquExc HarmComp, nonreact. *0,96	exc T2/Tm40856 pTan(0 19 bar)	0,0%	0,0%	0,0%	0,3%	19,3%	13,9%	14,0%	14,0%	-0,3%	-11,6%	7,0%	10,7%	10,7%	
12	SimX, v3.8	5x TorquExc HarmComp, nonreact.	exc T2/Tm40856 Texc(0 19 bar)	0,0%	0,0%	0,0%	0,2%	11,8%	6,7%	6,8%	6,8%	-0,3%	-13,5%	4,7%	8,4%	8,3%	
15	SimX, v3.8	5x TorquExc HarmComp, nonreact. *0,96	exc T2/Tm40856 Texc(0 19 bar)	0,0%	0,0%	0,0%	0,3%	19,3%	13,9%	14,0%	14,0%	-0,3%	-11,6%	7,0%	10,7%	10,7%	

Figure 50. Comparison of simulation results for model 5S50 under misfiring conditions

Total torsional stress in the intermediate shaft across the entire engine operating range for the 5S50 model under misfiring conditions are shown as graphs in Figure 51, including the best-case simulation results from Figure 50, together with verification and validation data.

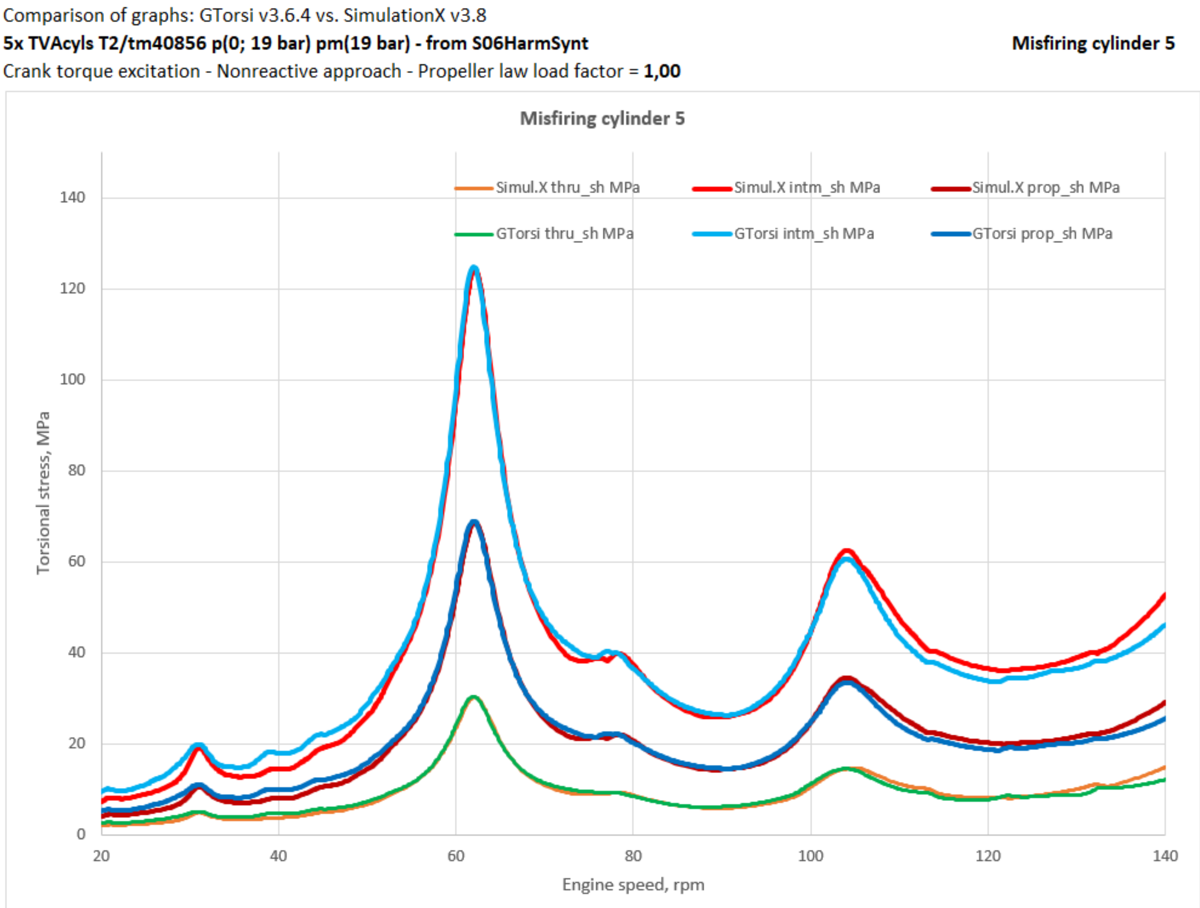

Figure 51. Graphical comparison of torsional stress results in complete shaft line for model 5S50 under misfiring conditions

6.3.2. Model 6S60 – propulsion system of 59315 GT crude oil Aframax tanker

Simulation model *6S60*, shown in Figure 52, represents propulsion system of crude oil tanker and her GT is 59315. It consists of one two-stroke slow-speed six-cylinders inline marine Diesel engine with MAN B&W 6S50MC-C Mark7, with MCR of 13560 kW at 105 rpm. Furthermore, the system contains forged intermediate (diameter 460 mm) and propeller shaft (diameter 660 mm), as well as the solid fixed pitch 4-bladed propeller (diameter 6900 mm, mean pitch 4998 mm, and area ratio 0.591). Calculation model of the propulsion shafting for the purpose of torsional vibrations analysis discretizes the actual system by means of contains the 11 concentrated masses represented by their mass moments of inertia, connected by shafts represented by means of torsional springs. The absolute damping is expressed in terms of dynamic magnifiers, on several concentrated masses, with no relative damping between any masses.

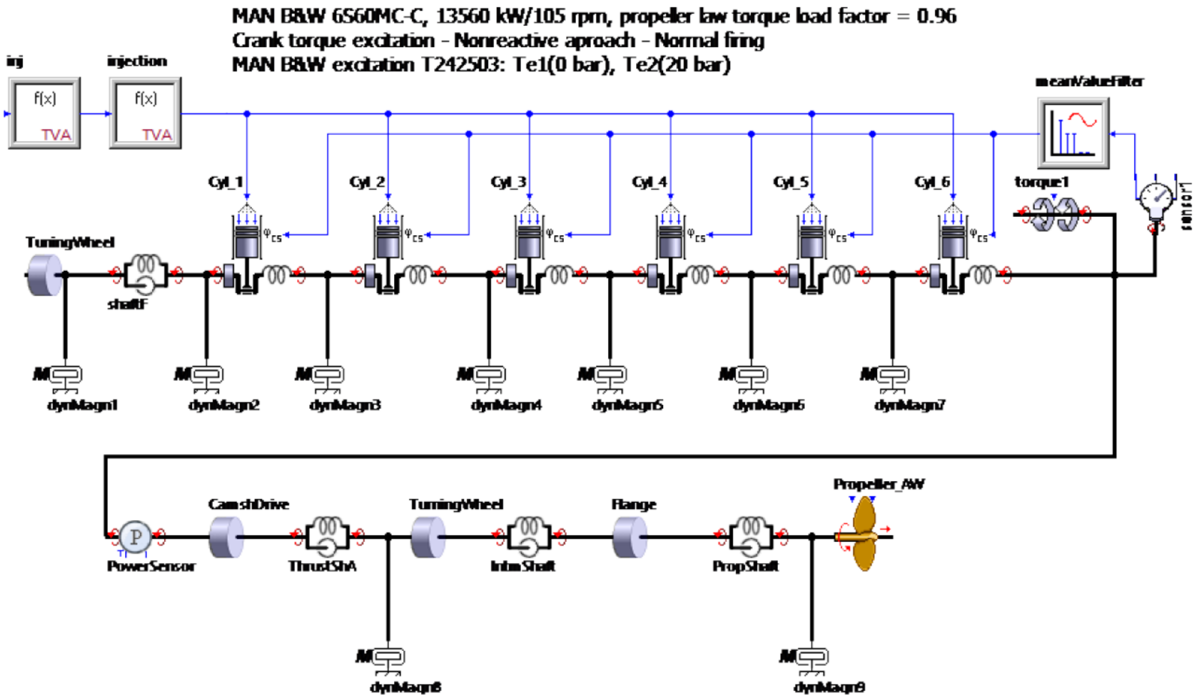

Figure 52. Structure of simulation model 6S60

The simulation results of natural frequencies and torsional stress amplitudes for the model *6S60* under normal firing conditions are evaluated, verified and validated, shown in Figure 53.

SimulationX evaluation of TVA

Excitation S06HarmSynt

MAN B&W 6S60MC-C, 13560 kW/105 rpm, comparison of results

Propeller law torque load factor: default = 1,00 otherwise = *

Normal firing

Compare results at critical speeds

case	program	system	excitation	natural frequencies n1 [rpm]	n2 [rpm]	n3 [rpm]	critical speed [rpm]	total tors. stress max. amplitude: tors. stress cylinder 6 [MPa]	tors. stress thrust shaft [MPa]	tors. stress intm. shaft [MPa]	tors. stress propeller shaft [MPa]	notes	average squ. deviation [%]
1	GTORSI, v3.6.4	5xcyl.	tang. press. coeff. T242503	**249,6**	**1072,6**	**2224,8**	**41,5**	**21,0**	**20,7**	**88,3**	**29,7**	**reference**	
2	SimX, v3.8	6x TVAcyl, cyl. press. nonreact.	exc T242503: p(0 20 bar)	249,6	1072,6	2224,8	41,4	17,4	18,1	77,2	25,9		5,5
3	SimX, v3.8	6x TVAcyl, crnk. torq. nonreact.	exc T242503: Te(0 20 bar)	249,6	1072,6	2224,8	41,6	17,8	18,5	79,0	26,6		4,7
4	SimX, v3.8	6x TVAcyl, cyl. press. nonreact.*0,96	exc T242503: p(0 20 bar)	249,6	1072,6	2224,8	41,3	18,8	19,5	83,1	27,9		2,9
5	SimX, v3.8	6x TVAcyl, cyl. press. nonreact. *0,96	exc T242503: Te(0 20 bar)	249,6	1072,6	2224,8	41,6	19,2	20,0	85,3	28,7	best match	2,1
6	SimX, v3.8	6x ForceExc, nonreact.	exc T242503: p(0 20 bar)	249,6	1072,6	2224,8	41,4	17,4	18,1	77,0	25,9		5,6
7	SimX, v3.8	6x ForceExc, nonreact. *0,96	exc T242503: p(0 20 bar)	249,6	1072,6	2224,8	41,3	18,7	19,5	72,9	27,9		4,4
8	SimX, v3.8	6x ForceExc, HC cylpress, nonreact.	exc T242503: cyl p(0 20 bar)	249,6	1072,6	2224,8	41,4	17,4	18,1	77,1	25,9		5,5
9	SimX, v3.8	6x ForceExc, HC cylpress, nonreact. *0,96	exc T242503: cyl p(0 20 bar)	249,6	1072,6	2224,8	41,3	18,8	19,5	83,1	27,9		2,9
10	SimX, v3.8	6x TorquExc, nonreact.	exc T242503: Te(0 20 bar)	249,6	1072,6	2224,8	41,6	17,6	18,3	78,3	26,3		5,0
11	SimX, v3.8	6x TorquExc HarmComp, nonreact.	exc T242503: tanp(0 20 bar)	249,6	1072,6	2224,8	41,6	17,8	18,5	78,9	26,6		4,7
12	SimX, v3.8	6x TorquExc HarmComp, nonreact.	exc T242503: exc T(0 20 bar)	249,6	1072,6	2224,8	41,6	17,8	18,5	78,9	26,6		4,7
13	SimX, v3.8	6x TorquExc, nonreact. *0,96	exc T242503: Te(0 20 bar)	249,6	1072,6	2224,8	41,5	19,0	19,8	84,5	28,4	3rd match	2,4
14	SimX, v3.8	6x TorquExc HarmComp, nonreact. *0,96	exc T242503: tanp(0 20 bar)	249,6	1072,6	2224,8	41,5	19,2	20,0	85,2	28,7	2nd match	2,1
15	SimX, v3.8	6x TorquExc HarmComp, nonreact. *0,96	exc T242503: exc T(0 20 bar)	249,6	1072,6	2224,8	41,5	19,2	20,0	85,2	28,7	2nd match	2,1
16	BIS Validation	Result of Sea Trial, norm. firing					41,4			90,0		intm. shaft, GphGrabb.	1,0

Relative values [%]

case	program	system	excitation	n1	n2	n3	critical speed	tors. stress cylinder 6	tors. stress thrust shaft	tors. stress intm. shaft	tors. stress propeller shaft	notes
1	GTORSI, v3.6.4	5xcyl.	tang. press. coeff. T242503	0,0%	0,0%	0,0%	0,0%	0,0%	0,0%	0,0%	0,0%	reference
2	SimX, v3.8	6x TVAcyl, cyl. press. nonreact.	exc T242503: p(0 20 bar)	0,0%	0,0%	0,0%	-0,3%	-16,8%	-12,4%	-12,6%	-12,6%	
3	SimX, v3.8	6x TVAcyl, crnk. torq. nonreact.	exc T242503: Te(0 20 bar)	0,0%	0,0%	0,0%	0,1%	-15,1%	-10,5%	-10,5%	-10,5%	
4	SimX, v3.8	6x TVAcyl, cyl. press. nonreact.*0,96	exc T242503: p(0 20 bar)	0,0%	0,0%	0,0%	-0,4%	-10,5%	-5,6%	-5,9%	-5,9%	
5	SimX, v3.8	6x TVAcyl, cyl. press. nonreact. *0,96	exc T242503: Te(0 20 bar)	0,0%	0,0%	0,0%	0,1%	-8,5%	-3,4%	-3,4%	-3,4%	best match
6	SimX, v3.8	6x ForceExc, nonreact.	exc T242503: p(0 20 bar)	0,0%	0,0%	0,0%	-0,3%	-17,0%	-12,6%	-12,8%	-12,8%	
7	SimX, v3.8	6x ForceExc, nonreact. *0,96	exc T242503: p(0 20 bar)	0,0%	0,0%	0,0%	-0,4%	-10,6%	-5,8%	-17,4%	-6,1%	
8	SimX, v3.8	6x ForceExc, HC cylpress, nonreact.	exc T242503: cyl p(0 20 bar)	0,0%	0,0%	0,0%	-0,3%	-16,8%	-12,4%	-12,6%	-12,6%	
9	SimX, v3.8	6x ForceExc, HC cylpress, nonreact. *0,96	exc T242503: cyl p(0 20 bar)	0,0%	0,0%	0,0%	-0,4%	-10,4%	-5,6%	-5,9%	-5,9%	
10	SimX, v3.8	6x TorquExc, nonreact.	exc T242503: Te(0 20 bar)	0,0%	0,0%	0,0%	0,1%	-15,9%	-11,3%	-11,3%	-11,3%	
11	SimX, v3.8	6x TorquExc HarmComp, nonreact.	exc T242503: tanp(0 20 bar)	0,0%	0,0%	0,0%	0,2%	-15,1%	-10,5%	-10,6%	-10,5%	
12	SimX, v3.8	6x TorquExc HarmComp, nonreact.	exc T242503: exc T(0 20 bar)	0,0%	0,0%	0,0%	0,2%	-15,1%	-10,5%	-10,6%	-10,5%	
13	SimX, v3.8	6x TorquExc, nonreact. *0,96	exc T242503: Te(0 20 bar)	0,0%	0,0%	0,0%	0,1%	-9,3%	-4,3%	-4,3%	-4,3%	3rd match
14	SimX, v3.8	6x TorquExc HarmComp, nonreact. *0,96	exc T242503: tanp(0 20 bar)	0,0%	0,0%	0,0%	0,1%	-8,5%	-3,4%	-3,4%	-3,4%	2nd match
15	SimX, v3.8	6x TorquExc HarmComp, nonreact. *0,96	exc T242503: exc T(0 20 bar)	0,0%	0,0%	0,0%	0,1%	-8,5%	-3,4%	-3,4%	-3,4%	2nd match
16	BIS Validation	Result of Sea Trial, norm. firing					-0,3%			2,0%		intm. shaft, GphGrabb.

Figure 53. Comparison of simulation results for model 6S60 under normal firing conditions

The torsional stress in the intermediate shaft for model *6S60*, under normal firing conditions across the complete engine operating range, is presented graphically in Figure 54. This includes the best-case simulation results from Figure 53. with verification and validation data.

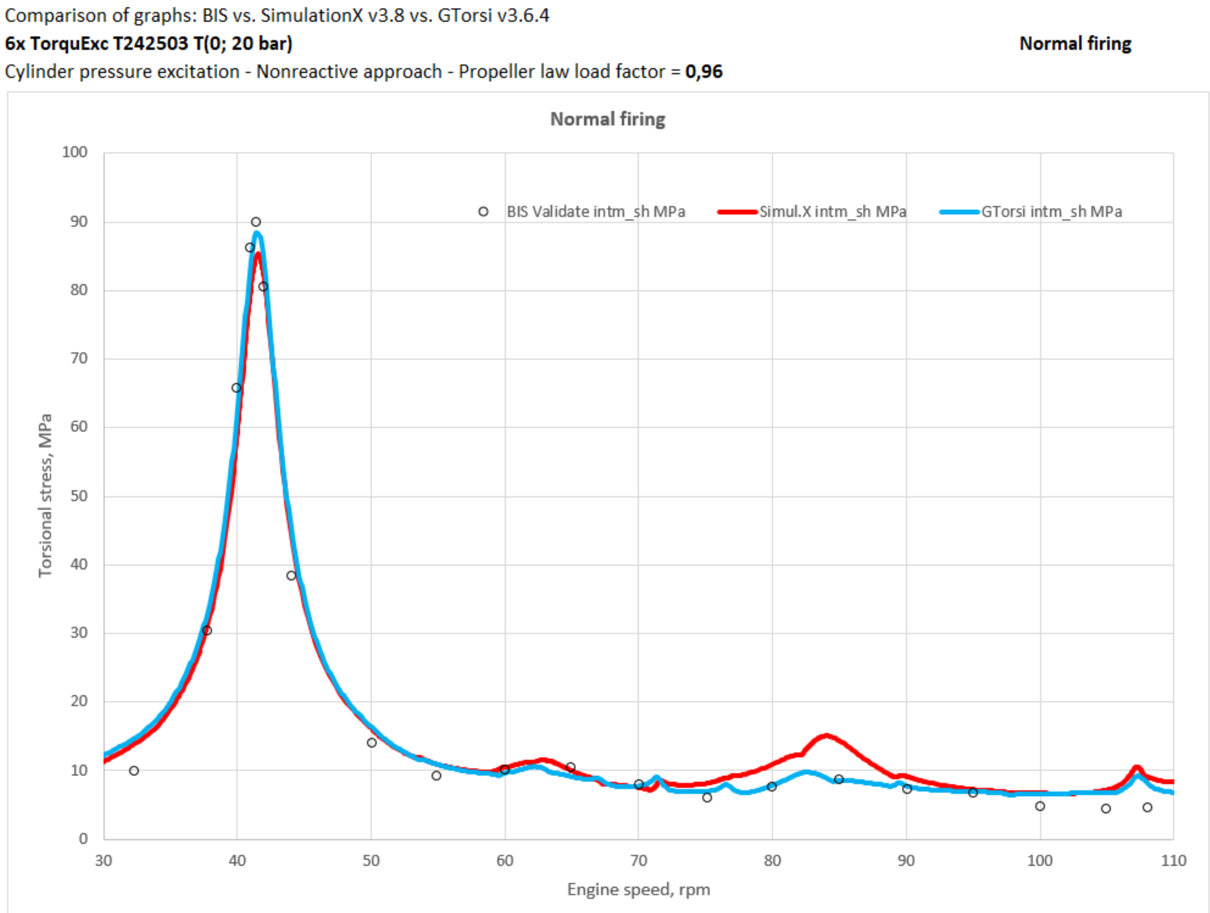

Figure 54. Graphical comparison of torsional stress results in the intermediate shaft for model 6S60 under normal firing conditions

The torsional stress in thrust shaft and propeller shaft for model *6S60*, under normal firing conditions across the complete engine operating range, is presented graphically in Figure 55. for the best-case simulation results from Figure 53. with verification and validation data.

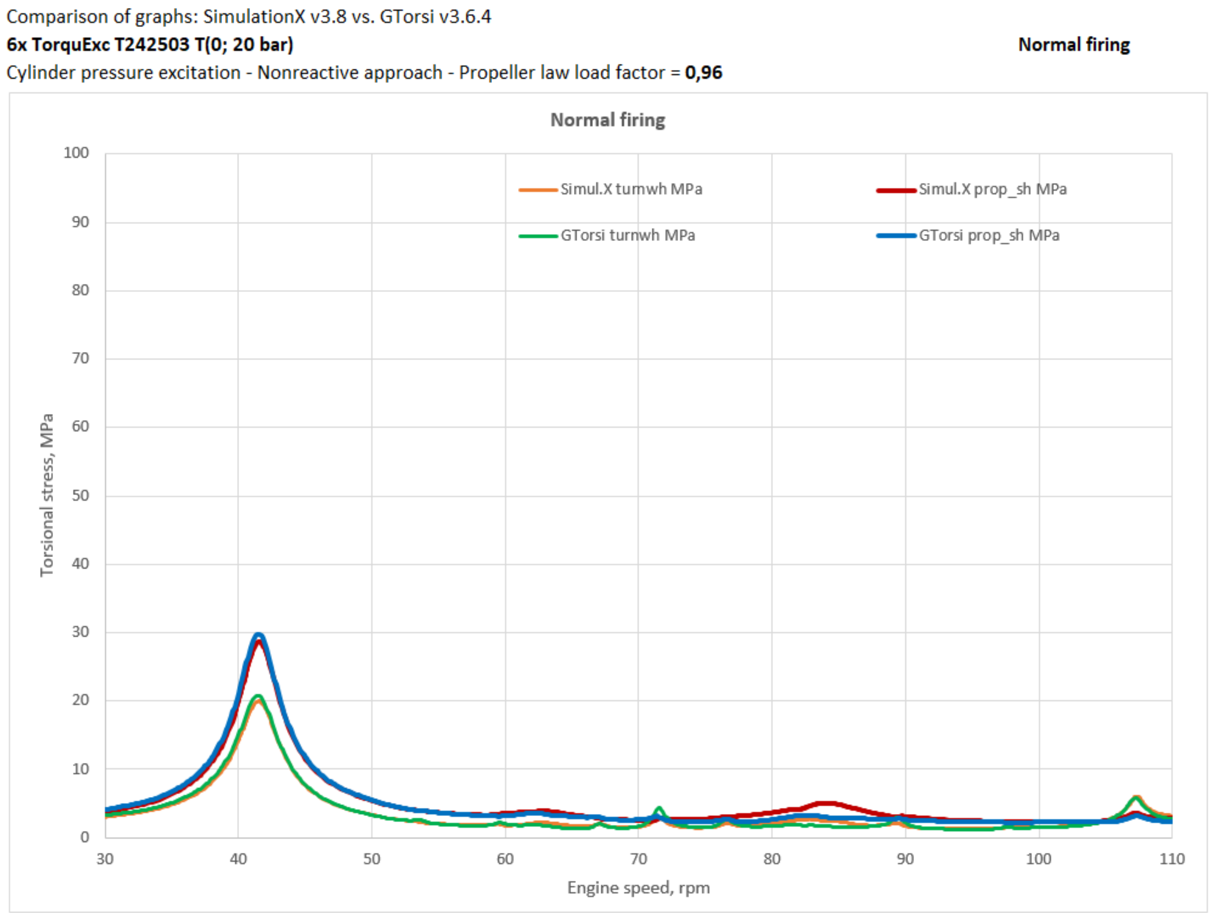

Figure 55. Graphical comparison of torsional stress results in thrust shaft and propeller shaft for model 6S60 under normal firing conditions

Evaluation, verification and validation of natural frequencies and torsional stress amplitudes of the model *6S60* under misfiring conditions are shown in Figure 56.

SimulationX evaluation of TVA

Excitation S06HarmSynt

MAN B&W 6S60MC-C, 13560 kW/105 rpm, comparison of results

Propeller law torque load factor: default = 1,00 otherwise = *

Misfiring cylinder 6

case	program	system	excitation	natural frequencies n1 [rpm]	n2 [rpm]	n3 [rpm]	critical speed 1 [rpm]	tors. stress max. ampl. tors. stress cylinder 6 [MPa]	tors. stress thrust shaft [MPa]	tors. stress inter. shaft [mrad]	tors. stress propeller shaft [mrad]	critical speed 2 [rpm]	tors. stress max. ampl. tors. stress cylinder 6 [MPa]	tors. stress thrust shaft [MPa]	tors. stress inter. shaft [mrad]	tors. stress propeller shaft [mrad]	notes	average squ. deviation [%]
1	GTORSI, v3.6.4	6S60MC-C	tang. press. coeff. T2/Tm42503	**249,6**	**1072,6**	**2224,8**	**41,5**	**21,3**	**21,7**	**92,2**	**31,0**	**82,7**	**21,2**	**16,1**	**60,6**	**20,4**	**reference**	
2	SimX, v3.8	6x TVAcyl, cyl. press. nonreact.	exc T2/Tm42503: p(0 20 bar)	249,6	1072,6	2224,8	41,4	18,8	19,6	83,0	27,9	83,0	16,6	16,2	59,3	19,9		3,0
4	SimX, v3.8	6x TVAcyl, crnk. torq. nonreact.	exc T2/Tm42503: Te(0 20 bar)	249,6	1072,6	2224,8	41,4	19,3	20,0	85,1	28,6	83,8	16,9	16,5	65,5	22,0		2,8
3	SimX, v3.8	6x TVAcyl, cyl. press. nonreact.*0,96	exc T2/Tm42503: p(0 20 bar)	249,6	1072,6	2224,8	41,3	20,5	21,3	90,2	30,3	83,0	17,0	16,7	60,8	20,4	best match	2,1
5	SimX, v3.8	6x TVAcyl, cyl. press. nonreact. *0,96	exc T2/Tm42503: Te(0 20 bar)	249,6	1072,6	2224,8	41,4	21,0	21,8	92,7	31,2	83,8	17,4	16,9	67,2	22,6	3rd match	2,4
6	SimX, v3.8	6x ForceExc, nonreact.	exc T2/Tm42503: p(0 20 bar)	249,6	1072,6	2224,8	41,4	18,8	19,5	82,8	27,8	83,4	16,5	16,2	59,0	19,9		3,1
7	SimX, v3.8	6x ForceExc, nonreact. *0,96	exc T2/Tm42503: p(0 20 bar)	249,6	1072,6	2224,8	41,4	20,4	21,2	89,9	30,2	83,4	17,0	16,6	60,9	20,5	2nd match	2,1
8	SimX, v3.8	6x ForceExc, HC cylpress, nonreact.	exc T2/Tm42503: cyl p(0 20 bar)	249,6	1072,6	2224,8	41,4	18,8	19,6	83,0	27,9	83,1	16,2	16,5	59,2	19,9		3,2
9	SimX, v3.8	6x ForceExc, HC cylpress, nonreact. *0,96	exc T2/Tm42503: cyl p(0 20 bar)	249,6	1072,6	2224,8	41,4	20,5	21,3	90,1	30,3	83,1	17,0	16,6	60,7	20,4	2nd match	2,1
10	SimX, v3.8	6x TorquExc, nonreact.	exc T2/Tm42503: Te(0 20 bar)	249,6	1072,6	2224,8	41,6	19,1	19,9	84,4	28,4	83,8	16,8	16,3	84,1	22,0		4,8
12	SimX, v3.8	6x TorquExc HarmComp, nonreact.	exc T2/Tm42503: tanp(0 20 bar)	249,6	1072,6	2224,8	41,5	19,3	20,0	85,1	28,6	83,8	16,9	16,4	65,4	22,0		2,9
14	SimX, v3.8	6x TorquExc HarmComp, nonreact.	exc T2/Tm42503: exc T(0 20 bar)	249,6	1072,6	2224,8	41,5	19,3	20,0	85,1	28,6	83,8	16,9	16,4	65,4	22,0		2,9
11	SimX, v3.8	6x TorquExc, nonreact. *0,96	exc T2/Tm42503: Te(0 20 bar)	249,6	1072,6	2224,8	41,6	20,9	21,6	91,8	30,9	83,8	17,3	16,8	67,0	22,5		2,5
13	SimX, v3.8	6x TorquExc HarmComp, nonreact. *0,96	exc T2/Tm42503: tanp(0 20 bar)	249,6	1072,6	2224,8	41,4	21,0	21,8	92,6	31,2	83,8	17,4	16,9	67,2	22,6		2,4
15	SimX, v3.8	6x TorquExc HarmComp, nonreact. *0,96	exc T2/Tm42503: exc T(0 20 bar)	249,6	1072,6	2224,8	41,5	21,0	21,8	92,6	31,2	83,8	16,4	16,9	67,2	22,6		2,8

Relative values [%]

case	program	system	excitation	n1	n2	n3	critical speed 1	tors. stress cylinder 6	tors. stress thrust shaft	tors. stress inter. shaft	tors. stress propeller shaft	critical speed 2	tors. stress cylinder 6	tors. stress thrust shaft	tors. stress inter. shaft	tors. stress propeller shaft	notes
1	GTORSI, v3.6.4	6S60MC-C	tang. press. coeff. T2/Tm42503														reference
2	SimX, v3.8	6x TVAcyl, cyl. press. nonreact.	exc T2/Tm42503: p(0 20 bar)	0,0%	0,0%	0,0%	-0,3%	-11,6%	-9,8%	-10,0%	-10,0%	0,3%	-22,0%	0,8%	-2,2%	-2,3%	
4	SimX, v3.8	6x TVAcyl, crnk. torq. nonreact.	exc T2/Tm42503: Te(0 20 bar)	0,0%	0,0%	0,0%	-0,1%	-9,3%	-7,7%	-7,6%	-7,6%	1,3%	-20,2%	2,6%	8,0%	8,1%	
3	SimX, v3.8	6x TVAcyl, cyl. press. nonreact.*0,96	exc T2/Tm42503: p(0 20 bar)	0,0%	0,0%	0,0%	-0,4%	-3,8%	-1,9%	-2,2%	-2,2%	0,3%	-19,8%	3,7%	0,4%	0,4%	best match
5	SimX, v3.8	6x TVAcyl, cyl. press. nonreact. *0,96	exc T2/Tm42503: Te(0 20 bar)	0,0%	0,0%	0,0%	-0,2%	-1,2%	0,5%	0,6%	0,6%	1,3%	-17,9%	5,5%	10,9%	11,0%	3rd match
6	SimX, v3.8	6x ForceExc, nonreact.	exc T2/Tm42503: p(0 20 bar)	0,0%	0,0%	0,0%	-0,3%	-11,9%	-10,1%	-10,2%	-10,2%	0,9%	-22,3%	0,6%	-2,7%	-2,0%	
7	SimX, v3.8	6x ForceExc, nonreact. *0,96	exc T2/Tm42503: p(0 20 bar)	0,0%	0,0%	0,0%	-0,3%	-4,1%	-2,2%	-2,4%	-2,4%	0,9%	-20,1%	3,4%	0,5%	0,6%	2nd match
8	SimX, v3.8	6x ForceExc, HC cylpress, nonreact.	exc T2/Tm42503: cyl p(0 20 bar)	0,0%	0,0%	0,0%	-0,2%	-11,7%	-9,9%	-10,0%	-10,0%	0,5%	-23,8%	2,9%	-2,3%	-2,3%	
9	SimX, v3.8	6x ForceExc, HC cylpress, nonreact. *0,96	exc T2/Tm42503: cyl p(0 20 bar)	0,0%	0,0%	0,0%	-0,2%	-3,8%	-1,9%	-2,2%	-2,2%	0,5%	-20,0%	3,5%	0,2%	0,3%	2nd match
10	SimX, v3.8	6x TorquExc, nonreact.	exc T2/Tm42503: Te(0 20 bar)	0,0%	0,0%	0,0%	0,2%	-10,1%	-8,5%	-8,5%	-8,5%	1,3%	-20,9%	1,8%	38,8%	7,9%	
12	SimX, v3.8	6x TorquExc HarmComp, nonreact.	exc T2/Tm42503: tanp(0 20 bar)	0,0%	0,0%	0,0%	-0,1%	-9,4%	-7,7%	-7,7%	-7,7%	1,3%	-20,4%	2,4%	8,0%	8,1%	
14	SimX, v3.8	6x TorquExc HarmComp, nonreact.	exc T2/Tm42503: exc T(0 20 bar)	0,0%	0,0%	0,0%	-0,1%	-9,4%	-7,7%	-7,7%	-7,7%	1,3%	-20,4%	2,3%	8,0%	8,1%	
11	SimX, v3.8	6x TorquExc, nonreact. *0,96	exc T2/Tm42503: Te(0 20 bar)	0,0%	0,0%	0,0%	0,2%	-2,1%	-0,4%	-0,3%	-0,3%	1,3%	-18,7%	4,7%	10,6%	10,7%	
13	SimX, v3.8	6x TorquExc HarmComp, nonreact. *0,96	exc T2/Tm42503: tanp(0 20 bar)	0,0%	0,0%	0,0%	-0,1%	-1,3%	0,4%	0,5%	0,5%	1,3%	-18,1%	5,3%	10,8%	11,0%	
15	SimX, v3.8	6x TorquExc HarmComp, nonreact. *0,96	exc T2/Tm42503: exc T(0 20 bar)	0,0%	0,0%	0,0%	-0,1%	-1,3%	0,4%	0,5%	0,5%	1,3%	-22,5%	5,3%	10,8%	11,0%	

Figure 56. Comparison of simulation results for model 6S60 under misfiring conditions

For model *6S60* under misfiring conditions across the complete engine operating range, the torsional stress in the intermediate shaft is presented graphically in Figure 57. This includes the best-case simulation results from Figure 56. along with verification and validation data.

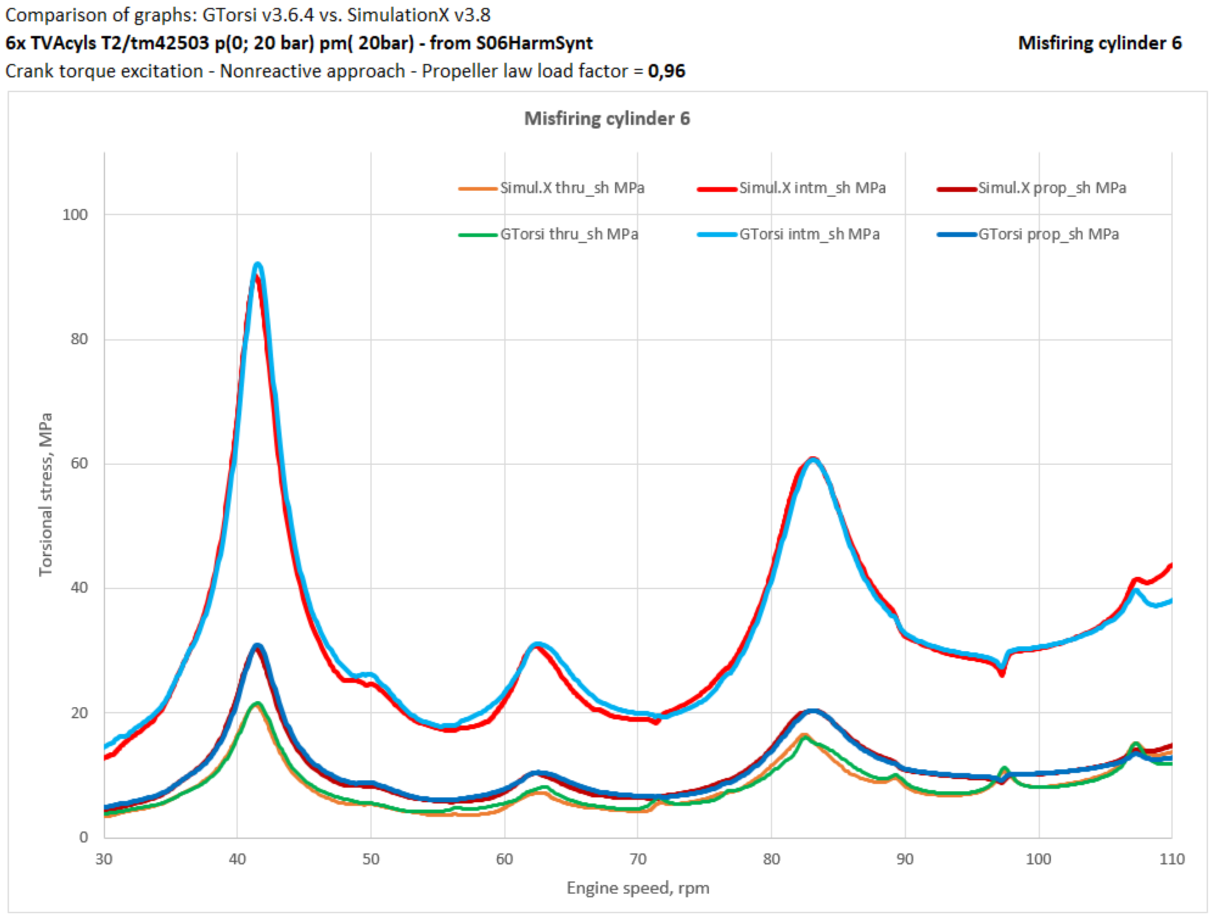

Figure 57. Graphical comparison of torsional stress results in complete shaft line for model 6S60 under misfiring conditions

6.3.3. Model 7L60 - propulsion system of 11443 GT reefer

Simulation model *7L60*, shown in Figure 58, represents propulsion system of reefer ship and her GT is 11443. It consists of one two-stroke slow-speed seven-cylinders inline marine Diesel engine MAN B&W 7L60MC Mark 5, with MCR of 13440 kW at 123 rpm. Furthermore, the system contains intermediate (diameter 450 mm) and propeller shaft (diameter 570 mm), and the solid fixed pitch 4-bladed propeller (diameter 5880 mm, mean pitch 5640 mm and area ratio 0.686). The propulsion shafting model for TVA discretized the actual system into 12 concentrated masses, each represented by its mass moments of inertia, connected by shafts represented by means of torsional springs. Absolute damping at certain masses is expressed in terms of dynamic magnifiers, with no relative damping occurring between any masses.

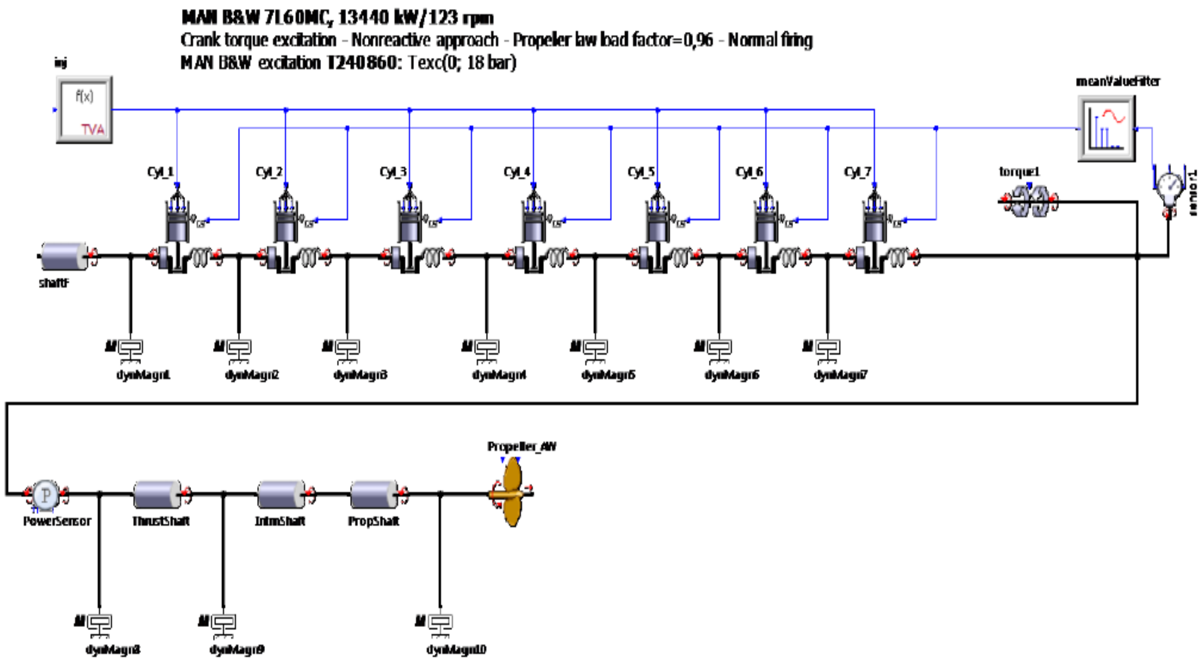

Figure 58. Structure of simulation model 7L60

Simulation results of natural frequencies and torsional stress amplitudes for the model *7L60* under normal firing conditions are evaluated, verified and validated, shown in Figure 59.

SimulationX evaluation of TVA — MAN B&W 7L60MC, 13440 kW/123 rpm, comparison of results

Excitation S06HarmSynt — Propeller law torque load factor: default = 1,00 otherwise = *

Normal firing — Compare results at critical speeds

case	program	system	excitation	natural frequencies n1 [rpm]	n2 [rpm]	n3 [rpm]	critical speed [rpm]	total tors. stress max. amplitude: tors. stress cylinder 7 [MPa]	tors. stress thrust shaft [MPa]	tors. stress intm. shaft [MPa]	tors. stress propeller shaft [MPa]	notes	average squ. deviation [%]
1	GTORSI, v3.6.4	7xcyl	tang. press. coeff. T240860	**315,4**	**1501,7**	**2939,9**	**44,9**	**21,1**	**20,4**	**72,0**	**35,2**	**reference**	
2	SimX, v3.8	7x TVAcyl, cyl. press. nonreact.	exc T240860 pCyl(0 18 bar)	315,3	1501,7	2939,9	44,7	17,5	17,4	61,3	30,0		6,2
3	SimX, v3.8	7x TVAcyl, crnk. torq. nonreact.	exc T240860 Texc(0 18 bar)	315,3	1501,7	2939,9	45,0	17,8	17,8	62,7	30,7		5,4
4	SimX, v3.8	7x TVAcyl, cyl. press. nonreact.*0,96	exc T240860 pCyl(0 18 bar)	315,3	1501,7	2939,9	44,8	18,6	18,5	65,3	31,9		4,0
5	SimX, v3.8	7x TVAcyl, crnk. torq. nonreact. *0,96	exc T240860 Texc(0 18 bar)	315,3	1501,7	2939,9	45,0	19,0	18,9	66,9	32,8	best match	3,1
6	SimX, v3.8	7x ForceExc, nonreact.	exc T240860 pCyl(0 18 bar)	315,3	1501,7	2939,9	44,8	17,4	17,3	60,9	29,8		6,4
7	SimX, v3.8	7x ForceExc HarmComp, nonreact.	exc T240860 pCyl(0 18 bar)	315,3	1501,7	2939,9	44,8	17,5	17,4	61,2	30,0		6,2
8	SimX, v3.8	7x ForceExc, nonreact. *0,96	exc T240860 pCyl(0 18 bar)	315,3	1501,7	2939,9	44,8	18,5	18,4	65,0	31,8		4,2
9	SimX, v3.8	7x ForceExc HarmComp, nonreact. *0,96	exc T240860 pCyl(0 18 bar)	315,3	1501,7	2939,9	44,7	18,6	18,5	65,3	32,0		4,0
10	SimX, v3.8	7x TorquExc, nonreact.	exc T240860 Texc(0 18 bar)	315,3	1501,7	2939,9	45,0	17,6	17,5	62,0	30,3		5,9
11	SimX, v3.8	7x TorquExc HarmComp, nonreact.	exc T240860 pTan(0 18 bar)	315,3	1501,7	2939,9	45,1	17,8	17,7	62,7	30,7		5,5
12	SimX, v3.8	7x TorquExc HarmComp, nonreact.	exc T240860 Texc(0 18 bar)	315,3	1501,7	2939,9	45,1	17,8	17,7	62,7	30,7		5,5
13	SimX, v3.8	7x TorquExc, nonreact. *0,96	exc T240860 Texc(0 18 bar)	315,3	1501,7	2939,9	45,0	18,8	18,7	66,2	32,4		3,6
14	SimX, v3.8	7x TorquExc HarmComp, nonreact. *0,96	exc T240860 pTan(0 18 bar)	315,3	1501,7	2939,9	45,0	19,0	18,9	67,0	32,8	2nd match	3,1
15	SimX, v3.8	7x TorquExc HarmComp, nonreact. *0,96	exc T240860 Texc(0 18 bar)	315,3	1501,7	2939,9	45,0	19,0	18,9	67,0	32,8	2nd match	3,1
16	BIS Validation	Result of Sea Trial, norm. firing					45,2			63,3		intm. shaft, GphGrabb.	6,1

Relative values [%]

case	program	system	excitation	n1	n2	n3	critical speed		tors. stress thrust shaft	tors. stress intm. shaft	tors. stress propeller shaft	notes
1	GTORSI, v3.6.4	7xcyl	tang. press. coeff. T240860	0,0%	0,0%	0,0%	0,0%	0,0%	0,0%	0,0%	0,0%	reference
2	SimX, v3.8	7x TVAcyl, cyl. press. nonreact.	exc T240860 pCyl(0 18 bar)	0,0%	0,0%	0,0%	-0,5%	-17,0%	-14,8%	-14,9%	-14,9%	
3	SimX, v3.8	7x TVAcyl, crnk. torq. nonreact.	exc T240860 Texc(0 18 bar)	0,0%	0,0%	0,0%	0,2%	-15,3%	-12,9%	-12,9%	-12,9%	
4	SimX, v3.8	7x TVAcyl, cyl. press. nonreact.*0,96	exc T240860 pCyl(0 18 bar)	0,0%	0,0%	0,0%	-0,3%	-11,6%	-9,2%	-9,4%	-9,4%	
5	SimX, v3.8	7x TVAcyl, crnk. torq. nonreact. *0,96	exc T240860 Texc(0 18 bar)	0,0%	0,0%	0,0%	0,3%	-9,7%	-7,1%	-7,1%	-7,1%	best match
6	SimX, v3.8	7x ForceExc, nonreact.	exc T240860 pCyl(0 18 bar)	0,0%	0,0%	0,0%	-0,2%	-17,5%	-15,2%	-15,4%	-15,4%	
7	SimX, v3.8	7x ForceExc HarmComp, nonreact.	exc T240860 pCyl(0 18 bar)	0,0%	0,0%	0,0%	-0,2%	-17,1%	-14,8%	-15,0%	-15,0%	
8	SimX, v3.8	7x ForceExc, nonreact. *0,96	exc T240860 pCyl(0 18 bar)	0,0%	0,0%	0,0%	-0,3%	-12,1%	-9,7%	-9,8%	-9,8%	
9	SimX, v3.8	7x ForceExc HarmComp, nonreact. *0,96	exc T240860 pCyl(0 18 bar)	0,0%	0,0%	0,0%	-0,4%	-11,7%	-9,2%	-9,3%	-9,3%	
10	SimX, v3.8	7x TorquExc, nonreact.	exc T240860 Texc(0 18 bar)	0,0%	0,0%	0,0%	0,2%	-16,4%	-14,0%	-14,0%	-14,0%	
11	SimX, v3.8	7x TorquExc HarmComp, nonreact.	exc T240860 pTan(0 18 bar)	0,0%	0,0%	0,0%	0,4%	-15,4%	-13,0%	-13,0%	-13,0%	
12	SimX, v3.8	7x TorquExc HarmComp, nonreact.	exc T240860 Texc(0 18 bar)	0,0%	0,0%	0,0%	0,4%	-15,4%	-13,0%	-13,0%	-13,0%	
13	SimX, v3.8	7x TorquExc, nonreact. *0,96	exc T240860 Texc(0 18 bar)	0,0%	0,0%	0,0%	0,3%	-10,8%	-8,2%	-8,1%	-8,1%	
14	SimX, v3.8	7x TorquExc HarmComp, nonreact. *0,96	exc T240860 pTan(0 18 bar)	0,0%	0,0%	0,0%	0,3%	-9,8%	-7,1%	-7,0%	-7,0%	2nd match
15	SimX, v3.8	7x TorquExc HarmComp, nonreact. *0,96	exc T240860 Texc(0 18 bar)	0,0%	0,0%	0,0%	0,3%	-9,8%	-7,1%	-7,0%	-7,0%	2nd match
16	BIS Validation	Result of Sea Trial, norm. firing					0,7%			-12,1%		intm. shaft, GphGrabb.

Figure 59. Comparison of simulation results for model 7L60 under normal firing conditions

The torsional stress in the intermediate shaft for model *7L60*, under normal firing conditions across the complete engine operating range, is presented graphically in Figure 60. This includes the best-case simulation results from Figure 59. along with verification and validation data.

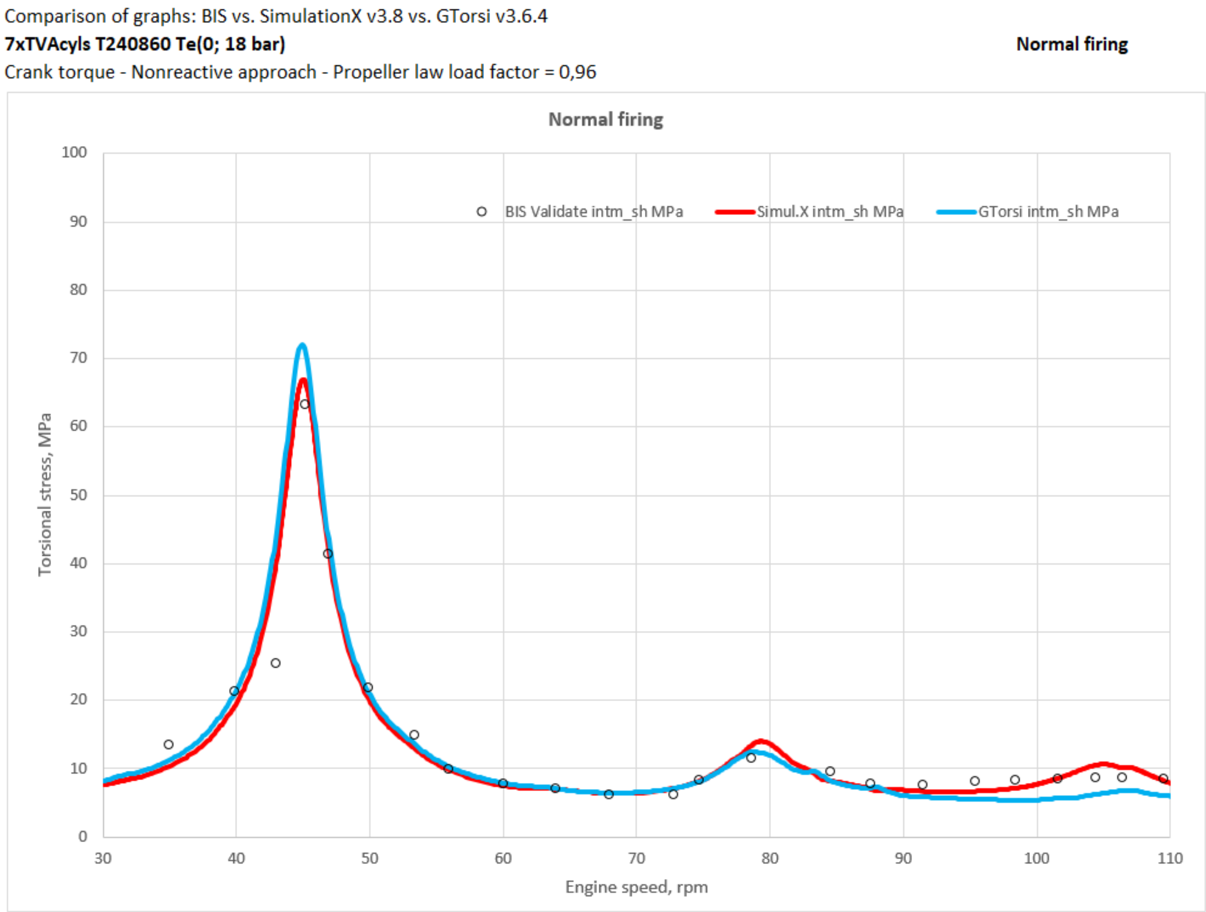

Figure 60. Graphical comparison of torsional stress results in the intermediate shaft for model 7L60 under normal firing conditions

The torsional stress in thrust and propeller shaft for model *7L60*, under normal firing conditions across the complete engine operating range, is presented graphically in Figure 61. This includes the best-case simulation results from Figure 59. along with verification and validation data.

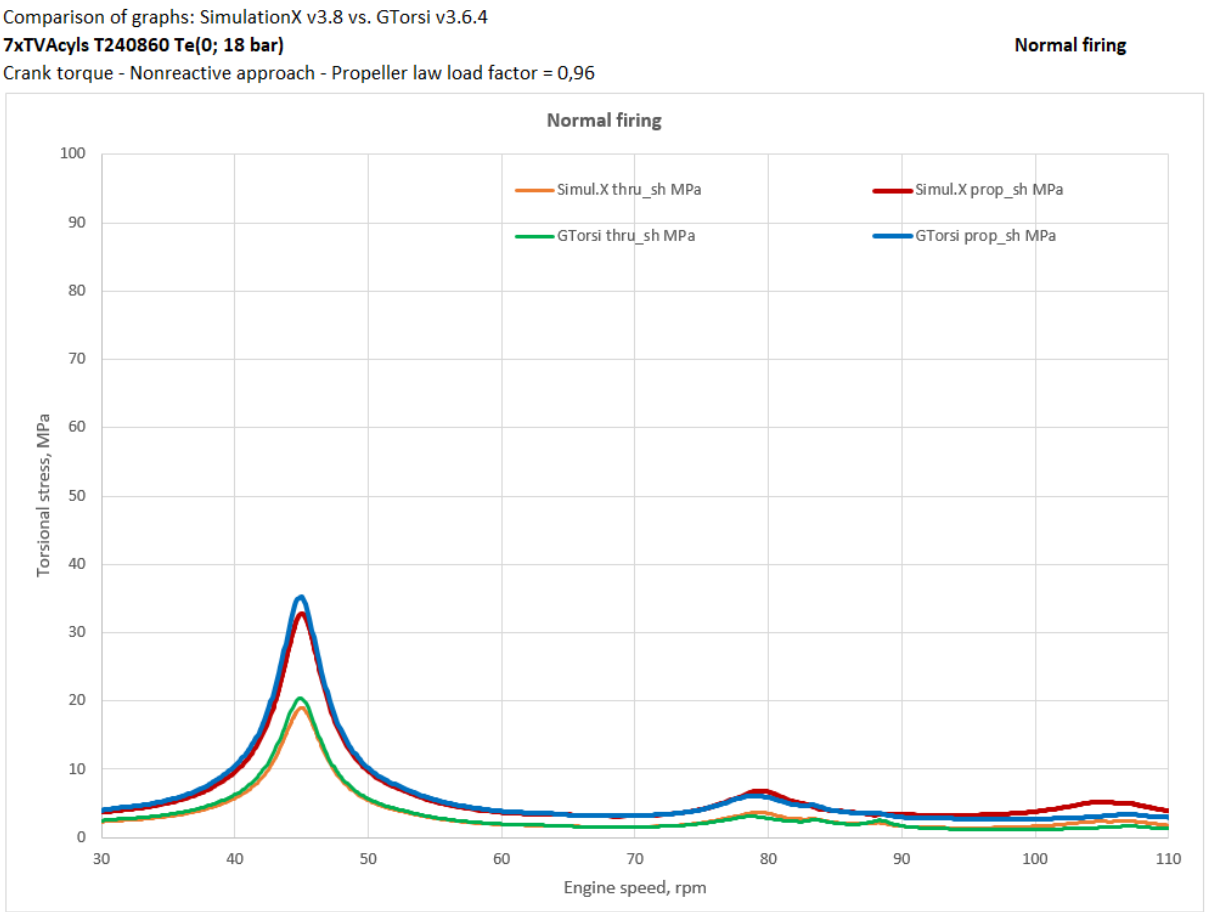

Figure 61. Graphical comparison of torsional stress results in thrust shaft and propeller shaft for model 7L60 under normal firing conditions

The simulation results of natural frequencies and torsional stress amplitudes for the model *7L60* under misfiring conditions are evaluated, verified and validated as shown in Figure 62.

SimulationX evaluation of TVA

Excitation S06HarmSynt

MAN B&W 7L60MC, 13440 kW/123 rpm, comparison of results vs. Gtorsi

Propeller law torque load factor: default = 1,00 otherwise = *

Misfiring cylinder 7				natural frequencies			tors. stress max. ampl.					tors. stress max. ampl.						
case	program	system	excitation	n1	n2	n3	critical speed 1	tors. stress cylinder 7	tors. stress thrust shaft	tors. stress inter. shaft	tors. stress propeller shaft	critical speed 2	tors. stress cylinder 7	tors. stress thrust shaft	tors. stress inter. shaft	tors. stress propeller shaft	notes	average squ. deviation
				[rpm]	[rpm]	[rpm]	[rpm]	[MPa]	[MPa]	[mrad]	[mrad]	[rpm]	[MPa]	[MPa]	[mrad]	[mrad]		[%]
1	GTORSI, v3.6.4	7xcyl	tang. press. coeff. Tm40860	**315,4**	**1501,7**	**2939,9**	**44,9**	**20,9**	**20,9**	**65,5**	**36,1**	**105,1**	**19,0**	**16,4**	**58,9**	**28,9**	**reference**	
2	SimX, v3.8	7x TVAcyl, cyl. press. nonreact.	exc T2/Tm40860 pCyl(0 18 bar)	315,3	1501,7	2939,9	44,7	18,5	18,3	64,3	31,4	104,3	16,2	16,4	59,5	29,1		2,6
3	SimX, v3.8	7x TVAcyl, crnk. torq. nonreact.	exc T2/Tm40860 Texc(0 18 bar)	315,3	1501,7	2939,9	45,0	19,1	19,0	66,7	32,6	105,9	18,3	18,1	65,9	32,3		2,6
4	SimX, v3.8	7x TVAcyl, cyl. press. nonreact.*0,96	exc T2/Tm40860 pCyl(0 18 bar)	315,3	1501,7	2939,9	44,8	19,9	19,7	69,2	33,8	104,3	16,5	16,7	60,6	29,7	3rd match	1,8
5	SimX, v3.8	7x TVAcyl, crnk. torq. nonreact. *0,96	exc T2/Tm40860 Texc(0 18 bar)	315,3	1501,7	2939,9	45,0	20,7	20,5	72,0	35,2	105,9	18,7	18,4	67,0	32,8		2,5
6	SimX, v3.8	7x ForceExc, nonreact.	exc T2/Tm40860 pCyl(0 18 bar)	315,3	1501,7	2939,9	44,8	18,4	18,2	64,0	31,3	104,3	16,4	16,4	59,5	29,1		2,6
7	SimX, v3.8	7x ForceExc HarmComp, nonreact.	exc T2/Tm40860 pCyl(0 18 bar)	315,3	1501,7	2939,9	44,8	18,5	18,3	64,3	31,5	104,3	16,3	16,5	59,6	29,2		2,6
8	SimX, v3.8	7x ForceExc, nonreact. *0,96	exc T2/Tm40860 pCyl(0 18 bar)	315,3	1501,7	2939,9	44,7	19,8	19,6	68,8	33,7	104,3	16,7	16,7	60,6	29,7	2nd match	1,8
9	SimX, v3.8	7x ForceExc HarmComp, nonreact. *0,96	exc T2/Tm40860 pCyl(0 18 bar)	315,3	1501,7	2939,9	44,7	19,9	19,7	69,2	33,9	104,7	16,8	16,5	60,4	29,6	best match	1,7
10	SimX, v3.8	7x TorquExc, nonreact.	exc T2/Tm40860 Texc(0 18 bar)	315,3	1501,7	2939,9	45,0	18,9	18,7	65,9	32,2	105,9	18,3	18,1	65,6	32,1		2,6
11	SimX, v3.8	7x TorquExc HarmComp, nonreact.	exc T2/Tm40860 pTan(0 18 bar)	315,3	1501,7	2939,9	44,9	19,1	19,0	66,6	32,6	105,9	18,3	18,1	65,8	32,2		2,5
12	SimX, v3.8	7x TorquExc HarmComp, nonreact.	exc T2/Tm40860 Texc(0 18 bar)	315,3	1501,7	2939,9	44,9	19,1	19,0	66,6	32,6	105,9	18,3	18,1	65,8	32,2		2,5
13	SimX, v3.8	7x TorquExc, nonreact. *0,96	exc T2/Tm40860 Texc(0 18 bar)	315,3	1501,7	2939,9	44,9	20,5	20,2	71,0	34,8	105,9	18,6	18,4	66,7	32,7		2,4
14	SimX, v3.8	7x TorquExc HarmComp, nonreact. *0,96	exc T2/Tm40860 pTan(0 18 bar)	315,3	1501,7	2939,9	44,9	20,7	20,5	71,9	35,2	105,9	18,7	18,4	66,9	32,8		2,5
15	SimX, v3.8	7x TorquExc HarmComp, nonreact. *0,96	exc T2/Tm40860 Texc(0 18 bar)	315,3	1501,7	2939,9	44,9	20,7	20,5	71,9	35,2	105,9	18,7	18,4	66,9	32,8		2,5

Relative values [%]																	
case	program	system	excitation	n1	n2	n3	critical speed 1	tors. stress cylinder 7	tors. stress thrust shaft	tors. stress inter. shaft	tors. stress propeller shaft	critical speed 2	tors. stress cylinder 7	tors. stress thrust shaft	tors. stress inter. shaft	tors. stress propeller shaft	notes
1	GTORSI, v3.6.4	7xcyl	tang. press. coeff. Tm40860														reference
2	SimX, v3.8	7x TVAcyl, cyl. press. nonreact.	exc T2/Tm40860 pCyl(0 18 bar)	0,0%	0,0%	0,0%	-0,4%	-11,9%	-12,5%	-1,8%	-12,9%	-0,8%	-14,5%	-0,1%	1,0%	0,9%	
3	SimX, v3.8	7x TVAcyl, crnk. torq. nonreact.	exc T2/Tm40860 Texc(0 18 bar)	0,0%	0,0%	0,0%	0,2%	-8,6%	-9,2%	1,9%	-9,6%	0,8%	-3,4%	10,3%	11,8%	11,8%	
4	SimX, v3.8	7x TVAcyl, cyl. press. nonreact.*0,96	exc T2/Tm40860 pCyl(0 18 bar)	0,0%	0,0%	0,0%	-0,3%	-5,1%	-5,9%	5,7%	-6,2%	-0,8%	-13,0%	1,7%	2,8%	2,8%	3rd match
5	SimX, v3.8	7x TVAcyl, crnk. torq. nonreact. *0,96	exc T2/Tm40860 Texc(0 18 bar)	0,0%	0,0%	0,0%	0,1%	-1,2%	-1,9%	9,9%	-2,5%	0,8%	-1,7%	12,2%	13,7%	13,7%	
6	SimX, v3.8	7x ForceExc, nonreact.	exc T2/Tm40860 pCyl(0 18 bar)	0,0%	0,0%	0,0%	-0,2%	-12,2%	-12,9%	-2,2%	-13,2%	-0,8%	-13,4%	0,0%	1,0%	0,9%	
7	SimX, v3.8	7x ForceExc HarmComp, nonreact.	exc T2/Tm40860 pCyl(0 18 bar)	0,0%	0,0%	0,0%	-0,2%	-11,8%	-12,5%	-1,7%	-12,8%	-0,8%	-13,9%	0,2%	1,2%	1,2%	
8	SimX, v3.8	7x ForceExc, nonreact. *0,96	exc T2/Tm40860 pCyl(0 18 bar)	0,0%	0,0%	0,0%	-0,4%	-5,6%	-6,4%	5,2%	-6,7%	-0,8%	-12,2%	1,8%	2,8%	2,8%	2nd match
9	SimX, v3.8	7x ForceExc HarmComp, nonreact. *0,96	exc T2/Tm40860 pCyl(0 18 bar)	0,0%	0,0%	0,0%	-0,3%	-5,1%	-5,9%	5,7%	-6,2%	-0,4%	-11,7%	0,4%	2,5%	2,5%	best match
10	SimX, v3.8	7x TorquExc, nonreact.	exc T2/Tm40860 Texc(0 18 bar)	0,0%	0,0%	0,0%	0,2%	-9,6%	-10,3%	0,6%	-10,7%	0,8%	-3,7%	9,9%	11,4%	11,4%	
11	SimX, v3.8	7x TorquExc HarmComp, nonreact.	exc T2/Tm40860 pTan(0 18 bar)	0,0%	0,0%	0,0%	0,1%	-8,6%	-9,3%	1,8%	-9,7%	0,8%	-3,4%	10,3%	11,7%	11,7%	
12	SimX, v3.8	7x TorquExc HarmComp, nonreact.	exc T2/Tm40860 Texc(0 18 bar)	0,0%	0,0%	0,0%	0,1%	-8,6%	-9,3%	1,8%	-9,7%	0,8%	-3,4%	10,3%	11,7%	11,7%	
13	SimX, v3.8	7x TorquExc, nonreact. *0,96	exc T2/Tm40860 Texc(0 18 bar)	0,0%	0,0%	0,0%	0,0%	-2,3%	-3,1%	8,5%	-3,7%	0,8%	-2,0%	11,8%	13,3%	13,3%	
14	SimX, v3.8	7x TorquExc HarmComp, nonreact. *0,96	exc T2/Tm40860 pTan(0 18 bar)	0,0%	0,0%	0,0%	0,0%	-1,1%	-2,0%	9,8%	-2,5%	0,8%	-1,7%	12,2%	13,6%	13,6%	
15	SimX, v3.8	7x TorquExc HarmComp, nonreact. *0,96	exc T2/Tm40860 Texc(0 18 bar)	0,0%	0,0%	0,0%	0,0%	-1,1%	-2,0%	9,8%	-2,5%	0,8%	-1,7%	12,2%	13,6%	13,6%	

Figure 62. Comparison of simulation results for model 7L60 under misfiring conditions

For model *7L60* under misfiring conditions across the complete engine operating range, the torsional stress in the intermediate shaft is presented graphically in Figure 63. This includes the best-case simulation results along from Figure 62. with verification and validation data.

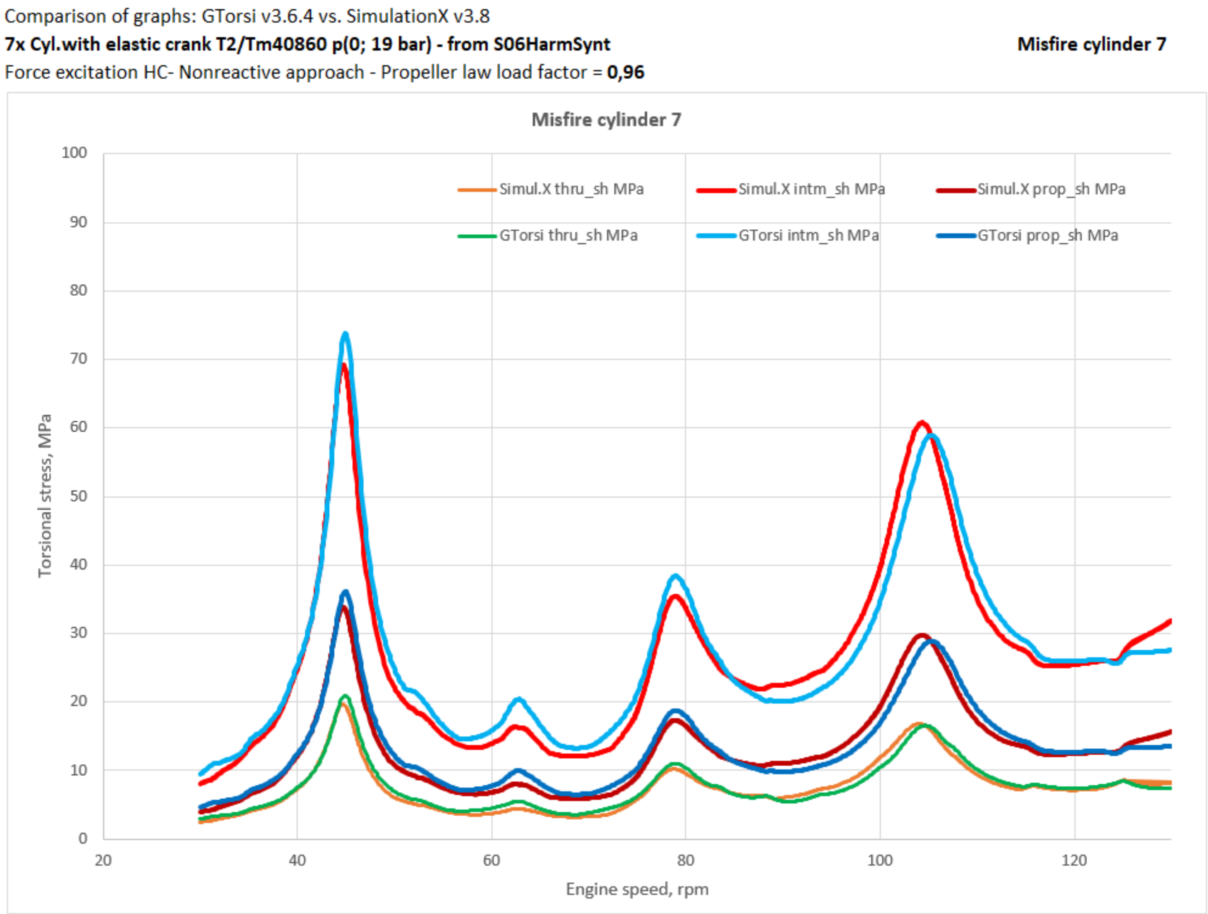

Figure 63. Graphical comparison of torsional stress results in complete shaft line for model 7L60 under misfiring conditions

6.3.4. Model 12K98 - propulsion system of 11388 TEU container ship

Simulation model *12K98*, shown in Figure 64, represents propulsion system of 11388 twenty-foot equivalent unit (TEU) container ship. It consists of one two-stroke slow-speed twelve-cylinders inline marine Diesel engine MAN B&W 12K98ME-C7 Mark 7, with MCR of 72240 kW at 104 rpm. Also, the system contains intermediate (diameter 805 mm) and propeller shaft (diameter 980 mm), and the solid fixed pitch 4-bladed propeller (diameter 8900 mm, mean pitch 8320 mm and area ratio 0.54). The propulsion shafting model for TVA discretized the actual system into 21 concentrated masses, each represented by its mass moments of inertia, connected by shafts represented by means of torsional springs. Absolute damping at certain masses is expressed in terms of dynamic magnifiers, while relative damping occurring between crank shaft masses is expressed within spring-damper elements.

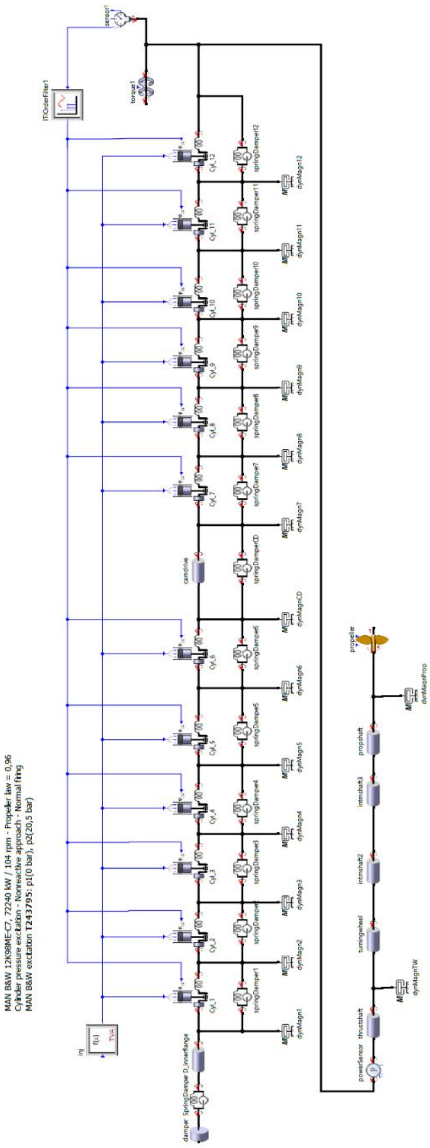

Figure 64. Structure of simulation model 12K98

Evaluation, verification and validation of natural frequencies and torsional stress amplitudes of the model *12K98* under misfiring conditions are shown in Figure 65.

SimulationX evaluation of TVA — Excitation S06HarmSynt

MAN B&W 12K98ME-C7, 72240 kW/104 rpm, comparison of results

Propeller law torque load factor: default = 1,00 otherwise = *

Normal firing

Compare results at critical speeds

case	program	system	excitation	natural frequencies n1 [rpm]	n2 [rpm]	n3 [rpm]	critical speed [rpm]	total tors. stress max. amplitude: tors. stress intm. sh. 2 [MPa]	tors. stress intm. sh. 3 [MPa]	tors. stress prop. shaft [MPa]	ang. disp. Cyl 1 [mrad]	ang. disp. propeller [mrad]	notes	average squ. deviation [%]
1	Hyndai TVC	12K98ME-C7	MIP 20,5 bar	**164,0**	**691,2**	**834,1**	**54,4**	**8,3**	**8,3**	**4,4**	**6,540**	**5,340**	**reference** (Gph Grabber)	
2	GTORSI, v3.6.4	12K98ME-C7	tang. press. coeff. T243795	164,0	691,2	834,1	54,4	7,0	7,1	3,9	5,322	4,422		5,9
3	SimX, v3.8	12x TVAcyl, cyl. press. nonreact.	exc T243795: p(0 20,5 bar)	164,0	713,8	809,0	54,1	9,1	9,1	5,0	7,074	5,936	2nd match	4,0
4	SimX, v3.8	12x TVAcyl, crnk. torq. nonreact.	exc T243795: Te(0 20,5 bar)	164,0	713,8	809,0	55,3	9,5	9,5	5,2	7,503	5,885		5,6
5	SimX, v3.8	12x TVAcyl, cyl. press. nonreact. *0,96	exc T243795: p(0 20,5 bar)	164,0	713,8	809,0	54,0	10,3	10,3	5,7	7,997	6,745		9,5
6	SimX, v3.8	12x TVAcyl, crnk. torq. nonreact. *0,96	exc T243795: Te(0 20,5 bar)	164,0	713,8	809,0	55,3	10,7	10,7	5,9	8,480	6,659		11,1
7	SimX, v3.8	12x ForceExc, nonreact.	exc T243795: p(0 20,5 bar)	164,0	713,8	809,0	54,1	9,1	9,1	5,0	7,096	5,961		4,2
8	SimX, v3.8	12x ForceExc, nonreact. *0,96	exc T243795: p(0 20,5 bar)	164,0	713,8	809,0	54,0	10,4	10,3	5,7	8,021	6,771		9,7
9	SimX, v3.8	12x ForceExc, HC cylpress, nonreact.	exc T243795: p(0 20,5 bar)	164,0	713,8	809,0	54,1	9,1	9,1	5,0	7,057	5,922	best match	3,9
10	SimX, v3.8	12x ForceExc, HC cylpress, nonreact. *0,96	exc T243795: p(0 20,5 bar)	164,0	713,8	809,0	54,0	10,3	10,3	5,6	7,979	6,729		9,4
11	SimX, v3.8	12x TorquExc, nonreact.	exc T243795: Te(0 20,5 bar)	164,0	713,8	809,0	55,3	9,4	9,4	5,2	7,461	5,854	3rd match	5,3
12	SimX, v3.8	12x TorquExc HarmComp, nonreact.	exc T243795: tan p(0 20,5 bar)	164,0	713,8	809,0	55,3	9,5	9,5	5,2	7,499	5,882		5,5
13	SimX, v3.8	12x TorquExc HarmComp, nonreact.	exc T243795: exc T(0 20,5 bar)	164,0	713,8	809,0	55,3	9,5	9,5	5,2	7,499	5,882		5,5
14	SimX, v3.8	12x TorquExc, nonreact. *0,96	exc T243795: Te(0 20,5 bar)	164,0	713,8	809,0	55,3	10,7	10,7	5,9	8,435	6,627		11,0
15	SimX, v3.8	12x TorquExc HarmComp, nonreact. *0,96	exc T243795: tan p(0 20,5 bar)	164,0	713,8	809,0	55,3	10,7	10,7	5,9	8,476	6,656		11,0
16	SimX, v3.8	12x TorquExc HarmComp, nonreact. *0,96	exc T243795: exc T(0 20,5 bar)	164,0	713,8	809,0	55,3	10,7	10,7	5,9	8,476	6,656		11,0
17	HHI Validation	Result of Sea Trial, norm. firing					54,8			4,2			propeller shaft, GphGrabb.	2,0

Relative values [%]

case	program	system	excitation	n1	n2	n3	critical speed	tors. stress intm. sh. 2	tors. stress intm. sh. 3	tors. stress prop. shaft	ang. disp. Cyl 1	ang. disp. propeller	notes
1	Hyndai TVC	12K98ME-C7	MIP 20,5 bar	0,0%	0,0%	0,0%	0,0%	0,0%	0,0%	0,0%	0,0%	0,0%	reference (Gph Grabber)
2	GTORSI, v3.6.4	12K98ME-C7	tang. press. coeff. T243795	0,0%	0,0%	0,0%	0,0%	-15,9%	-14,9%	-11,2%	-18,6%	-17,2%	
3	SimX, v3.8	12x TVAcyl, cyl. press. nonreact.	exc T243795: p(0 20,5 bar)	0,0%	3,3%	-3,0%	-0,6%	9,7%	9,5%	14,1%	8,2%	11,2%	2nd match
4	SimX, v3.8	12x TVAcyl, crnk. torq. nonreact.	exc T243795: Te(0 20,5 bar)	0,0%	3,3%	-3,0%	1,7%	14,5%	14,4%	19,2%	14,7%	10,2%	
5	SimX, v3.8	12x TVAcyl, cyl. press. nonreact. *0,96	exc T243795: p(0 20,5 bar)	0,0%	3,3%	-3,0%	-0,7%	24,4%	24,2%	29,3%	22,3%	26,3%	
6	SimX, v3.8	12x TVAcyl, crnk. torq. nonreact. *0,96	exc T243795: Te(0 20,5 bar)	0,0%	3,3%	-3,0%	1,7%	29,4%	29,2%	34,7%	29,7%	24,7%	
7	SimX, v3.8	12x ForceExc, nonreact.	exc T243795: p(0 20,5 bar)	0,0%	3,3%	-3,0%	-0,6%	10,2%	10,0%	14,6%	8,5%	11,6%	
8	SimX, v3.8	12x ForceExc, nonreact. *0,96	exc T243795: p(0 20,5 bar)	0,0%	3,3%	-3,0%	-0,7%	24,9%	24,7%	29,9%	22,6%	26,8%	3rd match
9	SimX, v3.8	12x ForceExc, HC cylpress, nonreact.	exc T243795: p(0 20,5 bar)	0,0%	3,3%	-3,0%	-0,6%	9,4%	9,2%	13,8%	7,9%	10,9%	
10	SimX, v3.8	12x ForceExc, HC cylpress, nonreact. *0,96	exc T243795: p(0 20,5 bar)	0,0%	3,3%	-3,0%	-0,7%	24,1%	23,9%	29,0%	22,0%	26,0%	
11	SimX, v3.8	12x TorquExc, nonreact.	exc T243795: Te(0 20,5 bar)	0,0%	3,3%	-3,0%	1,7%	14,0%	13,8%	18,6%	14,1%	9,6%	
12	SimX, v3.8	12x TorquExc HarmComp, nonreact.	exc T243795: tan p(0 20,5 bar)	0,0%	3,3%	-3,0%	1,7%	14,5%	14,4%	19,2%	14,7%	10,1%	
13	SimX, v3.8	12x TorquExc HarmComp, nonreact.	exc T243795: exc T(0 20,5 bar)	0,0%	3,3%	-3,0%	1,7%	14,5%	14,4%	19,2%	14,7%	10,1%	
14	SimX, v3.8	12x TorquExc, nonreact. *0,96	exc T243795: Te(0 20,5 bar)	0,0%	3,3%	-3,0%	1,7%	29,1%	29,1%	35,0%	29,0%	24,1%	
15	SimX, v3.8	12x TorquExc HarmComp, nonreact. *0,96	exc T243795: tan p(0 20,5 bar)	0,0%	3,3%	-3,0%	1,7%	29,1%	29,2%	34,6%	29,6%	24,6%	
16	SimX, v3.8	12x TorquExc HarmComp, nonreact. *0,96	exc T243795: exc T(0 20,5 bar)	0,0%	3,3%	-3,0%	1,7%	29,1%	29,2%	34,6%	29,6%	24,6%	
17	HHI Validation	Result of Sea Trial, norm. firing					0,7%			-3,9%			propeller shaft, GphGrabb.

Figure 65. Comparison of simulation results for model 12K98 under normal firing conditions

The torsional stress in the propeller shaft for model *12K98*, under normal firing conditions across the complete engine operating range, is presented graphically in Figure 66. This includes the best-case simulation results from Figure 66. along with verification and validation data.

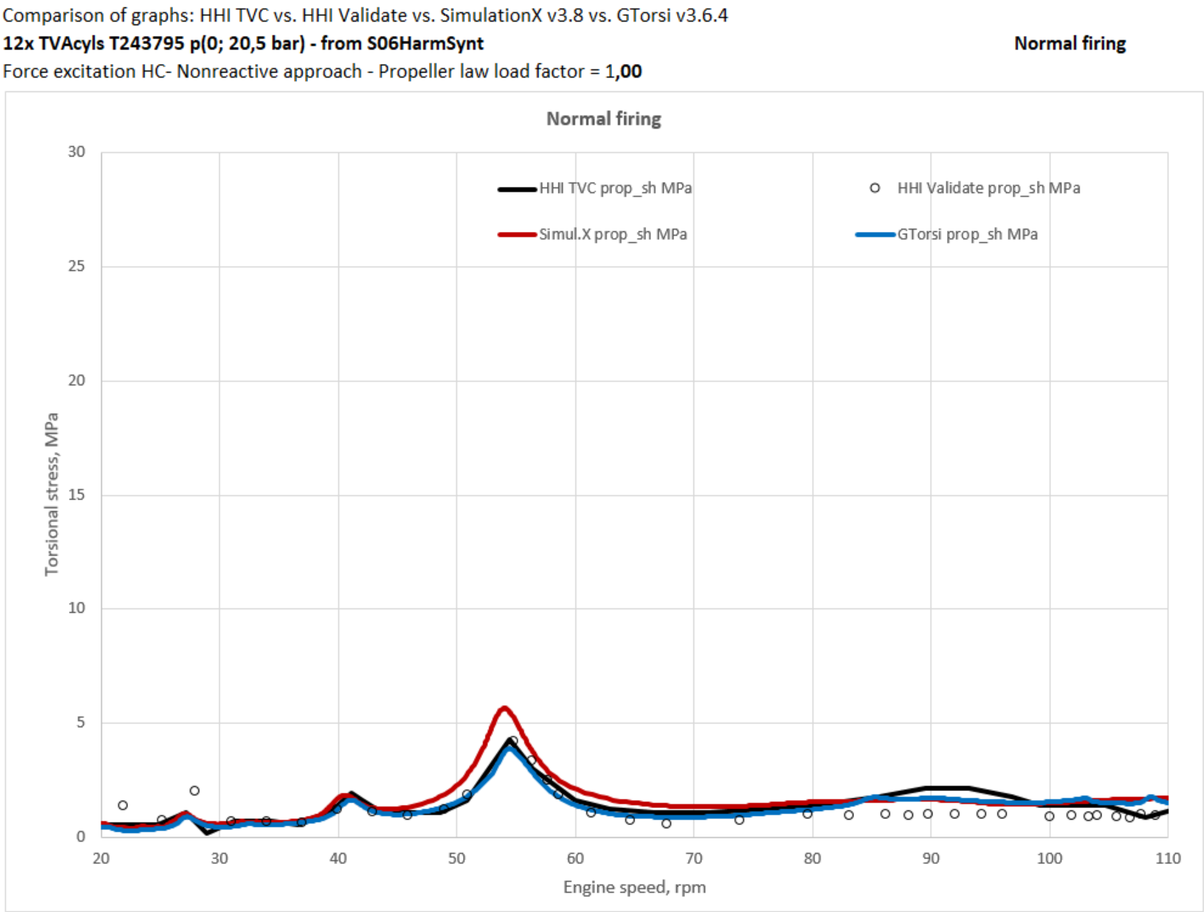

Figure 66. Graphical comparison of torsional stress results in the propeller shaft for model 12K98 under normal firing conditions

Torsional stresses in the thrust and intermediate shaft for model *12K98*, under normal firing conditions across the entire engine operating range, are shown graphically in Figure 67. This includes the best-case simulation results from Figure 65. with verification and validation data.

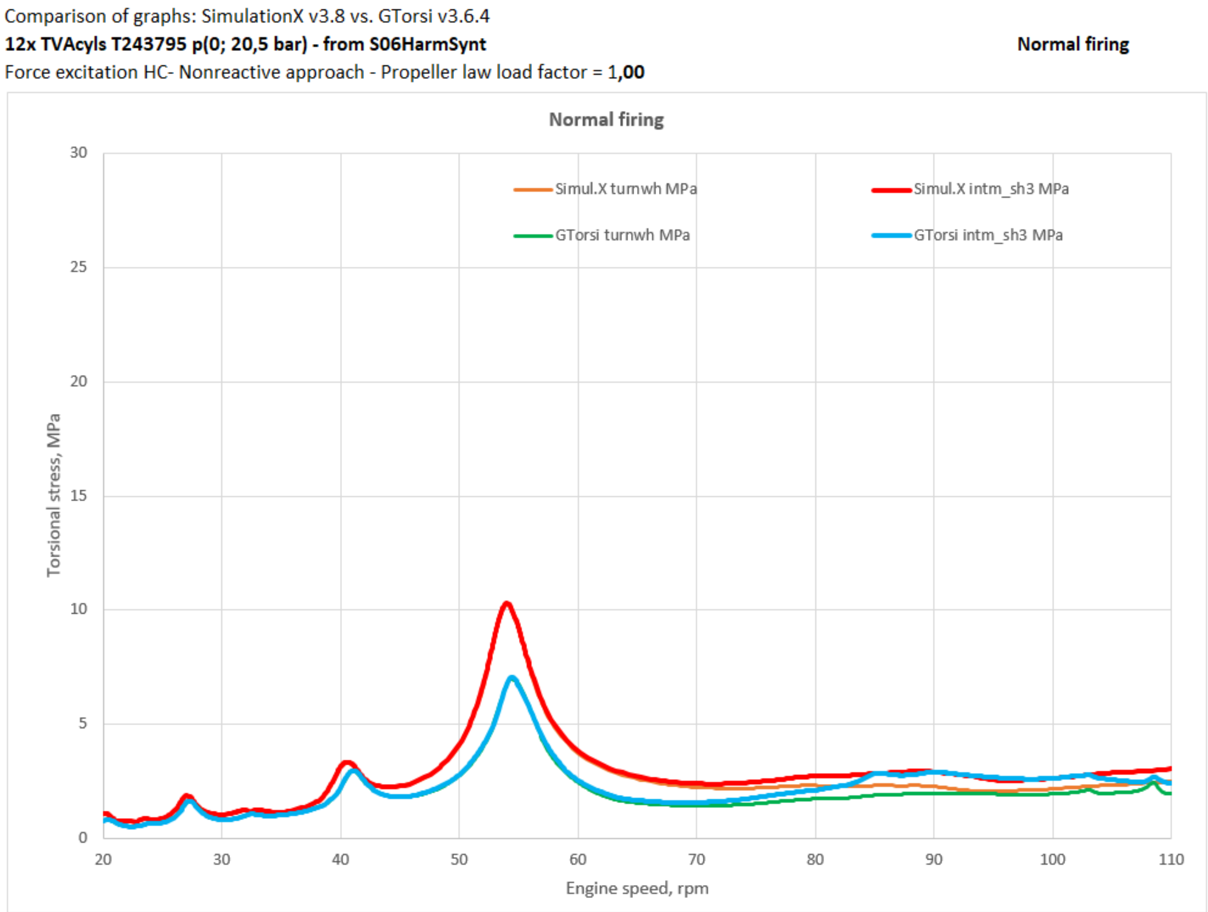

Figure 67. Graphical comparison of torsional stress results in thrust shaft and intermediate shaft for model 12K98 under normal firing conditions

Simulation results of natural frequencies and torsional stress amplitudes for the model *12K98* under normal firing conditions are evaluated, verified and validated as in Figure 68.

SimulationX evaluation of TVA

Excitation S06HarmSynt

MAN B&W 12K98ME-C7, 72240 kW/104 rpm, comparison of results

Propeller law torque load factor: default = 1,00 otherwise = *

Misfiring cylinder 1				natural frequencies				tors. stress max. ampl.					tors. stress max. ampl.					
case	program	system	excitation	n1 [rpm]	n2 [rpm]	n3 [rpm]	critical speed 1 [rpm]	turn. wheel sh. [MPa]	prop. shaft [MPa]	ang. disp. Cyl 1 [mrad]	ang. disp. propeller [mrad]	critical speed 2 [rpm]	tor. stress tur. wh. sh. [MPa]	tors. stress prop. shaft [MPa]	ang. disp. Cyl 1 [mrad]	ang. disp. propeller [mrad]	notes	average squ. deviation [%]
1	Hyndai TVC	12K98ME-C7	MIP 20,5 bar	164,0	691,2	834,1	54,2	10,1	5,43	15	15,6	81,6	45,8	25,1	35,4	36,4	reference (Graph Grabber)	
2	GTORSI, v3.6.4	12K98ME-C7	tang. press. coeff. T2/Tm43795	164,0	691,2	834,1	54,4	11,924	6,5853	15,87	17,076	81,9	51,078	28,202	38,181	39,84		3,7
3	SimX, v3.8	12x TVAcyl, cyl. press. nonreact.	exc T2/Tm43795: p(0 20,5 bar)	164,0	713,8	809,0	54,0	8,4	4,6	12,970	13,096	81,2	43,9	24,3	35,390	35,267		3,1
4	SimX, v3.8	12x TVAcyl, crnk. torq. nonreact.	exc T2/Tm43795: Te(0 20,5 bar)	164,0	713,8	809,0	54,6	8,9	4,8	15,308	16,202	84,4	52,8	29,1	43,841	39,939		3,8
5	SimX, v3.8	12x TVAcyl, cyl. press. nonreact. *0,96	exc T2/Tm43795: p(0 20,5 bar)	164,0	713,8	809,0	53,9	9,4	5,2	14,422	14,470	81,2	44,9	24,8	36,175	36,142	best match	1,2
6	SimX, v3.8	12x TVAcyl, crnk. torq. nonreact. *0,96	exc T2/Tm43795: Te(0 20,5 bar)	164,0	713,8	809,0	54,7	9,8	5,4	17,006	17,963	84,4	53,9	29,7	44,770	40,825		4,4
7	SimX, v3.8	12x ForceExc, nonreact.	exc T2/Tm43795: p(0 20,5 bar)	164,0	713,8	809,0	54,0	8,5	4,7	12,993	13,095	81,2	43,9	24,3	35,378	35,256		3,1
8	SimX, v3.8	12x ForceExc, nonreact. *0,96	exc T2/Tm43795: p(0 20,5 bar)	164,0	713,8	809,0	53,9	9,5	5,2	14,447	14,470	81,2	44,9	24,8	36,163	36,131	2nd match	1,2
9	SimX, v3.8	12x ForceExc, HC cylpress, nonreact.	exc T2/Tm43795: p(0 20,5 bar)	164,0	713,8	809,0	54,2	8,4	4,5	12,808	13,087	81,1	44,0	24,3	35,388	35,307		3,3
10	SimX, v3.8	12x ForceExc, HC cylpress, nonreact. *0,96	exc T2/Tm43795: p(0 20,5 bar)	164,0	713,8	809,0	54,2	9,4	5,2	14,306	14,459	81,5	44,9	24,8	36,173	36,183	3rd match	1,3
11	SimX, v3.8	12x TorquExc, nonreact.	exc T2/Tm43795: Te(0 20,5 bar)	164,0	713,8	809,0	54,7	8,8	4,8	15,273	16,188	84,4	52,7	29,1	43,754	39,886		3,8
12	SimX, v3.8	12x TorquExc HarmComp, nonreact.	exc T2/Tm43795: tan p(0 20,5 bar)	164,0	713,8	809,0	55,2	8,8	4,8	15,296	16,195	84,4	52,8	29,1	43,828	39,929		3,8
13	SimX, v3.8	12x TorquExc HarmComp, nonreact.	exc T2/Tm43795: exc T(0 20,5 bar)	164,0	713,8	809,0	55,2	8,8	4,8	15,297	16,195	84,4	52,8	29,1	43,823	39,929		3,8
14	SimX, v3.8	12x TorquExc, nonreact. *0,96	exc T2/Tm43795: Te(0 20,5 bar)	164,0	713,8	809,0	54,6	9,8	5,4	16,979	17,925	84,4	53,8	29,7	44,683	40,772		4,3
15	SimX, v3.8	12x TorquExc HarmComp, nonreact. *0.96	exc T2/Tm43795: tan p(0 20,5 bar)	164,0	713,8	809,0	54,8	9,8	5,3	17,008	17,934	84,4	53,9	29,7	44,757	40,815		4,4
16	SimX, v3.8	12x TorquExc HarmComp, nonreact. *0.96	exc T2/Tm43795: exc T(0 20,5 bar)	164,0	713,8	809,0	54,8	9,8	5,3	17,008	17,936	84,4	53,9	29,7	44,757	40,815		4,4
17	HHI Validation	Result of Sea Trial, misfiring cyl ???					54,8		7,1								propeller shaft, GphGrabb.	14,9

Relative values [%]																	
case	program	system	excitation	n1	n2	n3	critical speed 1	turn. wheel sh.	prop. shaft	ang. disp. Cyl 1	ang. disp. propeller	critical speed 2	tor. stress tur. wh. sh.	tors. stress prop. shaft	ang. disp. Cyl 1	ang. disp. propeller	notes
1	Hyndai TVC	12K98ME-C7	MIP 20,5 bar														reference (Graph Grabber)
2	GTORSI, v3.6.4	12K98ME-C7	tang. press. coeff. T2/Tm43795	0,0%	0,0%	0,0%	0,4%	18,1%	21,3%	5,8%	9,5%	0,4%	11,5%	12,4%	7,9%	9,5%	
3	SimX, v3.8	12x TVAcyl, cyl. press. nonreact.	exc T2/Tm43795: p(0 20,5 bar)	0,0%	3,3%	-3,0%	-0,3%	-16,5%	-14,7%	-13,5%	-16,1%	-0,5%	-4,1%	-3,3%	0,0%	-3,1%	
4	SimX, v3.8	12x TVAcyl, crnk. torq. nonreact.	exc T2/Tm43795: Te(0 20,5 bar)	0,0%	3,3%	-3,0%	0,8%	-12,4%	-11,1%	2,1%	3,9%	3,4%	15,2%	16,1%	23,8%	9,7%	
5	SimX, v3.8	12x TVAcyl, cyl. press. nonreact. *0,96	exc T2/Tm43795: p(0 20,5 bar)	0,0%	3,3%	-3,0%	-0,5%	-6,6%	-4,6%	-3,9%	-7,2%	-0,5%	-1,9%	-1,2%	2,2%	-0,7%	best match
6	SimX, v3.8	12x TVAcyl, crnk. torq. nonreact. *0,96	exc T2/Tm43795: Te(0 20,5 bar)	0,0%	3,3%	-3,0%	0,9%	-2,7%	-1,2%	13,4%	15,1%	3,4%	17,6%	18,5%	26,5%	12,2%	
7	SimX, v3.8	12x ForceExc, nonreact.	exc T2/Tm43795: p(0 20,5 bar)	0,0%	3,3%	-3,0%	-0,3%	-16,2%	-14,3%	-13,4%	-16,1%	-0,5%	-4,1%	-3,3%	-0,1%	-3,1%	
11	SimX, v3.8	12x ForceExc, nonreact. *0,96	exc T2/Tm43795: p(0 20,5 bar)	0,0%	3,3%	-3,0%	-0,5%	-6,3%	-4,2%	-3,7%	-7,2%	-0,5%	-1,9%	-1,2%	2,2%	-0,7%	
8	SimX, v3.8	12x ForceExc, HC cylpress, nonreact.	exc T2/Tm43795: p(0 20,5 bar)	0,0%	3,3%	-3,0%	0,1%	-16,9%	-17,1%	-14,6%	-16,1%	-0,6%	-4,0%	-3,3%	0,0%	-3,0%	2nd match
14	SimX, v3.8	12x ForceExc, HC cylpress, nonreact. *0,96	exc T2/Tm43795: p(0 20,5 bar)	0,0%	3,3%	-3,0%	0,0%	-7,3%	-4,7%	-4,6%	-7,3%	-0,2%	-1,9%	-1,1%	2,2%	-0,6%	
12	SimX, v3.8	12x TorquExc, nonreact.	exc T2/Tm43795: Te(0 20,5 bar)	0,0%	3,3%	-3,0%	0,8%	-12,5%	-11,2%	1,8%	3,8%	3,4%	15,1%	15,9%	23,6%	9,6%	
13	SimX, v3.8	12x TorquExc HarmComp, nonreact.	exc T2/Tm43795: tan p(0 20,5 bar)	0,0%	3,3%	-3,0%	1,9%	-12,5%	-11,5%	2,0%	3,8%	3,4%	15,2%	16,1%	23,8%	9,7%	
15	SimX, v3.8	12x TorquExc HarmComp, nonreact.	exc T2/Tm43795: exc T(0 20,5 bar)	0,0%	3,3%	-3,0%	1,9%	-12,5%	-11,7%	2,0%	3,8%	3,4%	15,2%	16,1%	23,8%	9,7%	
16	SimX, v3.8	12x TorquExc, nonreact. *0,96	exc T2/Tm43795: Te(0 20,5 bar)	0,0%	3,3%	-3,0%	0,7%	-2,8%	-1,4%	13,2%	14,9%	3,4%	17,5%	18,3%	26,2%	12,0%	
17	HHI Validation	Result of Sea Trial, misfiring cyl ???					1,1%		29,8%								propeller shaft, GphGrabb.

Figure 68. Comparison of simulation results for model 12K98 under misfiring conditions

For model *12K98* under misfiring conditions across entire engine operating range, the torsional stress in the propeller shaft is presented graphically in Figure 69. This includes the best-case simulation results from Figure 68. along with verification and validation data.

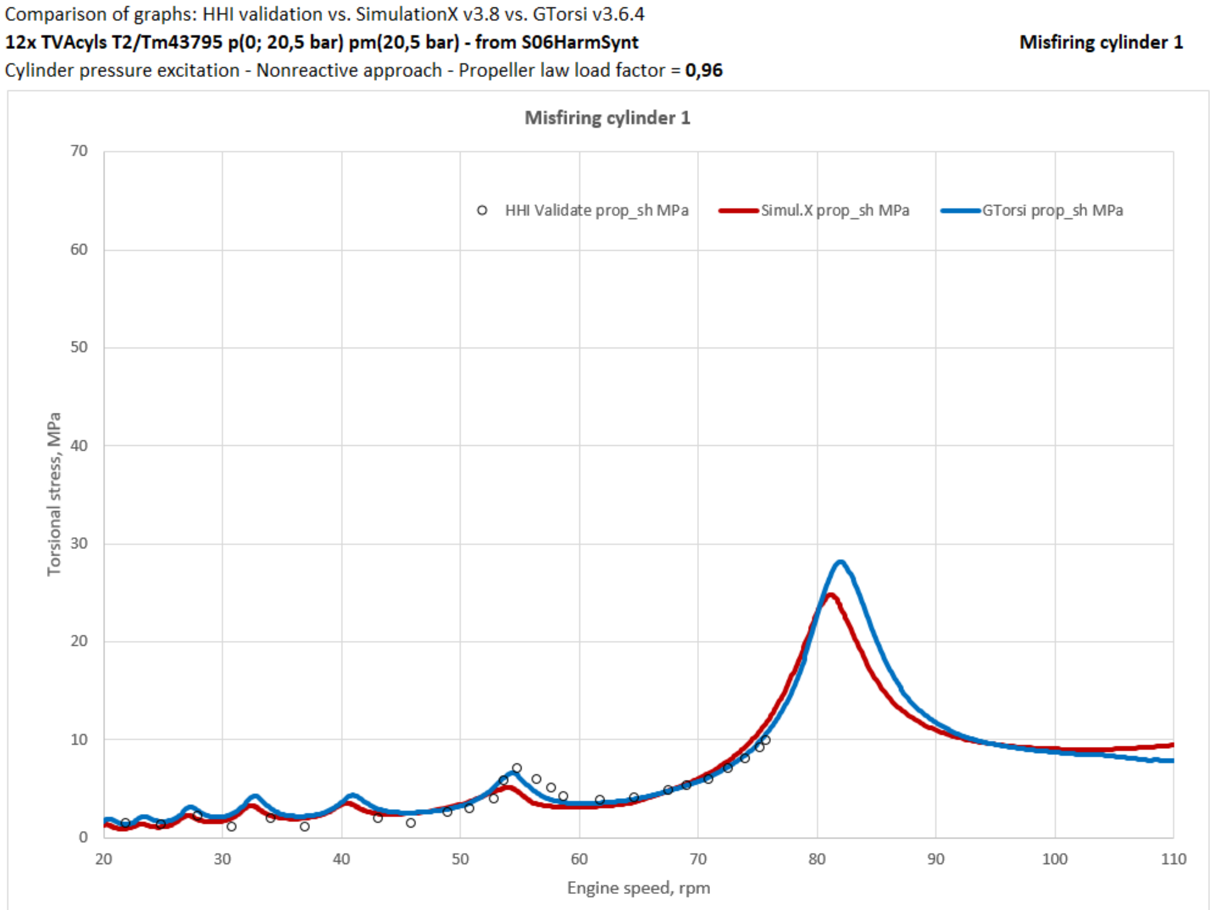

Figure 69. Graphical comparison of torsional stress results in propeller shaft for model 12K98 under misfiring conditions

Under misfiring condition, torsional stresses in the thrust and intermediate shaft for model *12K98* across the complete engine operating range are graphically shown in Figure 70, including best-case simulation results from Figure 68. with verification and validation data.

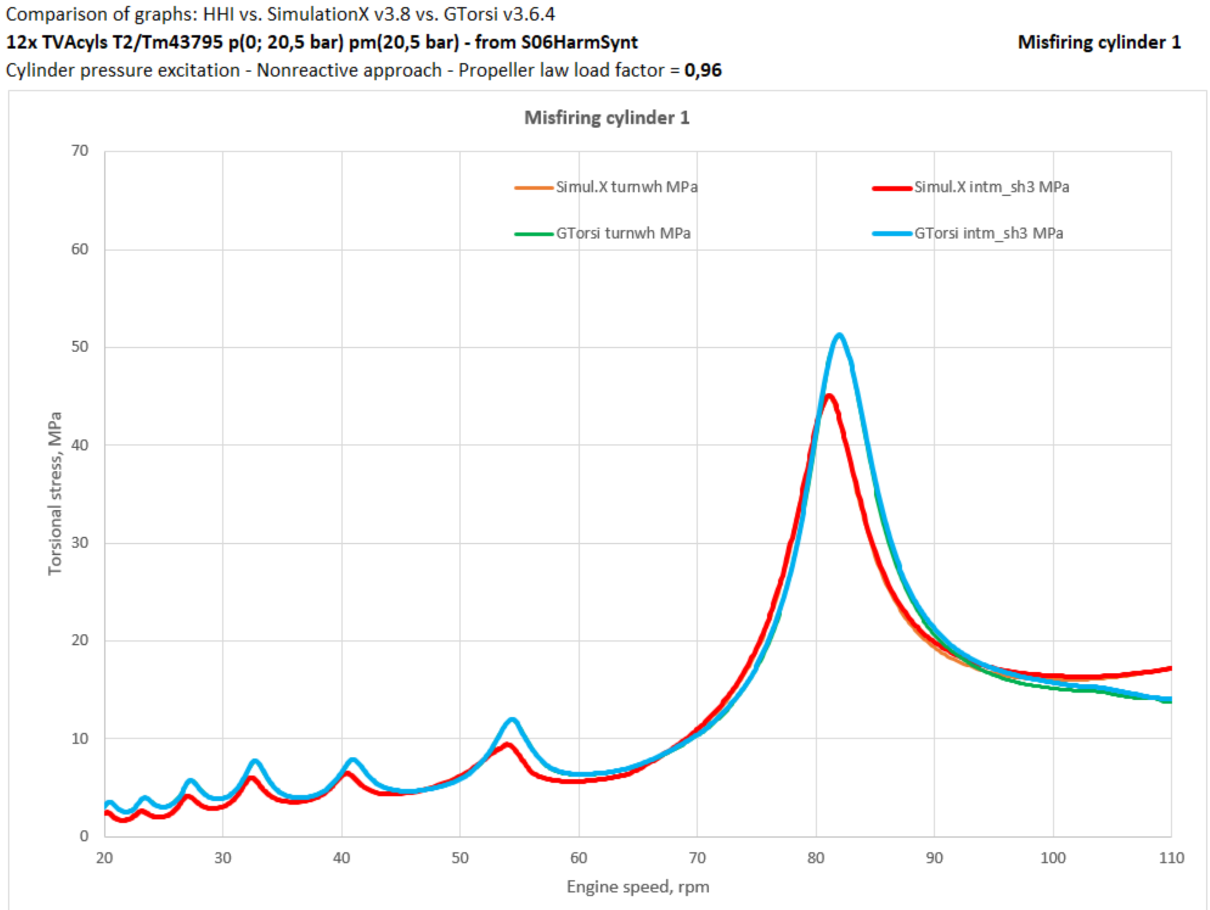

Figure 70. Graphical comparison of torsional stress results in thrust and intermediate shaft for model 12K98 under misfiring conditions

6.3.5. Model QSK-19M – four stroke engine based propulsion system of 496 GT Passenger/Ro-Ro Cargo Ship

The hereafter presented simulation model has been chosen to show the actual power of SimulationX torsional vibration analysis capabilities, because the model is nonlinear (due to the nonlinear characteristic of highly flexible coupling) and branched (due to the reduction gearbox normally implemented in such 4-stroke Diesel engine propulsion systems). Simulation model *QSK-19M*, shown in Figure 71, represents branched propulsion system consists of one four-stroke high speed six-cylinders inline marine Cummins Diesel engine type QSK-19M with power of delivers 560 kW at 1800 rpm. Engine power is transmitted to via highly elastic coupling and reduction gear to the propulsion shafting. The TVA model of this propulsion system is discretized into 28 concentrated masses, each represented by its mass moments of inertia, connected by shafts represented by means of torsional springs.

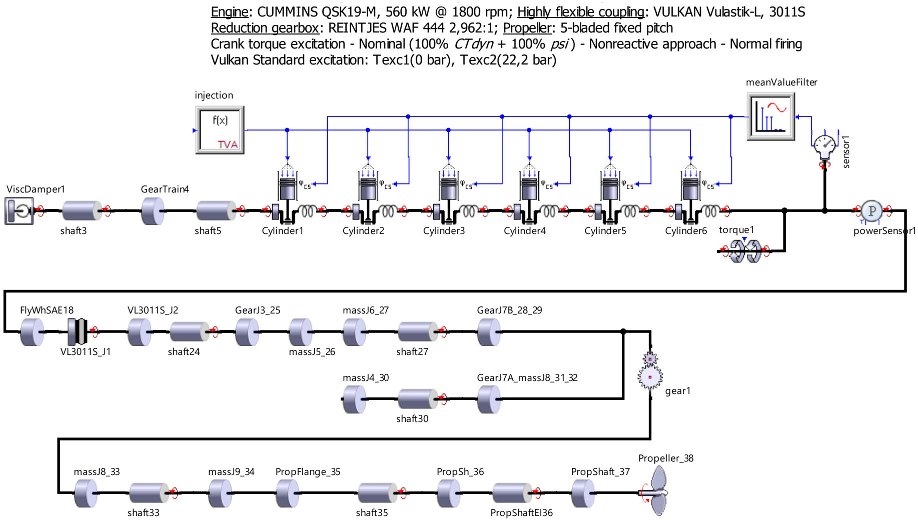

Figure 71. Structure of simulation model QSK-19M

The dependence of dynamic stiffness on mean torque is shown in Figure 72. The resulting diagram shows the nonlinear influence of torque variation on stiffness characteristics.

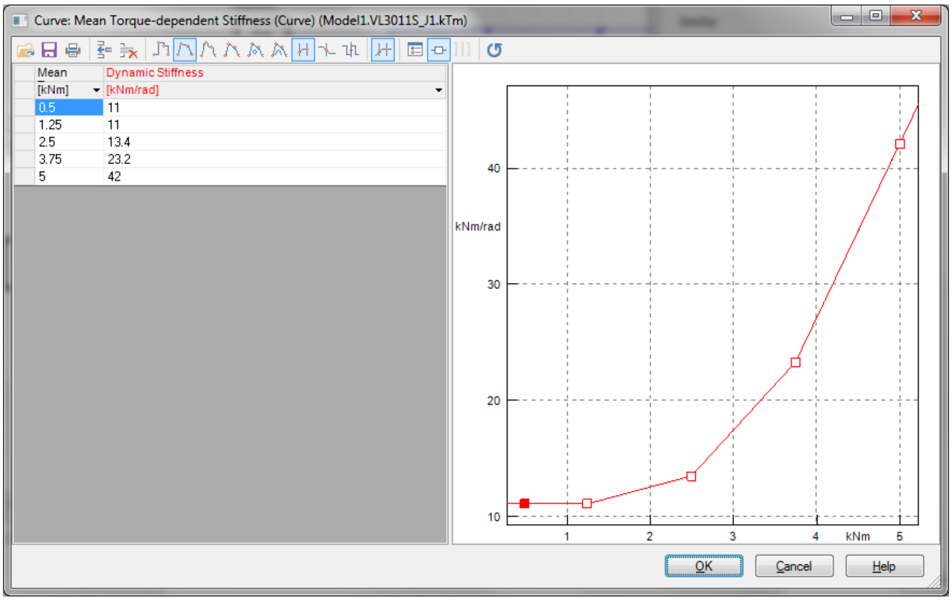

Figure 72. Dependence of dynamic stiffness on mean torque

The dependence of dynamic stiffness on mean torque is shown in Figure 72. The resulting diagram shows the nonlinear influence of torque variation on stiffness characteristics.

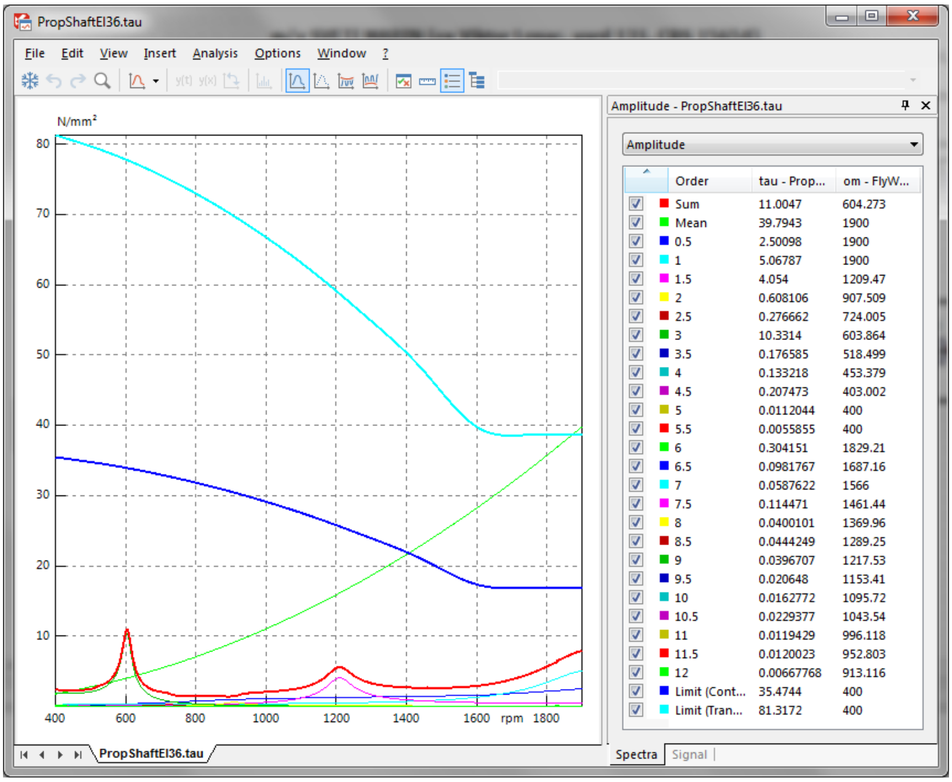

Figure 73. Additional torsional stress in propeller shaft

7. DISCUSSION

This research explores the application of simulation modelling, using SimulationX software, to analyse the dynamic response of marine shaft lines, especially the torsional vibration analysis (TVA), judged as the suitable showcase. Appropriate simulation models, with the same structure, have been developed to accurately represent real ship propulsion systems. For each model, TVA has been conducted under both all cylinders normal firing and one cylinder misfiring operating conditions. Engine and propeller loading have been examined by applying various modelling options to each simulation. The resulting data were statistically evaluated, as well as verified and validated through comparison with reliable reference values.

In simulation model *5S50* representing bulk carrier with 24533 GT, torsional stress results that most closely match the reference values under normal firing conditions are observed in Case 5 (TVA cylinder element, crank torque loading, combinator propeller curve), with the statistical deviation of 0.1%. Here, the lowest relative deviation is 0.1%, and the highest is 0.2%. The poorest results occur in Case 2, which has the statistical deviation of 3.4%, with relative deviations ranging from -8.3% to -8.5%. Under misfiring conditions in simulation model 5S50, Case 3 (TVA cylinder element, crank torque loading, propeller curve at nominal point) shows the closest alignment with reference values, exhibiting the statistical deviation of 1.9%. In this case, the lowest relative deviation is 0.4%, and the highest is -17.6%. Conversely, Case 15 provides the worst results, with the statistical deviation of 3.7% and relative deviations between -7.0% and 19.3%.

For simulation model 6S60 representing crude oil tanker with 59315 GT, the results under normal firing conditions most closely align with the reference values in Case 5 (TVA cylinder element, cylinder pressure loading, combinator propeller curve), with the statistical deviation of 2.1%. The relative deviations in this case range from -3.4% to -8.5%. The poorest results occur in Case 2, where the statistical deviation is 5.5%, and the relative deviations span from -12.4% to -16.8%. In misfiring conditions for the 6S60 model, Case 4 (TVA cylinder element, cylinder pressure loading, combinator propeller curve) demonstrates the best alignment with the reference values, showing the statistical deviation of 2.1%. The relative deviations in this case range from 0.4% to -19.8%. On the other hand, Case 10 delivers the poorest results with the statistical deviation of 4.8%, where the relative deviations range from 1.8% to -20.9%.

In simulation model 7L60 representing reefer ship with 11443 GT, the torsional stress results under normal firing conditions most closely match the reference values in Case 5 (TVA cylinder element, crank torque loading, combinator propeller curve), which has the statistical deviation of 3.1%. The relative deviations here are between -7.1% and -9.7%. The worst performance occurs in Case 6, where the statistical deviation is 6.4%, and the relative deviations range from -15.2% to -17.5%. For the 7L60 model under misfiring conditions, Case 9 (*Cylinder with elastic crank* element, cylinder pressure loading in form of harmonic components, combinator propeller curve) gives the closest match to the reference values, with the statistical deviation of 1.7%. In this case, the relative deviations range from 0.4% to -11.7%. The poorest results are found in Case 2, which has the statistical deviation of 2.6% and relative deviations from -0.1% to -14.5%.

In simulation model 12K98 representing 11388 TEU container ship, the results for torsional stresses that most closely match the reference values under normal firing conditions are found in Case 9 (*Cylinder with elastic crank* element, cylinder pressure loading in form of harmonic components, propeller curve at nominal point), which exhibits the statistical deviation of 3.9%. The relative deviations in this case are between 7.9% and 13.8%. The worst results occur in Case 6, with the statistical deviation of 11.1% and relative deviations from 1.7% to 34.7%. Under misfiring conditions in simulation model 12K98, Case 5 (TVA cylinder element, cylinder pressure loading, combinator propeller curve) shows the closest alignment with the reference values, with the statistical deviation of 1.2%. The relative deviations here range from -0.7% to -7.2%. The poorest results are observed in Case 6, where the statistical deviation is 4.4%, and the relative deviations range from -1.2% to -26.5%.

As described in Section 5.5.1., within cylinder elements two models are available for computation of the acceleration force, namely the physical model and non-reactive model. Valuable insight is gained as both models are tested in this research, with the presented simulation results derived from the latter. The average deviation of simulation results using the physical model compared to the non-reactive model is approximately -4% for critical speeds and -17.5% for torsional stresses in the shaft line components and therefore, these results are omitted from the presentation in all the tables.

Furthermore, simulation models in this research are developed and tested both in compact and expanded form, with the presented simulation results derived from the latter. However, the compact version of the *6S60* simulation model was also developed, utilizing the available 6-cylinder inline engine element. The results obtained from this model showed as less accurate in comparison with the reference data and, therefore, were omitted from the presentation. However, valuable insights into the limitations of this approach were gained. It was found that the model cannot account for compact engines with the odd number of cylinders, engines incorporating the camshaft drive between cylinders, or absolute damping defined using user-defined elements, as specified in this research.

It should be noted that only TVA is performed with the developed models, meaning that the interaction between axial, lateral, and torsional vibrations is not examined in this research. This is due the fact the software tool employed is limited in its ability to simulate vibration coupling effects. Additionally, the strong agreement between the obtained simulation results and the reference data suggests that, while vibration coupling certainly exists, its effects are negligible in the case studies examined. Both linear and nonlinear methods, as described in Section 5.2.2, were used to compute the obtained simulation results. However, the presented results are based on the linear method, as the nonlinear method proved to be significantly time-consuming while providing negligible differences in results.

In SimulationX, engine excitation for normal and misfiring conditions is defined by two curves, each representing the specific load state. To model engine excitation under normal firing conditions, both the normal and drag curves are necessary and have to be prepared. For misfiring conditions, engine excitation for the specific cylinder can be modelled by activating the default misfire parameter. This option was thoroughly examined in this research but showed extremely poor agreement with the reference data, leading to the exclusion of these results. This issue is explained within the theoretical background provided in Sections 5.5.1 and 5.5.3. When the default misfire parameter is used, the cylinder excitation is linked only to the drag load curve, which limits the accuracy of the model. This limitation prompted the development of the more accurate method for modelling misfire, and the results based on this approach are presented in Chapter 6. For misfiring conditions, it is necessary to prepare the normal, misfiring and drag curves. Consequently, this research identified that three load curves, representing normal, misfiring, and drag load states, are essential to accurately model both operating conditions.

In each simulation model, the first three natural frequencies are evaluated under both normal and misfiring conditions. The results from the *5S50*, *6S60*, and *7L60* simulation models exactly match the reference values for both operating conditions. However, in the *12K98* simulation model, only the first natural frequency completely matches with the reference values under both operating conditions. The second natural frequency shows the relative deviation of 3.3%, while the third natural frequency exhibits the relative deviation of -3.0%.

It is important to emphasize the issue excitation activation within simulation models, as it impacts the natural frequency analysis in SimulationX. Although this influence is stated in Section 5.5.3, it is nowhere accompanied by physical explanation or mathematical expressions for their computation. This influence is rather difficult to explain, especially as natural frequency depends solely upon inertia and stiffness as according to expression (16) in Section 3.1.1. The workaround has been found in the terms of switching the excitation in cylinders off during the calculation of natural frequencies.

However, the relative deviation in the natural frequency analysis is quantified in this research, although it is not presented tabularly. The third natural frequency remains unaffected in all models, except in the case of the *12K98* simulation model. The relative deviation is most pronounced for the first natural frequency, ranging from 0.2% to 0.5%, while for the second natural frequency, the deviation is generally much smaller, around 0.1% in most cases.

The simulation results, presented in tabular form, only provide peak values, namely the total torsional stress amplitudes within marine shaft line components at designated critical speeds. Comparison graphs are included to evaluate the overlap between curves derived from the simulation results and those derived from verification and validation data across the entire operating range of the engine. Graphical representations of the simulation results are provided solely for cases exhibiting the least statistical deviation from the reference results. These curves are constructed as collections of discrete time points, with the relative step size ranging from 0.01 to 0.1 rpm in the simulation results and 0.1 rpm in the GTORSI program. The validation results are based on the significantly smaller number of relative steps, graphically represented using dots rather than curves to enhance clarity. Comparison graphs or diagrams which include validation results are separately illustrated for all simulation models.

Overall, for each ship propulsion system examined, the curves derived from SimulationX and the GTORSI program exhibit satisfactory overlap across the entire engine operating range. Accurate and satisfactory curve overlap is crucial, particularly for propulsion systems equipped with engines having fewer or odd number of cylinders, as well as for misfiring conditions in regardless of the propulsion system configuration. The accuracy of the curve overlap is especially notable in the *12K98* simulation model for misfiring conditions, because it incorporates both TVC and validation results, which is particularly rare.

In addition, during the preparation and input of data, several important details were observed. When excitation is defined by cylinder pressure, as in Cases 1, 3, 6, and 8, the pressure input data can be entered using any appropriate physical unit. Similarly, when excitation is defined by crank torque, as in Cases 2, 5, 10, and 13, the torque input data can be entered using any appropriate physical unit. However, when excitation is defined by harmonic components, as in Cases 7, 9, 11, 12, 14 and 15, the same does not apply. In Cases 7 and 9, excitation is defined by the harmonic components of cylinder pressure, which must be specifically prepared and entered using the basic SI unit for pressure (N/m^2). The same applies to Cases 11 and 14, where excitation is defined by the harmonic components of tangential pressure. In Cases 12 and 15, excitation is defined by the harmonic components of excitation torque, which must be prepared and entered using the basic SI unit for torque (Nm).

The engine excitation data provided by the manufacturer are used in VBA programs to prepare excitation data for the SimulationX models in this research. These data, presented as harmonic components of tangential pressures in N/mm^2, cannot be directly entered in Cases 11 and 14 and must be converted to the SI unit, N/m^2. This conversion has been performed in the research, though the details are omitted for simplicity. The simulation results obtained in this manner are effectively identical to those derived using excitation data prepared by the VBA programs, with any differences being negligible, as relative deviations are confined to the second decimal.

Another important detail pertains to the simulation models where excitation is defined using harmonic components, as in Cases 7, 9, 11, 12, 14, and 15. This detail is related to the computation basis outlined in Table 3 of Section 5.5.2. The provided computation expressions include the constant c as the first term. However, this is incorrect, as according to the relevant literature [41, 75, 77], so the first term in the Fourier transform, commonly denoted as A_0, should always be divided by two. This issue posed the challenge in this research and was thoroughly investigated for each simulation model with excitation defined by harmonic components, although the details are omitted for simplicity. The average relative deviation in total torsional stress amplitudes in the shaft line components is approximately 25% due to this error.

The research objectives, focused on the dynamic response of marine shaft lines using simulation modelling, are achieved as they closely align with the findings discussed. The first objective, applying the simulation tool to develop scientific models and conduct TVA, is fulfilled by using SimulationX to model various propulsion systems and perform TVA under normal and misfiring conditions. The second objective, involving data preparation and parameter evaluation, is achieved through meticulous data preparation using the VBA program, along with the comparison and statistical analysis of torsional stresses and natural frequencies.

Verification and validation, as outlined in the third objective, were achieved by comparing simulation results with reference values. This process confirmed the obtained simulation results as satisfactory and highly accurate, in accordance with [92]. Challenges, such as discrepancies with default misfire parameters, led to the development of proper misfiring modelling methodology, supporting the goal of refining the modelling approach.

The research hypothesis, proposing that numerical simulation modelling can identify the most accurate methods for analysing steady-state torsional vibrations in marine shaft lines, is confirmed valid through the research findings. Supporting hypotheses AH1 and AH2, which suggest that the developed procedure can contribute to TVA of ship propulsion systems and enhance ship machinery design practices, are also validated by the findings. The simulation procedure, including the adjustments made to model misfiring and excitation accurately, provides the useful framework for enhancing the design and analysis of marine machinery systems, thus meeting the research objectives and confirming the relevance of the supporting hypotheses.

In accordance with formal specifications, the key application steps of SimulationX in vibration system modelling and analysis are summarized in Table 5.

Table 5. Overview of SimulationX vibration system modelling methodology

No.	Item	Remarks
1.	**Design characteristics**	The propulsion shafting is modelled as circular or hollow sections, assuming a homogeneous and isotropic material defined by the shear modulus.
2.	**Vibration system modelling**	Mass and stiffness are represented by lumped masses and massless springs. Damping is configurable via available options, with viscous damping requiring a defined damping constant *b*.
3.	**Simulation model structure**	Models can be structured in either expanded or compact form.
4.	**Natural frequency analysis**	This step can be performed once the simulation model is fully interconnected and properly configured.
5.	**Modelling approaches / limitations**	The crank mechanism can be modelled using either physical or non-reactive approach. Under normal and misfiring conditions, two curves for two load states are required by default.
6.	**Engine excitation data**	Excitation in engine cylinders is provided as cylinder pressure vs. crank angle (from engine type testing) or as crank torque harmonics expressed as tangential pressure (from the engine licensor). Both can be used as input for data preparation programs.
7.	**Simulation results**	Simulation results are selected and visualized in the result window, from which numerical data can be extracted.

8. CONCLUSION

This research thoroughly investigates the application of simulation modelling approach using SimulationX software to perform torsional vibration analysis (TVA) of marine propulsion shaft line driven by Diesel engines. The series of simulation models, representing real-world ship propulsion systems, were developed and evaluated under both normal firing and misfiring engine conditions. The models shared the unified structural approach, reflecting realistic configurations and enabling consistent comparison across cases. To support the interpretation of the research outcomes, Table 5. is provided to summarize the crucial modelling highlights and findings as the most important outcome of the entire research.

The modelling framework incorporates critical structural design characteristics. Specifically, the propulsion shafting has been modelled using elements with circular or hollow sections, while the material was assumed to be homogeneous and isotropic, characterized by shear modulus. The dynamic system was represented using concentrated masses and massless springs to model mass and stiffness, respectively. Damping modelling, however, proved to be less straightforward due to the input data format in SimulationX, as the damping constant *b* could not be applied directly. This required the development and implementation of additional user-defined elements to represent energy dissipation.

Natural frequency analysis revealed another important finding. Although theory dictates that natural frequencies are governed solely by system mass and stiffness, SimulationX demonstrated minor but not negligible deviations in these frequencies due to the active excitation parameter, obviously due to spring effect of air or gas in engine cylinders. This influence, while difficult to explain theoretically, was systematically tested and documented for all the research models. Notably, natural frequencies in three of the four models matched the reference values exactly, with the *12K98* model showing minimal deviations of 3.3% and -3.0% for the second and third frequencies, respectively. These findings validate the precision of the modelling approach and support its use for predictive analysis of marine propulsion systems. Disabling excitation during frequency analysis proved essential to achieving accurate results, confirming the sensitivity of numerical solvers to input conditions.

Simulation models were developed in both expanded and compact forms. The expanded model forms, featuring individually modelled engine cylinders, demonstrated superior flexibility and result accuracy, especially in systems with the odd number of cylinders or specific crank arrangements. In contrast, compact engine models where available were found deficient and unable to implement the developed absolute damping elements thus significantly affecting the final results. They did not capture key structural or damping details in the proper way. The most accurate simulation results were obtained using the expanded model architecture, with statistical deviations in torsional stress amplitudes ranging from as low as 0.1% to the maximum of 11.1%, depending on the configuration and operating condition.

An essential aspect of this research was engine excitation modelling under normal and misfiring conditions. Classification rules of IACS classification societies require both calculations with normal firing in all of the engine cylinders and misfiring in one cylinder. While excitation modelling for normal conditions performed flawlessly, the default misfire function in SimulationX failed to produce correct results. In fact, the results obtained by means of the SimulationX built-in misfire function were completely messy and thus useless! The author's own custom modelling strategy had to be developed, introducing three excitation curves (normal, misfiring, and drag), resulting in significantly improved accuracy for misfire simulations. Additionally, the study compared two connecting rod force models, physical and non-reactive, within cylinder elements. The non-reactive model was ultimately preferred for its computational efficiency and reasonable accuracy, while the physical model produced deviations of up to -17.5% in stress amplitudes.

Verification and validation of the obtained results are considered of utmost importance and were performed for each and every model throughout this research. Simulation results were benchmarked against GTORSI program, widely accepted TVA calculation tool, and validated through the available results of experimental onboard torsional vibration stress measurements. Obtained simulation results from the developed models *5S50*, *6S60*, *7L60*, and *12K98*, demonstrate strong agreement with the reference data. Statistical deviations for torsional stress amplitudes under both normal and misfiring conditions generally ranged between 0.1% and 4%, with the highest deviation observed at 11.1% in the specific case of the *12K98* model. Graphical comparisons showed excellent overlap between SimulationX and GTORSI outputs across the entire engine operating range. This was especially evident in models of engines with smaller or odd-numbered cylinders, and under misfiring conditions where dynamic behaviour can be more unpredictable.

Data preparation and handling were critical to the success of this research. Engine excitation data were input in the form of cylinder pressure, crank torque or harmonic components, depending on the observed calculation case. When using harmonic data, conversion to SI units (e.g., N/m² or Nm) was necessary to ensure consistency and prevent scaling errors, though it has nowhere been requested in the SimulationX reference manuals or help files! Furthermore, the error was identified in the default Fourier transformation expression for the A_0 term. This error, if uncorrected, would have introduced the 25% deviation in torsional stress amplitudes. VBA programs have been developed and used to automate and refine excitation data processing, enhancing repeatability and accuracy across model variations. This emphasizes the importance of understanding not only physical parameters but also the computational basis and mathematical formulations embedded in simulation tools.

In the terms of analysis methodology, the study confirmed that linear modelling approaches are generally sufficient for steady-state TVA. Although nonlinear methods were also tested, they yielded negligible improvements at the significantly higher computational cost. This finding supports the pragmatic use of linear solvers in engineering workflows, provided that the input data are properly calibrated and structured.

The research met all its predefined objectives, developing scientific simulation models, conducting rigorous TVA under various engine conditions, ensuring precise data preparation, and performing thorough verification and validation. Obtained simulation results confirm that SimulationX is the robust tool for assessing marine propulsion system dynamics but it has to be used *cum-grano-salis*. The central hypothesis, that simulation modelling can be effective tool for TVA of marine shaft line, is fully validated. Auxiliary hypotheses, which suggest these frameworks enhance TVA practices and inform better ship design, are also affirmed. Further on, comparison of the calculation results with the ones of the experimental validation onboard show that there is no need to analyse coupled axial and torsional vibration calculation results in the analysed and presented cases. Calculation results of torsional vibrations only are in a very good match with their experimental validation. This applies both to 2-stroke and 4-stroke engines based main propulsion shafting systems.

To support the interpretation of the research outcomes, Table 6. is provided to summarize the crucial modelling highlights and findings as the most important outcome of the entire research

Table 6. Necessary deviations from normally expected calculation procedure in implementation of SimulationX to TVC modelling and analysis

№	SimulationX model(s)	Quantity, property, or phase	Ordinary calc. procedure // Effect	Workaround	Final outcome
1.	Compact engine models	Dynamic magnification elements missing in models.	Open compound and try to add required elements (e.g. dynamic magnification). // Cannot be done.	Avoid compact engine models. Implement expanded engine models instead of compact ones.	Correct results.
2.	Engine cylinder models	Model for consideration of oscillating mass in cylinder *mOSC*. *kindFaP*: Physical model vs Approach by crank angle (nonreactive)	Physical model expected to be more precise than nonreactive. // Physical model gives highly underestimated torsional stress amplitudes.	Physical model not to be implemented ever. *kindFaP*: Physical model → Approach by crank angle (nonreactive)	Correct results.
3.	Engine cylinder models	Crank damping coefficient *bC*	Enter dependence upon inertia when necessary. // *bC* does not accept analytical expression. The results are completely incorrect.	Develop and implement user defined element of e.g. dynamic magnification *M* related to the selected inertia.	Correct results.
4.	Engine cylinder models	Misfiring in engine cylinder	Misfiring → true. Program uses drag and normal curves only. // Torsional stress amplitudes completely incorrect.	Misfiring → false. In misfiring cylinders input compression curve as second curve (*pCylCurve2* or *TeCurve2* etc.)	Correct results. Misfiring calculation requires drag, normal and misfiring curves.
5.	Engine cylinder models with excitation expressed as Harmonic components for 2 load states	Components: Cylinder pressure, Excitation force, Tangential pressure, Excitation torque	Select measurement units (bar, kNm, …). // Measurement units can nowhere be selected.	Excitation assumes basic SI units only: pressure [N/m²], torque [Nm]. Enter values expressed in these units only.	Correct results. Somewhat difficult to follow the quantities in N/m² and N/m.
6.	Engine cylinder models with excitation expressed as Harmonic components for 2 load states	Components: Cylinder pressure, Excitation force, Tangential pressure, Excitation torque	Trigonometric approximation constant term, *c*. // Calculated stress amplitudes deviate by ~25% from the correct ones.	Calculate harmonic components A_0, A_1, B_1, A_2, B_2, … A_n, B_n and enter $c = A_0 / 2$ into the Table editor.	Correct results.
7.	All TVC models, always	Natural frequencies and mode shapes	Should be dependent upon elements inertia and stiffness only. However, different elements to model engine cylinders and their loading produce different natural frequencies.	Turn off excitation in engine cylinders. Consideration of excitation, *swe*: true → false	Correct results. Dependence of natural frequencies only upon elements inertia and stiffness.
8.	Some TVC models, rarely	Steady state simulation	Simulation → Mode → Steady state; Simulation → Start // Message: "In period calculation: Inaccurate or wrong period vector". Calculation stops.	Steady State Settings → change both Reference quantity and Period variable (e.g. set to *om* and *phi* of the first inertia)	Calculation normal running and completion.

In conclusion, this research confirms the efficacy of simulation-based TVA for marine propulsion systems under normal and misfiring operating conditions, and provides validated, adaptable application approach for engineers and designers. This research underscores the significant potential of simulation modelling, especially when validated, for optimizing the design and analysis of marine propulsion systems. The developed models for TVA provide the reliable framework for predicting torsional stresses and natural frequencies, offering significant advantages in terms of time and cost savings compared to traditional physical testing though the classification rules require testing for the first newly built ship in series. However, the study also demonstrates the inherent risks of relying solely on simulation models without proper calibration and validation, as discrepancies in the results can lead to inaccurate or unsafe design decisions.

The findings offer the comprehensive foundation for future design improvements, potential diagnostic practices, and continued innovation in the field of marine engineering. While the findings of this study are promising, there are several limitations that need to be addressed in future research. One significant limitation is the inability to simulate vibration coupling effects (axial and torsional) within the SimulationX software that may be important in some cases. Future studies should explore more advanced simulation tools that can account for these coupled vibrations, as this would provide more comprehensive understanding of the dynamic behaviour of marine shaft lines.

Furthermore, the study suggests that there is potential for simulation modelling to be applied to design optimization, as well as for TVA of other marine propulsion systems such as steam turbine based or Diesel electric propulsion systems, though their nature of excitation forces is expected to produce much less severe impact than in reciprocating engine systems. It should also be applied in broader context, such as for TVA of ship machinery systems, such as on ship genset auxiliary, cargo turbo-pumps, etc.

Finally, correctly and rigorously performed simulation modelling of torsional vibrations in marine shaft lines can provide sufficiently reliable results to classification societies and design offices in the design, approval, and control of this essential part of the ship's propulsion system. The research findings suggest that simulation modelling can be used as the design optimization tool, leading to more cost-effective ships. As the maritime industry continues to prioritize efficiency and sustainability, the role of simulation modelling will certainly become crucial.

LITERATURE

[1] J. P. Den Hartog, Mechanical vibrations, New York and London: McGraw-Hill Book Company, 1947.

[2] E. J. Nestorides, A Handbook on Torsional Vibration, Cambridge: Cambridge University Press, 1958.

[3] W. K. Wilson, Practical Solution of Torsional Vibration Problems, London: Chapman and Hall, 1956.

[4] R. L. Eshleman, "Torsional vibration of machine systems," in *Proceeding of the Sixth Turbomachinery Symposium*, College Station, 1977.

[5] N. Vulić, A. Šestan and C. V., "Shafting alignment calculation and validation criteria," in *5th Internation Congress of Croatian Society of Mechanics – ICCSM*, Trogir/Split, 2006.

[6] N. Vulić, A. Šestan and V. Cvitanić, "Verification of Crankshaft Design and Fatigue Strength for in-line and v-type Marine Diesel Engines," *Strojarstvo,* vol. 49, no. 4, pp. 317-331, 2007.

[7] M. Savolainen, H. Tienhaara, T. Resch and B. Smiljanic, "Comparison of Crankshaft Calculation Methods with Reference to Classification Societies' Requirements," in *CIMAC Congress*, Bergen, 2010.

[8] A. S. Mendes, P. Meirelles and D. E. Zampieri, "Analysis of torsional vibration in internal combustion engines: modelling and experimental validation," *Journal of Multi-body Dynamics,* vol. 222, no. 2, pp. 155-178, 2008.

[9] J. C. Wachel and F. R. Szenasi, "Analysis of torsional vibrations in rotating machinery," in *Proceeding of the 22nd Turbomachinery Symposium,* College Station, 1993.

[10] L. Bryndum and S. B. Jakobsen, An Introduction to Vibration Aspects of Two-stroke Diesel Engines in Ships", 1992., MAN B&W Diesel A/S, 1992.

[11] L. Bryndum and S. B. Jakobsen, "Vibration Characteristics of Two-Stroke Low Speed Diesel Engines," in *Proceeding of 9th International Marine Propulsion Conference*, London, 1987.

[12] J. E. Margaronis, "The torsional vibrations of marine Diesel engines under fault operation of its cylinders," *Engineering Research,* vol. 58, pp. 13-25, 1992.

[13] Y. Batrak, "Torsional vibration calculation issues with propulsion systems," ShaftDesigner, 2010.

[14] D. Hesterman and B. Stone, "A systems approach to the torsional vibration of multi-cylinder reciprocating engines and pumps," *Journal of Mechanical Engineering Science,* pp. 395-408, 1994.

[15] D. C. Hesterman and B. J. Stone, "A comparison of secondary inertia effects in a range of reciprocating engines," in *Proceedings of the International Mechanical Engineers Congress*, Canberra, 1994.

[16] D. Hesterman and B. Stone, "Secondary inertia effects in the torsional vibration of reciprocating engines – a literature review," *ournal of Mechanical Engineering Science,* vol. 208, pp. 11-15, 1994.

[17] N. Vulić, Đ. Dobrota and I. Komar, "Damping and excitation in the torsional vibrations calculation of ship propulsion systems," in *Proceeding of the Contemporary Issues in Economy & Technology - CIET*, Split, 2016.

[18] H. Tienhaara and H. Mikonaho, "Engine Dynamics and Vibration Control," in *CIMAC Congress*, Vienna, 2007.

[19] J. Holm, Comparison of methods to measure torsional vibration, Vassa: University of Applied Sciences, 2014.

[20] S. Schramm, Damping of Torsional Interaction Effects in Power Systems Doctoral thesis, Munchen: Technische Universitat, 2010.

[21] N. Vulić, K. Bratić, B. Lalić and L. Stazić, "Implementing SimulationX in the modelling of marine shafting steady state torsional vibrations",, No. 2 (110), Vol. 28, 2021., pp. 63-71," *Polish Maritime Research,* vol. 28, no. 2, pp. 63-71, 2021.

[22] N. Vulić, I. Komar and P. Jurišić, "Selection and evaluation of marine shafting torsional vibrations calculation software," in *Proceedings of International Maritime Science Conference*, Solin, 2017.

[23] N. Vulić, K. L. B. Bratić and L. Stazić, "Propeller load modelling in the calculations of marine shafting torsional vibrations," *Pedagogika,* vol. 93, no. 6, pp. 204-216, 2021.

[24] H. Rimstad, Dynamic Modelling, Vibration and Fatigue Analysis of Slow Rotating Propulsion Systems, Trondheim: Norwegian University of Scisence and Technology, 2018.

[25] G. P. Gunnarsson and S. P. Sigurðsson, Dimensioning of marine propulsion shafts, Gothenburg: Chalmers University of Technology, 2021.

[26] L. Murawski and A. Charchalis, "An Estimation Method for the Torsional Vibration of the Marine Propulsion System," *Solid State Phenomena,* Vols. 220-221, pp. 71-80, 2015.

[27] V. D. Doan and M. L., "Vibrations in marine power transmission system," *Scientific Journal of Gdynia Maritime University,* no. 100, pp. 37-50, 2017.

[28] M. L., "Vibrations resonance estimation in marine structures," *Journal of KONES Powertrain and Transport,* vol. 21, no. 1, pp. 175-182, 2014.

[29] L. Murawski and A. Charchalis, "Simplified method of torsional vibration alculation of marie power transmission system," *Marine structures,* vol. 39, pp. 335-349, 2014.

[30] L. Murawski and M. Dereszewski, "Theoretical and practical backgrounds of monitoring system of ship power transmission systems´ torsional vibration," *Journal of Marine Science and Technology,* vol. 25, pp. 272-284, 2019.

[31] I. Senjanović, N. Hadžić, L. Murawski, N. Vladimir, N. Alujević and D. S. Cho, "Analytical procedures for torsional vibration analysis of ship power transmission system," *Engineering Structures,* vol. 178, pp. 227-244, 2019.

[32] I. Senjanović, I. Ančić, G. Magazinović, Alujević, V. N. N. and D. S. Cho, "Validation of analytical methods for the estimation of the torsional vibrations of ship power transmission system," *Ocean Engineering,* vol. 184, pp. 107-120, 2019.

[33] Y. Batrak, "Ice Induced Propulsion Shafting Torsional Vibration Analysis Issues and Case Studies," in *Torsional Vibration Symposium*, Salzburg, 2017.

[34] A. Y. Batrak., A. M. Serdjuchenko and A. I. Tarasenko, "Calculation of Torsional Vibration Responses in Propulsion Shafting System Caused by Ice Impacts," in *Torsional Vibration Symposium*, Salzburg, 2014.

[35] A. Zambon and L. Moro, "Torsional vibration analysis of diesel driven propulsion systems: The case of a polar-class vessel," *Ocean Engineering,* vol. 245, 2022.

[36] G. Burella, L. Moro and D. Oldford, "Analysis and validation of a procedure for a lumped model of Polar," *Journal of Marine Science and Technology,* vol. 23, pp. 633-646, 2018.

[37] A. Zambon, L. Moro, A. Kennedy and D. Oldford, "Torsional vibrations of Polar-Class shaftlines: Correlating ice–propeller," *Ocean Engineering,* vol. 267, 2023.

[38] ISO, "ISO 2014:2018 Mechanical cibration, shock and condition monitoring - Vocabulary," International Organization for Standardization, Geneaa, 2018.

[39] G. Vizentin, G. Vukelić and M. Srok, "Common failures of the ship propulsion shafts," *Scientific Journal of Maritime Research,* vol. 31, pp. 85-90, 2017.

[40] G. Vizentin, G. Vukelić, L. Murawski, N. Recho and J. Orović, "Marine Propulsion System Failures – A Review," *Journal of Marine Science and Engineering,* vol. 8, no. 9, 2020.

[41] S. S. Rao, Mechanical vibrations 6th Edition, Pearson, 2018.

[42] K. Kuiken, The Diesel Engines I: for Ship Propulsion and Power Plants, 2012.

[43] G. Magazinović, "Screening of Slow Speed Marine Diesel Propulsion Shafting Design Space," *Strojarstvo,* vol. 51, no. 6, pp. 575-586, 2009.

[44] G. Magazinović, "Shafting vibration primer," CADEA, Split, 2009.

[45] CRS, CRS Rules for the Classification of Ships, "Part 7 – Machinery installation", Split: Croatian Register of Shipping, 2020.

[46] W. Schiffer, "Shaft vibration: Axial vibration," in *Encyclopedia of Maritime and Offshore Engineering*, New Jersey, Wiley, 2017, pp. 1215-1225.

[47] L. Murawski, Static and Dynamic Analysis of Marine Populsion Systems, Warszawa: Oficyna Wydawnicza Politecniki Waeszawskiej, 2003.

[48] Y. Batrak, "Lateral vibration prediction issues," ShaftDesigner, 2011.

[49] D. Ziu, L. Ling, Z. Rao and T. Na, "Coupled longitudinal-transverse dynamics of a marine propulsion shafting under primary and internal resonances," *Journal of sound and vibration,* vol. 372, pp. 299-316, 2016.

[50] Y. Yi, Z. Lun, Y. Zhengyang, W. Bozheng, S. Guoji, Z. Yang and H. Niaoqing, “Vibration Analysis of a Marine Propulsion Shaft System with the Torsional-longitudinal Coupling Effect Induced by Propeller and Crankshaft,” in *Global Reliability and Prognostics and Health Management*, Nanjing, 2021.

[51] Z. Hu, J. Tang and C. Siyu, “Analysis of coupled lateral-torsional vibration response of a geared shaft rotor system with and without gyroscopic effect,” *Journal of mechanical engineering science,* vol. 24, pp. 232-246, 2018.

[52] Q. Huang, X. Yan, C. Zhang and H. Zhu, “Coupled transverse and torsional vibrations of the marine propeller shaft with multiple impact factors,” *Ocean engineering,* vol. 178, pp. 48-58, 2019.

[53] J. Guo-Yong and Y. Tian-Gui , “Ship Machinery Design,” in *Encyclopedia of Ocean Engineering*, Springer, 2022, pp. 1614-1622.

[54] IACS, “IACS Z21 "Surveys of Propeller Shafts and Tube Shafts",” International Association of Classification Societies, London, 2015.

[55] N. Vulić, “Numerical Modelling of Crack Propagation Arrest Procedures,” FSB, 1995.

[56] B. R. G. and J. K. Nisbett, Shigley’s Mechanical Engineering Design, New York: McGraw-Hill Education, 2015.

[57] Z. Kulenović and N. Vulić, Elementi brodskih strojeva i pomorskih konstrukcija, Split: Faculty of Maritime Studies, 2020.

[58] DIN, “DIN 743-1 Calculation of load capacity of shafts and axles,” Deutsches Institut für Normung, 2012.

[59] DNV, DNV CG-0038, “Calculation of shafts in marine applications”, Høvik: Det Norske Veritas, 2021.

[60] R. l. Mott, Machine Elements in Mechanical Design (5th Edition), Pearson, 2013.

[61] N. P. Kyrtatos, “Slow-Speed Two-Stroke Engines,” in *Encyclopedia of Maritime and Offshore Engineerin*, Wiley, 2018, pp. 1227-1237.

[62] IACS, “IACS M68 "Dimensions of propulsion shafts and their permissible torsional vibration stresses",” International Association of Classification Societies, London, 2014.

[63] M. E. Solutions, “Basic principles of ship propulsion,” 2023.

[64] IACS, "IACS: Safer and Cleaner Shipping," International Association of Classification Societies, [Online]. Available: https://iacs.org.uk/. [Accessed 15 May 2023].

[65] ISO, “ISO 3046-5:2001 "Reciprocatinginternal combustion engines — Performance — Part 5: Torsional vibrations",” Organization for Standardization, Geneva, 2001.

[66] ISO, “ISO 21940 – 12:2016 "Mechanical vibration — Rotor balancing",” International Organization for Standardization, Geneva, 2016.

[67] VDI, VDI 2039 "Torsional vibration of drivelines – Calculation, measurement, reduction", Düsseldorf: Verein Deutscher Ingenieure, 2016.

[68] Croatian Register of Shipping, “CRS Rules for the Classification of Ships, “Part 9 – Machines”,” Croatian Register of Shipping, Split, 2022.

[69] G. T. Beckwith, D. R. Marangoni and H. J. Lienhard, Mechanical Measurements, Pearson, 2011.

[70] G. J. Webster and H. Eren, Measurement, Instrumentation, and Sensors Handbook, CRC Press, Taylor & Francis Group, 2014.

[71] S. A. Morris and R. Langari, Measuremnt and instrumentation, Academic Press, Elsevier, 2012.

[72] B. R. Northrop, Introduction to instrumentation and measurements, CRC Press, Taylor & Francis Group, 2014.

[73] I. Alfirević, “Vibracije,” in *Tehnička enciklopedija*, Zagreb, 1997, pp. 462-477.

[74] M. Cvitković, S. Dolanski Babić, D. Hrupec, Z. Jakobović, V. Lopac, M. Mihaljević, A. Milković, I. Movre Šapić, B. Nahod, S. Popović, T. Roginić, A. Tonejc and D. Veža, “Hrvatsko nazivlje u fizici,” Institut za hrvatski jezik i jezikoslovlje, Zagreb, 2015.

[75] D. J. Inman, Engineering Vibrations, Pearson Education, 2014.

[76] C. W. de Silva, Vibration: Fundamentals and Practice, CRC Press LLC, 1999.

[77] G. S. Kelly, Mechanical Vibrations: Theory and Applications, Cengage Learning, 2012.

[78] D. Pustaić, H. Wolf and Z. Tonković, Mehanika III., Zagreb: Golden marketing - Tehnička knjiga, 2005.

[79] D. &. T. MAN, “Torsional Vibration Calculation Program GTORSI, User’s Manual, Version 3.6.1 External,” Copenhagen, 2012.

[80] ESI, “SimulationX Torsional Vibration Analysis, in the SimulationX Library Manual,” Dresden, 2013.

[81] D. Woodyard, Pounder’s Marine Diesel Engines and Gas Turbines, Elsevier, 2004.

[82] K. Lal, Procedure for Torsional-Vibration Calculations in Ice, Rostock: University of Rostock, 2021.

[83] Soofastaei and Ali, “Introductory Chapter: Numerical Simulation,” in *Numerical Simulation - Advanced Techniques for Science and Engineering*, IntechOpen, 2023.

[84] “Green, safe, reliable - ITI presenting latest SimulationX release at SMM 2012,” aecaffe, 24 July 2012. [Online]. Available: https://aeccafe.com/nbc/articles/1/1107572/Green-safe-reliable-ITI-presenting-latest-SimulationX-release-SMM-2012. [Accessed 23 2 2025].

[85] J.-F. Prevéraud, “Ils s’équipent : Bureau Veritas adopte SimulationX d’ITI,” L'Usine Nouvelle, 31 August 2011. [Online]. Available: https://www.usinenouvelle.com/article/ils-s-equipent-bureau-veritas-adopte-simulationx-d-iti.N1896622. [Accessed 13 April 2025].

[86] “SimulationX Multi-domain System Simulation Software,” ESI-group, [Online]. Available: https://www.esi-group.com/products/simulationx. [Accessed 9 April 2025].

[87] ESI, “User Manual SimulationX,” ITI Software GmbH, Dresden, 2013.

[88] G. Group, “(I-1-22) Guidelines for the Construction of Polar Class Ships,” GL, 2008.

[89] FMA, “FMA "Ice Class Regulations (Finnish-Swedish Ice Class Rules)",” Finnish Maritime Administration, 2008.

[90] IACS, “IACS "Unified Requirements for Polar Ships",” International Association of Classification Societies, London, 2011.

[91] MAN Energy Solutions SE, “MAN Energy Solutions Login portal,” MAN Energy Solutions, 2020. [Online]. Available: https://extranet.man-es.com/. [Accessed 15 4 2025].

[92] VDI, “VDI 3843 Part 1. "Modelling of vibrating systems",” Verein Deutscher Ingenieure e.V., Düsseldorf, 2018.

[93] M53, “Calculation of crankshafts for I.C. engines,” International Association of Classification Societies, London, 2019.

LIST OF FIGURES

LIST OF TABLES

LIST OF ABBREVIATIONS

ABBREVIATION	DEFINITION
BDF	Backward Differentiation Formula
CAD	Computer-Aided Design
CAE	Computer-Aided Engineering
COM	Component Object Model
CRS	Croatian Register of Shipping
CSR	Continuous Service Rating
DAE	Differential-Algebraic Equation
DIN	Deutsche Industrie-Norm
DOF	Degree-of-freedom
DNV	DNV (ex Det Norske Veritas)
FEM	Finite Element Method
FFT	Fast Fourier Transform
GL	ex Germanischer Loyd
GMRES	Generalized Minimal Residual Method
HMH	Huber-von Mises-Hencky criterion
IACS	International Association of Classification Societies
IEC	International Electrotechnical Commission
ISO	International Organization for Standardization
MCR	Maximum Continuous Rating
MSD	Mean Square Deviation
TVC	Torsional Vibration Calculation
TVA	Torsional Vibration Analysis (broader than TVC)
UR	Unified Requirement
VDI	Verein Deutscher Ingenieure (German Engineers Association)
VBA	Visual Basic for Applications

LIST OF SYMBOLS

SYMBOL	DESCRIPTION	UNIT
b	Damping constant | relative damping	Nms/rad
b_{θ}	Physical damping	
b_{Cabs}	Absolute damping parameter	Nms/rad
c	Damping coefficient	Ns/m
c	Vector of real filter coefficient |	
c_{c}	Critical damping	Ns/m
c_{t}	Torsional damping	Nms/rad
c_{tc}	Critical torsional stiffness	Nms/rad
d	Minimum diameter of the shaft	m
d_{cyl}	Cylinder diameter (bore)	m
d_i	Inner diameter of the shaft	m
d_o	Outside diameter of the shaft	m
d_H	Hub diameter	m
d	Rotor diameter	m
ex	Eccentricity parameter	
$\mathbf{f}$	Excitation force vector	
f_{C}	Cosine component of the vector of external forces	
f_{S}	Sine component of the vector of external forces	
f_i	*i-th* fundamental frequency	Hz
f_n	Natural frequency	Hz
inj	Injection parameter	
k	Spring stiffness constant	N/m
k_d	Low-cycle fatigue factor for particular shaft design feature	
k_t	Torsional stiffness	Nm/rad
l	Length of the shaft	mm
l_{rod}	Length of connecting rod	mm
m	Mass	kg
m_{osc}	Reciprocating mass	kg
$\mathbf{m_t}$	Harmonic excitation torque	
n	Rotational speed of the shaft	rpm
n	Number of blades	
n_0	Rotational speed of the shaft at rated power	rpm
p_{Cylx}	Pressure for load state	Pa
p_{cyl}	Cylinder pressure	Pa
per	Fundamental period	
p_i	*i-th* period	
r	Coefficient of cycle asymmetry	
r_1, r_2	Roots of characteristic equation	
r_C	Crank radius	mm
s	Piston stroke	mm
t	Time	s
x	Vector of displacement	m
$\dot{x}$	Vector of velocity	m/s
$\ddot{x}$	Vector of acceleration	m/s^2

SYMBOL	DESCRIPTION	UNIT
x_0	Initial displacement	m
$\dot{x}_0$	Initial velocity	m/s
x_{ref}	Reference quantity	
$\dot{x}_{ref}$	Relative speed of contact surfaces	m/s
x_{st}	Static displacement	m
x_h	Homogenous part of differentia equation	
x_p	Homogenous part of differentia equation	
x_p	Constant period vector with dimension of steady state variables	
A_i, B_i	Coefficients of *i-th* parameter	
B	Estimation damping factor	
$\mathbf{C}$	Damping matrix	Ns/m
C_1, C_2…	Integration constants	m, m/s
C_D	Size factor	
C_K	High-cycle fatigue factor for particular shaft design feature	
D	Discriminant	$(Ns/m)^2$
D	Diameter	m
D	Leh′s damping factor	
$F(t)$, F_e	Force excitation	N
F_0	Amplitude of the excitation force	m
F_c	Damping force	N
F_i	Inertia force	N
F	Factor for type of propulsion installation	
F_s	Spring force	N
G	Shear modulus of the material	Pa
I_p	Polar moment of inertia	m^4
$\mathbf{J}$	Inertia matrix	kgm^2
J, J_0	Mass moment of inertia	kgm^2
J_C	Crank inertia	kgm^2
J_r	Rotor inertia in air	kgm^2
J_{ref}	Reference inertia	
J_{rw}	Rotor inertia in air plus water inertia	kgm^2
$\mathbf{K}$	Stiffness matrix	Nm
$\mathbf{M}$	Mass matrix	kg
M	Magnification factor	
N	The number of spectral components	
O_i	Order	
P	Rated power transmitter trough the shaft	kW
P_{07}	Adjustable pitch at 70% rotor radius	m
P_{07m}	Nominal pitch at 70% rotor radius	m
P_n	Nominal power	kW
R_i	Magnitude	m
T	Period duration of the vibration	s
T_d	Viscous damping torque	

SYMBOL	DESCRIPTION	UNIT
T_e	Excitation torque	Nm
T_{e1x}	Torque for load state	Nm
T_E	Torque for frequency damping	Nm
T_i	Internal torque	Nm
T_{iC}	Internal torque of the crank	Nm
T_{load}	External (mean) load torque	Nm
T_n	Period of free undamped vibration	S
T_n	Nominal torque	Nm
T_{nc}	Period of damped vibration	s
W_D	Damper work	W
W_S	Spring work	W
W_p	Polar moment of resistance	m^3
X	Displacement amplitude	m
$\underline{\hat{x}}[k]$	Complex amplitude of the *k-th* spectral component	
$\hat{x}_R[k]$	the real part of the complex amplitude	
$\hat{x}_I[k]$	the imaginary part of the complex amplitude	
$\hat{x}[0]$	the constant signal component (mean value)	
$\underline{\hat{y}}[k]$	Complex amplitude of the output signal	
$\hat{y}[0]$	Mean value of output signal	
ζ	Damping factor	
η	Dimensionless radial frequency	
γ	Phase angle	rad
λ	Speed ratio | Connecting rod ratio	
θ	Angular displacement	rad
ρ_{inner}	Modal damping with respect to stiffness	
ρ_θ	Relative damping	
σ_a	Amplitude stress (dynamic component)	Pa
σ_B	Specified minimum tensile strength of the shaft material	Pa
$\sigma_{\max}$	Maximum stress under dynamic load	Pa
$\sigma_{\min}$	Minimum stress under dynamic load	Pa
σ_m	Mean stress (static component)	Pa
τ_C	Torsional stress	Pa
τ_{tor}	Tangential stress due to torsion	Pa
τ_c, τ_1	Allowable stress for continuous operation	Pa
τ_t, τ_2	Allowable stress for transient operation	Pa
φ	Vector of angular displacement	rad
$\dot{\varphi}$	Vector of angular velocity	rad/s
$\ddot{\varphi}$	Vector of angular acceleration	rad/s^2

SYMBOL	DESCRIPTION	UNIT
φ_0	Initial angular displacement	rad
φ_{01}	Phase position of the harmonic *i*	rad
φ_C	Crank angle	rad
φ_{C0}	Initial phase angle	rad
φ_{CS}	Crankshaft angle	rad
ψ	Relative damping | phase damping	
ω	Phase velocity of the vibration	rad/s
ω_C	Crank speed	rpm
ω_{C0}	Initial rotational speed	rad/s
ω_n	Nominal speed	rpm
ω_n	Natural angular frequency of free undamped vibration	rad/s
ω_{nc}	Natural angular frequency of free damped vibration	rad/s
Λ	Logarithmic decrement	
Ω	Angular excitation frequency	rad/s

APPENDIX A - Theoretical background of VBA programs

A.1 Program *S06PropLaw*

The theoretical background for the S06PropLaw program is based on the calculation procedures outlined in MAN B&W documentation, with detailed expressions derived from source [23]. Steady state propeller torque *T*, at operating speed *n*, is expressed as:

$$T = T_{MCR}\left(\frac{n}{n_{MCR}}\right)^2 \tag{A1-1}$$

where:

T_{MCR} is prime mover torque produced at MCR power, Nm

n_{MCR} is nominal engine speed at MCR power, rpm

Torque expressed in terms of engine power (valid for the MCR power) is defined as follows:

$$T = \frac{30 \cdot P}{\pi \cdot n} \tag{A1-2}$$

Thereby, the propeller curve is defined as:

$$P = P_{MCR}\left(\frac{n}{n_{MCR}}\right)^3 \tag{A1-3}$$

where:

P is actual power absorbed by the propeller, kW

n is actual steady state speed, rpm

P_{MCR} is MCR power, kW

n_{MCR} is nominal speed at MCR power, rpm

The loads can be represented in terms of mean pressures, as follows:

$$p_{m,i} = \left[0,96 \cdot \left(\frac{n}{n_{MCR}}\right)^2 + 0,04\right] \cdot p_{m,e\,MCR} + p_D \tag{A1-4}$$

where:

$P_{m,i}$ is mean indicated pressure at speed *n*,

$P_{m,eMCR}$ is mean effective pressure at MCR,

P_D is drag pressure.

Mean effective pressure at MCR is defined as:

$$p_{m,e} = \left[0,96 \cdot \left(\frac{n}{n_{MCR}} \right)^2 + 0,04 \right] \cdot p_{m,e\,MCR} \tag{A1-5}$$

Drag pressure is defined as follows:

$$p_D = p_{m,i\,MCR} - p_{m,e\,MCR} \tag{A1-6}$$

Mechanical efficiency ratio is expressed as:

$$\eta_m = \frac{p_{m,e\,MCR}}{p_{m,i\,MCR}} \tag{A1-7}$$

By substituting formula (A1-7) and (A1-6) into (A1-4), the following is obtained:

$$p_{m,i} = \left[0,96\,\eta_m \cdot \left(\frac{n}{n_{MCR}} \right)^2 + \left(1 - \eta_m\right) \right] \cdot p_{m,i\,MCR} \tag{A1-8}$$

Expressed in terms of torque, and upon simplification, the following expression is obtained:

$$T = \left[0,96 \cdot \left(\frac{n}{n_{MCR}} \right)^2 + 0,04 \right] \cdot T_{MCR} \tag{A1-9}$$

UNIVERSITY OF SPLIT - FACULTY OF MARITIME STUDIES		
TORSIONAL VIBRATIONS CALCULATION - PROPELLER LAW LOADING		
in accordance with MAN B&W formula for fixed pitch propellers		
Program: **S06PropLaw.xlsm**	Author: N.Vulić	ver. **1.0** (22 OCT 2020)

Ship: **Hyundai Heavy Industries, yard 1992** Engine: **MAN B&W, 12K98ME-C7**

INPUT DATA

number of engine cylinders	z_{cyl} =	12	
cylinder bore	D =	980	mm
piston stroke	s =	2400	mm
effective power at max. continuous rating, total	$P_{e,\,MCR}$ =	**72240**	kW
engine speed at max. continuous rating	n_{MCR} =	**104**	rpm
mechanical efficiency ratio	η_m =	0,950	
engine speed, minimal	n_{min} =	20	rpm
engine speed, maximal	n_{max} =	120	rpm
engine speed, step increment	Δn =	5	rpm
propeller curve factor (MAN B&W: *k* = 0,96)	k =	0,96	
loss pressure	p_{loss} =	1	bar

CALCULATED RESULTS

crank radius	r =	1200	mm
effective power at max. continuous rating, per cylinder	$P_{e1,\,MCR}$ =	6020	kW/cyl
torque at max. continuous rating, total	T_{MCR} =	6.633,09	kNm
Direct calculation			
mean indicated pressure	$p_{m,i}$ =	20,18	bar
mean effective pressure	$p_{e,i}$ =	19,18	bar
MAN B&W calculation			
mean indicated pressure	$p_{m,i}$ =	20,18	bar
mean effective pressure	$p_{e,i}$ =	19,18	bar

Propeller law curve, acc. to direct calculation

n	T	$p_{m,i}$
rpm	kNm	bar
20	500,818	1,68
25	633,283	2,06
30	795,186	2,53
35	986,525	3,09
40	1207,301	3,72
45	1457,513	4,45
50	1737,163	5,26
55	2046,249	6,15
60	2384,772	7,13
65	2752,732	8,19
70	3150,128	9,34
75	3576,962	10,58
80	4033,232	11,90
85	4518,939	13,30
90	5034,082	14,79
95	5578,663	16,37
100	6152,680	18,03
105	6756,134	19,77
110	7389,025	21,60
115	8051,353	23,52
120	8743,117	25,52

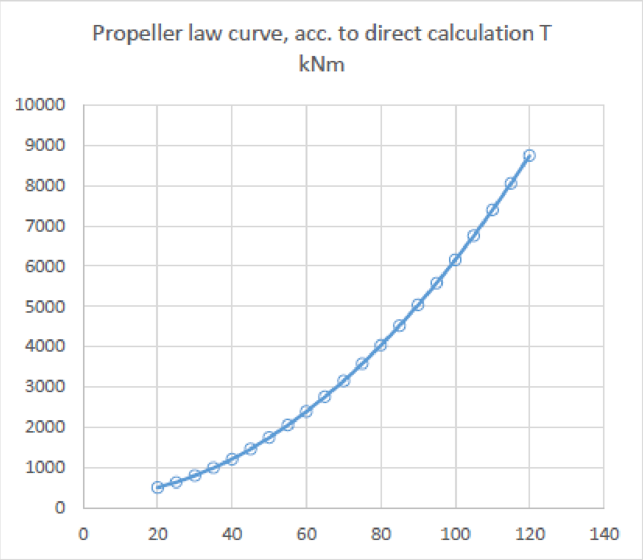

A.2. Program *S06 ViBra*

The program *Torsional Vibrations of Rotational Branched Systems with or without the Gearbox* or abbreviated *S06 ViBra* is completely written using VBA code. The program is used for calculation of eigenfrequencies and eigenvectors for steady-state torsional free undamped vibrations of the rotational in-line system comprising or not comprising the change of rotational speed, described by:

$$\mathbf{J_u} \cdot \ddot{\boldsymbol{\psi}} + \mathbf{C_u} \cdot \boldsymbol{\psi} = \mathbf{0} \tag{A2-1}$$

where

$\boldsymbol{\psi} = [\phi_1 \quad \phi_2 \quad \dots \quad \phi_{k-1} \quad \phi_k \quad u \cdot \phi_{k+1} \quad \dots \quad u \cdot \phi_{N-1} \quad u \cdot \phi_N]^T$ - vector of transformed rotations,

u – reduction gear ratio $(z_k'' / z_k' \geq 1)$ (if any),

N – number of masses.

Eigenfrequencies and eigenvectors, based upon Jacobi's method, are calculated from the frequency equation:

$$\left(\mathbf{J_u^{-1}} \cdot \mathbf{C_u} - \lambda_i \cdot \mathbf{I}\right) \cdot \boldsymbol{\psi}_i = \mathbf{0} \tag{A2-2}$$

or:

$$\mathbf{C_u} \cdot \boldsymbol{\psi} = \mathbf{J_u} \cdot \boldsymbol{\Psi} \cdot \boldsymbol{\Lambda} \tag{A2-3}$$

transforming the eigenproblem to the symmetrical one:

$$\mathbf{A} \cdot \mathbf{x}_i = \lambda_i \cdot \mathbf{x}_i \tag{A2-4}$$

where:

$\mathbf{A} = \mathbf{L}^T \cdot \mathbf{C_u} \cdot \mathbf{L}$ – symmetric matrix of the vibrating system;

$\mathbf{L} = diag\left(1/\sqrt{J_{u1}} \quad 1/\sqrt{J_{u2}} \quad \dots \quad 1/\sqrt{J_{uN}}\right)$ – transformation matrix;

$\boldsymbol{\Lambda} = diag\left(\lambda_{\min} \quad \dots \quad \lambda_{\max}\right)$ –matrix of eigenvalues;

$\boldsymbol{\psi}_i = \mathbf{L} \cdot \mathbf{x}_i$

Numerical precision (error) of the calculation is checked upon the following:

$|\Delta\lambda|_{\max} = \max\left|\boldsymbol{\Lambda} - \mathbf{X}^T \cdot \mathbf{A} \cdot \mathbf{X}\right|$ – numerical error of eigenvalues;

$\left|\Delta\omega\right|_{\max} = \dfrac{\left|\Delta\lambda\right|_{\max}}{2\sqrt{\lambda_{\min}}}$ – numerical error of natural frequencies;

$\left|\Delta n\right|_{\max} = \dfrac{30 \cdot \left|\Delta\omega\right|_{\max}}{\pi}$ – numerical error of natural frequencies expressed as rotational speed;

$\max\left|\mathbf{C_u} \cdot \boldsymbol{\psi} - \mathbf{J_u} \cdot \boldsymbol{\Psi} \cdot \boldsymbol{\Lambda}\right|$ – numerical error due to eigenvectors;

where:

$\boldsymbol{\Lambda} = diag\left(\lambda_1 \quad \lambda_2 \quad \dots \quad \lambda_N\right)$ – matrix of eigenvalues;

$\mathbf{X} = \left[\mathbf{x}_1 \quad \mathbf{x}_2 \quad \dots \quad \mathbf{x}_N\right]$ – matrix of transformed eigenvectors;

λ_{min} – minimal positive eigenvalue;

$\left|\dots\right|$ – absolute value (i.e., not the determinant).

CROATIAN REGISTER OF SHIPPING
TORSIONAL VIBRATIONS OF ROTATING SYSTEMS - FREE VIBRATIONS OF BRANCHED SYSTEMS WITH OR WITHOUT THE REDUCTION GEARBOX
(Jacobi method for eigenfrequencies and eigenvectors)

Program: **S06ViBra.xls / vba** — Author: N.Vulić — Ver.: **1.0** (25 MAR 2007)

Calculation case:	**HHI Yard 1992**					
Engine:	MAN B&W 12K98ME-C7		72240 kW @		104 rpm	
Flexible coupling:	n/a					
Gearbox:	n/a			i =	1 :1	
Propeller:	6 blades	D/H = 8900/8319,89	mm / mm	A_e/A_0 =		0,8409

INPUT DATA

Number of concentrated masses	N =	21
Number of elastic elements	Nc =	20
Required numerical precision of calculation	e =	1,00E-09

CONCENTRATED MASSES

Mass No.	**Inertia** [kgm^2]	**Mass Description**
1	9340,00	DAMPD_250/7/3
2	3444,00	D_INNER+FLG
3	36824,00	CYLINDERl
4	36824,00	CYLINDER2
5	36824,00	CYLINDER3
6	36824,00	CYLINDER4
7	36824,00	CYLINDER5
8	36824,00	CYLINDER6
9	13223,00	CAMDRIVE
10	36824,00	CYLINDER7
11	36824,00	CYLINDER8
12	36824,00	CYLINDER9
13	36824,00	CYLINDER10
14	36824,00	CYLINDER11
15	36824,00	CYLINDER12
16	10600,00	THRUST_SHAFT
17	20398,00	TURNING_WH
18	4214,00	FLANGE1
19	4528,00	FLANGE2
20	6689,00	FLANGE3
21	540142,00	PROPELLER

Red. Node	**Inertia of Gear Wheel** [kgm^2]		**Gear ratio**
20	0	None	1

ELASTIC ELEMENTS

Elem. No.	**Fore Node**	**Aft Node**	**Stiffness** [Nm/rad]	**Elem. No.**	**Fore Node**	**Aft Node**	**Stiffness** [Nm/rad]
1	1	2	5,70E+07	11	11	12	4,27E+09
2	2	3	5,29E+09	12	12	13	4,18E+09
3	3	4	4,22E+09	13	13	14	4,27E+09
4	4	5	4,35E+09	14	14	15	4,41E+09
5	5	6	4,37E+09	15	15	16	6329100000
6	6	7	4,33E+09	16	16	17	9434000000
7	7	8	4,27E+09	17	17	18	307600000
8	8	9	5,78E+09	18	18	19	305400000
9	9	10	5,78E+09	19	19	20	264500000
10	10	11	4,31E+09	20	20	21	603400000

TORSIONAL VIBRATIONS - FREE VIBRATIONS CALCULATION RESULTS

Eigenfrequencies

Vibr Mode	Lambda [1/s2]	Omega [rad/s]	RotSpeed [rpm]	Frequency [Hz]
1	0			
2	295,0869	17,1781	164,0387	2,734
3	5239,7212	72,3859	691,2346	11,5206
4	7629,8917	87,3493	834,1239	13,9021
5	25658,2106	160,1818	1529,6236	25,4937
6	46584,8437	215,8352	2061,0746	34,3512
7	58639,5203	242,156	2312,4193	38,5403
8	98779,5558	314,2922	3001,269	50,0211
9	133617,6819	365,5375	3490,6262	58,1771
10	146647,3274	382,9456	3656,861	60,9477
11	199976,365	447,1872	4270,3229	71,172
12	220491,8222	469,5656	4484,0209	74,7337
13	253553,3826	503,5408	4808,4609	80,141
14	309817,3757	556,6124	5315,257	88,5876
15	357605,8308	598,0015	5710,494	95,1749
16	398231,9592	631,0562	6026,1431	100,4357
17	439879,7261	663,2343	6333,421	105,557
18	448477,3715	669,6845	6395,0162	106,5836
19	1054007,177	1026,6485	9803,7712	163,3962
20	1706296,574	1306,2529	12473,796	207,8966
21	1852676,686	1361,1307	12997,84	216,6307

Maximal error of calculation...Delta_N= 0 [rpm]
Maximal error of eigenequation..........= 0,0003 [Nm]

Eigenvectors, taking gear ratio into account

Mode	1	2	3	4	5	6	7	8	9	10	11	12	13	14	15	16	17	18	19	20
Mass																				
1	0,001	0,001	0,008	0,006	-0,001	0	0	0	0	0	0	0	0	0	0	0	0	0	0	0
2	0,001	0,001	0,001	-0,001	0,002	0,001	0,002	-0,002	0,001	-0,002	0,001	-0,001	-0,002	0,001	-0,001	0	-0,001	0	0	0,016
3	0,001	0,001	0,001	-0,002	0,002	0,001	0,002	-0,002	0,001	-0,002	0,001	-0,001	-0,001	0,001	-0,001	0	-0,001	0	0	-0,002
4	0,001	0,001	0,001	-0,002	0,001	0,001	0,001	0	0	0,001	-0,001	0,001	0,002	-0,002	0,002	-0,001	0,002	0,001	0	0
5	0,001	0,001	0,001	-0,001	0,001	0	-0,001	0,001	-0,001	0,002	-0,001	0,001	0,001	0	-0,002	0,001	-0,003	-0,001	0	0
6	0,001	0,001	0,001	-0,001	0	-0,001	-0,002	0,002	-0,001	0,001	0,001	0	-0,002	0,001	-0,001	0	0,003	0,001	0	0
7	0,001	0,001	0	-0,001	-0,001	-0,001	-0,002	0,001	0	-0,001	0,002	-0,001	-0,001	-0,001	0,002	0	-0,002	-0,001	0	0
8	0,001	0,001	0	-0,001	-0,002	-0,001	-0,001	-0,001	0,001	-0,002	0	0	0,002	-0,001	-0,002	0,001	0,001	0,001	-0,002	0
9	0,001	0,001	0	0	-0,002	-0,001	0	-0,002	0,001	-0,001	-0,001	0,001	0,001	0,001	-0,001	-0,001	0,001	0	0,008	0
10	0,001	0,001	0	0	-0,002	0	0,001	-0,002	0	0,001	-0,002	0	-0,001	0,002	0,001	-0,002	0	-0,001	-0,002	0
11	0,001	0,001	-0,001	0	-0,002	0	0,002	-0,001	-0,001	0,002	0,001	-0,001	-0,001	-0,002	0	0,003	0	0,002	0	0
12	0,001	0,001	-0,001	0,001	-0,001	0,001	0,002	0,001	-0,001	0	0,002	-0,001	0,001	-0,001	-0,001	-0,002	0,001	-0,002	0	0
13	0,001	0,001	-0,001	0,001	0	0,001	0,001	0,002	0	-0,002	0	0,001	0,001	0,002	0,001	0	-0,001	0,002	0	0
14	0,001	0,001	-0,001	0,001	0,001	0,001	0	0,001	0,001	-0,001	-0,002	0,001	-0,002	-0,001	0	0,002	0,001	-0,002	0	0
15	0,001	0,001	-0,001	0,001	0,002	0	-0,001	-0,001	0	0	-0,001	0	-0,001	-0,002	-0,001	-0,002	-0,001	0,002	0	0
16	0,001	0,001	-0,001	0,002	0,002	0	-0,002	-0,002	0	0,001	0,001	-0,001	0,001	0,001	0	0	0	0	0	0
17	0,001	0,001	-0,001	0,002	0,002	-0,001	-0,002	-0,002	-0,001	0,002	0,002	-0,001	0,002	0,002	0,001	0,002	0,001	-0,001	0	0
18	0,001	0	-0,001	0,001	0,002	-0,007	0,002	-0,001	-0,008	-0,003	0,002	0,009	-0,002	-0,001	0	-0,001	0	0	0	0
19	0,001	0	-0,001	0,001	0,002	-0,009	0,005	0,001	-0,001	-0,002	-0,004	-0,009	0,001	0	0	0	0	0	0	0
20	0,001	-0,001	0	0	0,001	-0,004	0,003	0,002	0,009	0,004	0,002	0,004	0	0	0	0	0	0	0	0
21	0,001	-0,001	0	0	0	0	0	0	0	0	0	0	0	0	0	0	0	0	0	0

A.3 Program *S02CrankL*

The program *Crankshaft Calculations for In-Line Type Internal Combustion Engines* or abbreviated *S02CrankL* is completely written using VBA code. The program is used for calculation of crankshaft strength by determining the absolute maximal torque based on the number of cylinders, mean torque per cylinder (from engine power), and nominal alternating torque (from nominal stress), while also incorporating shrink-fit calculations and comparing the input maximal torque with the calculated value. However, it also allows for the harmonic analysis of cylinder pressures function vs. crank angle and for tangential force function vs. crank angle, it is used within this research for calculations of torsional vibration excitations. The theory and formulae of the program presented hereafter are based upon rules and requirements provided in [68, 93].

A.3.1. Kinematic analysis

In the analysis of internal combustion engine mechanisms, the description of piston motion, i.e. the displacement is commonly the starting point. By differentiating displacement with respect to time, piston velocity and acceleration are obtained, which are essential for further dynamic analysis. Simplifications are often introduced in this process, such as series expansion and the neglect of higher-order terms. However, the method presented here deviates from the conventional approach by considering the motion of the connecting rod rather than the piston. This approach yields significantly simplified expressions without the need for approximations or simplifications. The kinematic scheme of the engine mechanism is shown in Figure A3-1.

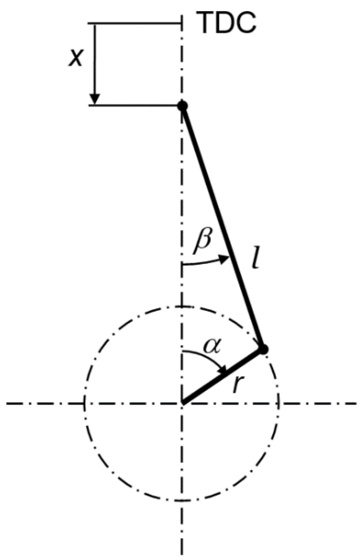

Figure A3-1. Kinematic diagram of the engine mechanism

Steady-state conditions are assumed, where the crankshaft rotates uniformly about its axis with angular velocity ω. The connecting rod undergoes complex planar motion, consisting of the translation of its centre of mass and its rotation around this centre. The position of the connecting rod at any given moment is uniquely determined by the angles α and β, with their positive directions indicated in the corresponding diagram. For the angle β, the relationship is: $-\beta_{max} \leq \beta \leq \beta_{max}$. For the angle α the relationship is: for four-stroke engines: $-360° \leq \alpha \leq +360°$, and for two-stroke engines: $-180° \leq \alpha \leq +180°$.

Angular velocity of the crankshaft:

$$\omega = \frac{\pi \cdot n}{30} \tag{A3-1}$$

The ratio of the crank radius to the connecting rod length:

$$\lambda = r/l \tag{A3-2}$$

Geometric relationship between the connecting rod angle β and the crankshaft angle α:

$$\sin\beta = \lambda \cdot \sin\alpha \tag{A3-3}$$

Connecting rod angular velocity:

$$\omega_{CR} = \frac{d\beta}{dt} = \omega \cdot \lambda \frac{\cos\alpha}{\cos\beta} \tag{A3-4}$$

Connecting rod angular acceleration:

$$\varepsilon_{CR} = \frac{d\omega_{CR}}{dt} = -\omega^2 \lambda \left(1-\lambda^2\right) \frac{\sin\alpha}{\cos^3\beta} \tag{A3-5}$$

Piston displacement (from TDC, positive downwards):

$$x = r\left(1-\cos\alpha + \frac{1-\cos\beta}{\lambda}\right) \tag{A3-6}$$

Piston velocity (positive downwards):

$$v = \frac{dx}{dt} = r\omega\left(\sin\alpha + \frac{\lambda}{2} \cdot \frac{\sin 2\alpha}{\cos\beta}\right) \tag{A3-7}$$

Piston acceleration (positive downwards):

$$a = \frac{dv}{dt} = r\omega^2 \left(\cos\alpha + \lambda \cdot \frac{\cos 2\alpha}{\cos\beta} + \frac{\lambda^3}{4} \cdot \frac{\sin^2 2\alpha}{\cos^3\beta} \right) \tag{A3-8}$$

Stroke:

$$s = 2r \tag{A3-9}$$

Mean piston velocity:

$$v_m = \frac{s \cdot n}{30} \tag{A3-10}$$

A.3.2 Dynamic analysis

In dynamic analysis of the slider-crank mechanism, it is also advantageous to start from the motion of the connecting rod since the following parameters are known:

- mass of the connecting rod m_{cr},
- the distance from the centre of the journal bearing l_{cr}, used position of the connecting rod's centre of mass,
- radius of inertia of the connecting rod i_{cr}, about its centre of gravity (COG).

The mass of the connecting rod is conveniently divided into three components, treated as concentrated masses in the model:

- The translational component m_T (moves together with the piston).
- The rotational component m_R (moves with the crankshaft journal).
- Central component m_C, (the remaining mass associated with the rod's centre of mass).

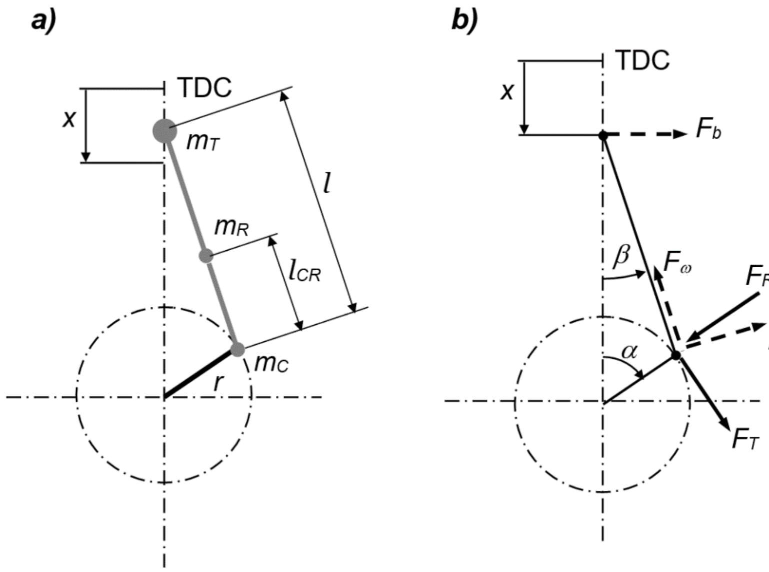

Figure A3-2. Dynamics of connecting rod: a) point masses, b) forces to the connecting rod (F_b, F_ε, F_ω), forces to the crank (F_T, F_R)

This distribution of masses is carried out based on the solution of the linear system of 3 equations with 3 unknowns, where the unknowns are the given masses shown in Figure A3-2 a). The equations are formulated based on three conditions: the sum of all three masses is equal to the total mass of the connecting rod, the sum of the static moments of the masses around the centroid of the connecting rod is equal to zero, and finally, the sum of the moments of inertia of the given masses around the centroid of the connecting rod is equal to the moment of inertia of the connecting rod. Solving this system of equations yields the following expressions for the unknown masses, which is defined as:

$$m_{CR} = m_R + m_C + m_T \tag{A3-11}$$

$$m_R \cdot l_{CR} = m_T \cdot \left(l - l_{CR}\right) = 0 \tag{A3-12}$$

$$m_{CR} \cdot i_{CR}^2 = m_R \cdot l_{CR}^2 + m_T \cdot \left(l - l_{CR}\right)^2 \tag{A3-13}$$

By solving the system of linear equations, the concentrated masses of the dynamic model of the connecting rod are determined:

$$m_T = m_{CR} \cdot \frac{i_{CR}^2}{\left(l - l_{cr}\right) l} \tag{A3-14}$$

$$m_R = m_{CR} \cdot \frac{i_{CR}^2}{l_{CR} \cdot l} \tag{A3-15}$$

$$m_C = m_{CR} - \left(m_T + m_R\right) \tag{A3-16}$$

The forces acting on the connecting rod exclusively due to the inertia of its concentrated masses (inertial forces) acting in positive direction and marked with dashed lines in the Figure A3-2 b). From the conditions of dynamic equilibrium considering the uniform rotation of the crankshaft with angular velocity and the acceleration of the piston, the following expressions are obtained:

Lateral force (acting on the cylinder liner or the crosshead bearing), F_b

$$F_b = \varepsilon_{CR} \cdot l_{CR} \frac{m_C}{\cos\beta}\left(1 - \frac{l_{CR}}{l}\right) - \left(m_T + m_C \frac{l_{CR}}{l}\right) \cdot a_p \tan\beta \tag{A3-17}$$

Longitudinal force (along the axis of the connecting rod), $F\omega$

$$F_\omega = \omega_{CR}^2 \cdot l \cdot \left[m_C \cdot \left(1 - \frac{l_{CR}}{l}\right) + m_R\right] - m_{CR} \cdot a_p \cos\beta + F_b \sin\beta \tag{A3-18}$$

Transverse force (perpendicular to the axis of the connecting rod) $F\varepsilon$

$$F_\varepsilon = \varepsilon_{CR} \cdot l \cdot \left[m_C \cdot \left(1 - \frac{l_{CR}}{l}\right) + m_R\right] - m_{CR} \cdot a_p \sin\beta - F_b \cos\beta \tag{A3-19}$$

A.3.3 Engine cylinder load

In the thermodynamic process underlying the operation of the internal combustion engine, the cylinder gas pressure *p* (air/fuel mixture, combustion gases) varies depending on the crank angle *α*. These pressures can be determined through thermodynamic analysis of the engine cycle or directly measured by recording the indicator diagram. In both cases, the pressures must be known as the dataset, i.e., the table of points (*p, α*) for the complete cycle of the engine process −360° ≤ α ≤ +360° for four-stroke engines, along with −180° ≤ α ≤ +180° for two-stroke engines). Pressure values are typically presented for the constant crank angle increment, such as *Δα*=3°. However, for sufficient precision, the increment should not exceed *Δα*=5°. The mean indicated pressure is determined by integrating the gas pressure curve in the cylinder, where the crank angle is expressed as alpha [rad]:

$$p_{m,i} = \frac{1}{s}\int_{x(\alpha_{\min})}^{x(\alpha_{\max})} p(x)\,dx = \frac{1}{s}\int_{\alpha_{\min}}^{\alpha_{\max}} p(\alpha)\cdot\left(\sin\alpha + \frac{\lambda}{2}\cdot\frac{\sin 2\alpha}{\sqrt{1-\lambda^2\sin^2\alpha}}\right)\cdot d\alpha \qquad \text{(A3-20)}$$

In practice, numerical integration using the trapezoidal rule provides satisfactory results.

A.3.4 Forces acting to the crankshaft crank

When determining the total load on the crankpin of the single-cylinder engine mechanism, the starting point is the forces due to the pressure of combustion gases in the cylinder, which act on the piston, as well as the inertial forces due to the mass of the piston, which moves in reciprocating, i.e. translational oscillatory motion (up and down).

$$F_{gas} = p\cdot\frac{\pi D^2}{4} \qquad \text{(A3-21)}$$

$$F_{in} = -m_{Tadd}\cdot a \qquad \text{(A3-22)}$$

where:

p – gas pressure in the cylinder, dependent on the crank angle α

m_{Tadd} – mass of the other parts of the engine mechanism in translational motion (excluding the mass of the connecting rod, as it has already been accounted for)

The connecting rod transmits the specified forces to the crankpin of the crankshaft via its lower bearing. To this, the previously calculated forces due to the inertia of the connecting rod should be added. The positive direction of the transmitted force components (F_T, F_R) is shown with solid arrows in the previous Figure A3-2 illustrate the forces on the connecting rod and the crankpin. By rotating the coordinate system from the connecting rod axis to the crankpin axis, incorporating kinematic quantities (β, ω_{CR}, and ε_{CR}), and subsequently simplifying, the tangential force F_T, radial force F_R, and the torque M_T acting on the crankshaft at the connecting rod bearing are determined as follows:

$$F_T = \left(F_{gas} + F_{in}\right) \cdot \frac{\sin\left(\alpha+\beta\right)}{\cos\beta} + F_\omega \sin\left(\alpha+\beta\right) - F_\varepsilon \cos\left(\alpha+\beta\right) \tag{A3-23}$$

$$F_R = \left(F_{gas} + F_{in}\right) \cdot \frac{\cos\left(\alpha+\beta\right)}{\cos\beta} + F_\omega \cos\left(\alpha+\beta\right) + F_\varepsilon \sin\left(\alpha+\beta\right) \tag{A3-24}$$

$$M_T = F_T \cdot r \tag{A3-25}$$

The positive direction of the tangential force and torque corresponds to the direction of rotation. The positive direction of the radial force is towards the crankshaft axis. All the forces shown act on the bearing pin, i.e., on the crankpin. From these forces, the stresses are determined, followed by their ranges required for calculating the fatigue strength in the fillet radii of the crankshaft bearing pins.

CROATIAN REGISTER OF SHIPPING		
CRANKSHAFT CALCULATIONS FOR IN-LINE TYPE INTERNAL COMBUSTION ENGINES		
CRS *Rules*, Part 9-*Machines* (2009), item 2.4; IACS UR M53(2004)		
Program: S02CrankL.xls/vba	Author: N.Vulić	Ver.: 3.2 (10 FEB 2013)

Engine manufacturer: **HHI MAN B&W (T243795)** Type: **12K98ME-C7, norm. fir.**

ENGINE INPUT DATA

engine working cycle (two stroke-2, four stroke-4)	$cycle=$	2	
cylinder bore	$D=$	980	mm
crank radius	$r=$	1200	mm
length of connecting rod	$l=$	3090	mm
nominal number of revolutions	$n=$	104	rpm
mass of reciprocating parts (excluding connecting rod)	$m_{Tadd}=$	0	kg
mass of rotating parts (excluding connecting rod)	$m_{Radd}=$	0,00	kg
mass of connecting rod	$m_{CR}=$	0	kg
distance of connecting rod COG to the crank pin	$l_R=$	1500	mm
radius of inertia of connecting rod about its COG	$i_{CR}=$	1500	mm
acceleration of gravity	$g=$	9,80665	m/s^2
mechanical efficiency	$\eta_m=$	0,950	
maximal cylinder overpressure	$p_{max}=$	143,71	bar
cylinder overpressure vs. crank angle	$p(a)$	*see the next worksheet*	

CALCULATED RESULTS

stroke	$s=$	2.400,00	mm
mean piston speed	$v_m=$	8,32	m/s
crankshaft angular rotational speed	$\omega=$	10,89	rad/s
ratio of crank radius to the connecting rod length	$\lambda=$	0,39	
mean indicated pressure	$p_{mi}=$	20,42	bar
mean indicated power per cylinder	$P_i=$	6.408,92	kW/cyl
mean effective pressure	$p_{me}=$	19,41	bar
mean effective power per cylinder	$P_e=$	6.091,33	kW/cyl
mass of connecting rod translational part	$m_T=$	0,00	kg
mass of connecting rod rotational part	$m_R=$	0,00	kg
remaining mass of connecting rod (in the COG)	$m_S=$	0,00	kg

		min	*max*	
tangential force on the crank journal	$F_t=$	-2.276,43	5.016,45	kN
radial force on the crank journal	$F_r=$	-466,93	10.420,48	kN
corresponding torque moment	$T_t=$	-2.731,71	6.019,74	kNm

		mean	*amplitude*	
tangential force on the crank journal	$F_t=$	1.370,01	**3.646,44**	kN
radial force on the crank journal	$F_r=$	4.976,77	**5.443,70**	kN
corresponding torque moment	$T_t=$	1.644,01	4.375,72	kNm

A.4 Program *S06HarmSynt – Engine excitation Harmonic Synthesis*

The program *Engine excitation Harmonic Synthesis* or abbreviated *S06HarmSynt* is completely written using VBA code. Basic formulae described in for program *S02CrankL* is applied in this program, which is used to calculate tangential force, cylinder pressure and crank torque, all vs. crank angle, for the two cases: case of gas normal firing and gas compression only (misfiring) for 2-stroke and 4-stroke internal combustion engines, from the following input data: cylinder bore diameter, ratio of crank radius and connecting rod length, crank radius and harmonic cosine and sine components of Fourier series expansion of gas normal firing and gas compression only tangential pressure values, given for orders 0,5; 1; 1,5; 2; … for 4-stroke engines or orders 1; 2; 3; … for 2-stroke engines. Input data are denoted by pale yellow background: Gas normal firing and misfiring N harmonic (cosine and sine) components F_{TC} and F_{TS} expressed as:

$$p = F_T / A_{cyl} \tag{A3-26}$$

where

F_T - force in tangential direction

$A_{cyl} = \pi d^2 / 4$ - cylinder area

<u>Calculation procedure</u>

Crank angle, α, range for 2-stroke engines $-360° \le \alpha \le +360°$

Crank angle, α, range for 4-stroke engines $-180° \le \alpha \le +180°$

Ratio of crank radius to the connecting rod length:

$$\lambda = r / l_{CR} \tag{A3-27}$$

Connecting rod angle:

$$\sin\beta = \lambda \cdot \sin\alpha \tag{A3-28}$$

Gas force (positive downwards):

$$F_{gas} = p \cdot \frac{\pi\, d^2}{4} \tag{A3-29}$$

Tangential force on the crank journal due to gas forces:

$$F_T = F_{gas} \cdot \frac{\sin(\alpha+\beta)}{\cos\beta} \tag{A3-30}$$

Cylinder pressure from tangential force:

direct calculation

$$p = \frac{4F_T(\alpha)}{\pi\, d^2} \cdot \frac{\cos\beta}{\sin(\alpha+\beta)} \tag{A3-31}$$

when: $\sin(\alpha+\beta) \neq 0$

or by linear interpolation from nearby values

$$p = \frac{4\cos\beta}{\pi\, d^2} \cdot \frac{1}{2}\left[\frac{F_T(\alpha+\Delta\alpha)}{\sin(\alpha+\Delta\alpha+\beta)} + \frac{F_T(\alpha-\Delta\alpha)}{\sin(\alpha-\Delta\alpha+\beta)}\right]; \quad \Delta\alpha = 0{,}0001° \tag{A3-32}$$

when: $\sin(\alpha+\beta) = 0$

Trigonometric approximation for tangential forces:

$$F_T = \frac{F_{T0}}{2} + \sum_{k=1}^{N} F_{TC,k} \cos(k\alpha) + F_{TS,k} \sin(k\alpha) \tag{A3-33}$$

for crank angle $\alpha = \pi$, tangential force $F_T(\pi)=0$, giving:

$$F_{T0} = -2\sum_{k=1}^{N} F_{TC,k} \cos k\pi \tag{A3-34}$$

Mean indicated pressure:

$$p_{m,i} = \frac{1}{2}\int_{\alpha_{\min}}^{\alpha_{\max}} p(\alpha)\left(\sin\alpha + \lambda\frac{\sin\alpha\cdot\cos\alpha}{\sqrt{1-\lambda^2\sin^2\alpha}}\right)\cdot d\alpha \tag{A3-35}$$

It should be noted that in order to change direction of rotation (negative to positive work), the sign (+/-) of sine components may need to be changed, e. g. when expressed as parts (*Re* and *Im*) of complex numbers.

FACULTY OF MARITIME STUDIES - UNIVERSITY OF SPLIT

ENGINE EXCITATION HARMONIC SYNTHESIS

(cylinder pressures and torques from tangential pressure coefficients)

Program: S06HarmSynt.xlsm/vba Author: N.Vulić Ver. **2.0** (12 NOV 2020)

Yard / ship name: **Hyundai Heavy Industries (HHI), yard 1992 / normal vs drag** CRS No: -

Engine licence: **MAN B&W, 12K98ME-C Mk. 7** Type: **excitation T243795, pmi = 20,5 bar**

engine working cycle (two stroke-2, four stroke-4)	*cycle* =	2	
cylinder bore	*d* =	980	mm
piston stroke	*s* =	2400	mm
length of connecting rod	L_{CR} =	3090	mm
crank angle step increment	Δα =	3	°

	Inertia	Gas normal firing		Total	Gas compression only			[Nmm/mm³]
Order	SIN	COS	SIN	Ampl	COS	SIN	Ampl	
0	A_0=	**1,2998974**		A_{0comp}=	**-0,0002**			[Nmm/mm³]
1	0	0,749335	1,594644		-0,0002	0,1744		
2	0	-0,0599024	1,779473		-0,0009	0,2499		
3	0	-0,2795427	1,263371		-0,0009	0,2221		
4	0	-0,2815592	0,862528		0,0003	0,1625		
5	0	-0,2953467	0,541984		0,0004	0,1175		
6	0	-0,2145815	0,298211		-0,0001	0,0842		
7	0	-0,1489063	0,179203		0,0001	0,0583		
8	0	-0,1151648	0,084877		0,0004	0,0403		
9	0	-0,063029	0,02569		0,0001	0,0281		
10	0	-0,033944	0,007356		0	0,019		
11	0	-0,0180005	-0,011085		0,0002	0,0128		
12	0	0,000426	-0,017185		0,0001	0,0089		
13	0	0,008028	-0,014189		0	0,0059		
14	0	0,0118337	-0,013531		0,0001	0,0039		
15	0	0,0142602	-0,009976		0	0,0028		
16	0	0,0143112	-0,006383		0	0,0018		
17	0	0,0131415	-0,003387		0,0001	0,0011		
18	0	0,0107755	-0,001115		0	0,0008		
19	0	0,009234	0,000319		0	0,0005		
20	0	0,0070303	0,001873		0	0,0003		
21	0	0	0		0	0		
22	0	0	0		0	0		
23	0	0	0		0	0		
24	0	0	0		0	0		

Tangential force, cylinder pressures and crank torque

calculated $p_{m,i}$ = **20,424** bar

crank angle°	tangential pressures................[Nmm/mm^3] total	gas	inertia	compression	F_T [kN]	T [kNm]	T_{comp} [kNm]	p [bar]	p_{comp} [bar]
-180	-0,64995	-0,64995	0,00000	0,00010	0,000	0,000	0,000	0,037	-0,018
-177	-0,65173	-0,65173	0,00000	0,00015	-1,344	-1,613	0,041	0,556	-0,014
-174	-0,65599	-0,65599	0,00000	0,00008	-4,559	-5,471	-0,015	0,943	0,003
-171	-0,65976	-0,65976	0,00000	-0,00011	-7,398	-8,877	-0,188	1,018	0,022
-168	-0,66057	-0,66057	0,00000	-0,00031	-8,015	-9,618	-0,373	0,826	0,032
-165	-0,65911	-0,65911	0,00000	-0,00039	-6,908	-8,290	-0,443	0,568	0,030
-162	-0,65842	-0,65842	0,00000	-0,00031	-6,393	-7,671	-0,370	0,437	0,021
-159	-0,66077	-0,66077	0,00000	-0,00016	-8,161	-9,793	-0,239	0,476	0,012
-156	-0,66518	-0,66518	0,00000	-0,00007	-11,486	-13,783	-0,157	0,584	0,007
-153	-0,66845	-0,66845	0,00000	-0,00005	-13,958	-16,750	-0,139	0,629	0,005
-150	-0,66846	-0,66846	0,00000	-0,00001	-13,966	-16,759	-0,100	0,563	0,003
-147	-0,66626	-0,66626	0,00000	0,00016	-12,307	-14,769	0,055	0,449	-0,002
-144	-0,66487	-0,66487	0,00000	0,00047	-11,253	-13,504	0,334	0,375	-0,009
-141	-0,66595	-0,66595	0,00000	0,00082	-12,073	-14,487	0,655	0,369	-0,017
-138	-0,66808	-0,66808	0,00000	0,00113	-13,678	-16,413	0,931	0,387	-0,022
-135	-0,66833	-0,66833	0,00000	0,00136	-13,867	-16,640	1,139	0,364	-0,025
-132	-0,66568	-0,66568	0,00000	0,00155	-11,869	-14,242	1,315	0,291	-0,027
-129	-0,66248	-0,66248	0,00000	0,00174	-9,451	-11,341	1,485	0,217	-0,028
-126	-0,66231	-0,66231	0,00000	0,00189	-9,320	-11,185	1,622	0,201	-0,029
-123	-0,66641	-0,66641	0,00000	0,00195	-12,414	-14,897	1,675	0,253	-0,028
-120	-0,67242	-0,67242	0,00000	0,00189	-16,948	-20,337	1,624	0,327	-0,026
-117	-0,67690	-0,67690	0,00000	0,00173	-20,331	-24,397	1,473	0,372	-0,022
-114	-0,67919	-0,67919	0,00000	0,00138	-22,056	-26,467	1,161	0,385	-0,017
-111	-0,68250	-0,68250	0,00000	0,00064	-24,551	-29,461	0,490	0,410	-0,007
-108	-0,69106	-0,69106	0,00000	-0,00082	-31,008	-37,209	-0,835	0,496	0,011
-105	-0,70609	-0,70609	0,00000	-0,00326	-42,347	-50,816	-3,044	0,652	0,039
-102	-0,72480	-0,72480	0,00000	-0,00671	-56,460	-67,752	-6,168	0,838	0,076
-99	-0,74352	-0,74352	0,00000	-0,01102	-70,581	-84,697	-10,065	1,014	0,121
-96	-0,76181	-0,76181	0,00000	-0,01604	-84,380	-101,256	-14,607	1,177	0,170
-93	-0,78327	-0,78327	0,00000	-0,02186	-100,562	-120,674	-19,874	1,365	0,225
-90	-0,81205	-0,81205	0,00000	-0,02880	-122,270	-146,724	-26,159	1,621	0,289
-87	-0,84878	-0,84878	0,00000	-0,03722	-149,975	-179,970	-33,776	1,948	0,366
-84	-0,89010	-0,89010	0,00000	-0,04723	-181,148	-217,378	-42,845	2,313	0,456
-81	-0,93256	-0,93256	0,00000	-0,05874	-213,171	-255,806	-53,263	2,685	0,559
-78	-0,97674	-0,97674	0,00000	-0,07159	-246,501	-295,801	-64,895	3,073	0,674
-75	-1,02738	-1,02738	0,00000	-0,08585	-284,692	-341,631	-77,795	3,525	0,803
-72	-1,08892	-1,08892	0,00000	-0,10182	-331,115	-397,338	-92,253	4,088	0,949
-69	-1,16133	-1,16133	0,00000	-0,11990	-385,731	-462,877	-108,619	4,766	1,118
-66	-1,24049	-1,24049	0,00000	-0,14032	-445,441	-534,529	-127,101	5,530	1,315
-63	-1,32322	-1,32322	0,00000	-0,16311	-507,843	-609,412	-147,735	6,361	1,542
-60	-1,41164	-1,41164	0,00000	-0,18834	-574,541	-689,449	-170,564	7,292	1,804
-57	-1,51214	-1,51214	0,00000	-0,21623	-650,348	-780,418	-195,812	8,401	2,108
-54	-1,62961	-1,62961	0,00000	-0,24721	-738,957	-886,748	-223,858	9,762	2,464
-51	-1,76292	-1,76292	0,00000	-0,28166	-839,507	-1007,408	-255,034	11,399	2,886
-48	-1,90661	-1,90661	0,00000	-0,31969	-947,896	-1137,475	-289,458	13,300	3,385
-45	-2,05759	-2,05759	0,00000	-0,36128	-1061,778	-1274,134	-327,101	15,485	3,975
-42	-2,21960	-2,21960	0,00000	-0,40647	-1183,984	-1420,781	-368,007	18,060	4,678
-39	-2,40023	-2,40023	0,00000	-0,45547	-1320,232	-1584,279	-412,364	21,211	5,521
-36	-2,60244	-2,60244	0,00000	-0,50834	-1472,756	-1767,307	-460,220	25,114	6,540
-33	-2,81900	-2,81900	0,00000	-0,56443	-1636,107	-1963,329	-510,988	29,871	7,774
-30	-3,03573	-3,03573	0,00000	-0,62199	-1799,584	-2159,501	-563,088	35,533	9,265
-27	-3,24000	-3,24000	0,00000	-0,67816	-1953,664	-2344,396	-613,935	42,212	11,054
-24	-3,42410	-3,42410	0,00000	-0,72902	-2092,531	-2511,037	-659,971	50,177	13,188
-21	-3,57666	-3,57666	0,00000	-0,76912	-2207,605	-2649,126	-696,265	59,781	15,712
-18	-3,66790	-3,66790	0,00000	-0,79047	-2276,427	-2731,712	-715,593	71,181	18,646
-15	-3,64420	-3,64420	0,00000	-0,78190	-2258,555	-2710,266	-707,828	84,014	21,941
-12	-3,44316	-3,44316	0,00000	-0,73016	-2106,910	-2528,292	-660,999	97,274	25,431
-9	-3,02341	-3,02341	0,00000	-0,62388	-1790,295	-2148,355	-564,798	109,604	28,815
-6	-2,38838	-2,38838	0,00000	-0,45915	-1311,293	-1573,552	-415,690	119,947	31,687

-3	-1,58420	-1,58420	0,00000	-0,24424	-704,704	-845,645	-221,166	128,620	33,639
0	-0,67160	-0,67160	0,00000	-0,00030	-16,333	-19,599	-0,362	130,682	34,249
3	0,30655	0,30655	0,00000	0,24331	721,483	865,779	220,142	131,682	33,483
6	1,33504	1,33504	0,00000	0,45736	1497,269	1796,723	413,892	136,959	31,550
9	2,40456	2,40456	0,00000	0,62105	2304,005	2764,806	562,057	141,054	28,675
12	3,47663	3,47663	0,00000	0,72648	3112,667	3735,200	657,483	143,709	25,296
15	4,46690	4,46690	0,00000	0,77778	3859,619	4631,543	703,921	143,570	21,820
18	5,26559	5,26559	0,00000	0,78639	4462,073	5354,487	711,711	139,524	18,545
21	5,78487	5,78487	0,00000	0,76539	4853,762	5824,514	692,703	131,437	15,632
24	6,00055	6,00055	0,00000	0,72579	5016,448	6019,738	656,866	120,290	13,126
27	5,95944	5,95944	0,00000	0,67547	4985,439	5982,527	611,319	107,718	11,007
30	5,74889	5,74889	0,00000	0,61985	4826,619	5791,943	560,971	95,303	9,230
33	5,45188	5,45188	0,00000	0,56287	4602,591	5523,109	509,398	84,032	7,750
36	5,11797	5,11797	0,00000	0,50740	4350,722	5220,867	459,190	74,189	6,525
39	4,76383	4,76383	0,00000	0,45514	4.083,596	4.900,316	411,878	65,606	5,514
42	4,39356	4,39356	0,00000	0,40665	3.804,304	4.565,165	367,987	58,031	4,678
45	4,01690	4,01690	0,00000	0,36184	3.520,186	4.224,223	327,432	51,338	3,979
48	3,65138	3,65138	0,00000	0,32055	3.244,475	3.893,370	290,059	45,524	3,392
51	3,31184	3,31184	0,00000	0,28281	2.988,365	3.586,038	255,897	40,577	2,896
54	3,00114	3,00114	0,00000	0,24872	2.754,003	3.304,804	225,038	36,382	2,477
57	2,71185	2,71185	0,00000	0,21814	2.535,792	3.042,950	197,361	32,757	2,125
60	2,43638	2,43638	0,00000	0,19064	2.328,009	2.793,610	172,465	29,546	1,824
63	2,17491	2,17491	0,00000	0,16569	2.130,783	2.556,940	149,885	26,689	1,564
66	1,93394	1,93394	0,00000	0,14302	1.949,017	2.338,821	129,369	24,196	1,338
69	1,71827	1,71827	0,00000	0,12265	1.786,341	2.143,609	110,928	22,071	1,142
72	1,52532	1,52532	0,00000	0,10465	1.640,799	1.968,958	94,631	20,256	0,974
75	1,34727	1,34727	0,00000	0,08887	1.506,493	1.807,791	80,352	18,654	0,829
78	1,17828	1,17828	0,00000	0,07493	1.379,026	1.654,832	67,735	17,190	0,704
81	1,01910	1,01910	0,00000	0,06240	1.258,958	1.510,750	56,389	15,856	0,592
84	0,87458	0,87458	0,00000	0,05105	1.149,949	1.379,939	46,121	14,683	0,491
87	0,74725	0,74725	0,00000	0,04095	1.053,905	1.264,686	36,977	13,689	0,400
90	0,63377	0,63377	0,00000	0,03220	968,305	1.161,966	29,055	12,837	0,321
93	0,52776	0,52776	0,00000	0,02474	888,343	1.066,012	22,306	12,059	0,252
96	0,42574	0,42574	0,00000	0,01831	811,389	973,667	16,484	11,314	0,192
99	0,32973	0,32973	0,00000	0,01260	738,968	886,762	11,317	10,617	0,135
102	0,24380	0,24380	0,00000	0,00749	674,150	808,980	6,691	10,011	0,083
105	0,16806	0,16806	0,00000	0,00310	617,021	740,425	2,716	9,499	0,035
108	0,09633	0,09633	0,00000	-0,00034	562,919	675,503	-0,398	9,010	-0,005
111	0,01997	0,01997	0,00000	-0,00268	505,319	606,383	-2,514	8,436	-0,035
114	-0,06571	-0,06571	0,00000	-0,00393	440,693	528,831	-3,652	7,695	-0,053
117	-0,15830	-0,15830	0,00000	-0,00429	370,848	445,017	-3,973	6,795	-0,061
120	-0,25106	-0,25106	0,00000	-0,00399	300,884	361,060	-3,706	5,802	-0,060
123	-0,33820	-0,33820	0,00000	-0,00334	235,150	282,179	-3,116	4,788	-0,053
126	-0,41770	-0,41770	0,00000	-0,00264	175,185	210,222	-2,476	3,780	-0,045
129	-0,48930	-0,48930	0,00000	-0,00213	121,179	145,415	-2,020	2,780	-0,039
132	-0,55093	-0,55093	0,00000	-0,00193	74,693	89,632	-1,838	1,829	-0,038
135	-0,59798	-0,59798	0,00000	-0,00192	39,200	47,041	-1,832	1,029	-0,040
138	-0,62672	-0,62672	0,00000	-0,00186	17,520	21,024	-1,776	0,495	-0,042
141	-0,63844	-0,63844	0,00000	-0,00155	8,677	10,413	-1,492	0,265	-0,038
144	-0,63993	-0,63993	0,00000	-0,00100	7,555	9,066	-0,992	0,252	-0,028
147	-0,63933	-0,63933	0,00000	-0,00042	8,012	9,614	-0,469	0,292	-0,014
150	-0,64103	-0,64103	0,00000	-0,00005	6,728	8,074	-0,136	0,271	-0,005
153	-0,64418	-0,64418	0,00000	0,00005	4,354	5,225	-0,048	0,196	-0,002
156	-0,64568	-0,64568	0,00000	0,00002	3,220	3,864	-0,075	0,164	-0,003
159	-0,64447	-0,64447	0,00000	0,00006	4,131	4,957	-0,037	0,241	-0,002
162	-0,64278	-0,64278	0,00000	0,00024	5,408	6,490	0,124	0,369	0,007
165	-0,64356	-0,64356	0,00000	0,00044	4,820	5,784	0,308	0,396	0,021
168	-0,64719	-0,64719	0,00000	0,00050	2,078	2,493	0,366	0,214	0,031
171	-0,65106	-0,65106	0,00000	0,00038	-0,835	-1,002	0,256	-0,115	0,029
174	-0,65233	-0,65233	0,00000	0,00019	-1,794	-2,152	0,081	-0,371	0,014
177	-0,65102	-0,65102	0,00000	0,00008	-0,807	-0,969	-0,018	-0,334	-0,006
180	-0,64995	-0,64995	0,00000	0,00010	0,000	0,000	0,000	0,037	-0,018

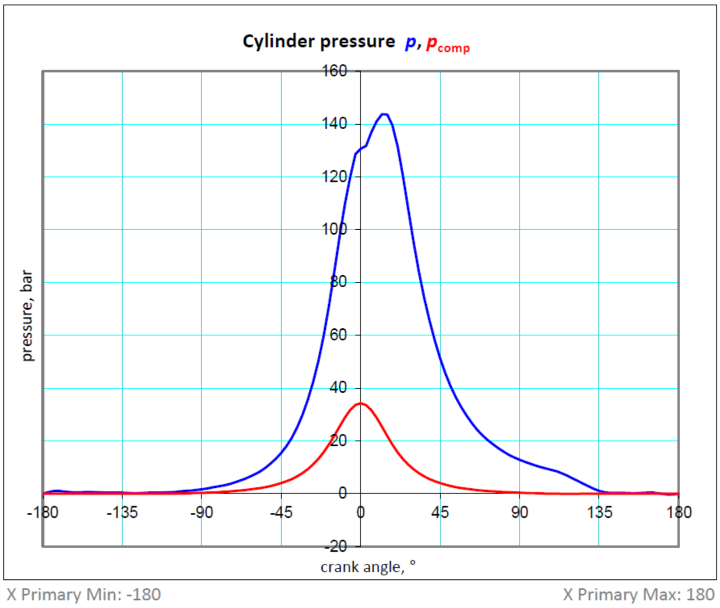
Cylinder pressure p, p_{comp}
pressure, bar
crank angle, °
X Primary Min: -180
X Primary Max: 180

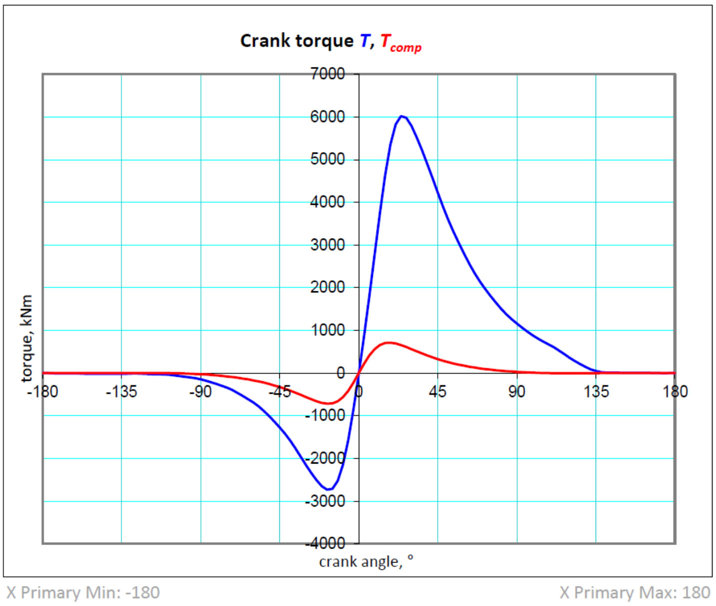
Crank torque T, T_{comp}
torque, kNm
crank angle, °
X Primary Min: -180
X Primary Max: 180

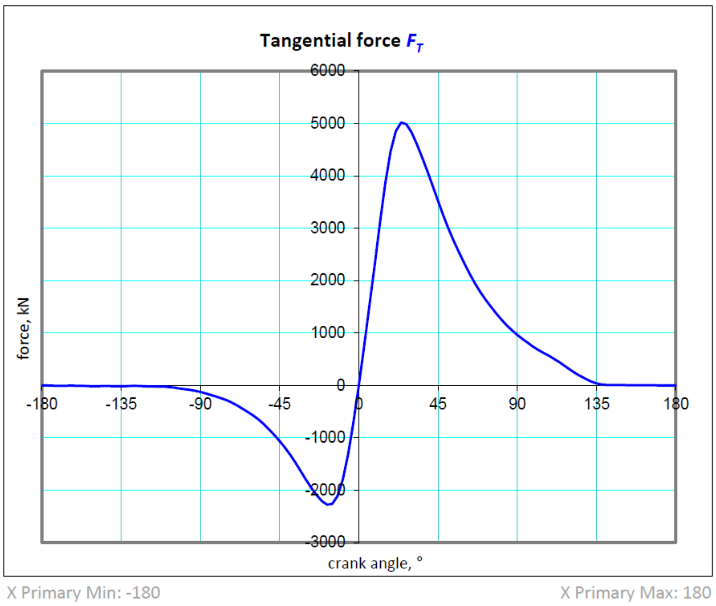
Tangential force F_T
force, kN
crank angle, °
X Primary Min: -180
X Primary Max: 180

APPENDIX B – Engine specifications and excitation data

To perform the calculation of torsional vibrations, it is necessary to know the values of the driving load. In reciprocating engines, due to its irregularity, the driving load is extremely difficult to define analytically. The data required for TVC in this study was obtained from the manufacturer's website with restricted access. For the engine MAN B&W 12K98ME-C7 he following data is:

- Cylinder diameter – 980 mm
- Piston stroke – 2400 mm
- Power per cylinder – 6020 kW
- Maximum crankshaft rotational speed – 104 rpm
- Mean effective pressure – 19,2 bar
- Mean indicated pressure – 20,2 bar
- Measured absolute ambient air pressure – 1 bar
- Maximum cylinder pressure – 150 bar
- Fourier series coefficients of the tangential component of the mean indicated pressure at the crankshaft axis centre during normal engine operation
- Fourier series coefficients of the radial component of the mean indicated pressure at the crankshaft axis centre during normal engine operation
- Fourier series coefficients of the tangential component of the mean indicated pressure at the crankshaft axis centre in case of misfire
- Fourier series coefficients of the radial component of the mean indicated pressure at the crankshaft axis centre in case of misfire

The tangential load is obtained using Fourier coefficients provided by the manufacturer. The data for tangential load is presented below in form of cosine and sine harmonic components for normal firing operating condition, along with only sine components for misfiring operating condition. It is important to underline that the torque on the crankshaft is determined by the product of the tangential load and the crankshaft radius.

B & W ENGINEERING COPENHAGEN DATE 16 JAN 2004

HARMONIC ANALYSIS OF T A N G E N T I A L PRESSURE NO. 243795

Bore: 0.980 m Stroke: 2.400 m
Dpistrod: 0.381 m Excen: 0.000 m
Lconrod: 3.090 m Sign: po
Diagrams: S:\2412-software\harmon calc\Indika\K98ME-C Mark 7\F275T276
TANGENT.TRYK

****
no. * 243795 *
****

FAMILY NO. 275

COSINE COMPONENTS IN N/mm2

MEAN INDICATED PRESSURE IN BAR

ORDER	0.0000	1.4429	2.8858	4.3287	5.7716	7.2145	8.6574	10.1003	11.5432	12.9861	14.4290	15.8719	17.3148	18.7577	20.2006	21.6435
1	-0.0002	0.0545	0.1092	0.1639	0.2186	0.2733	0.3279	0.3796	0.4312	0.4828	0.5351	0.5874	0.6400	0.6934	0.7456	0.7636
2	-0.0009	-0.0020	-0.0032	-0.0043	-0.0055	-0.0066	-0.0079	-0.0146	-0.0212	-0.0279	-0.0322	-0.0364	-0.0398	-0.0417	-0.0460	-0.1130
3	-0.0009	-0.0187	-0.0366	-0.0545	-0.0724	-0.0903	-0.1083	-0.1308	-0.1534	-0.1759	-0.1947	-0.2131	-0.2314	-0.2492	-0.2684	-0.3221
4	0.0003	-0.0180	-0.0363	-0.0546	-0.0730	-0.0913	-0.1097	-0.1329	-0.1562	-0.1794	-0.1983	-0.2169	-0.2360	-0.2562	-0.2766	-0.3005
5	0.0004	-0.0201	-0.0406	-0.0612	-0.0817	-0.1022	-0.1228	-0.1464	-0.1700	-0.1936	-0.2130	-0.2321	-0.2518	-0.2729	-0.2935	-0.3024
6	-0.0001	-0.0162	-0.0324	-0.0485	-0.0646	-0.0808	-0.0969	-0.1135	-0.1301	-0.1467	-0.1601	-0.1733	-0.1871	-0.2022	-0.2162	-0.2084
7	0.0001	-0.0114	-0.0229	-0.0344	-0.0459	-0.0574	-0.0688	-0.0801	-0.0914	-0.1027	-0.1123	-0.1217	-0.1315	-0.1421	-0.1515	-0.1390
8	0.0004	-0.0096	-0.0196	-0.0296	-0.0396	-0.0496	-0.0595	-0.0673	-0.0752	-0.0831	-0.0903	-0.0975	-0.1046	-0.1118	-0.1178	-0.1051
9	0.0001	-0.0065	-0.0131	-0.0197	-0.0263	-0.0329	-0.0394	-0.0427	-0.0460	-0.0492	-0.0530	-0.0569	-0.0606	-0.0639	-0.0661	-0.0513
10	0.0000	-0.0041	-0.0082	-0.0122	-0.0163	-0.0203	-0.0243	-0.0254	-0.0265	-0.0275	-0.0299	-0.0323	-0.0345	-0.0360	-0.0366	-0.0238
11	0.0002	-0.0030	-0.0062	-0.0095	-0.0127	-0.0160	-0.0191	-0.0185	-0.0179	-0.0172	-0.0184	-0.0198	-0.0207	-0.0208	-0.0202	-0.0096
12	0.0001	-0.0016	-0.0032	-0.0048	-0.0064	-0.0080	-0.0095	-0.0074	-0.0052	-0.0030	-0.0032	-0.0035	-0.0035	-0.0027	-0.0014	0.0074
13	0.0000	-0.0006	-0.0012	-0.0018	-0.0024	-0.0030	-0.0035	-0.0010	0.0016	0.0041	0.0042	0.0041	0.0044	0.0054	0.0067	0.0131
14	0.0001	-0.0002	-0.0004	-0.0007	-0.0010	-0.0013	-0.0016	0.0014	0.0044	0.0074	0.0078	0.0080	0.0085	0.0097	0.0109	0.0154
15	0.0000	0.0004	0.0007	0.0010	0.0014	0.0017	0.0021	0.0051	0.0081	0.0111	0.0115	0.0117	0.0121	0.0129	0.0137	0.0164
16	0.0000	0.0006	0.0013	0.0020	0.0026	0.0033	0.0040	0.0067	0.0094	0.0121	0.0125	0.0127	0.0130	0.0136	0.0140	0.0155
17	0.0001	0.0008	0.0016	0.0023	0.0031	0.0038	0.0046	0.0071	0.0097	0.0123	0.0126	0.0127	0.0129	0.0131	0.0131	0.0133
18	0.0000	0.0009	0.0019	0.0028	0.0037	0.0046	0.0056	0.0076	0.0097	0.0117	0.0118	0.0117	0.0116	0.0114	0.0109	0.0103
19	0.0000	0.0009	0.0019	0.0028	0.0038	0.0047	0.0057	0.0074	0.0091	0.0108	0.0108	0.0107	0.0105	0.0102	0.0094	0.0086
20	0.0000	0.0010	0.0020	0.0029	0.0039	0.0049	0.0058	0.0071	0.0085	0.0098	0.0096	0.0094	0.0090	0.0083	0.0073	0.0060

SINE COMPONENTS IN N/mm2

MEAN INDICATED PRESSURE IN BAR

ORDER	0.0000	1.4429	2.8858	4.3287	5.7716	7.2145	8.6574	10.1003	11.5432	12.9861	14.4290	15.8719	17.3148	18.7577	20.2006	21.6435
1	0.1744	0.2493	0.3243	0.3993	0.4742	0.5492	0.6251	0.7361	0.8471	0.9581	1.0803	1.2035	1.3246	1.4411	1.5547	1.7472
2	0.2499	0.3268	0.4038	0.4807	0.5577	0.6346	0.7127	0.8352	0.9577	1.0801	1.2167	1.3544	1.4897	1.6198	1.7437	1.9161
3	0.2221	0.2694	0.3167	0.3640	0.4113	0.4586	0.5069	0.5930	0.6790	0.7651	0.8641	0.9642	1.0627	1.1579	1.2459	1.3301
4	0.1625	0.1935	0.2244	0.2554	0.2863	0.3172	0.3489	0.4063	0.4638	0.5212	0.5896	0.6590	0.7272	0.7931	0.8529	0.8993
5	0.1175	0.1355	0.1535	0.1715	0.1896	0.2076	0.2260	0.2600	0.2940	0.3280	0.3718	0.4164	0.4598	0.5007	0.5369	0.5614
6	0.0842	0.0908	0.0974	0.1039	0.1105	0.1170	0.1239	0.1407	0.1575	0.1743	0.2003	0.2270	0.2526	0.2759	0.2957	0.3078
7	0.0583	0.0611	0.0640	0.0669	0.0697	0.0726	0.0756	0.0843	0.0929	0.1015	0.1182	0.1355	0.1516	0.1654	0.1769	0.1880
8	0.0403	0.0400	0.0396	0.0393	0.0389	0.0386	0.0383	0.0404	0.0424	0.0445	0.0535	0.0631	0.0717	0.0782	0.0833	0.0909
9	0.0281	0.0248	0.0216	0.0183	0.0151	0.0118	0.0086	0.0074	0.0061	0.0048	0.0095	0.0147	0.0191	0.0221	0.0243	0.0310
10	0.0190	0.0160	0.0129	0.0098	0.0068	0.0037	0.0006	-0.0013	-0.0033	-0.0053	-0.0026	0.0006	0.0032	0.0046	0.0058	0.0133
11	0.0128	0.0094	0.0060	0.0025	-0.0009	-0.0043	-0.0077	-0.0106	-0.0135	-0.0165	-0.0155	-0.0143	-0.0133	-0.0130	-0.0126	-0.0053
12	0.0089	0.0051	0.0013	-0.0025	-0.0063	-0.0101	-0.0139	-0.0164	-0.0189	-0.0214	-0.0209	-0.0202	-0.0197	-0.0194	-0.0187	-0.0114
13	0.0059	0.0029	-0.0001	-0.0032	-0.0062	-0.0093	-0.0123	-0.0141	-0.0160	-0.0178	-0.0177	-0.0173	-0.0169	-0.0165	-0.0156	-0.0088
14	0.0039	0.0011	-0.0017	-0.0045	-0.0073	-0.0101	-0.0128	-0.0143	-0.0157	-0.0171	-0.0171	-0.0170	-0.0167	-0.0161	-0.0149	-0.0083
15	0.0028	0.0002	-0.0023	-0.0049	-0.0075	-0.0100	-0.0125	-0.0131	-0.0137	-0.0142	-0.0141	-0.0139	-0.0135	-0.0126	-0.0112	-0.0053
16	0.0018	-0.0002	-0.0022	-0.0042	-0.0062	-0.0082	-0.0101	-0.0102	-0.0103	-0.0104	-0.0103	-0.0101	-0.0098	-0.0088	-0.0074	-0.0025
17	0.0011	-0.0006	-0.0023	-0.0040	-0.0057	-0.0074	-0.0090	-0.0086	-0.0082	-0.0078	-0.0075	-0.0073	-0.0068	-0.0057	-0.0043	0.0001
18	0.0008	-0.0006	-0.0020	-0.0034	-0.0048	-0.0062	-0.0075	-0.0066	-0.0057	-0.0048	-0.0046	-0.0044	-0.0040	-0.0030	-0.0018	0.0015
19	0.0005	-0.0005	-0.0016	-0.0027	-0.0038	-0.0049	-0.0059	-0.0048	-0.0038	-0.0028	-0.0026	-0.0025	-0.0021	-0.0012	-0.0002	0.0023
20	0.0003	-0.0005	-0.0014	-0.0022	-0.0031	-0.0039	-0.0047	-0.0034	-0.0021	-0.0007	-0.0005	-0.0004	0.0000	0.0007	0.0015	0.0033

MAN B&W Diesel A/S HARMONIC ANALYSIS OF
Copenhagen MISFIRING TANGENTIAL
Date: 20 Jan 2004 PRESSURE NO. 243795

Based on T243795 dated 16 Jan 2004
Bore: 0.980 m
Stroke: 2.400 m
Con. rod length: 3.090 m
S:\2412-software\harmon calc\Indika\K98M

****
NO. * 243795 MISFIRING *
****

FAMILY NO. 275

SINE COMPONENTS in MPa

MEAN INDICATED PRESSURE IN BAR

ORDER	0.0000	1.4429	2.8858	4.3287	5.7716	7.2145	8.6574	10.1003	11.5432	12.9861	14.4290	15.8719	17.3148	18.7577	20.2006	21.6435
1	0.1742	0.1881	0.2024	0.2173	0.2309	0.2456	0.2605	0.3079	0.3556	0.4029	0.4625	0.5231	0.5816	0.6358	0.6859	0.7896
2	0.2497	0.2677	0.2857	0.3036	0.3217	0.3396	0.3588	0.4224	0.4861	0.5498	0.6294	0.7103	0.7886	0.8610	0.9278	1.0580
3	0.2230	0.2386	0.2544	0.2703	0.2859	0.3017	0.3185	0.3750	0.4313	0.4877	0.5577	0.6288	0.6974	0.7607	0.8187	0.9241
4	0.1635	0.1748	0.1862	0.1975	0.2088	0.2201	0.2323	0.2735	0.3148	0.3560	0.4075	0.4599	0.5106	0.5575	0.6003	0.6785
5	0.1176	0.1259	0.1343	0.1428	0.1512	0.1596	0.1685	0.1987	0.2291	0.2592	0.2969	0.3352	0.3720	0.4060	0.4371	0.4953
6	0.0843	0.0901	0.0959	0.1017	0.1075	0.1132	0.1196	0.1411	0.1626	0.1842	0.2112	0.2387	0.2652	0.2898	0.3122	0.3530
7	0.0587	0.0627	0.0669	0.0711	0.0750	0.0793	0.0836	0.0987	0.1138	0.1288	0.1476	0.1667	0.1851	0.2023	0.2178	0.2457
8	0.0404	0.0432	0.0460	0.0488	0.0516	0.0544	0.0573	0.0678	0.0782	0.0888	0.1020	0.1153	0.1283	0.1403	0.1512	0.1712
9	0.0280	0.0298	0.0318	0.0337	0.0356	0.0376	0.0396	0.0468	0.0541	0.0614	0.0704	0.0797	0.0885	0.0968	0.1042	0.1178
10	0.0191	0.0204	0.0217	0.0228	0.0242	0.0253	0.0266	0.0316	0.0366	0.0415	0.0477	0.0541	0.0603	0.0660	0.0711	0.0802
11	0.0129	0.0137	0.0147	0.0155	0.0163	0.0172	0.0181	0.0216	0.0251	0.0285	0.0327	0.0370	0.0412	0.0450	0.0484	0.0549
12	0.0088	0.0092	0.0097	0.0102	0.0106	0.0111	0.0115	0.0138	0.0161	0.0183	0.0213	0.0243	0.0271	0.0298	0.0322	0.0366
13	0.0059	0.0063	0.0068	0.0071	0.0074	0.0077	0.0080	0.0098	0.0114	0.0131	0.0150	0.0170	0.0190	0.0208	0.0224	0.0250
14	0.0039	0.0040	0.0041	0.0041	0.0042	0.0043	0.0044	0.0054	0.0065	0.0075	0.0088	0.0102	0.0115	0.0128	0.0141	0.0161
15	0.0027	0.0027	0.0028	0.0029	0.0028	0.0030	0.0031	0.0038	0.0046	0.0054	0.0063	0.0072	0.0081	0.0089	0.0098	0.0111
16	0.0019	0.0016	0.0016	0.0014	0.0013	0.0012	0.0011	0.0015	0.0020	0.0025	0.0031	0.0039	0.0045	0.0053	0.0060	0.0069
17	0.0011	0.0010	0.0009	0.0007	0.0006	0.0005	0.0005	0.0008	0.0012	0.0015	0.0020	0.0024	0.0029	0.0034	0.0038	0.0044
18	0.0007	0.0004	0.0000	-0.0003	-0.0007	-0.0010	-0.0013	-0.0011	-0.0010	-0.0008	-0.0005	0.0000	0.0003	0.0010	0.0015	0.0023
19	0.0005	0.0003	0.0000	-0.0004	-0.0007	-0.0010	-0.0013	-0.0010	-0.0008	-0.0006	-0.0004	-0.0001	0.0003	0.0007	0.0012	0.0016
20	0.0003	-0.0005	-0.0015	-0.0023	-0.0033	-0.0041	-0.0051	-0.0054	-0.0057	-0.0059	-0.0055	-0.0051	-0.0045	-0.0036	-0.0024	-0.0014

APPENDIX C - SimulationX TVA report

C.1. Normal firing condition

get it right®

Torsional Vibration Analysis

HHI 1992

Client: Faculty of Maritime Studies

Contractor:
ESI ITI GmbH
Schweriner Str. 1
01067 Dresden, Germany

Dresden, 14.5.2025.

General Remarks

This document template is a prototype. The enclosed analysis results demonstrate the possibilities of result evaluation and post-processing in SimulationX® and the ESI ITI Report Generator.
The analyses have been executed according to state-of-the art vibration analysis.

More descriptions …

Project name: CGA CGM Andromeda

Customer: Faculty of Maritime Studies

Project number: HHI 1992

Date: May 14, 2025

Issued by: *Karlo Bratić*

Checked by: *Nenad Vulić*

Remark:

Model structure

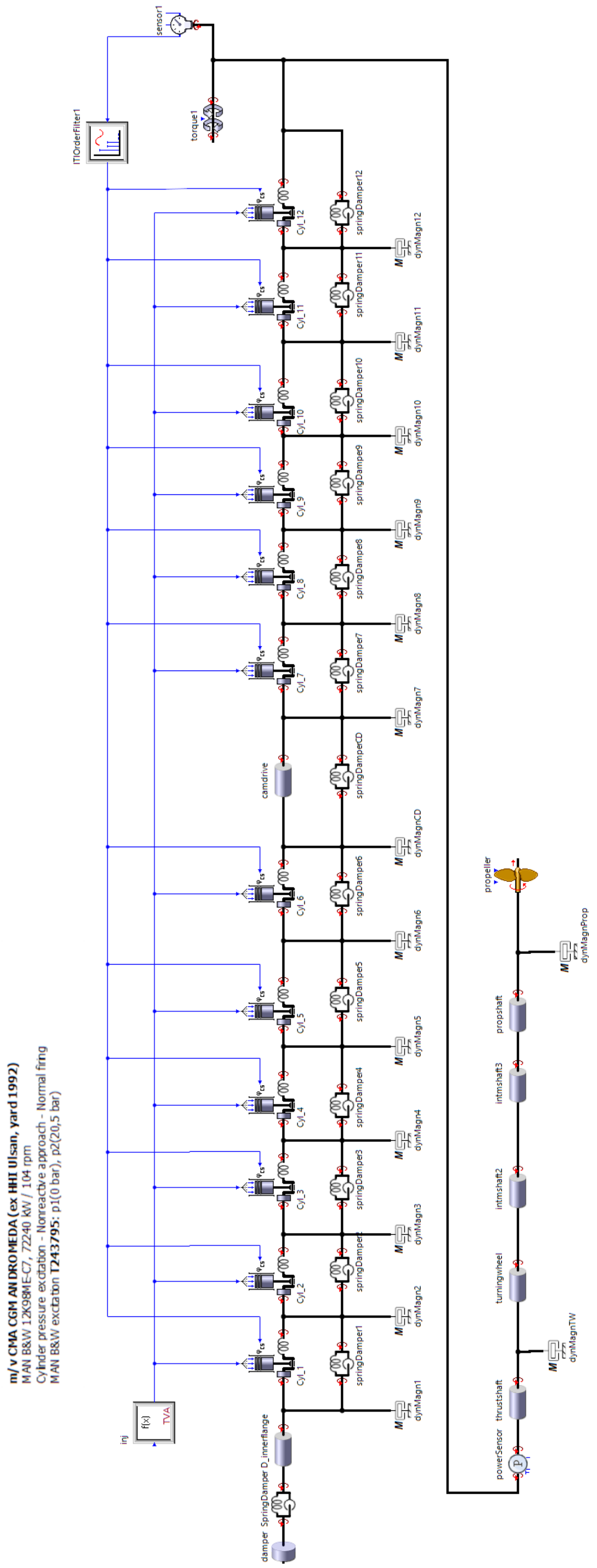

Table C1-1. Torsional System input data

Element	Inertia	Torsional Stiffness	Damping	Ratio: i_{12}	Description
turningwheel	20398 kgm^2	3.0760e+2 MNm/rad	-	-	Shaft Model
intmshaft3	4528 kgm^2	2.6450e+2 MNm/rad	-	-	Shaft Model
propshaft	6689 kgm^2	6.0340e+2 MNm/rad	-	-	Shaft Model
intmshaft2	4214 kgm^2	3.0540e+2 MNm/rad	-	-	Shaft Model
thrustshaft	10600 kgm^2	9.4340e+3 MNm/rad	-	-	Shaft Model
D_innerflange	3444 kgm^2	5.2910e+3 MNm/rad	-	-	Shaft Model
SpringDamper	-	5.7000e+1 MNm/rad	210000 Nms/rad	-	Spring-Damper
damper	9340 kgm^2	-	-	-	
camdrive	13223 kgm^2	5.7803e+3 MNm/rad	-	-	Shaft Model
springDamperCD	-	-	psi = 0	-	Spring-Damper
springDamper1	-	-	psi = 0	-	Spring-Damper
springDamper2	-	-	psi = 0	-	Spring-Damper
springDamper3	-	-	psi = 0	-	Spring-Damper
springDamper4	-	-	psi = 0	-	Spring-Damper
springDamper5	-	-	psi = 0	-	Spring-Damper
springDamper6	-	-	psi = 0	-	Spring-Damper
springDamper7	-	-	psi = 0	-	Spring-Damper
springDamper8	-	-	psi = 0	-	Spring-Damper
springDamper9	-	-	psi = 0	-	Spring-Damper
springDamper10	-	-	psi = 0	-	Spring-Damper
springDamper11	-	-	psi = 0	-	Spring-Damper
springDamper12	-	-	psi = 0	-	Spring-Damper
Cyl_1	36824 kgm^2	4.2194e+3 MNm/rad	-	-	Inline Cylinder
Cyl_2	36824 kgm^2	4.3478e+3 MNm/rad	-	-	Inline Cylinder
Cyl_3	36824 kgm^2	4.3668e+3 MNm/rad	-	-	Inline Cylinder
Cyl_4	36824 kgm^2	4.3290e+3 MNm/rad	-	-	Inline Cylinder
Cyl_5	36824 kgm^2	4.2735e+3 MNm/rad	-	-	Inline Cylinder
Cyl_6	36824 kgm^2	5.7803e+3 MNm/rad	-	-	Inline Cylinder
Cyl_7	36824 kgm^2	4.3103e+3 MNm/rad	-	-	Inline Cylinder
Cyl_8	36824 kgm^2	4.2735e+3 MNm/rad	-	-	Inline Cylinder
Cyl_9	36824 kgm^2	4.1841e+3 MNm/rad	-	-	Inline Cylinder
Cyl_10	36824 kgm^2	4.2735e+3 MNm/rad	-	-	Inline Cylinder
Cyl_11	36824 kgm^2	4.4053e+3 MNm/rad	-	-	Inline Cylinder
Cyl_12	36824 kgm^2	6.3291e+3 MNm/rad	-	-	Inline Cylinder

Natural Frequency Analysis

Table C1-2. Natural vibration modes, natural frequencies, distribution of potential energy

Mode	1			2		
Frequency [rpm]	163.26			711.71		
Element	Rel. Angle	Torque	Pot. Energy	Rel. Angle	Torque	Pot. Energy
	rad	Nm	*(normalized)*	rad	Nm	*(normalized)*
turningwheel.springDamper.springDamper	0.377	1.1597e+8	0.5208	0.038	6.3206e+7	0.0068
intmshaft3.springDamper.springDamper	0.439	1.1618e+8	0.6079	0.064	4.0718e+8	0.0168
propshaft.springDamper.springDamper	0.191	1.1513e+8	0.2617	0.03	7.9913e+8	0.0082
intmshaft2.springDamper.springDamper	0.381	1.1631e+8	0.5277	0.048	1.6415e+8	0.0111
thrustshaft.springDamper.springDamper	0.012	1.1204e+8	0.0158	0.001	1.2545e+7	0.0001
D_innerflange.springDamper.springDamper	0.001	3.2980e+6	0	0.011	6.4884e+7	0.0107
SpringDamper.springDamper	0.043	2.4554e+6	0.0012	1	5.8806e+7	0.8845
camdrive.springDamper.springDamper	0.011	6.3332e+7	0.0083	0.028	1.4682e+9	0.071
Cyl_1.crank.relStiffDamp	0.004	1.6118e+7	0.0007	0.021	1.4977e+8	0.0282
Cyl_2.crank.relStiffDamp	0.006	2.5233e+7	0.0017	0.026	3.3952e+8	0.046
Cyl_2.forceExcitation	0.699	2.8352e+3	0			
Cyl_3.crank.relStiffDamp	0.008	3.4294e+7	0.0032	0.031	8.0200e+8	0.0653
Cyl_4.crank.relStiffDamp	0.01	4.3174e+7	0.0051	0.035	2.7891e+9	0.0827
Cyl_4.forceExcitation	1	6.7547e+4	0.0008			
Cyl_5.crank.relStiffDamp	0.012	5.2039e+7	0.0075	0.038	5.5742e+9	0.0947
Cyl_6.crank.relStiffDamp	0.01	6.0237e+7	0.0075	0.028	1.7795e+9	0.0722
Cyl_6.forceExcitation	0.654	1.5673e+6	0.0122			
Cyl_7.crank.relStiffDamp	0.017	7.1739e+7	0.0142	0.036	9.9030e+8	0.0848
Cyl_7.forceExcitation	0.948	7.1211e+4	0.0008	0.058	2.2270e+4	0
Cyl_8.crank.relStiffDamp	0.019	7.9487e+7	0.0176	0.032	7.1832e+8	0.0685
Cyl_8.forceExcitation	0.623	1.5758e+6	0.0117	0.065	9.3247e+5	0.0004
Cyl_9.crank.relStiffDamp	0.021	8.7610e+7	0.0219	0.027	5.1318e+8	0.0486
Cyl_10.crank.relStiffDamp	0.022	9.5508e+7	0.0254	0.02	3.3790e+8	0.0269
Cyl_11.crank.relStiffDamp	0.023	1.0286e+8	0.0286	0.012	1.7945e+8	0.0101

Cyl_11.forceExcitation	0.892	2.6915e+5	0.0029	0.198	5.9362e+5	0.0002
Cyl_12.crank.relStiffDamp	0.017	1.0996e+8	0.0228	0.003	4.1191e+7	0.0009
Cyl_12.forceExcitation	0.862	2.7172e+5	0.0028	0.213	8.0343e+5	0.0002
Cyl_3.forceExcitation				0.098	3.1526e+3	0
Max. Angle	Cyl_4.forceExcitation			SpringDamper.springDamper		
Max. Torque	intmshaft2.springDamper.springDamper			Cyl_5.crank.relStiffDamp		
Max. Energy	intmshaft3.springDamper.springDamper			SpringDamper.springDamper		

Mode	3			4		
Frequency [rpm]	**806.66**			**1527.65**		
Element	**Rel. Angle**	**Torque**	**Pot. Energy**	**Rel. Angle**	**Torque**	**Pot. Energy**
	rad	Nm	*(normalized)*	rad	Nm	*(normalized)*
turningwheel.springDamper.springDamper	0.04	2.5017e+7	0.0086	0.204	6.2691e+7	0.021
intmshaft3.springDamper.springDamper	0.078	6.4827e+7	0.0283	0.535	1.4164e+8	0.1252
propshaft.springDamper.springDamper	0.037	7.4440e+7	0.0142	0.322	1.9438e+8	0.1034
intmshaft2.springDamper.springDamper	0.056	4.5908e+7	0.0169	0.144	4.3929e+7	0.0104
thrustshaft.springDamper.springDamper	0.002	1.0329e+8	0.0006	0.05	4.7179e+8	0.039
D_innerflange.springDamper.springDamper	0.011	6.1334e+7	0.0104	0.009	6.5599e+7	0.0007
SpringDamper.springDamper	1	6.0674e+7	1	1	6.0394e+7	0.0941
camdrive.springDamper.springDamper	0.038	8.8672e+8	0.1458	0.038	2.2313e+8	0.0136
Cyl_1.crank.relStiffDamp	0.013	6.8208e+7	0.0129	0.177	7.5165e+8	0.2188
Cyl_2.crank.relStiffDamp	0.021	1.0369e+8	0.0348	0.3	1.3070e+9	0.6476
Cyl_2.crank.piston	0.167	1.7238e+3	0			
Cyl_3.crank.relStiffDamp	0.031	2.1070e+8	0.0734	0.362	1.5817e+9	0.9457
Cyl_3.forceExcitation	0.151	8.7830e+3	0			
Cyl_4.crank.relStiffDamp	0.04	3.6808e+8	0.1204	0.35	1.5160e+9	0.8765
Cyl_5.crank.relStiffDamp	0.047	5.6834e+8	0.1645	0.262	1.1210e+9	0.4851
Cyl_5.forceExcitation	0.045	1.5324e+4	0	0.166	6.7229e+3	0
Cyl_6.crank.relStiffDamp	0.038	8.0200e+8	0.1427	0.082	4.7839e+8	0.0648
Cyl_7.crank.relStiffDamp	0.05	1.1147e+9	0.1898	0.125	5.4013e+8	0.1111
Cyl_7.forceExcitation	0.031	2.1605e+4	0			
Cyl_8.crank.relStiffDamp	0.047	1.3164e+9	0.1643	0.276	1.1785e+9	0.5362
Cyl_8.forceExcitation	0.051	5.6353e+5	0.0004			
Cyl_9.crank.relStiffDamp	0.041	1.4572e+9	0.1236	0.372	1.5561e+9	0.9554
Cyl_10.crank.relStiffDamp	0.031	1.5139e+9	0.0722	0.371	1.5835e+9	0.9688
Cyl_11.crank.relStiffDamp	0.019	1.6334e+9	0.0292	0.287	1.2622e+9	0.5971
Cyl_11.forceExcitation	0.224	2.0102e+5	0.0003	0.428	2.9458e+5	0.0002
Cyl_12.crank.relStiffDamp	0.005	7.1422e+8	0.0031	0.106	6.7086e+8	0.1174
Cyl_12.forceExcitation	0.248	2.2087e+5	0.0004	0.787	2.9758e+5	0.0004
Cyl_2.forceExcitation				0.489	3.1075e+3	0
Max. Angle	SpringDamper.springDamper			SpringDamper.springDamper		
Max. Torque	Cyl_11.crank.relStiffDamp			Cyl_10.crank.relStiffDamp		
Max. Energy	SpringDamper.springDamper			Cyl_10.crank.relStiffDamp		

Mode	5		
Frequency [rpm]	2060.82		
Element	Rel. Angle	Torque	Pot. Energy
	rad	Nm	*(normalized)*
turningwheel.springDamper.springDamper	1	3.0760e+8	0.752
intmshaft3.springDamper.springDamper	0.748	1.9779e+8	0.3616
propshaft.springDamper.springDamper	0.661	3.9869e+8	0.6441
intmshaft2.springDamper.springDamper	0.314	9.5911e+7	0.0736
thrustshaft.springDamper.springDamper	0.041	3.8236e+8	0.0379
D_innerflange.springDamper.springDamper	0.003	3.7724e+7	0.0001
SpringDamper.springDamper	0.172	9.9904e+6	0.0041
camdrive.springDamper.springDamper	0.059	3.4257e+8	0.0495
Cyl_1.crank.relStiffDamp	0.064	2.6940e+8	0.0418
Cyl_2.crank.relStiffDamp	0.095	4.1228e+8	0.0955
Cyl_3.crank.relStiffDamp	0.09	3.9300e+8	0.0865
Cyl_4.crank.relStiffDamp	0.051	2.1988e+8	0.0273
Cyl_4.forceExcitation	0.121	3.8609e+3	0
Cyl_5.crank.relStiffDamp	0.01	4.5412e+7	0.001
Cyl_6.crank.relStiffDamp	0.049	2.8551e+8	0.0343
Cyl_6.forceExcitation	0.115	8.9056e+4	0
Cyl_7.crank.relStiffDamp	0.093	4.0018e+8	0.0908
Cyl_8.crank.relStiffDamp	0.07	2.9882e+8	0.0511
Cyl_9.crank.relStiffDamp	0.019	7.9150e+7	0.0036
Cyl_10.crank.relStiffDamp	0.041	1.7631e+8	0.0176
Cyl_11.crank.relStiffDamp	0.081	3.5823e+8	0.0711
Cyl_12.crank.relStiffDamp	0.063	4.0123e+8	0.0622
Max. Angle	turningwheel.springDamper.springDamper		
Max. Torque	Cyl_2.crank.relStiffDamp		
Max. Energy	turningwheel.springDamper.springDamper		

Table C1-3. Natural vibration modes, natural frequencies, distribution of kinetic energy

Mode	1		2	
Frequency [rpm]	163.26		711.71	
Element	Deviation	Kin. Energy	Deviation	Kin. Energy
	(normalized)	*(normalized)*	*(normalized)*	*(normalized)*
turningwheel.inertia.inertia	0.737	0.031	0.156	0.053
intmshaft3.inertia.inertia	0.111	0	0.079	0.003
propshaft.inertia.inertia	0.602	0.007	0.021	0
intmshaft2.inertia.inertia	0.315	0.001	0.122	0.007
thrustshaft.inertia.inertia	0.75	0.017	0.156	0.027
D_innerflange.inertia.inertia	0.952	0.009	0.155	0.009
damper.inertia	1	0.026	1	1
camdrive.inertia.inertia	0.896	0.03	0.024	0.001
Cyl_1.crank.inertiaCrank	0.952	0.093	0.146	0.085
Cyl_2.crank.inertiaCrank	0.947	0.092	0.129	0.066
Cyl_3.crank.inertiaCrank	0.941	0.091	0.107	0.045
Cyl_3.forceExcitation	0	0		
Cyl_4.crank.inertiaCrank	0.932	0.089	0.08	0.025
Cyl_5.crank.inertiaCrank	0.921	0.087	0.051	0.01
Cyl_5.forceExcitation	0	0		
Cyl_6.crank.inertiaCrank	0.907	0.084	0.024	0.002
Cyl_7.crank.inertiaCrank	0.883	0.08	0.043	0.007
Cyl_8.crank.inertiaCrank	0.865	0.077	0.073	0.021
Cyl_9.crank.inertiaCrank	0.844	0.073	0.101	0.04
Cyl_9.forceExcitation	0	0		
Cyl_10.crank.inertiaCrank	0.821	0.069	0.125	0.061
Cyl_11.crank.inertiaCrank	0.796	0.065	0.142	0.08
Cyl_12.crank.inertiaCrank	0.769	0.061	0.153	0.092
propeller.rotor	0.816	1	0.005	0.002
Cyl_2.forceExcitation			0	0
Cyl_4.forceExcitation			0	0
Cyl_6.forceExcitation			0	0
Max. Deviation	damper.inertia		damper.inertia	
Max. Energy	propeller.rotor		damper.inertia	

Mode	3		4	
Frequency [rpm]	806.66		1527.65	
Element	Deviation	Kin. Energy	Deviation	Kin. Energy
	(normalized)	*(normalized)*	*(normalized)*	*(normalized)*
turningwheel.inertia.inertia	0.234	0.108	0.794	0.53
intmshaft3.inertia.inertia	0.125	0.007	0.854	0.136
propshaft.inertia.inertia	0.035	0.001	0.312	0.027
intmshaft2.inertia.inertia	0.189	0.014	1	0.174
thrustshaft.inertia.inertia	0.232	0.055	0.743	0.241
D_innerflange.inertia.inertia	0.235	0.018	0.783	0.087
damper.inertia	1	0.899	0.28	0.03
camdrive.inertia.inertia	0.042	0.002	0.774	0.326
Cyl_1.crank.inertiaCrank	0.24	0.204	0.78	0.923
Cyl_2.crank.inertiaCrank	0.231	0.189	0.601	0.547
Cyl_2.forceExcitation	0	0		
Cyl_3.crank.inertiaCrank	0.209	0.155	0.297	0.134
Cyl_4.crank.inertiaCrank	0.175	0.109	0.072	0.008
Cyl_4.forceExcitation	0	0	0	0

Cyl_5.crank.inertiaCrank	0.131	0.061	0.425	0.274
Cyl_6.crank.inertiaCrank	0.08	0.023	0.691	0.723
Cyl_6.forceExcitation	0	0	0	0.002
Cyl_7.crank.inertiaCrank	0.029	0.003	0.812	1
Cyl_8.crank.inertiaCrank	0.073	0.019	0.686	0.713
Cyl_9.crank.inertiaCrank	0.124	0.054	0.406	0.25
Cyl_10.crank.inertiaCrank	0.169	0.102	0.03	0.001
Cyl_11.crank.inertiaCrank	0.204	0.148	0.346	0.181
Cyl_12.crank.inertiaCrank	0.226	0.181	0.636	0.613
propeller.rotor	0.007	0.002	0.014	0.005
Cyl_3.forceExcitation			0	0
Cyl_7.forceExcitation			0	0
Cyl_8.forceExcitation			0	0.002
Max. Deviation	damper.inertia		intmshaft2.inertia.inertia	
Max. Energy	damper.inertia		Cyl_7.crank.inertiaCrank	

Mode	**5**	
Frequency [rpm]	2060.82	
Element	**Deviation**	**Kin. Energy**
	(normalized)	*(normalized)*
turningwheel.inertia.inertia	0.057	0.014
intmshaft3.inertia.inertia	1	1
propshaft.inertia.inertia	0.463	0.317
intmshaft2.inertia.inertia	0.775	0.558
thrustshaft.inertia.inertia	0.027	0.002
D_innerflange.inertia.inertia	0.108	0.009
damper.inertia	0.021	0.001
camdrive.inertia.inertia	0.067	0.013
Cyl_1.crank.inertiaCrank	0.106	0.091
Cyl_2.crank.inertiaCrank	0.06	0.029
Cyl_3.crank.inertiaCrank	0.008	0.001
Cyl_4.crank.inertiaCrank	0.073	0.043
Cyl_5.crank.inertiaCrank	0.109	0.097
Cyl_6.crank.inertiaCrank	0.102	0.085
Cyl_7.crank.inertiaCrank	0.024	0.005
Cyl_8.crank.inertiaCrank	0.042	0.015
Cyl_8.forceExcitation	0	0
Cyl_9.crank.inertiaCrank	0.093	0.07
Cyl_10.crank.inertiaCrank	0.106	0.091
Cyl_11.crank.inertiaCrank	0.076	0.048
Cyl_11.forceExcitation	0	0
Cyl_12.crank.inertiaCrank	0.018	0.003
Cyl_12.forceExcitation	0	0
propeller.rotor	0.011	0.015
Max. Deviation	intmshaft3.inertia.inertia	
Max. Energy	intmshaft3.inertia.inertia	

Computation results of steady state analysis

Mechanical power

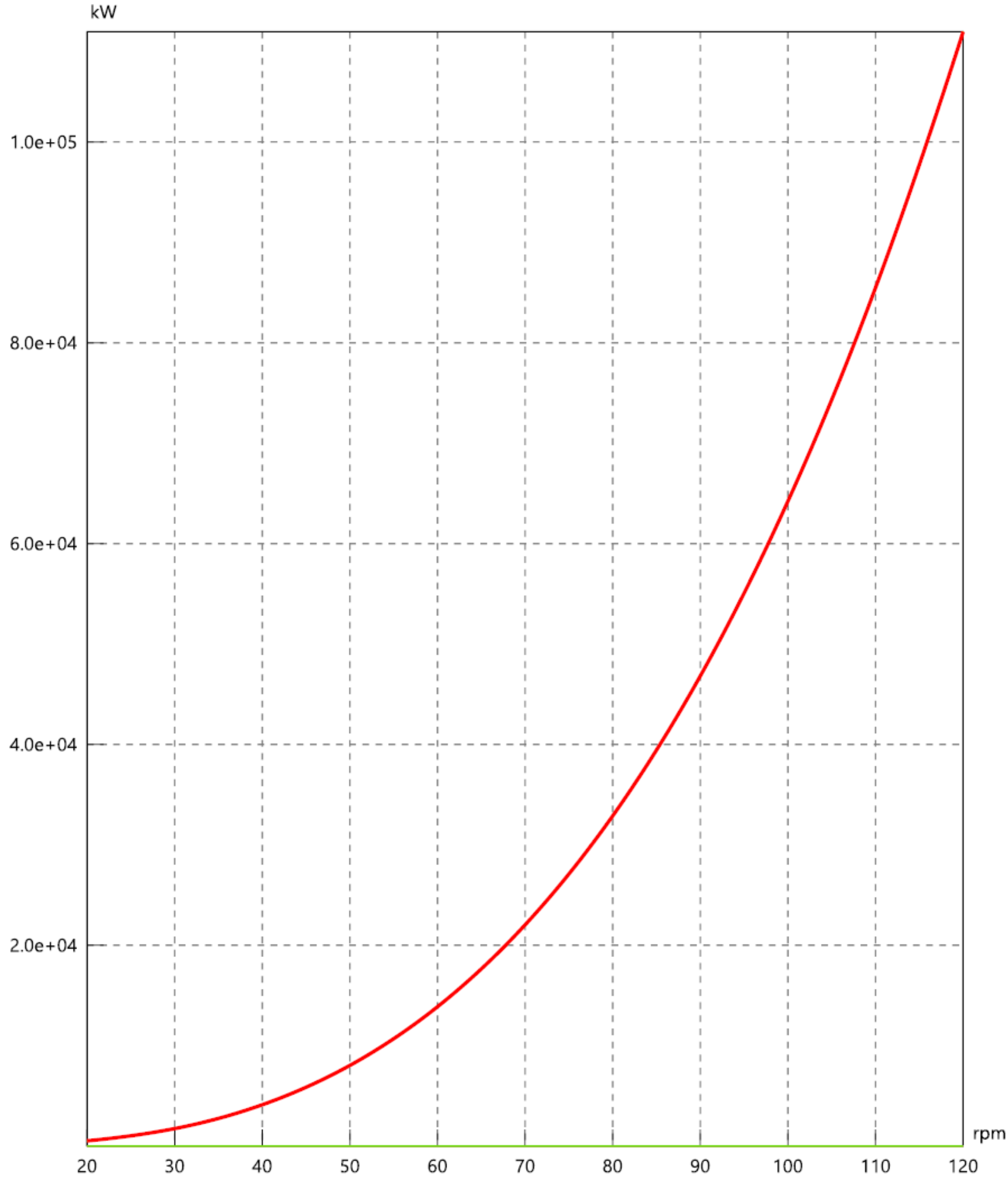

Total torsional stress in thrust shaft

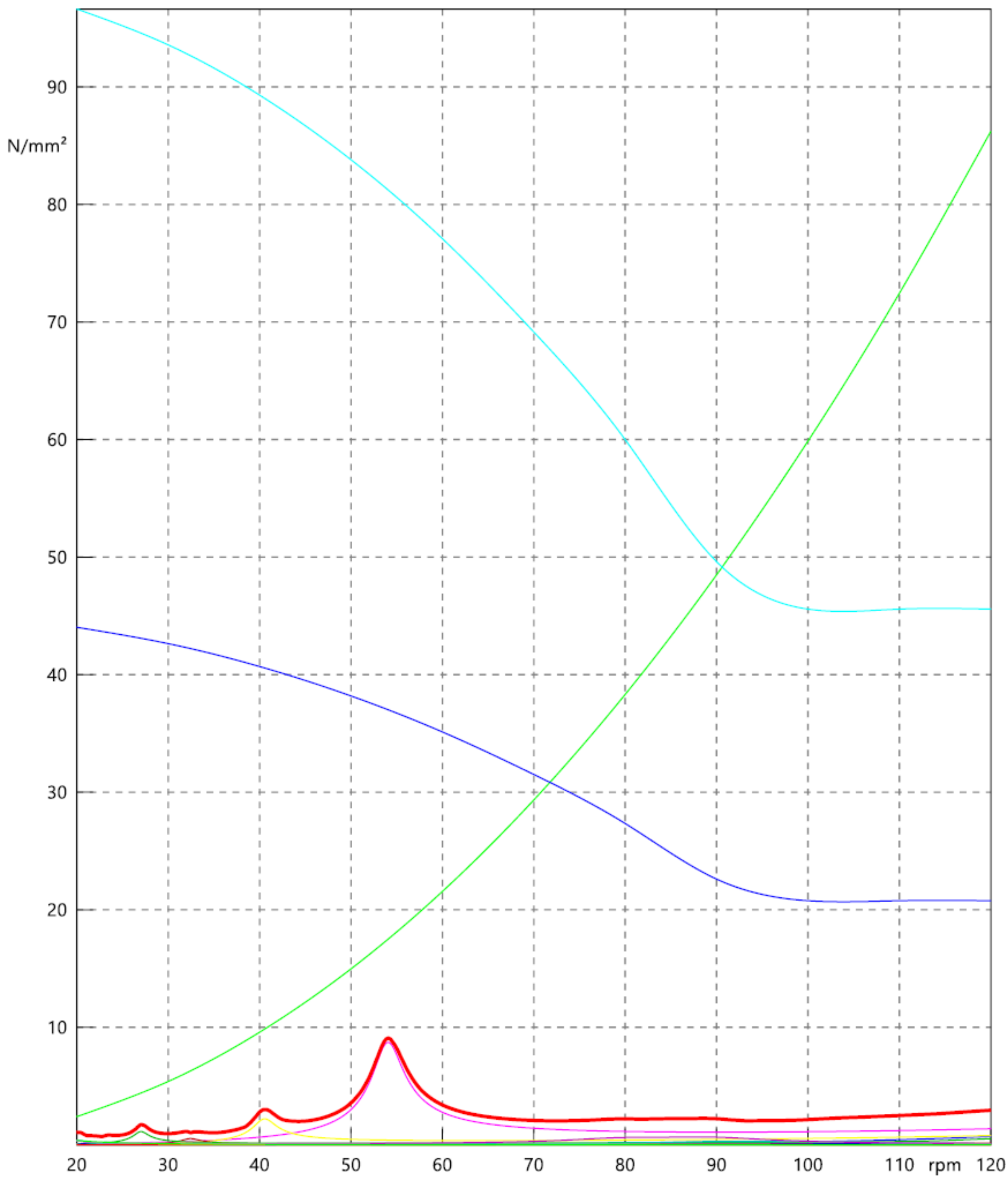

Total torsional stress in intermediate shaft 2

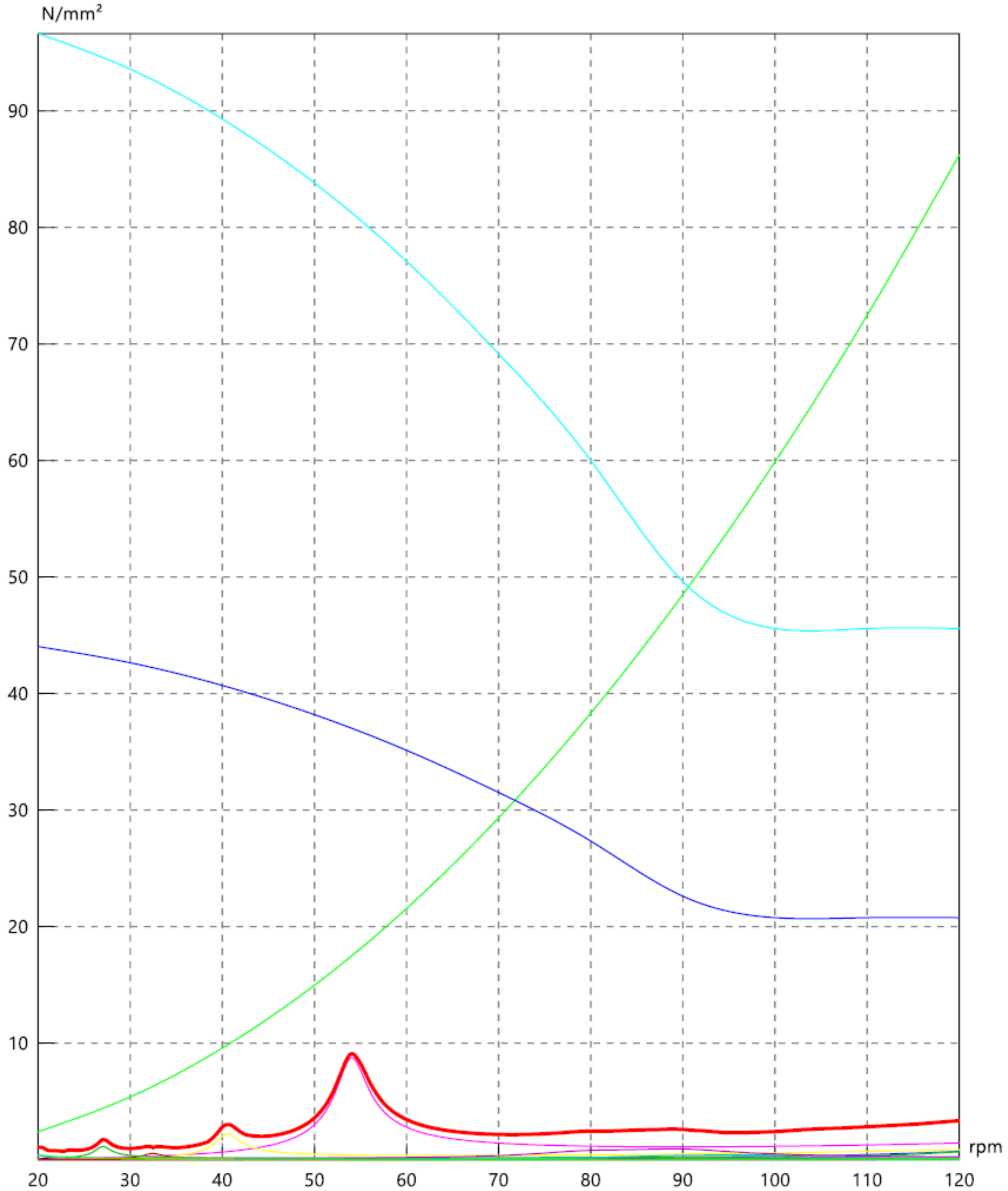

Total torsional stress in intermediate shaft 3

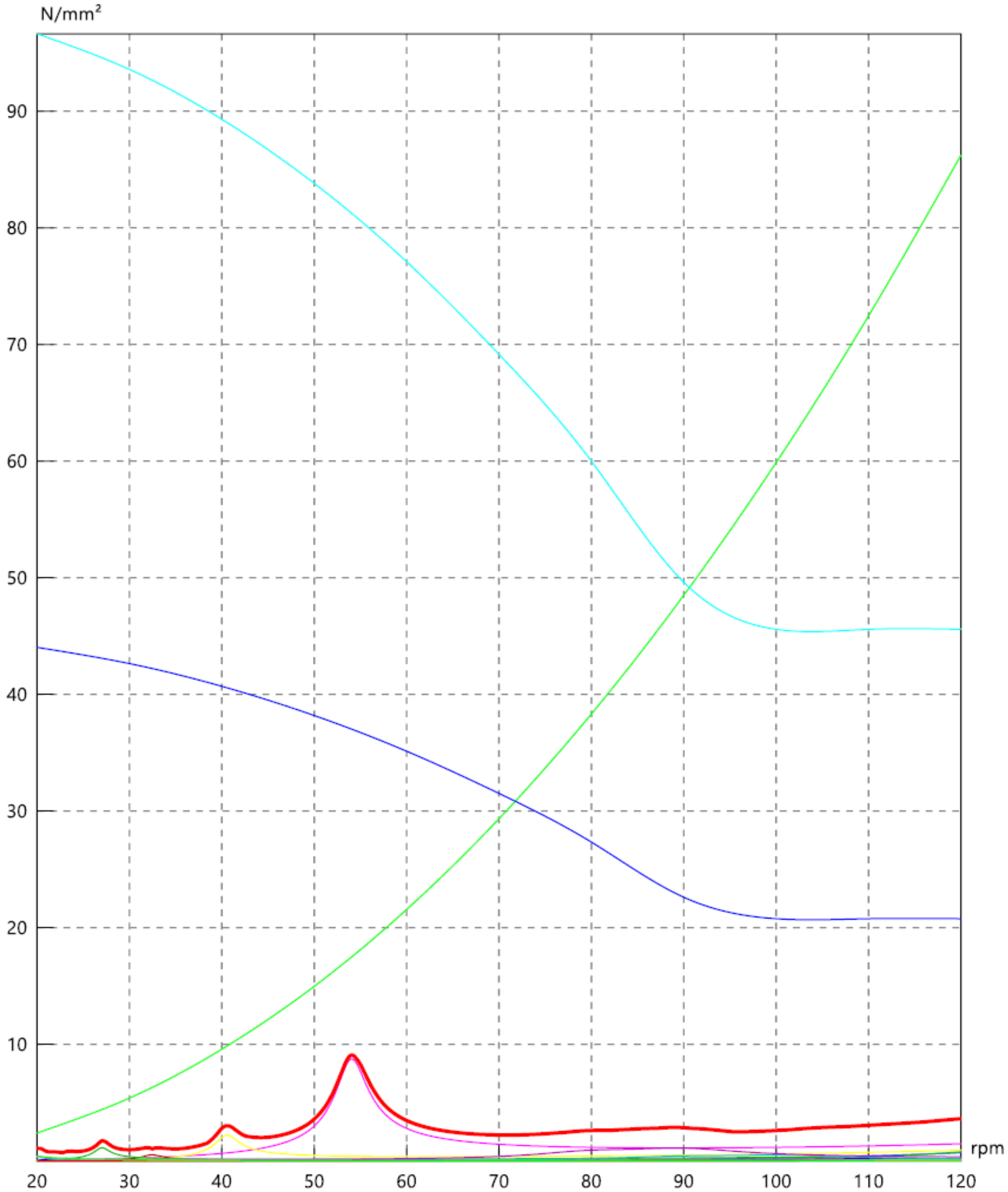

Total torsional stress in propeller shaft

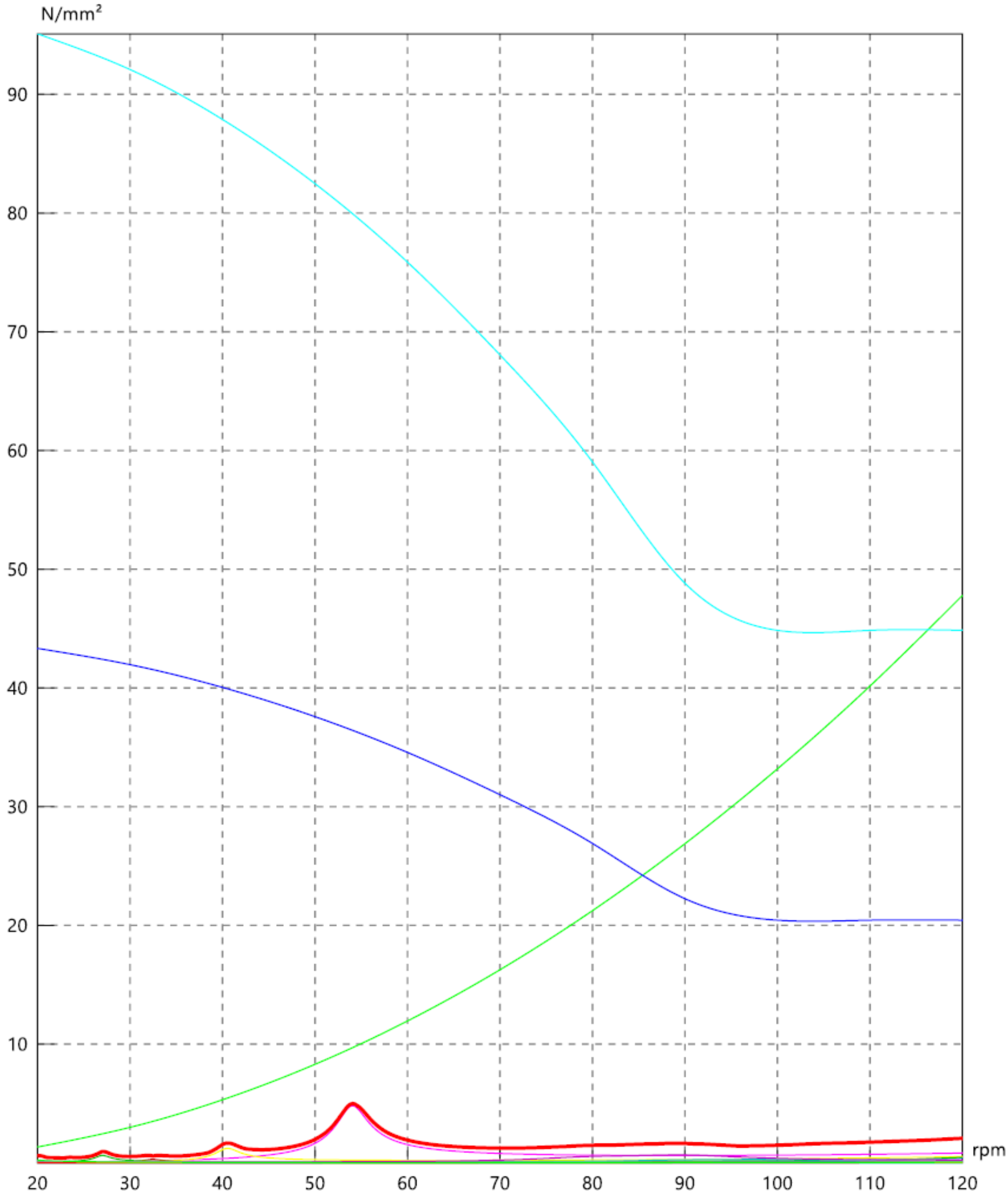

Angular displacement at cylinder 1

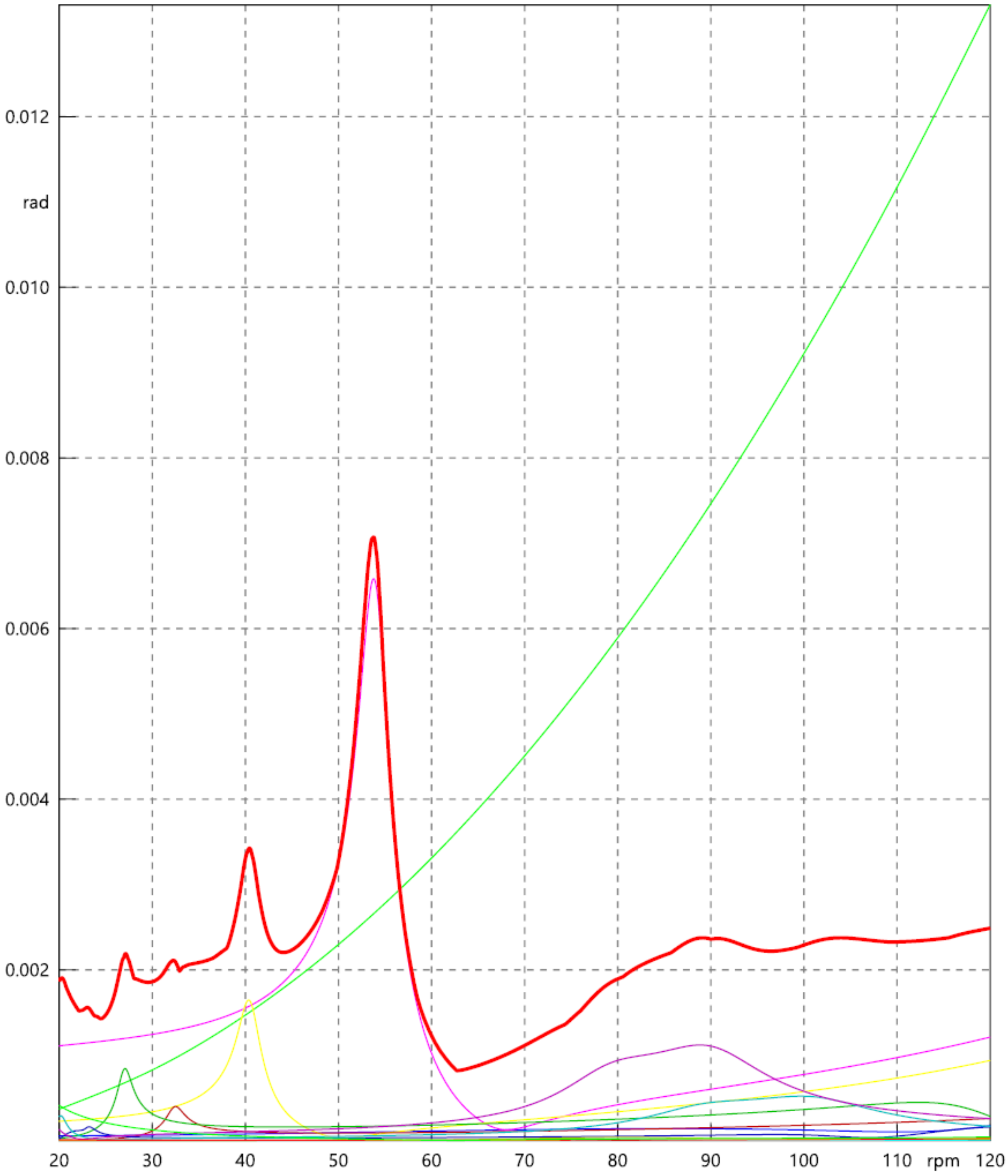

Angular displacement at propeller

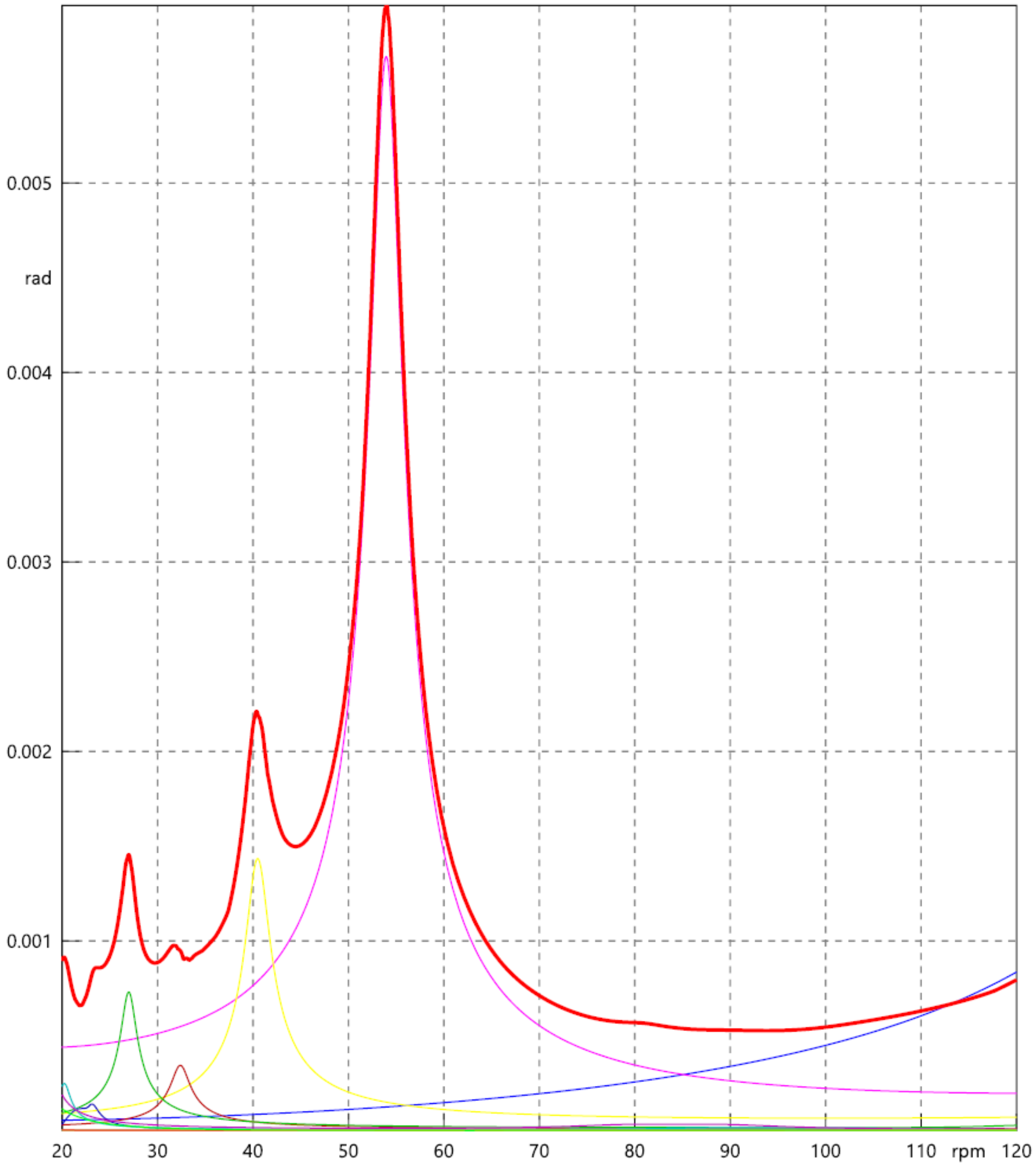

C.2. Misfiring condition

Torsional Vibration Analysis

HHI 1992

Client: Faculty of Maritime Studies

Contractor:
ESI ITI GmbH
Schweriner Str. 1
01067 Dresden, Germany

Dresden, 14.5.2025.

General Remarks

This document template is a prototype. The enclosed analysis results demonstrate the possibilities of result evaluation and post-processing in SimulationX® and the ESI ITI Report Generator.
The analyses have been executed according to state-of-the art vibration analysis.

More descriptions …

Project name: CGA CGM Andromeda

Customer: Faculty of Maritime Studies

Project number: HHI 1992

Date: May 14, 2025

Issued by: *Karlo Bratić*

Checked by: *Nenad Vulić*

Remark:

Model structure

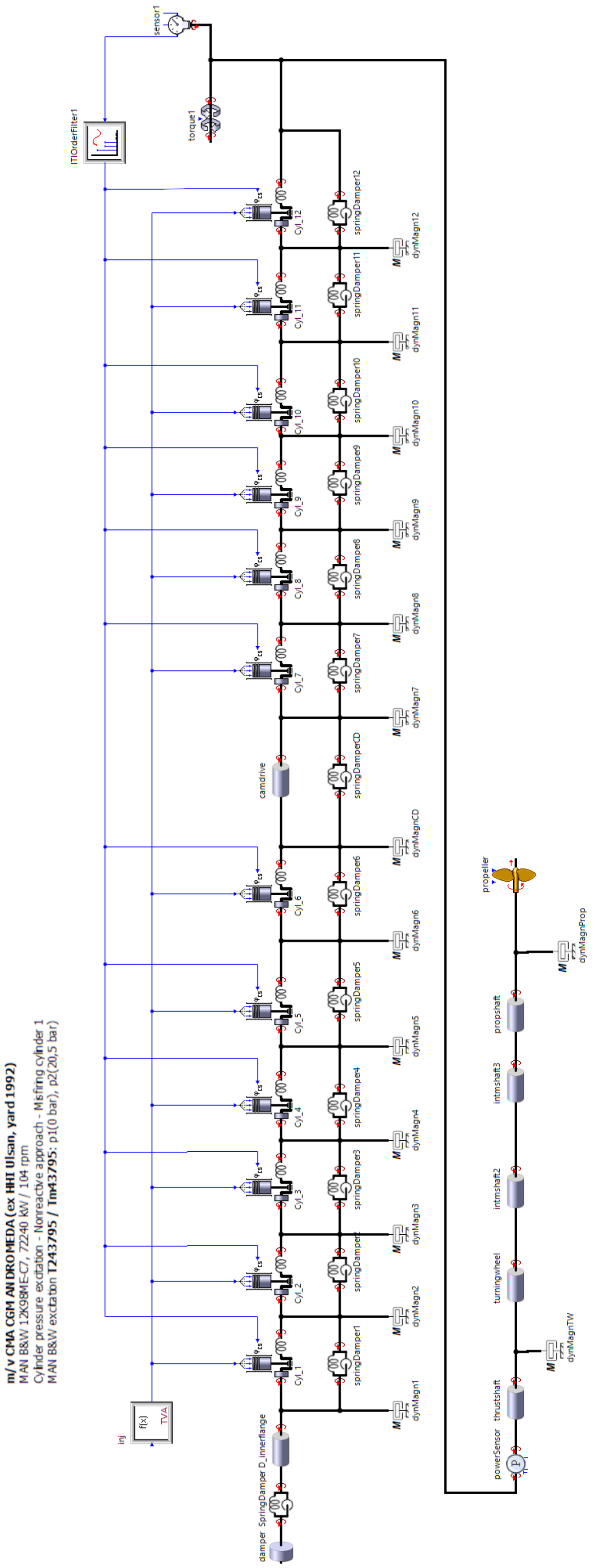

Table C 2-1. Torsional system input data

Element	Inertia	Torsional Stiffness	Damping	Ratio: i_{12}	Description
turningwheel	20398 kgm²	3.0760e+2 MNm/rad	-	-	Shaft Model
intmshaft3	4528 kgm²	2.6450e+2 MNm/rad	-	-	Shaft Model
propshaft	6689 kgm²	6.0340e+2 MNm/rad	-	-	Shaft Model
intmshaft2	4214 kgm²	3.0540e+2 MNm/rad	-	-	Shaft Model
thrustshaft	10600 kgm²	9.4340e+3 MNm/rad	-	-	Shaft Model
D_innerflange	3444 kgm²	5.2910e+3 MNm/rad	-	-	Shaft Model
SpringDamper	-	5.7000e+1 MNm/rad	210000 Nms/rad	-	Spring-Damper
damper	9340 kgm²	-	-	-	
camdrive	13223 kgm²	5.7803e+3 MNm/rad	-	-	Shaft Model
springDamperCD	-	-	psi = 0	-	Spring-Damper
springDamper1	-	-	psi = 0	-	Spring-Damper
springDamper2	-	-	psi = 0	-	Spring-Damper
springDamper3	-	-	psi = 0	-	Spring-Damper
springDamper4	-	-	psi = 0	-	Spring-Damper
springDamper5	-	-	psi = 0	-	Spring-Damper
springDamper6	-	-	psi = 0	-	Spring-Damper
springDamper7	-	-	psi = 0	-	Spring-Damper
springDamper8	-	-	psi = 0	-	Spring-Damper
springDamper9	-	-	psi = 0	-	Spring-Damper
springDamper10	-	-	psi = 0	-	Spring-Damper
springDamper11	-	-	psi = 0	-	Spring-Damper
springDamper12	-	-	psi = 0	-	Spring-Damper
Cyl_1	36824 kgm²	4.2194e+3 MNm/rad	-	-	Inline Cylinder
Cyl_2	36824 kgm²	4.3478e+3 MNm/rad	-	-	Inline Cylinder
Cyl_3	36824 kgm²	4.3668e+3 MNm/rad	-	-	Inline Cylinder
Cyl_4	36824 kgm²	4.3290e+3 MNm/rad	-	-	Inline Cylinder
Cyl_5	36824 kgm²	4.2735e+3 MNm/rad	-	-	Inline Cylinder
Cyl_6	36824 kgm²	5.7803e+3 MNm/rad	-	-	Inline Cylinder
Cyl_7	36824 kgm²	4.3103e+3 MNm/rad	-	-	Inline Cylinder
Cyl_8	36824 kgm²	4.2735e+3 MNm/rad	-	-	Inline Cylinder
Cyl_9	36824 kgm²	4.1841e+3 MNm/rad	-	-	Inline Cylinder
Cyl_10	36824 kgm²	4.2735e+3 MNm/rad	-	-	Inline Cylinder
Cyl_11	36824 kgm²	4.4053e+3 MNm/rad	-	-	Inline Cylinder
Cyl_12	36824 kgm²	6.3291e+3 MNm/rad	-	-	Inline Cylinder

Natural frequency analysis

Table C2-2. Natural vibration modes, natural frequencies, distribution of potential energy

Mode	1			2		
Frequency [rpm]	163.26			711.71		
Element	Rel. Angle	Torque	Pot. Energy	Rel. Angle	Torque	Pot. Energy
	rad	Nm	*(normalized)*	rad	Nm	*(normalized)*
turningwheel.springDamper.springDamper	0.377	1.1597e+8	0.5208	0.038	6.3206e+7	0.0068
intmshaft3.springDamper.springDamper	0.439	1.1618e+8	0.6079	0.064	4.0718e+8	0.0168
propshaft.springDamper.springDamper	0.191	1.1513e+8	0.2617	0.03	7.9913e+8	0.0082
intmshaft2.springDamper.springDamper	0.381	1.1631e+8	0.5277	0.048	1.6415e+8	0.0111
thrustshaft.springDamper.springDamper	0.012	1.1204e+8	0.0158	0.001	1.2545e+7	0.0001
D_innerflange.springDamper.springDamper	0.001	3.2980e+6	0	0.011	6.4884e+7	0.0107
SpringDamper.springDamper	0.043	2.4554e+6	0.0012	1	5.8806e+7	0.8845
camdrive.springDamper.springDamper	0.011	6.3332e+7	0.0083	0.028	1.4682e+9	0.071
Cyl_1.crank.relStiffDamp	0.004	1.6118e+7	0.0007	0.021	1.4977e+8	0.0282
Cyl_2.crank.relStiffDamp	0.006	2.5233e+7	0.0017	0.026	3.3952e+8	0.046
Cyl_2.forceExcitation	0.699	2.8352e+3	0			
Cyl_3.crank.relStiffDamp	0.008	3.4294e+7	0.0032	0.031	8.0200e+8	0.0653
Cyl_4.crank.relStiffDamp	0.01	4.3174e+7	0.0051	0.035	2.7891e+9	0.0827
Cyl_4.forceExcitation	1	6.7547e+4	0.0008			
Cyl_5.crank.relStiffDamp	0.012	5.2039e+7	0.0075	0.038	5.5742e+9	0.0947
Cyl_6.crank.relStiffDamp	0.01	6.0237e+7	0.0075	0.028	1.7795e+9	0.0722
Cyl_6.forceExcitation	0.654	1.5673e+6	0.0122			
Cyl_7.crank.relStiffDamp	0.017	7.1739e+7	0.0142	0.036	9.9030e+8	0.0848
Cyl_7.forceExcitation	0.948	7.1211e+4	0.0008	0.058	2.2270e+4	0
Cyl_8.crank.relStiffDamp	0.019	7.9487e+7	0.0176	0.032	7.1832e+8	0.0685
Cyl_8.forceExcitation	0.623	1.5758e+6	0.0117	0.065	9.3247e+5	0.0004
Cyl_9.crank.relStiffDamp	0.021	8.7610e+7	0.0219	0.027	5.1318e+8	0.0486
Cyl_10.crank.relStiffDamp	0.022	9.5508e+7	0.0254	0.02	3.3790e+8	0.0269
Cyl_11.crank.relStiffDamp	0.023	1.0286e+8	0.0286	0.012	1.7945e+8	0.0101

Cyl_11.forceExcitation	0.892	2.6915e+5	0.0029	0.198	5.9362e+5	0.0002
Cyl_12.crank.relStiffDamp	0.017	1.0996e+8	0.0228	0.003	4.1191e+7	0.0009
Cyl_12.forceExcitation	0.862	2.7172e+5	0.0028	0.213	8.0343e+5	0.0002
Cyl_3.forceExcitation				0.098	3.1526e+3	0
Max. Angle	Cyl_4.forceExcitation			SpringDamper.springDamper		
Max. Torque	intmshaft2.springDamper.springDamper			Cyl_5.crank.relStiffDamp		
Max. Energy	intmshaft3.springDamper.springDamper			SpringDamper.springDamper		

Mode	3			4		
Frequency [rpm]	806.66			1527.65		
Element	Rel. Angle	Torque	Pot. Energy	Rel. Angle	Torque	Pot. Energy
	rad	Nm	*(normalized)*	rad	Nm	*(normalized)*
turningwheel.springDamper.springDamper	0.04	2.5017e+7	0.0086	0.204	6.2691e+7	0.021
intmshaft3.springDamper.springDamper	0.078	6.4827e+7	0.0283	0.535	1.4164e+8	0.1252
propshaft.springDamper.springDamper	0.037	7.4440e+7	0.0142	0.322	1.9438e+8	0.1034
intmshaft2.springDamper.springDamper	0.056	4.5908e+7	0.0169	0.144	4.3929e+7	0.0104
thrustshaft.springDamper.springDamper	0.002	1.0329e+8	0.0006	0.05	4.7179e+8	0.039
D_innerflange.springDamper.springDamper	0.011	6.1334e+7	0.0104	0.009	6.5599e+7	0.0007
SpringDamper.springDamper	1	6.0674e+7	1	1	6.0394e+7	0.0941
camdrive.springDamper.springDamper	0.038	8.8672e+8	0.1458	0.038	2.2313e+8	0.0136
Cyl_1.crank.relStiffDamp	0.013	6.8208e+7	0.0129	0.177	7.5165e+8	0.2188
Cyl_2.crank.relStiffDamp	0.021	1.0369e+8	0.0348	0.3	1.3070e+9	0.6476
Cyl_2.crank.piston	0.167	1.7238e+3	0			
Cyl_3.crank.relStiffDamp	0.031	2.1070e+8	0.0734	0.362	1.5817e+9	0.9457
Cyl_3.forceExcitation	0.151	8.7830e+3	0			
Cyl_4.crank.relStiffDamp	0.04	3.6808e+8	0.1204	0.35	1.5160e+9	0.8765
Cyl_5.crank.relStiffDamp	0.047	5.6834e+8	0.1645	0.262	1.1210e+9	0.4851
Cyl_5.forceExcitation	0.045	1.5324e+4	0	0.166	6.7229e+3	0
Cyl_6.crank.relStiffDamp	0.038	8.0200e+8	0.1427	0.082	4.7839e+8	0.0648
Cyl_7.crank.relStiffDamp	0.05	1.1147e+9	0.1898	0.125	5.4013e+8	0.1111
Cyl_7.forceExcitation	0.031	2.1605e+4	0			
Cyl_8.crank.relStiffDamp	0.047	1.3164e+9	0.1643	0.276	1.1785e+9	0.5362
Cyl_8.forceExcitation	0.051	5.6353e+5	0.0004			
Cyl_9.crank.relStiffDamp	0.041	1.4572e+9	0.1236	0.372	1.5561e+9	0.9554
Cyl_10.crank.relStiffDamp	0.031	1.5139e+9	0.0722	0.371	1.5835e+9	0.9688
Cyl_11.crank.relStiffDamp	0.019	1.6334e+9	0.0292	0.287	1.2622e+9	0.5971
Cyl_11.forceExcitation	0.224	2.0102e+5	0.0003	0.428	2.9458e+5	0.0002
Cyl_12.crank.relStiffDamp	0.005	7.1422e+8	0.0031	0.106	6.7086e+8	0.1174
Cyl_12.forceExcitation	0.248	2.2087e+5	0.0004	0.787	2.9758e+5	0.0004
Cyl_2.forceExcitation				0.489	3.1075e+3	0
Max. Angle	SpringDamper.springDamper			SpringDamper.springDamper		
Max. Torque	Cyl_11.crank.relStiffDamp			Cyl_10.crank.relStiffDamp		
Max. Energy	SpringDamper.springDamper			Cyl_10.crank.relStiffDamp		

Mode	5		
Frequency [rpm]	2060.82		
Element	Rel. Angle	Torque	Pot. Energy
	rad	Nm	*(normalized)*
turningwheel.springDamper.springDamper	1	3.0760e+8	0.752
intmshaft3.springDamper.springDamper	0.748	1.9779e+8	0.3616
propshaft.springDamper.springDamper	0.661	3.9869e+8	0.6441
intmshaft2.springDamper.springDamper	0.314	9.5911e+7	0.0736
thrustshaft.springDamper.springDamper	0.041	3.8236e+8	0.0379
D_innerflange.springDamper.springDamper	0.003	3.7724e+7	0.0001
SpringDamper.springDamper	0.172	9.9904e+6	0.0041
camdrive.springDamper.springDamper	0.059	3.4257e+8	0.0495
Cyl_1.crank.relStiffDamp	0.064	2.6940e+8	0.0418
Cyl_2.crank.relStiffDamp	0.095	4.1228e+8	0.0955
Cyl_3.crank.relStiffDamp	0.09	3.9300e+8	0.0865
Cyl_4.crank.relStiffDamp	0.051	2.1988e+8	0.0273
Cyl_4.forceExcitation	0.121	3.8609e+3	0
Cyl_5.crank.relStiffDamp	0.01	4.5412e+7	0.001
Cyl_6.crank.relStiffDamp	0.049	2.8551e+8	0.0343
Cyl_6.forceExcitation	0.115	8.9056e+4	0
Cyl_7.crank.relStiffDamp	0.093	4.0018e+8	0.0908
Cyl_8.crank.relStiffDamp	0.07	2.9882e+8	0.0511
Cyl_9.crank.relStiffDamp	0.019	7.9150e+7	0.0036
Cyl_10.crank.relStiffDamp	0.041	1.7631e+8	0.0176
Cyl_11.crank.relStiffDamp	0.081	3.5823e+8	0.0711
Cyl_12.crank.relStiffDamp	0.063	4.0123e+8	0.0622
Max. Angle	turningwheel.springDamper.springDamper		
Max. Torque	Cyl_2.crank.relStiffDamp		
Max. Energy	turningwheel.springDamper.springDamper		

Table C2-3. Natural vibration modes, natural frequencies, distribution of potential energy

Mode	1		2	
Frequency [rpm]	163.26		711.71	
Element	Deviation	Kin. Energy	Deviation	Kin. Energy
	(normalized)	*(normalized)*	*(normalized)*	*(normalized)*
turningwheel.inertia.inertia	0.737	0.031	0.156	0.053
intmshaft3.inertia.inertia	0.111	0	0.079	0.003
propshaft.inertia.inertia	0.602	0.007	0.021	0
intmshaft2.inertia.inertia	0.315	0.001	0.122	0.007
thrustshaft.inertia.inertia	0.75	0.017	0.156	0.027
D_innerflange.inertia.inertia	0.952	0.009	0.155	0.009
damper.inertia	1	0.026	1	1
camdrive.inertia.inertia	0.896	0.03	0.024	0.001
Cyl_1.crank.inertiaCrank	0.952	0.093	0.146	0.085
Cyl_2.crank.inertiaCrank	0.947	0.092	0.129	0.066
Cyl_3.crank.inertiaCrank	0.941	0.091	0.107	0.045
Cyl_3.forceExcitation	0	0		
Cyl_4.crank.inertiaCrank	0.932	0.089	0.08	0.025
Cyl_5.crank.inertiaCrank	0.921	0.087	0.051	0.01
Cyl_5.forceExcitation	0	0		
Cyl_6.crank.inertiaCrank	0.907	0.084	0.024	0.002
Cyl_7.crank.inertiaCrank	0.883	0.08	0.043	0.007
Cyl_8.crank.inertiaCrank	0.865	0.077	0.073	0.021
Cyl_9.crank.inertiaCrank	0.844	0.073	0.101	0.04
Cyl_9.forceExcitation	0	0		
Cyl_10.crank.inertiaCrank	0.821	0.069	0.125	0.061
Cyl_11.crank.inertiaCrank	0.796	0.065	0.142	0.08
Cyl_12.crank.inertiaCrank	0.769	0.061	0.153	0.092
propeller.rotor	0.816	1	0.005	0.002
Cyl_2.forceExcitation			0	0
Cyl_4.forceExcitation			0	0
Cyl_6.forceExcitation			0	0
Max. Deviation	damper.inertia		damper.inertia	
Max. Energy	propeller.rotor		damper.inertia	

Mode	3		4	
Frequency [rpm]	806.66		1527.65	
Element	Deviation	Kin. Energy	Deviation	Kin. Energy
	(normalized)	*(normalized)*	*(normalized)*	*(normalized)*
turningwheel.inertia.inertia	0.234	0.108	0.794	0.53
intmshaft3.inertia.inertia	0.125	0.007	0.854	0.136
propshaft.inertia.inertia	0.035	0.001	0.312	0.027
intmshaft2.inertia.inertia	0.189	0.014	1	0.174
thrustshaft.inertia.inertia	0.232	0.055	0.743	0.241
D_innerflange.inertia.inertia	0.235	0.018	0.783	0.087
damper.inertia	1	0.899	0.28	0.03
camdrive.inertia.inertia	0.042	0.002	0.774	0.326
Cyl_1.crank.inertiaCrank	0.24	0.204	0.78	0.923
Cyl_2.crank.inertiaCrank	0.231	0.189	0.601	0.547
Cyl_2.forceExcitation	0	0		
Cyl_3.crank.inertiaCrank	0.209	0.155	0.297	0.134
Cyl_4.crank.inertiaCrank	0.175	0.109	0.072	0.008
Cyl_4.forceExcitation	0	0	0	0

Cyl_5.crank.inertiaCrank	0.131	0.061	0.425	0.274
Cyl_6.crank.inertiaCrank	0.08	0.023	0.691	0.723
Cyl_6.forceExcitation	0	0	0	0.002
Cyl_7.crank.inertiaCrank	0.029	0.003	0.812	1
Cyl_8.crank.inertiaCrank	0.073	0.019	0.686	0.713
Cyl_9.crank.inertiaCrank	0.124	0.054	0.406	0.25
Cyl_10.crank.inertiaCrank	0.169	0.102	0.03	0.001
Cyl_11.crank.inertiaCrank	0.204	0.148	0.346	0.181
Cyl_12.crank.inertiaCrank	0.226	0.181	0.636	0.613
propeller.rotor	0.007	0.002	0.014	0.005
Cyl_3.forceExcitation			0	0
Cyl_7.forceExcitation			0	0
Cyl_8.forceExcitation			0	0.002
Max. Deviation	damper.inertia		intmshaft2.inertia.inertia	
Max. Energy	damper.inertia		Cyl_7.crank.inertiaCrank	

Mode	**5**	
Frequency [rpm]	**2060.82**	
Element	**Deviation**	**Kin. Energy**
	(normalized)	*(normalized)*
turningwheel.inertia.inertia	0.057	0.014
intmshaft3.inertia.inertia	1	1
propshaft.inertia.inertia	0.463	0.317
intmshaft2.inertia.inertia	0.775	0.558
thrustshaft.inertia.inertia	0.027	0.002
D_innerflange.inertia.inertia	0.108	0.009
damper.inertia	0.021	0.001
camdrive.inertia.inertia	0.067	0.013
Cyl_1.crank.inertiaCrank	0.106	0.091
Cyl_2.crank.inertiaCrank	0.06	0.029
Cyl_3.crank.inertiaCrank	0.008	0.001
Cyl_4.crank.inertiaCrank	0.073	0.043
Cyl_5.crank.inertiaCrank	0.109	0.097
Cyl_6.crank.inertiaCrank	0.102	0.085
Cyl_7.crank.inertiaCrank	0.024	0.005
Cyl_8.crank.inertiaCrank	0.042	0.015
Cyl_8.forceExcitation	0	0
Cyl_9.crank.inertiaCrank	0.093	0.07
Cyl_10.crank.inertiaCrank	0.106	0.091
Cyl_11.crank.inertiaCrank	0.076	0.048
Cyl_11.forceExcitation	0	0
Cyl_12.crank.inertiaCrank	0.018	0.003
Cyl_12.forceExcitation	0	0
propeller.rotor	0.011	0.015
Max. Deviation	intmshaft3.inertia.inertia	
Max. Energy	intmshaft3.inertia.inertia	

Computation results of steady state analysis

Mechanical power

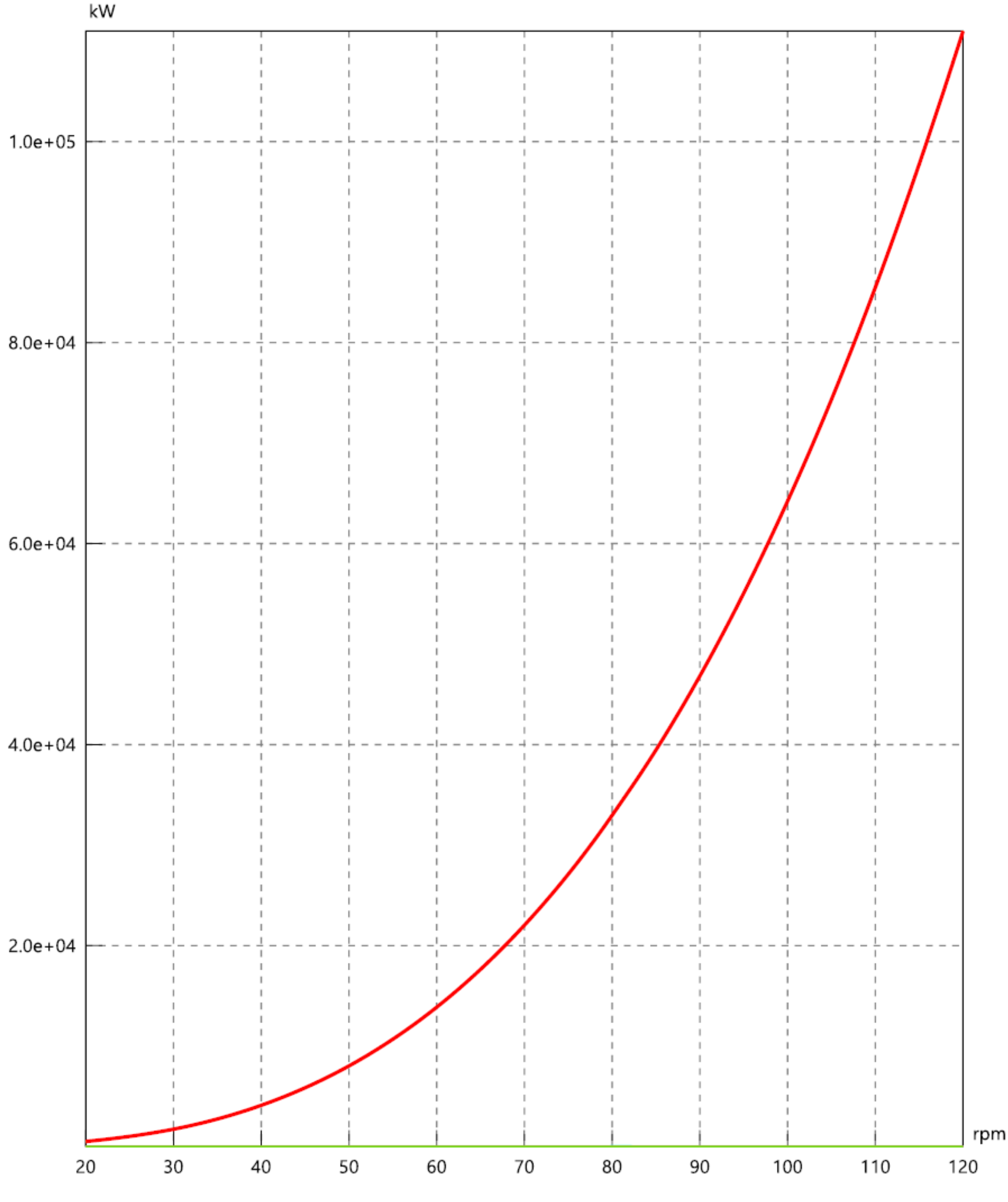

Total torsional stress in thrust shaft

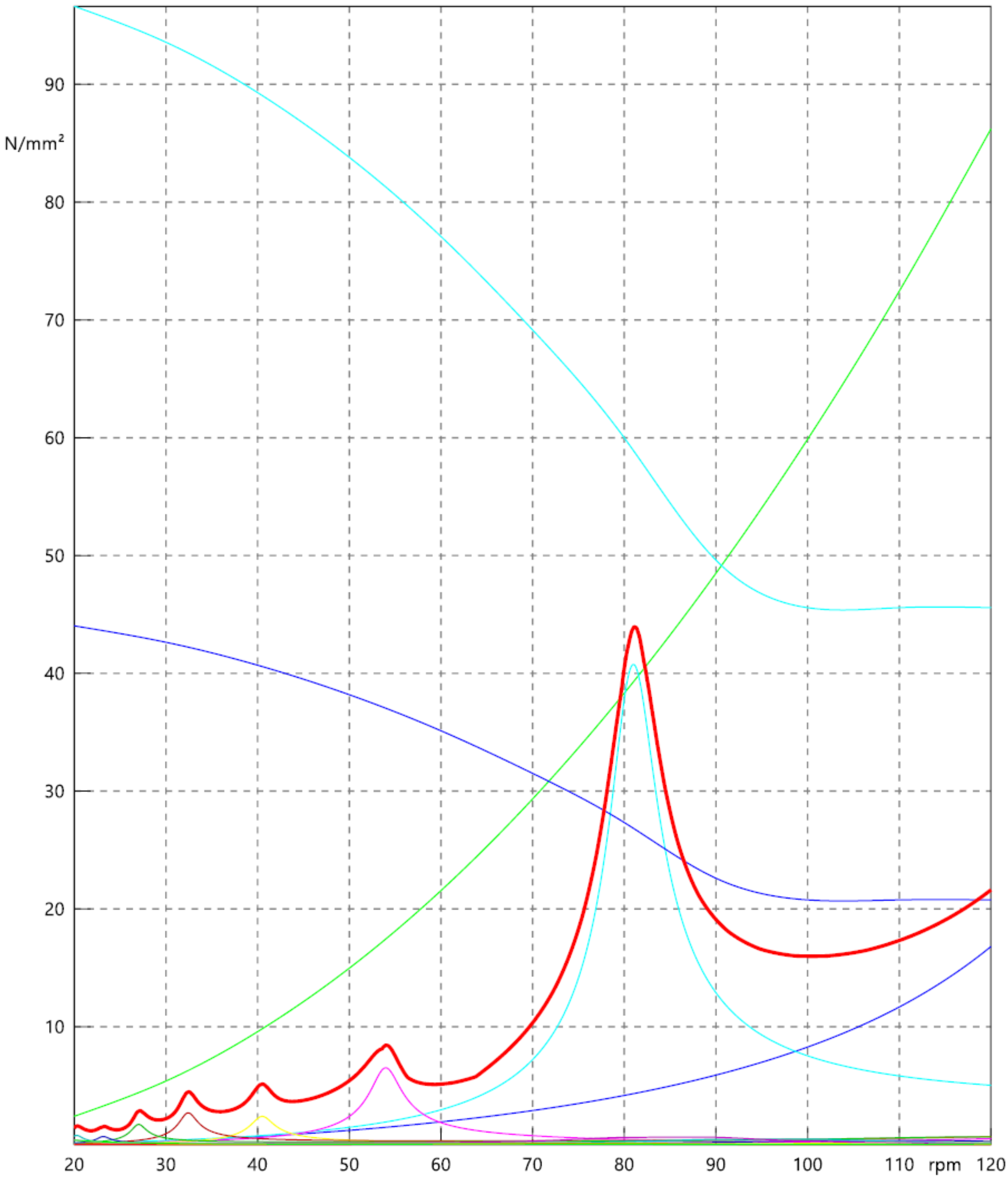

Total torsional stress in intermediate shaft 2

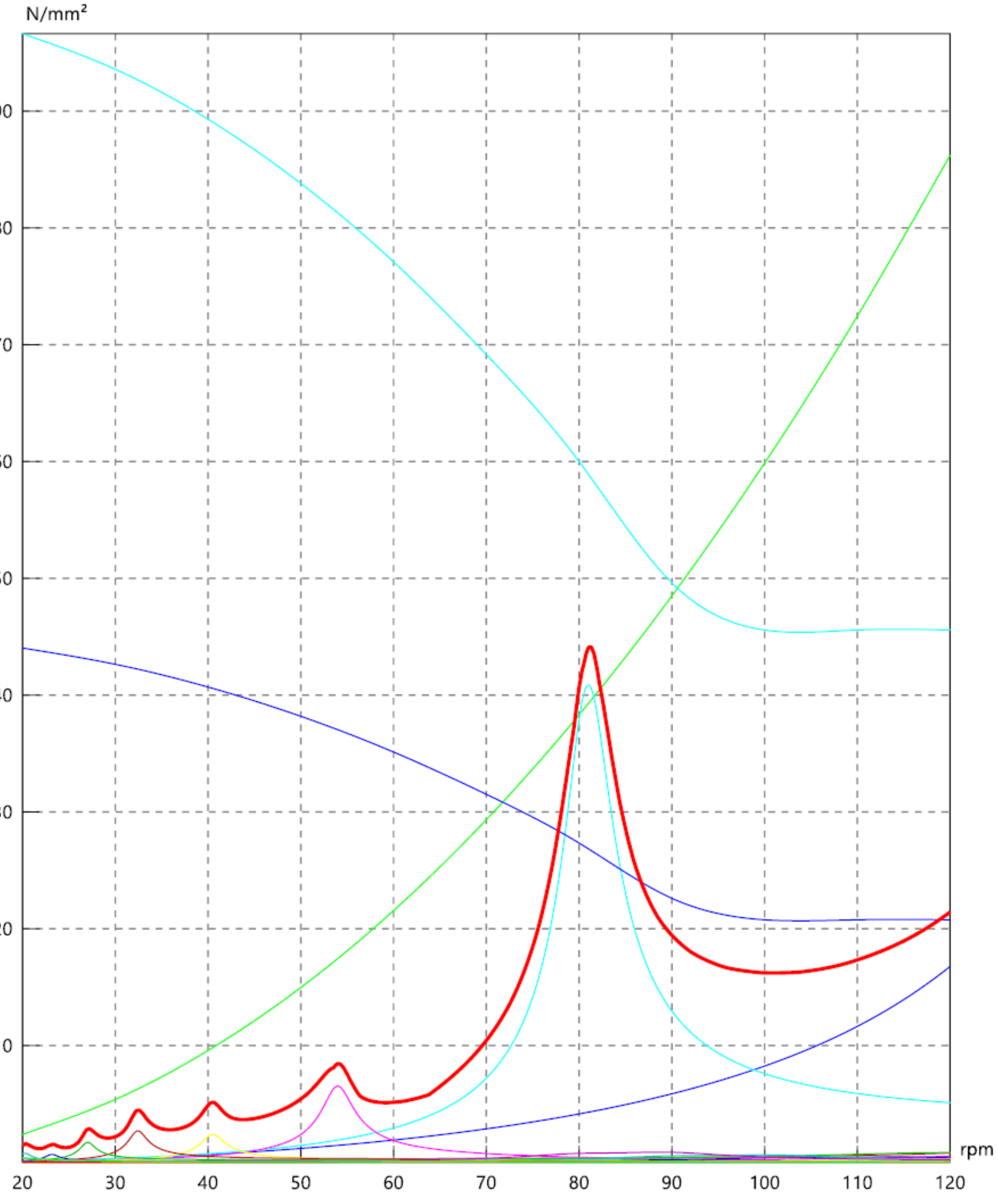

Total torsional stress in intermediate shaft 3

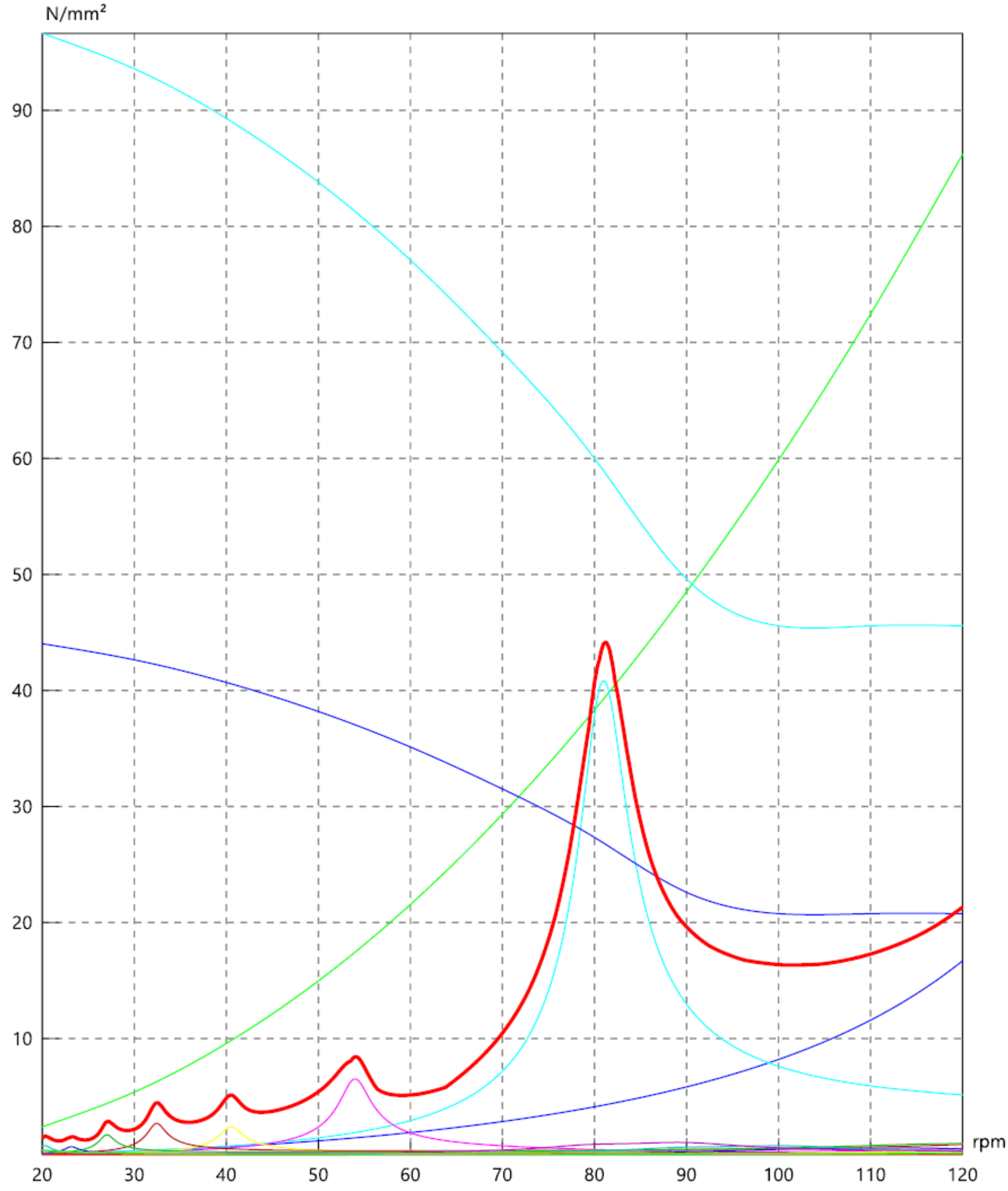

Total torsional stress in propeller shaft

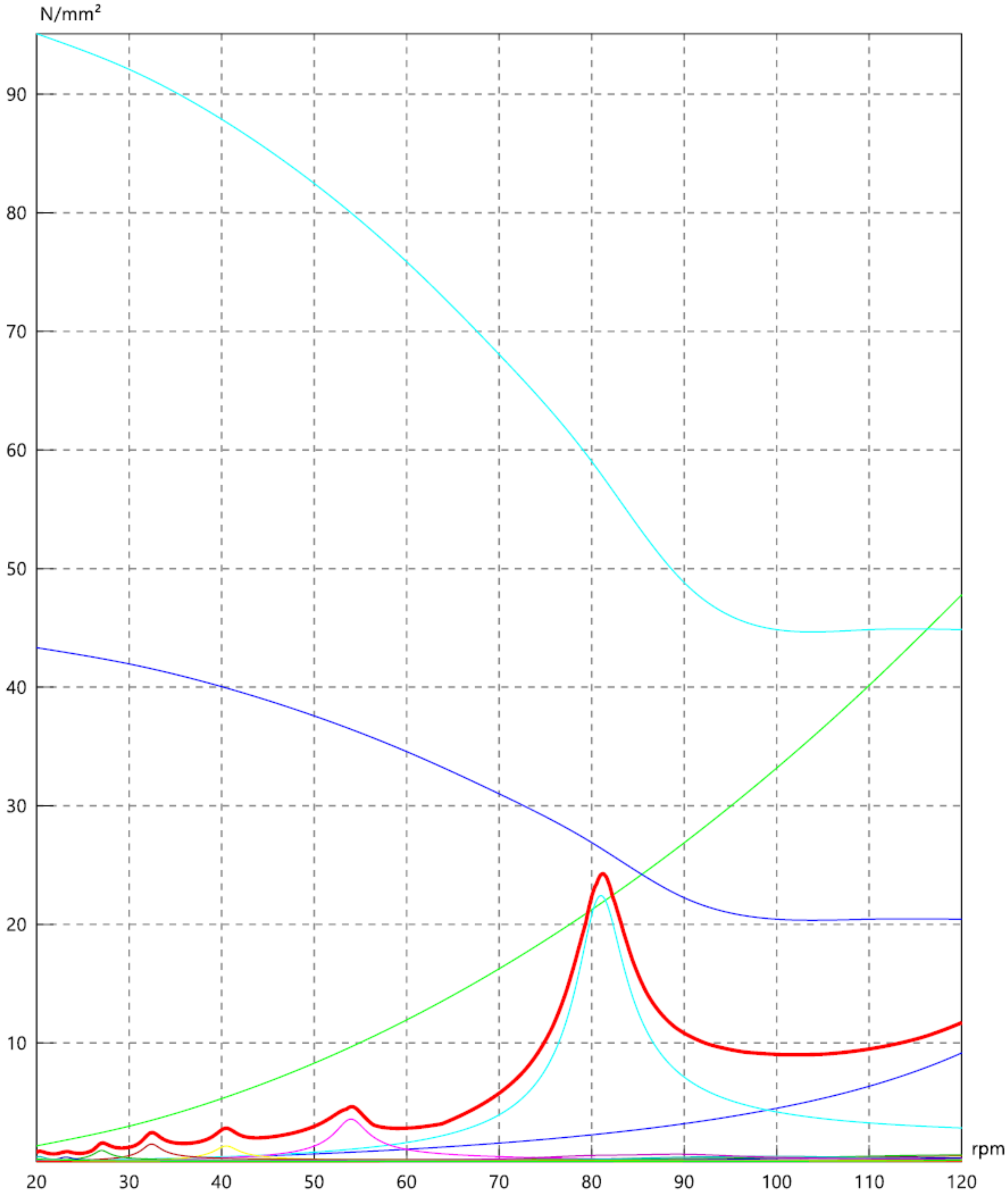

Angular displacement at cylinder 1

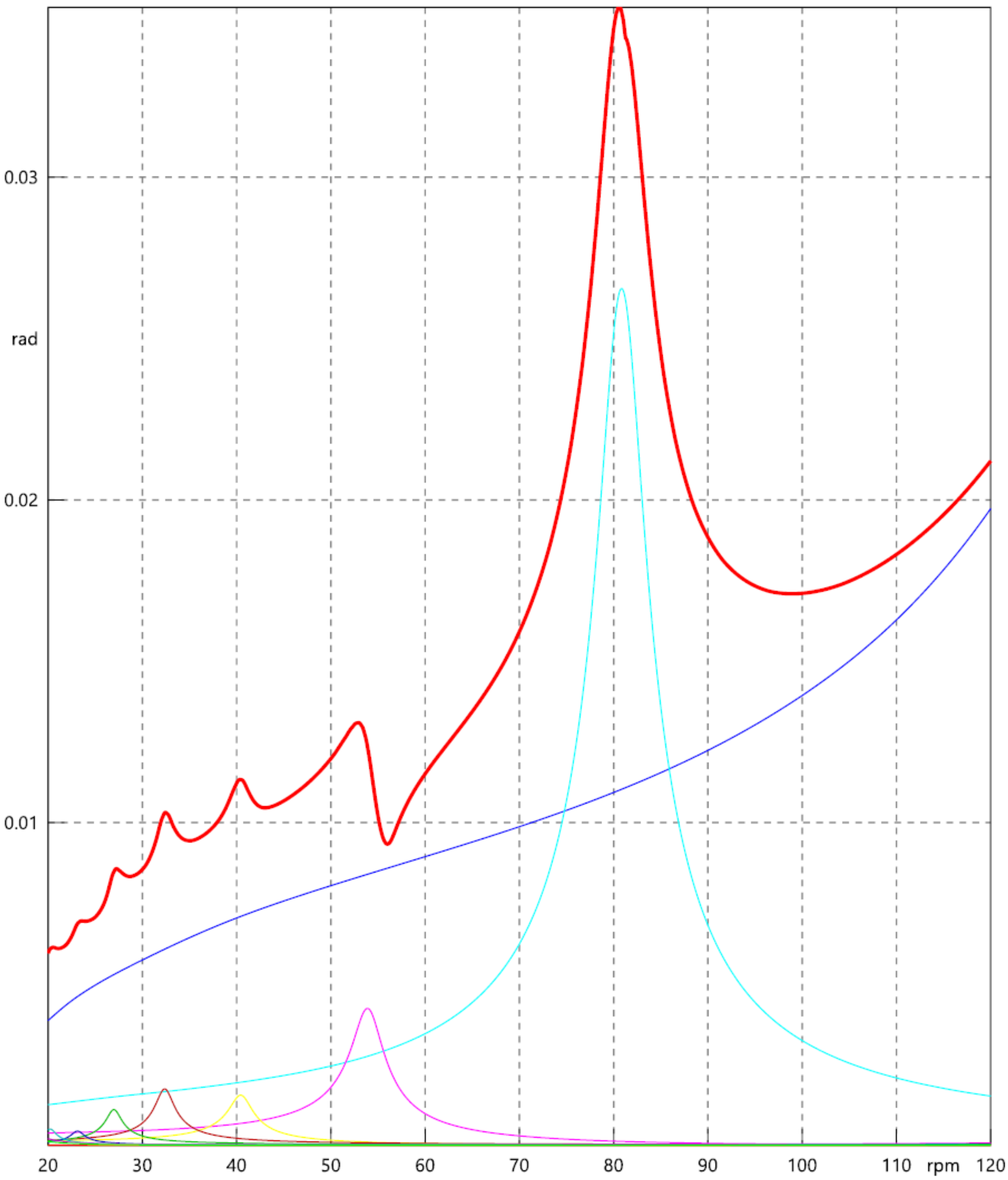

Angular displacement at propeller

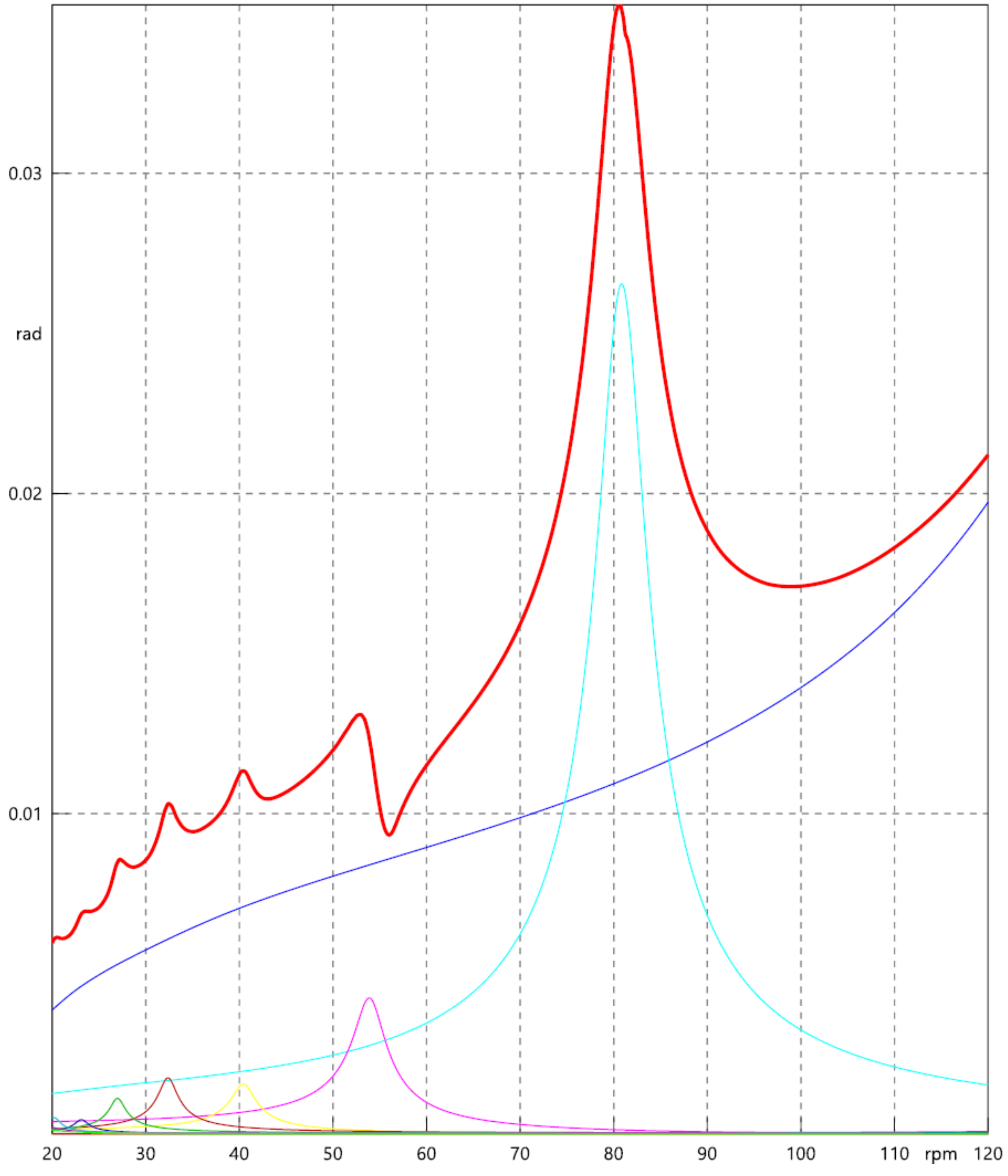

APPENDIX D - GTORSI TVA report

D.1. Normal firing condition

MAN Energy Solutions — T O R S I O N A L   V I B R A T I O N   C A L C U L A T I O N — Page 1

GTORSI 3.6.4/WIN32 — T A B L E   O F   I N F O R M A T I O N — 8 Aug 2024

Faculty of Maritime S — 09:45:49

Calculations made by anonymous user

12K98ME-C7, Mark VII, — Hyundai Heavy Industrires

MCR 72240 kW @ 104 r/min — 1992

NORMAL FIRING, PROPELLER DAMPING 5.5% FLAT

Excitation: T243795

ENGINE LOAD :	kW	r/min
Propeller	72240	104

COMBUSTION CONDITION :

Normal

Gas harmonic components : 243795

Bore: 980 Stroke: 2400 Connecting rod: 3090 R/L: 0.3883

Firing order: 1 8 12 4 2 9 10 5 3 7 11 6

Mass ID/Description	Tang. harmon ID	Firing angle (deg)	Osc. mass (kg)	Mom. of inertia (kgm^2)	Rot. speed (r/min)	Mass damping (Nms or %)	Tors. flex. (nrad/Nm)	Diameters outer/inner (mm)	Relative damping (Nms or %)
MAIN SHAFT									
61 Damper				9340	104.0	0.00%			
							17.544	0.0/ 0.0	210000
38 Flange				3444	104.0	0.00%			
							0.189	1061.0/150.0	0
1 Cylinder	243795	0.0	18756	36824	104.0	0.85%			
							0.237	1062.0/150.0	0.50%
2 Cylinder	243795	120.0	18756	36824	104.0	0.85%			
							0.230	1062.0/150.0	0.50%
3 Cylinder	243795	240.0	18756	36824	104.0	0.85%			
							0.229	1062.0/150.0	0.50%
4 Cylinder	243795	90.0	18756	36824	104.0	0.85%			
							0.231	1062.0/150.0	0.50%
5 Cylinder	243795	210.0	18756	36824	104.0	0.85%			
							0.234	1062.0/150.0	0.50%
6 Cylinder	243795	330.0	18756	36824	104.0	0.85%			
							0.173	1061.0/150.0	0.50%
23 Camshaft Drive				13223	104.0	0.85%			
							0.173	1061.0/150.0	0.50%
7 Cylinder	243795	270.0	18756	36824	104.0	0.85%			
							0.232	1062.0/150.0	0.50%
8 Cylinder	243795	30.0	18756	36824	104.0	0.85%			
							0.234	1062.0/150.0	0.50%
9 Cylinder	243795	150.0	18756	36824	104.0	0.85%			
							0.239	1062.0/150.0	0.50%
10 Cylinder	243795	180.0	18756	36824	104.0	0.85%			
							0.234	1062.0/150.0	0.50%
11 Cylinder	243795	300.0	18756	36824	104.0	0.85%			
							0.227	1062.0/150.0	0.50%
12 Cylinder	243795	60.0	18756	36824	104.0	0.85%			
							0.158	1061.0/150.0	0.50%
30 Thrst B/Ch driv				10600	104.0	0.00%			
							0.106	1062.0/150.0	0
32 Turning Wheel				20398	104.0	0.50%			
							3.251	805.0/ 0.0	0
43 Flange				4214	104.0	0.00%			
							3.274	805.0/ 0.0	0
44 Flange				4528	104.0	0.00%			
							3.781	805.0/ 0.0	0
45 Flange				6689	104.0	0.00%			

12K98ME-C7, Mark VII,   Hyundai Heavy Industrires
MCR 72240 kW @ 104 r/min   1992

Mass ID/Description	Tang. harmon ID	Firing angle (deg)	Osc. mass (kg)	Mom. of inertia (kgm^2)	Rot. speed (r/min)	Mass damping (Nms or %)	Tors. flex. (nrad/Nm)	Diameters outer/inner (mm)	Relative damping (Nms or %)
							1.657	980.0/ 0.0	0
73 Main Propeller				540142	104.0	170.02% FLAT			

END OF MAIN SHAFT

PROPELLER DAMPING <-> RPM DEPENDENCY

ID   73 FLAT
rho= 5.5%
F1=170.02 cpm (estimated)

Speed (r/min)	Physical damping (kNms	, %critical)
10	1058	5.5
20	1058	5.5
30	1058	5.5
40	1058	5.5
50	1058	5.5
60	1058	5.5
70	1058	5.5
80	1058	5.5
90	1058	5.5
100	1058	5.5
110	1058	5.5

12K98ME-C7, Mark VII,
MCR 72240 kW @ 104 r/min
Bore 980 mm
Stroke 2400 mm
Conn rod 3090 mm
Osc mass 18756 kg
Firing order 1 8 12 4 2 9 10 5 3 7 11 6

ENGINE LOAD :	kW	r/min
Propeller	72240	104

Gas harmonic components : 243795

Hyundai Heavy Industrires
1992

NORMAL FIRING, PROPELLER DAMPING 5.5% FLAT
Excitation: T243795

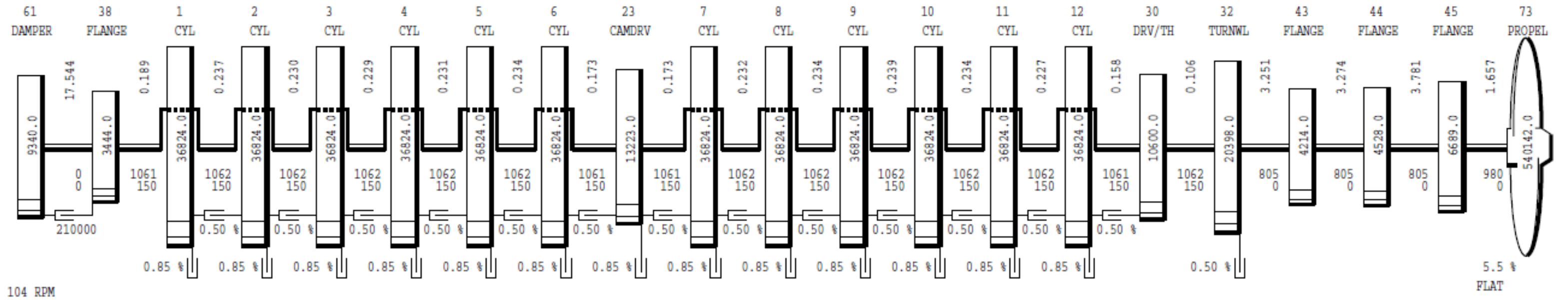

Units: Inertia kgm2
Diameter mm
Flexibility nanorad/Nm
Damping Nms/rad or % of critical

CALCULATION MODEL FOR TORSIONAL VIBRATIONS

MAN Energy Solutions
GTORSI 3.6.4/WIN32
8 Aug 2024 09:45:49
Page 3

MAN Energy Solutions GTORSI 3.6.4/WIN32 Faculty of Maritime S	TORSIONAL VIBRATION CALCULATION Hyundai Heavy Industrires	Page 4 8 Aug 2024 09:45:49
12K98ME-C7, Mark VII,	MCR 72240 kW @ 104 r/min	1992

NORMAL FIRING, PROPELLER DAMPING 5.5% FLAT
Excitation: T243795

ENGINE LOAD :	kW	r/min
Propeller	72240	104

Gas harmonic components : 243795

COMBUSTION CONDITION :
Normal

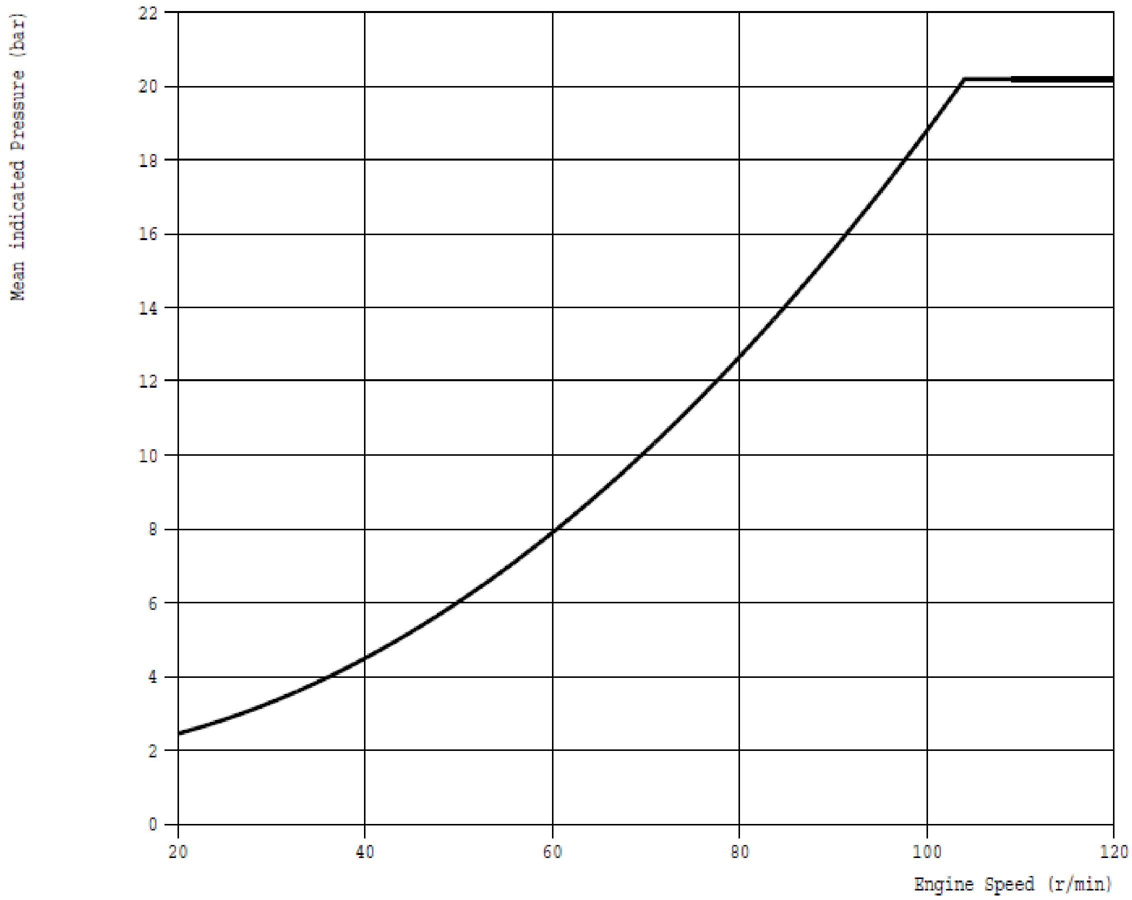

MAN Energy Solutions GTORSI 3.6.4/WIN32 Faculty of Maritime S	TORSIONAL VIBRATION CALCULATION Hyundai Heavy Industrires	Page 5 8 Aug 2024 09:45:49

12K98ME-C7, Mark VII,	MCR 72240 kW @ 104 r/min	1992

	NORMAL FIRING, PROPELLER DAMPING 5.5% FLAT Excitation: T243795
ENGINE LOAD : kW r/min Propeller 72240 104 Gas harmonic components : 243795	COMBUSTION CONDITION : Normal

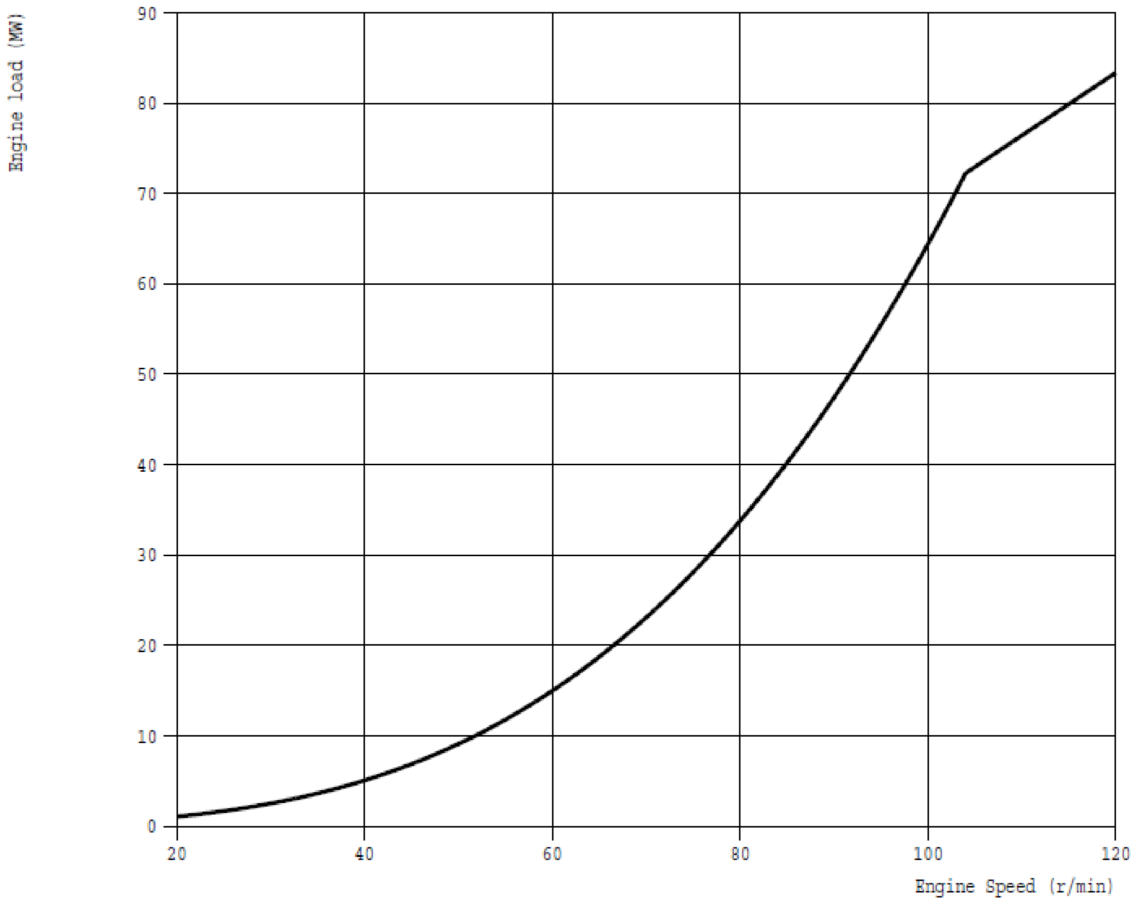

12K98ME-C7, Mark VII, Hyundai Heavy Industrires
MCR 72240 kW @ 104 r/min 1992

Modal form no. 1, Cyclic frequency = 17.178 rad/s , = 2.734 Hz , = 164.04 CPM

ID no	Mass name	Angular deflection (rad)	Shaft torque (kNm)	Torsional stress (MPa)	Kinetic energy (kNm)	Strain energy (kNm)	Damping loss per cycle external (kNm)	internal (kNm)
61	Damper	1.0516E+00			1.5239E+03		0.0000E+00	
38	Flange	1.0007E+00	-2.8983E+03	NaN	5.0890E+02	7.3686E+01	0.0000E+00	2.9301E+01
1	Cylinder	1.0000E+00	-3.9153E+03	-1.6702E+01	5.4332E+03	1.4487E+00	5.8034E+02	0.0000E+00
2	Cylinder	9.9650E-01	-1.4782E+04	-6.2877E+01	5.3952E+03	2.5892E+01	5.7628E+02	1.6268E+00
3	Cylinder	9.9061E-01	-2.5610E+04	-1.0894E+02	5.3316E+03	7.5425E+01	5.6949E+02	4.7391E+00
4	Cylinder	9.8228E-01	-3.6374E+04	-1.5473E+02	5.2423E+03	1.5149E+02	5.5995E+02	9.5186E+00
5	Cylinder	9.7141E-01	-4.7048E+04	-2.0013E+02	5.1269E+03	2.5566E+02	5.4763E+02	1.6064E+01
6	Cylinder	9.5793E-01	-5.7604E+04	-2.4503E+02	4.9856E+03	3.8823E+02	5.3254E+02	2.4393E+01
23	Camshaft Drive	9.4616E-01	-6.8013E+04	-2.9013E+02	1.7466E+03	4.0013E+02	1.8656E+02	2.5141E+01
7	Cylinder	9.3376E-01	-7.1705E+04	-3.0588E+02	4.7372E+03	4.4475E+02	5.0600E+02	2.7944E+01
8	Cylinder	9.1477E-01	-8.1851E+04	-3.4817E+02	4.5465E+03	7.7716E+02	4.8563E+02	4.8830E+01
9	Cylinder	8.9329E-01	-9.1792E+04	-3.9046E+02	4.3355E+03	9.8581E+02	4.6309E+02	6.1940E+01
10	Cylinder	8.6903E-01	-1.0150E+05	-4.3175E+02	4.1032E+03	1.2311E+03	4.3828E+02	7.7351E+01
11	Cylinder	8.4307E-01	-1.1094E+05	-4.7191E+02	3.8617E+03	1.4400E+03	4.1249E+02	9.0480E+01
12	Cylinder	8.1581E-01	-1.2010E+05	-5.1088E+02	3.6160E+03	1.6372E+03	3.8624E+02	1.0287E+02
30	Thrst B/Ch driv	7.9543E-01	-1.2897E+05	-5.5015E+02	9.8954E+02	1.3140E+03	0.0000E+00	8.2560E+01
32	Turning Wheel	7.8150E-01	-1.3146E+05	-5.5918E+02	1.8381E+03	9.1587E+02	1.1549E+02	0.0000E+00
43	Flange	3.3886E-01	-1.3616E+05	-1.3293E+03	7.1392E+01	3.0135E+04	0.0000E+00	0.0000E+00
44	Flange	-1.0837E-01	-1.3658E+05	-1.3334E+03	7.8453E+00	3.0541E+04	0.0000E+00	0.0000E+00
45	Flange	-6.2419E-01	-1.3644E+05	-1.3320E+03	3.8452E+02	3.5189E+04	0.0000E+00	0.0000E+00
73	Main Propeller	-8.4826E-01	-1.3520E+05	-7.3161E+02	5.7344E+04	1.5148E+04	0.0388*Cprop	0.0000E+00
				Total :	1.2113E+05	1.2113E+05	6.9628E+03 + prop.	(ext.+int.)

Resonances with vibration mode no. 1, natural frequency 164.04 c/min in the revolution range 26 - 130 r/min

Order	Critical speed (r/min)	Modal damping (%)	Vector sum	Indicated pressure (bar)	Harmonic components Total (bar)	Mass (bar)	Static amplitude cyl. 1 (mrad)
1	164.0	3.1562	0.0403	20.1850	27.8837	11.3352	0.4200
2	82.0	3.1562	0.0020	13.2226	0.5700	-10.5318	0.0004
3	54.7	3.1562	0.4896	6.8586	1.6796	-3.0259	0.3072
4	41.0	3.1562	0.1104	4.6312	2.4549	-0.2345	0.1013
5	32.8	3.1562	0.0406	3.6002	1.7375	0.0374	0.0263
6	27.3	3.1562	0.1384	3.0402	1.0447	0.0064	0.0540
7	23.4	3.1562	0.0406	2.7025	0.6707	-0.0008	0.0102

12K98ME-C7, Mark VII, Hyundai Heavy Industrires
MCR 72240 kW @ 104 r/min 1992

Modal form no. 2, Cyclic frequency = 72.386 rad/s , = 11.521 Hz , = 691.24 CPM

ID no	Mass name	Angular deflection (rad)	Shaft torque (kNm)	Torsional stress (MPa)	Kinetic energy (kNm)	Strain energy (kNm)	Damping loss per cycle external (kNm)	internal (kNm)
61	Damper	7.5937E+00			1.4110E+06		0.0000E+00	
38	Flange	1.0739E+00	-3.7163E+05	NaN	1.0406E+04	1.2115E+06	0.0000E+00	2.0300E+06
1	Cylinder	1.0000E+00	-3.9101E+05	-1.6680E+03	9.6474E+04	1.4448E+04	1.0305E+04	0.0000E+00
2	Cylinder	8.6160E-01	-5.8396E+05	-2.4840E+03	7.1618E+04	4.0409E+04	7.6498E+03	2.5390E+03
3	Cylinder	6.8906E-01	-7.5020E+05	-3.1911E+03	4.5806E+04	6.4722E+04	4.8927E+03	4.0666E+03
4	Cylinder	4.8681E-01	-8.8315E+05	-3.7567E+03	2.2863E+04	8.9305E+04	2.4421E+03	5.6112E+03
5	Cylinder	2.6111E-01	-9.7708E+05	-4.1562E+03	6.5773E+03	1.1027E+05	7.0255E+02	6.9283E+03
6	Cylinder	2.0682E-02	-1.0275E+06	-4.3705E+03	4.1265E+01	1.2351E+05	4.4077E+00	7.7606E+03
23	Camshaft Drive	-1.5776E-01	-1.0315E+06	-4.3999E+03	8.6219E+02	9.2027E+04	9.2094E+01	5.7822E+03
7	Cylinder	-3.3431E-01	-1.0205E+06	-4.3533E+03	1.0782E+04	9.0087E+04	1.1517E+03	5.6603E+03
8	Cylinder	-5.5611E-01	-9.5602E+05	-4.0666E+03	2.9835E+04	1.0602E+05	3.1868E+03	6.6615E+03
9	Cylinder	-7.5471E-01	-8.4872E+05	-3.6102E+03	5.4950E+04	8.4278E+04	5.8694E+03	5.2953E+03
10	Cylinder	-9.2275E-01	-7.0310E+05	-2.9908E+03	8.2144E+04	5.9075E+04	8.7741E+03	3.7118E+03
11	Cylinder	-1.0456E+00	-5.2506E+05	-2.2335E+03	1.0548E+05	3.2255E+04	1.1266E+04	2.0267E+03
12	Cylinder	-1.1190E+00	-3.2331E+05	-1.3753E+03	1.2080E+05	1.1864E+04	1.2903E+04	7.4544E+02
30	Thrst B/Ch driv	-1.1360E+00	-1.0740E+05	-4.5814E+02	3.5836E+04	9.1125E+02	0.0000E+00	5.7256E+01
32	Turning Wheel	-1.1407E+00	-4.4307E+04	-1.8847E+02	6.9532E+04	1.0405E+02	4.3688E+03	0.0000E+00
43	Flange	-8.8837E-01	7.7608E+04	7.5768E+02	8.7129E+03	9.7900E+03	0.0000E+00	0.0000E+00
44	Flange	-5.7003E-01	9.7223E+04	9.4919E+02	3.8546E+03	1.5475E+04	0.0000E+00	0.0000E+00
45	Flange	-1.5132E-01	1.1075E+05	1.0812E+03	4.0129E+02	2.3185E+04	0.0000E+00	0.0000E+00
73	Main Propeller	4.1005E-02	1.1605E+05	6.2797E+02	2.3793E+03	1.1160E+04	0.0004*Cprop	0.0000E+00
				Total :	2.1904E+06	2.1904E+06	2.1604E+06 + prop.	(ext.+int.)

Resonances with vibration mode no. 2, natural frequency 691.24 c/min in the revolution range 26 - 130 r/min

Order	Critical speed (r/min)	Modal damping (%)	Vector sum	Indicated pressure (bar)	Harmonic components Total (bar)	Mass (bar)	Static amplitude cyl. 1 (mrad)
5	138.2	7.8505	0.1183	20.1850	6.7053	0.6648	0.0164
6	115.2	7.8505	0.3398	20.1850	3.7488	0.1088	0.0263
7	98.7	7.8505	0.1183	18.3717	2.1231	-0.0146	0.0052
8	86.4	7.8505	1.2071	14.4801	1.0518	-0.0033	0.0262
9	76.8	7.8505	6.1330	11.8120	0.4697	0.0004	0.0595
10	69.1	7.8505	0.3285	9.9035	0.2527	0.0001	0.0017
11	62.8	7.8505	0.1144	8.4915	0.2012	0.0000	0.0005
12	57.6	7.8505	1.4132	7.4175	0.1344	0.0000	0.0039
13	53.2	7.8505	0.1144	6.5817	0.0840	0.0000	0.0002
14	49.4	7.8505	0.3285	5.9185	0.0765	0.0000	0.0005
15	46.1	7.8505	6.1330	5.3835	0.0692	0.0000	0.0088
16	43.2	7.8505	1.2071	4.9456	0.0554	0.0000	0.0014
17	40.7	7.8505	0.1183	4.5827	0.0494	0.0000	0.0001
18	38.4	7.8505	0.3398	4.2785	0.0435	0.0000	0.0003
19	36.4	7.8505	0.1183	4.0212	0.0359	0.0000	0.0001
20	34.6	7.8505	1.2071	3.8014	0.0320	0.0000	0.0008

MAN Energy Solutions T O R S I O N A L   V I B R A T I O N   C A L C U L A T I O N Page 8
GTORSI 3.6.4/WIN32 U N D A M P E D   N A T U R A L   F R E Q U E N C I E S 8 Aug 2024
Faculty of Maritime S 09:45:49
Calculations made by anonymous user

12K98ME-C7, Mark VII, Hyundai Heavy Industrires
MCR 72240 kW @ 104 r/min 1992

Modal form no. 3, Cyclic frequency = 87.349 rad/s , = 13.902 Hz , = 834.12 CPM

ID no	Mass name	Angular deflection (rad)	Shaft torque (kNm)	Torsional stress (MPa)	Kinetic energy (kNm)	Strain energy (kNm)	Damping loss per cycle external (kNm)	internal (kNm)
61	Damper	-3.8101E+00			5.1726E+05		0.0000E+00	
38	Flange	9.5342E-01	2.7152E+05	NaN	1.1943E+04	6.4670E+05	0.0000E+00	1.3076E+06
1	Cylinder	1.0000E+00	2.4647E+05	1.0514E+03	1.4048E+05	5.7405E+03	1.5005E+04	0.0000E+00
2	Cylinder	9.9182E-01	-3.4497E+04	-1.4674E+02	1.3819E+05	1.4102E+02	1.4761E+04	8.8604E+00
3	Cylinder	9.1980E-01	-3.1316E+05	-1.3321E+03	1.1885E+05	1.1278E+04	1.2695E+04	7.0863E+02
4	Cylinder	7.8890E-01	-5.7159E+05	-2.4314E+03	8.7431E+04	3.7409E+04	9.3389E+03	2.3505E+03
5	Cylinder	6.0566E-01	-7.9325E+05	-3.3742E+03	5.1532E+04	7.2677E+04	5.5044E+03	4.5664E+03
6	Cylinder	3.8022E-01	-9.6341E+05	-4.0981E+03	2.0309E+04	1.0860E+05	2.1693E+03	6.8233E+03
23	Camshaft Drive	1.9507E-01	-1.0702E+06	-4.5654E+03	1.9196E+03	9.9079E+04	2.0504E+02	6.2253E+03
7	Cylinder	6.5139E-03	-1.0899E+06	-4.6494E+03	5.9607E+00	1.0276E+05	6.3669E-01	6.4564E+03
8	Cylinder	-2.4677E-01	-1.0918E+06	-4.6440E+03	8.5549E+03	1.3826E+05	9.1379E+02	8.6874E+03
9	Cylinder	-4.8602E-01	-1.0224E+06	-4.3491E+03	3.3184E+04	1.2231E+05	3.5445E+03	7.6847E+03
10	Cylinder	-6.9774E-01	-8.8587E+05	-3.7682E+03	6.8393E+04	9.3779E+04	7.3053E+03	5.8923E+03
11	Cylinder	-8.5916E-01	-6.8983E+05	-2.9343E+03	1.0370E+05	5.5676E+04	1.1076E+04	3.4982E+03
12	Cylinder	-9.6096E-01	-4.4843E+05	-1.9075E+03	1.2973E+05	2.2824E+04	1.3857E+04	1.4341E+03
30	Thrst B/Ch driv	-9.8915E-01	-1.7844E+05	-7.6118E+02	3.9566E+04	2.5154E+03	0.0000E+00	1.5805E+02
32	Turning Wheel	-9.9958E-01	-9.8440E+04	-4.1874E+02	7.7753E+04	5.1359E+02	4.8853E+03	0.0000E+00
43	Flange	-8.1386E-01	5.7130E+04	5.5776E+02	1.0648E+04	5.3052E+03	0.0000E+00	0.0000E+00
44	Flange	-5.4111E-01	8.3298E+04	8.1323E+02	5.0579E+03	1.1360E+04	0.0000E+00	0.0000E+00
45	Flange	-1.5551E-01	1.0199E+05	9.9575E+02	6.1711E+02	1.9664E+04	0.0000E+00	0.0000E+00
73	Main Propeller	2.6674E-02	1.0993E+05	5.9484E+02	1.4661E+03	1.0014E+04	0.0002*Cprop	0.0000E+00
				Total :	1.5666E+06	1.5666E+06	1.4634E+06 + prop.	(ext.+int.)

Resonances with vibration mode no. 3, natural frequency 834.12 c/min in the revolution range 26 - 130 r/min

Order	Critical speed (r/min)	Modal damping (%)	Vector sum	Indicated pressure (bar)	Harmonic components Total (bar)	Mass (bar)	Static amplitude cyl. 1 (mrad)
6	139.0	7.4345	0.6547	20.1850	3.7894	0.1583	0.0717
7	119.2	7.4345	0.1872	20.1850	2.3114	-0.0213	0.0125
8	104.3	7.4345	1.0780	20.1850	1.4391	-0.0049	0.0448
9	92.7	7.4345	5.9778	16.3940	0.6049	0.0006	0.1045
10	83.4	7.4345	0.4832	13.6149	0.2884	0.0002	0.0040
11	75.8	7.4345	0.1869	11.5587	0.2243	0.0000	0.0012
12	69.5	7.4345	1.4423	9.9949	0.1789	0.0000	0.0075
13	64.2	7.4345	0.1869	8.7778	0.1288	0.0000	0.0007
14	59.6	7.4345	0.4832	7.8121	0.1131	0.0000	0.0016
15	55.6	7.4345	5.9778	7.0330	0.0983	0.0000	0.0170
16	52.1	7.4345	1.0780	6.3953	0.0764	0.0000	0.0024
17	49.1	7.4345	0.1872	5.8669	0.0661	0.0000	0.0004
18	46.3	7.4345	0.6547	5.4240	0.0566	0.0000	0.0011
19	43.9	7.4345	0.1872	5.0493	0.0463	0.0000	0.0003
20	41.7	7.4345	1.0780	4.7293	0.0401	0.0000	0.0012

MAN Energy Solutions GTORSI 3.6.4/WIN32 Faculty of Maritime S	TORSIONAL VIBRATION CALCULATION Hyundai Heavy Industrires	Page 9 8 Aug 2024 09:45:49
12K98ME-C7, Mark VII,	MCR 72240 kW @ 104 r/min	1992

Normal modes no. 1- 3 of main branch

Mode no 1, 164.04 cpm

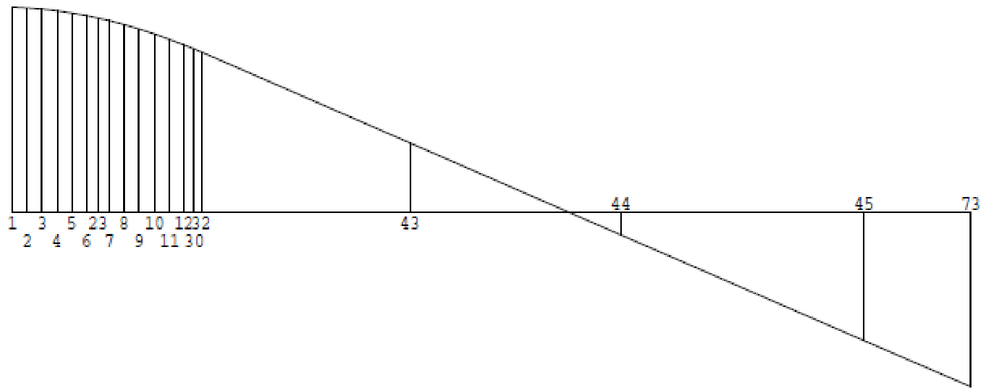

Mode no 2, 691.24 cpm

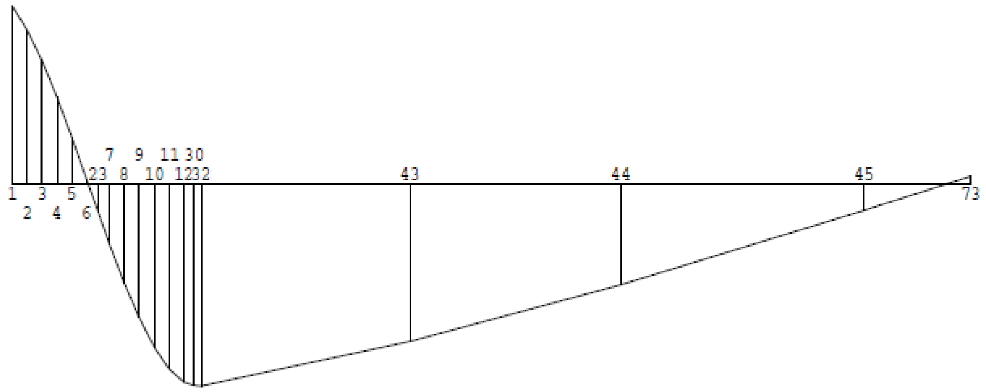

Mode no 3, 834.13 cpm

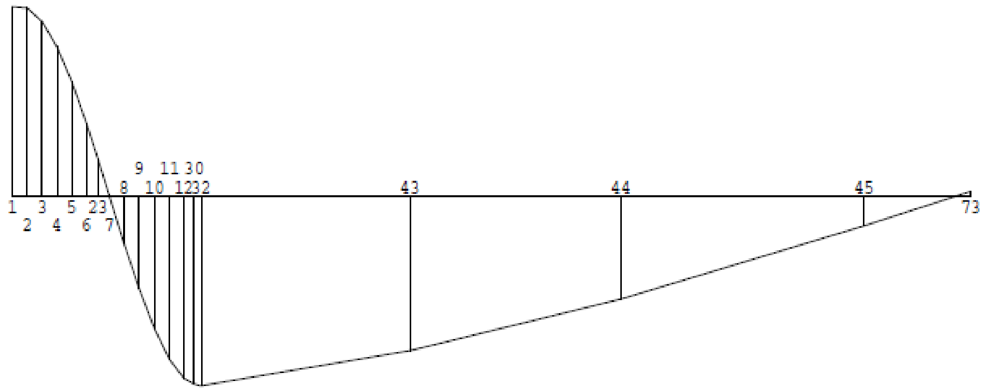

MAN Energy Solutions GTORSI 3.6.4/WIN32 Faculty of Maritime S	TORSIONAL VIBRATION CALCULATION Hyundai Heavy Industrires	Page 10 8 Aug 2024 09:45:49
12K98ME-C7, Mark VII,	MCR 72240 kW @ 104 r/min	1992

	NORMAL FIRING, PROPELLER DAMPING 5.5% FLAT Excitation: T243795
ENGINE LOAD : kW r/min Propeller 72240 104 Gas harmonic components : 243795	COMBUSTION CONDITION : Normal

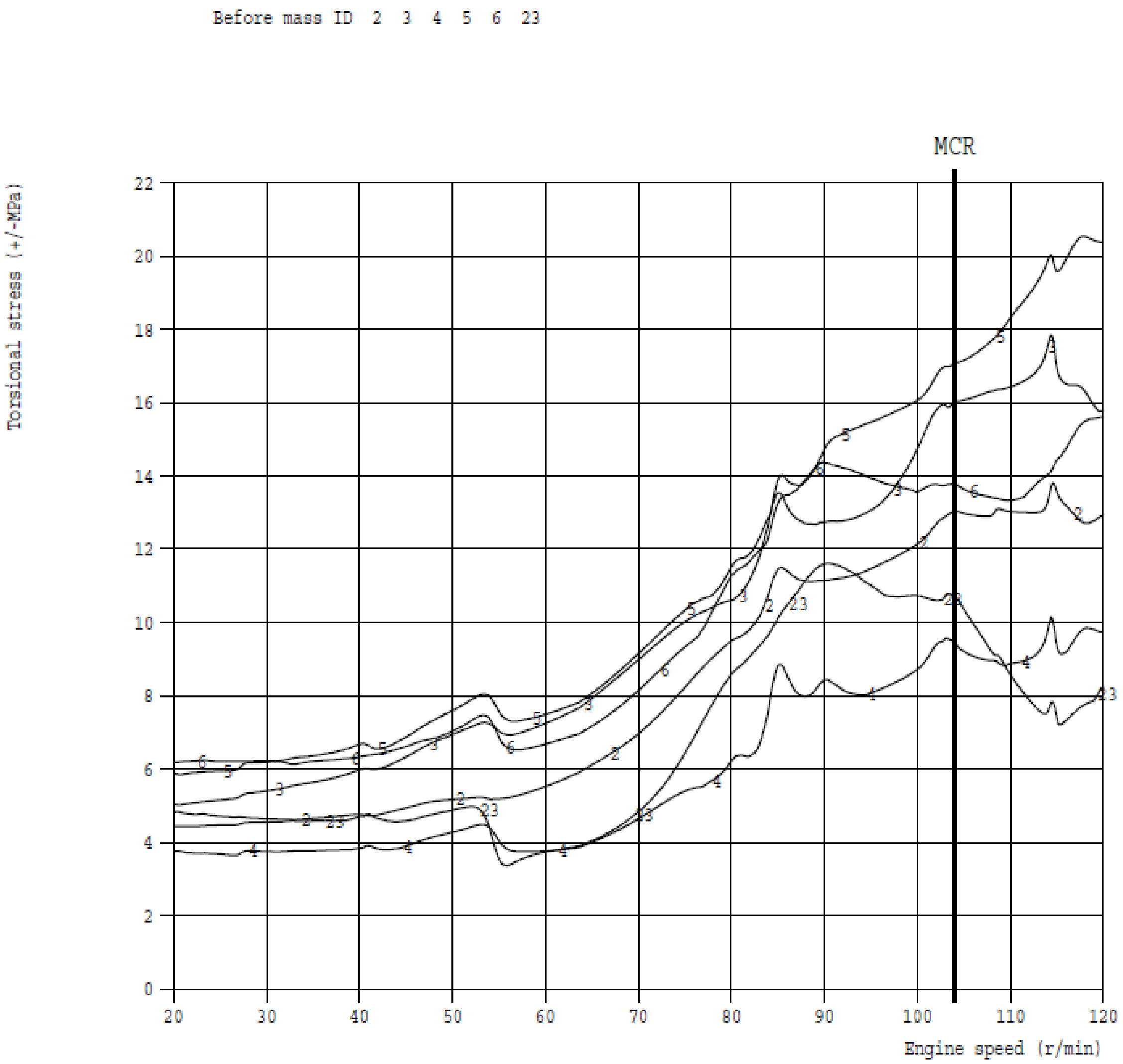

MAN Energy Solutions GTORSI 3.6.4/WIN32 Faculty of Maritime S	TORSIONAL VIBRATION CALCULATION Hyundai Heavy Industrires	Page 11 8 Aug 2024 09:45:49
12K98ME-C7, Mark VII,	MCR 72240 kW @ 104 r/min	1992

NORMAL FIRING, PROPELLER DAMPING 5.5% FLAT
Excitation: T243795

ENGINE LOAD : kW r/min
Propeller 72240 104

Gas harmonic components : 243795

COMBUSTION CONDITION :
Normal

Before mass ID 8 9 10 11 12 30

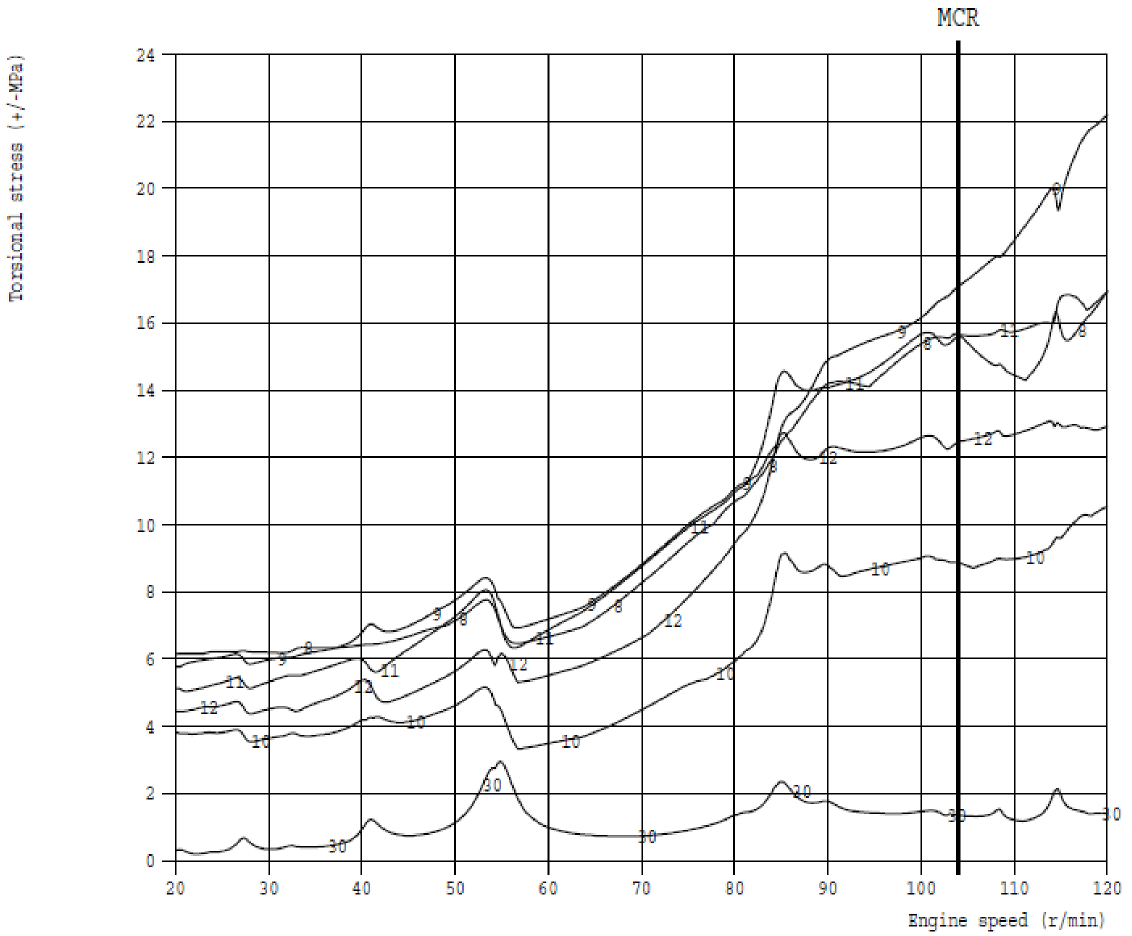

MAN Energy Solutions GTORSI 3.6.4/WIN32 Faculty of Maritime S	TORSIONAL VIBRATION CALCULATION Hyundai Heavy Industrires	Page 12 8 Aug 2024 09:45:49

12K98ME-C7, Mark VII,	MCR 72240 kW @ 104 r/min	1992

	NORMAL FIRING, PROPELLER DAMPING 5.5% FLAT Excitation: T243795
ENGINE LOAD : kW r/min Propeller 72240 104 Gas harmonic components : 243795	COMBUSTION CONDITION : Normal

CRANK_5 before mass ID 5 Cylinder

Order 1 2 3 4 5 6 8 9 18

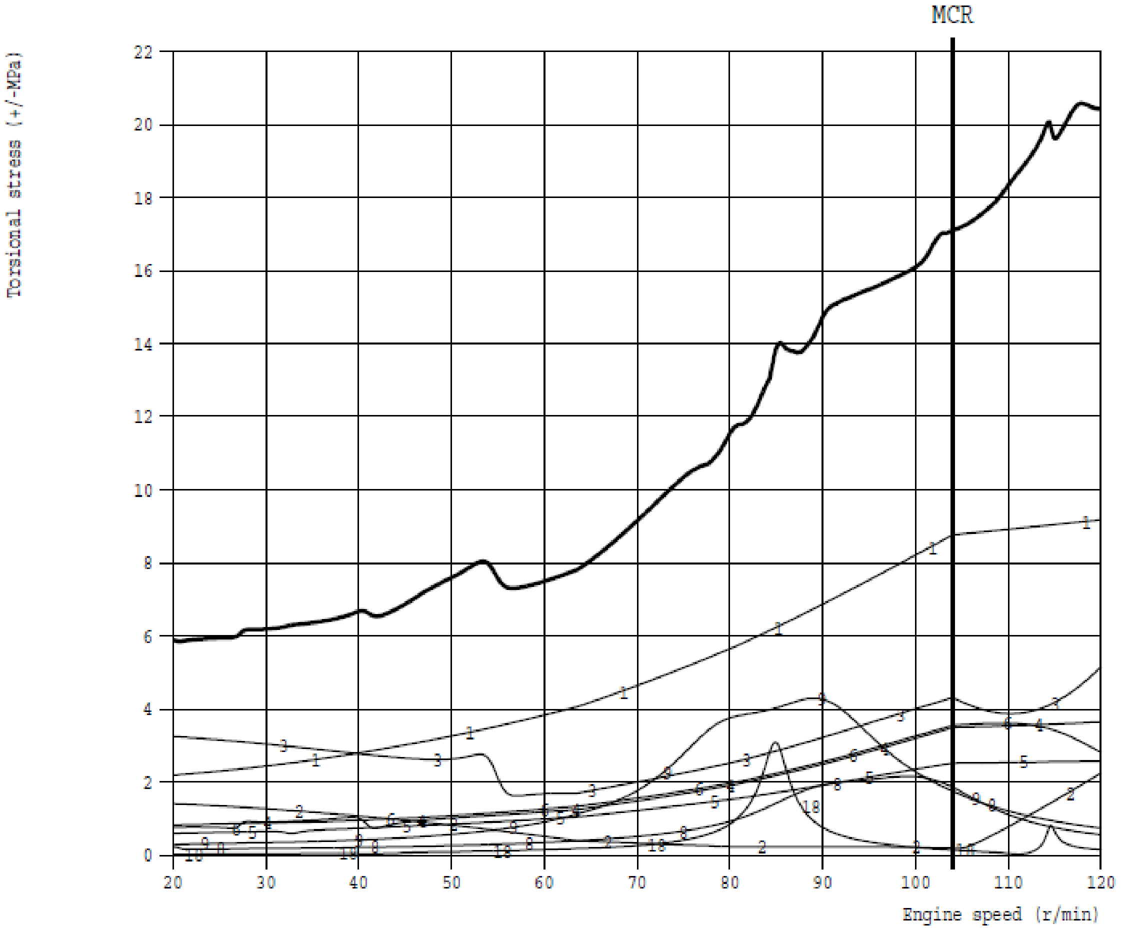

MAN Energy Solutions GTORSI 3.6.4/WIN32 Faculty of Maritime S	TORSIONAL VIBRATION CALCULATION Hyundai Heavy Industrires	Page 13 8 Aug 2024 09:45:49
12K98ME-C7, Mark VII,	MCR 72240 kW @ 104 r/min	1992

NORMAL FIRING, PROPELLER DAMPING 5.5% FLAT
Excitation: T243795

ENGINE LOAD :	kW	r/min
Propeller	72240	104

Gas harmonic components : 243795

COMBUSTION CONDITION :
Normal

CRANK_9 before mass ID 9 Cylinder

Order 1 2 3 4 5 6 9 18

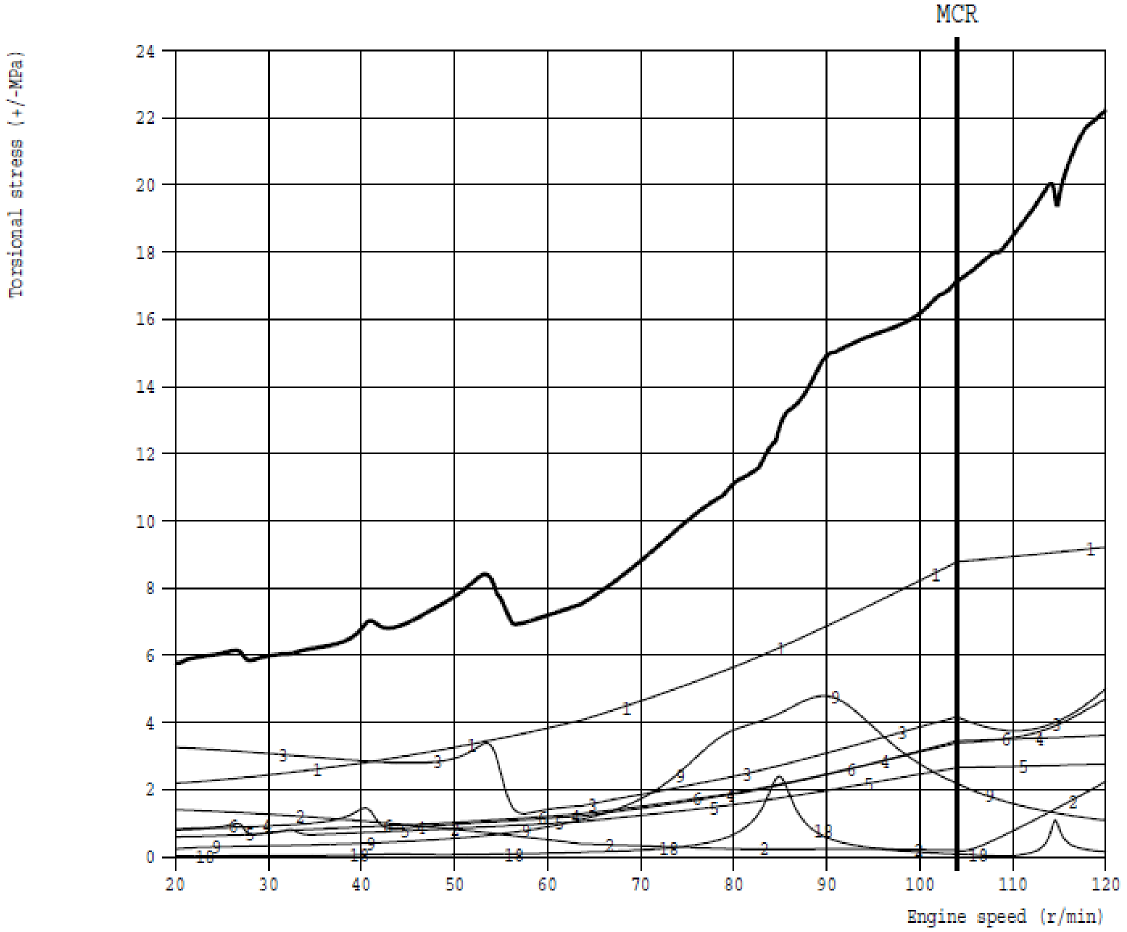

MAN Energy Solutions GTORSI 3.6.4/WIN32 Faculty of Maritime S	TORSIONAL VIBRATION CALCULATION Hyundai Heavy Industrires	Page 14 8 Aug 2024 09:45:49
12K98ME-C7, Mark VII,	MCR 72240 kW @ 104 r/min	1992

NORMAL FIRING, PROPELLER DAMPING 5.5% FLAT
Excitation: T243795

ENGINE LOAD : kW r/min
Propeller 72240 104

Gas harmonic components : 243795

COMBUSTION CONDITION :
Normal

FLANGE1 before mass ID 43 Flange

Order 3 4 6 9 18

Classification Society: IACS Rules

Dy= 805.0 mm Di= 0.0 mm SIGMAB= 800 MPa Ck= 1.00
Limits for synthesis:

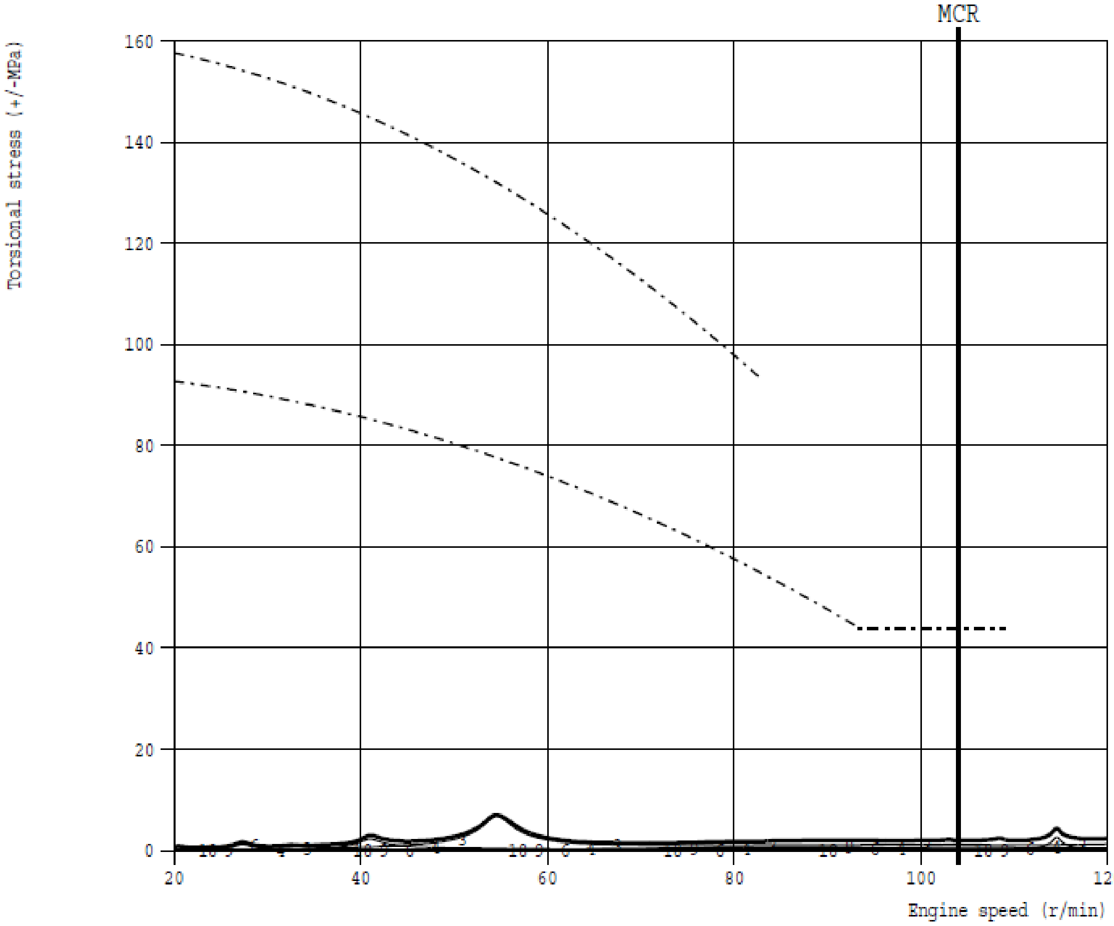

MAN Energy Solutions GTORSI 3.6.4/WIN32 Faculty of Maritime S	TORSIONAL VIBRATION CALCULATION Hyundai Heavy Industrires	Page 15 8 Aug 2024 09:45:49
12K98ME-C7, Mark VII,	MCR 72240 kW @ 104 r/min	1992

NORMAL FIRING, PROPELLER DAMPING 5.5% FLAT
Excitation: T243795

ENGINE LOAD : kW r/min
Propeller 72240 104

Gas harmonic components : 243795

COMBUSTION CONDITION :
Normal

PROPELLER before mass ID 73 Main Propeller

Order 3 4 6 9 18 19

Classification Society: IACS Rules

Dy= 980.0 mm Di= 0.0 mm SIGMAB= 600 MPa Ck= 0.55
Limits for synthesis:

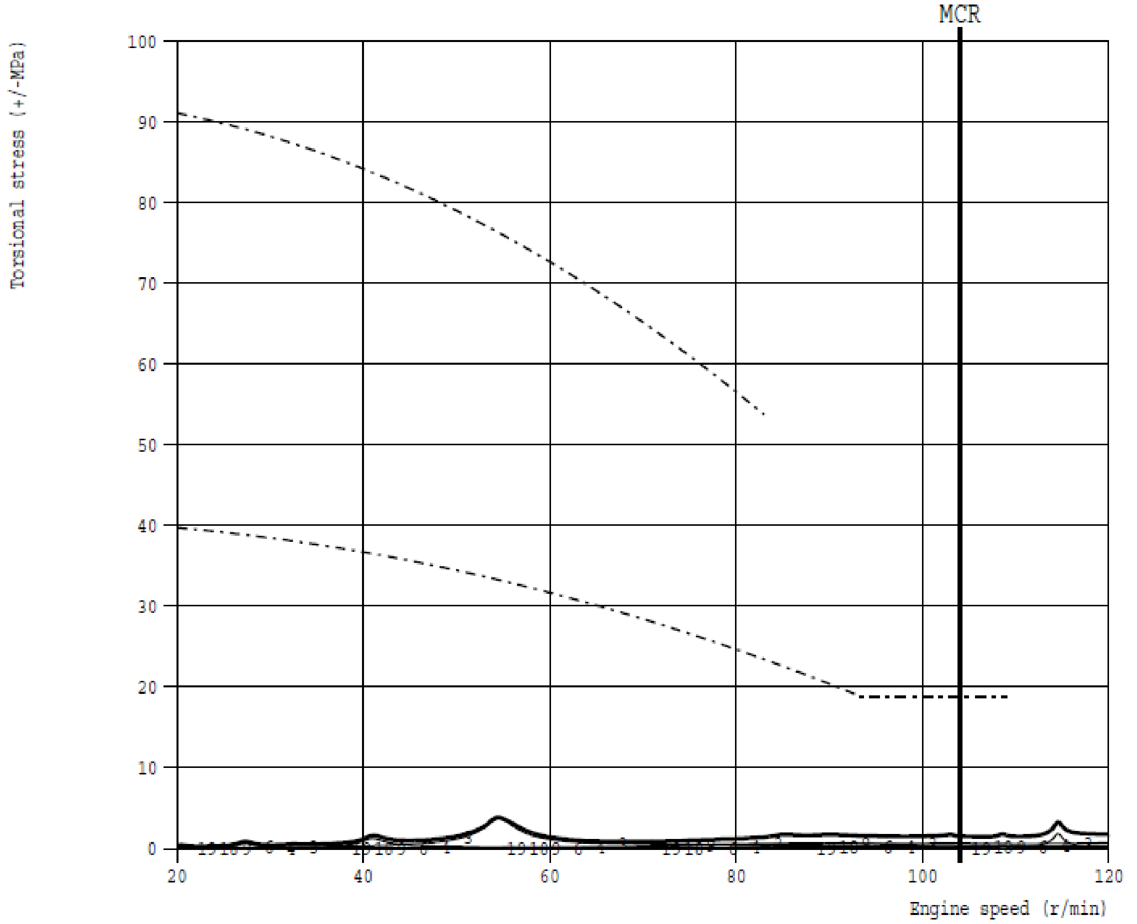

MAN Energy Solutions
GTORSI 3.6.4/WIN32
Faculty of Maritime S

TORSIONAL VIBRATION CALCULATION

Hyundai Heavy Industrires

Page 16
8 Aug 2024
09:45:49

12K98ME-C7, Mark VII,	MCR 72240 kW @ 104 r/min	1992

NORMAL FIRING, PROPELLER DAMPING 5.5% FLAT
Excitation: T243795

ENGINE LOAD : kW r/min
Propeller 72240 104

Gas harmonic components : 243795

COMBUSTION CONDITION :
Normal

D. INNER+FLG before mass ID 38 Flange

Order 6 8 9 15

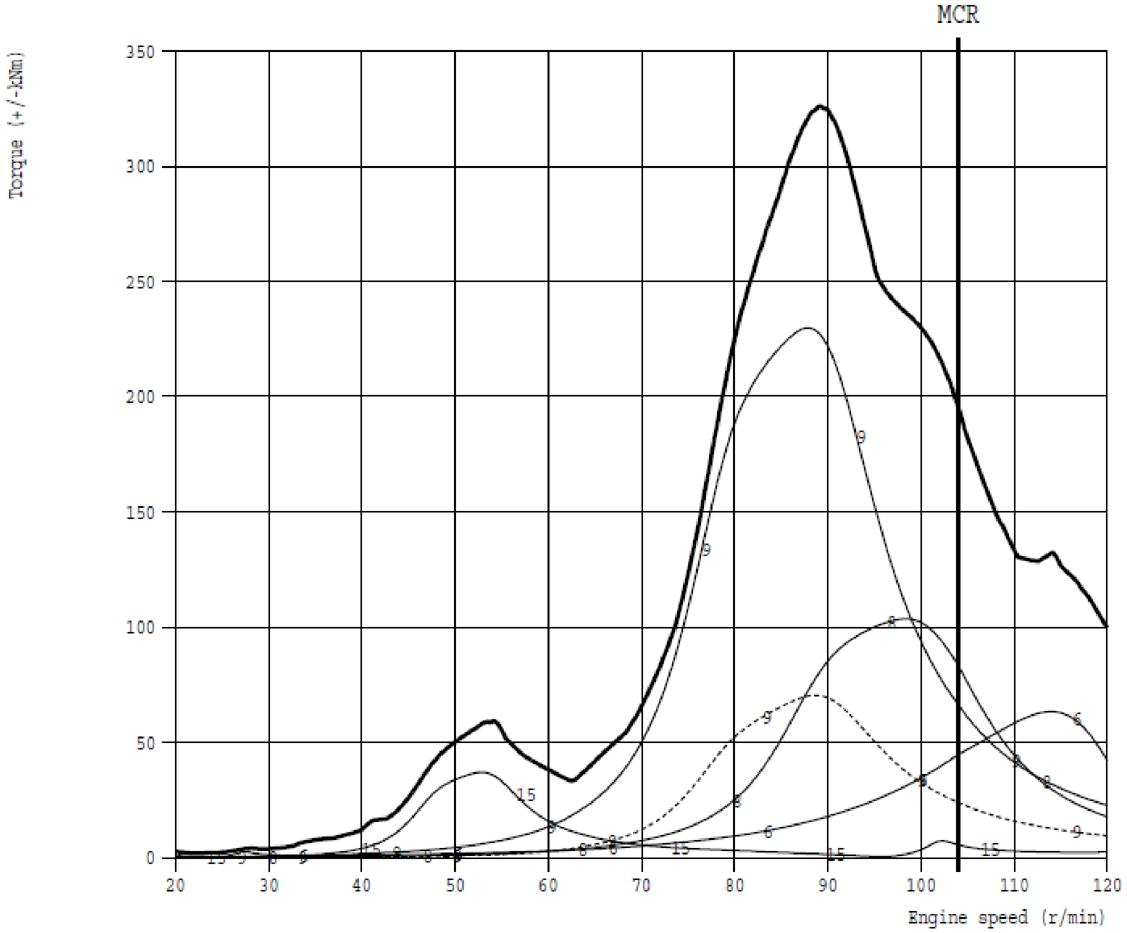

MAN Energy Solutions GTORSI 3.6.4/WIN32 Faculty of Maritime S	TORSIONAL VIBRATION CALCULATION Hyundai Heavy Industrires	Page 17 8 Aug 2024 09:45:49
12K98ME-C7, Mark VII,	MCR 72240 kW @ 104 r/min	1992

NORMAL FIRING, PROPELLER DAMPING 5.5% FLAT
Excitation: T243795

ENGINE LOAD :	kW	r/min
Propeller	72240	104

Gas harmonic components : 243795

COMBUSTION CONDITION :
Normal

D. INNER+FLG before mass ID 38 Flange

Order 8 9

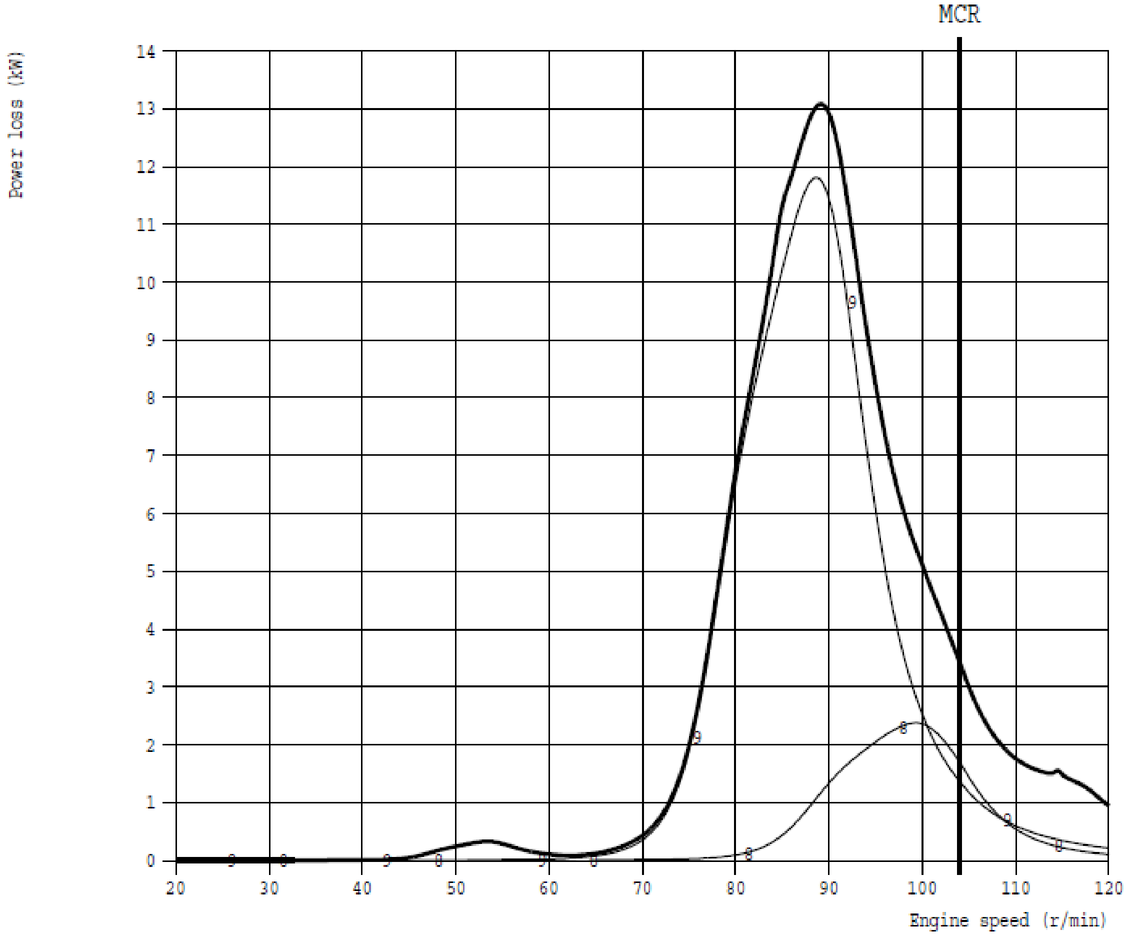

MAN Energy Solutions GTORSI 3.6.4/WIN32 Faculty of Maritime S	TORSIONAL VIBRATION CALCULATION Hyundai Heavy Industrires	Page 18 8 Aug 2024 09:45:49
12K98ME-C7, Mark VII,	MCR 72240 kW @ 104 r/min	1992

	NORMAL FIRING, PROPELLER DAMPING 5.5% FLAT Excitation: T243795
ENGINE LOAD : kW r/min Propeller 72240 104 Gas harmonic components : 243795	COMBUSTION CONDITION : Normal

Mass ID 1 Cylinder

Order 3 4 6 9

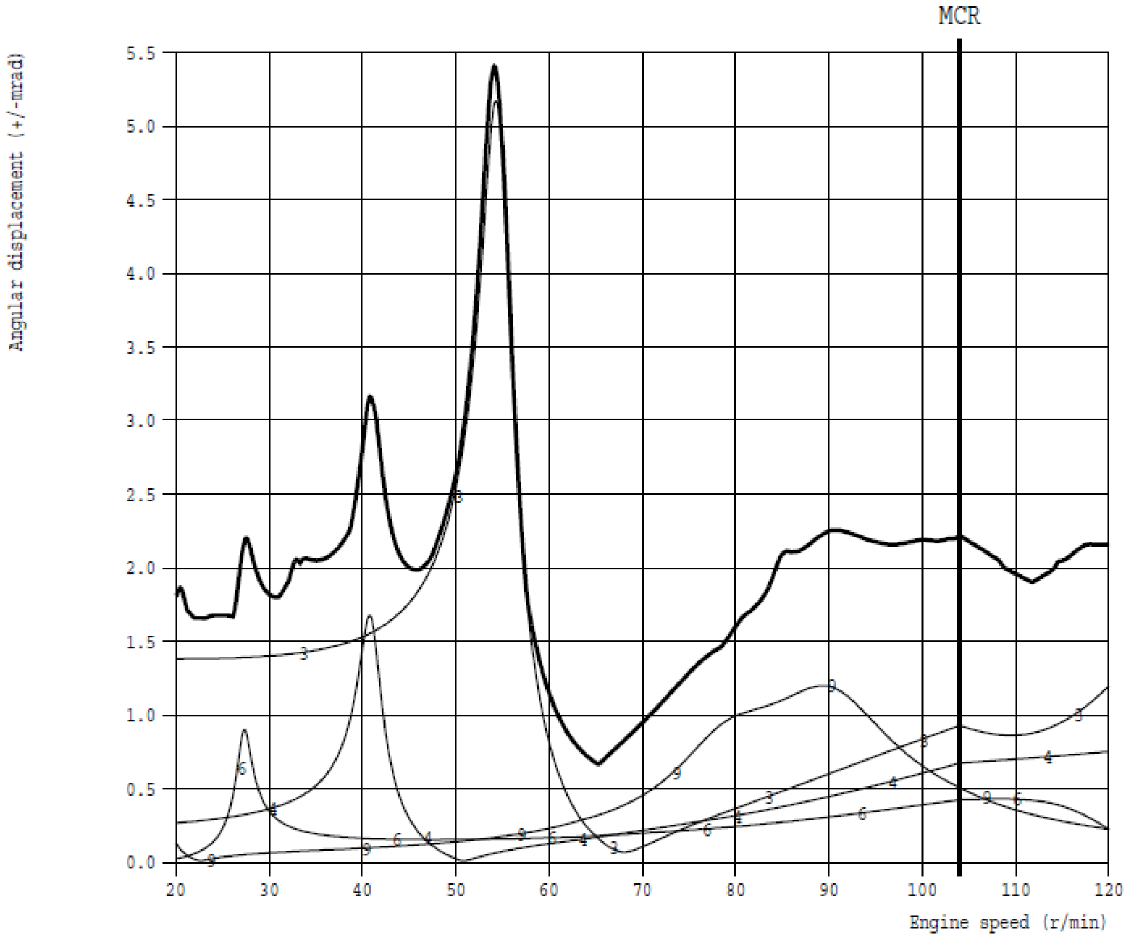

MAN Energy Solutions GTORSI 3.6.4/WIN32 Faculty of Maritime S	TORSIONAL VIBRATION CALCULATION Hyundai Heavy Industrires	Page 19 8 Aug 2024 09:45:49
12K98ME-C7, Mark VII,	MCR 72240 kW @ 104 r/min	1992

NORMAL FIRING, PROPELLER DAMPING 5.5% FLAT
Excitation: T243795

ENGINE LOAD :	kW	r/min
Propeller	72240	104

Gas harmonic components : 243795

COMBUSTION CONDITION :
Normal

Mass ID 73 Main Propeller

Order 1 3 4 6

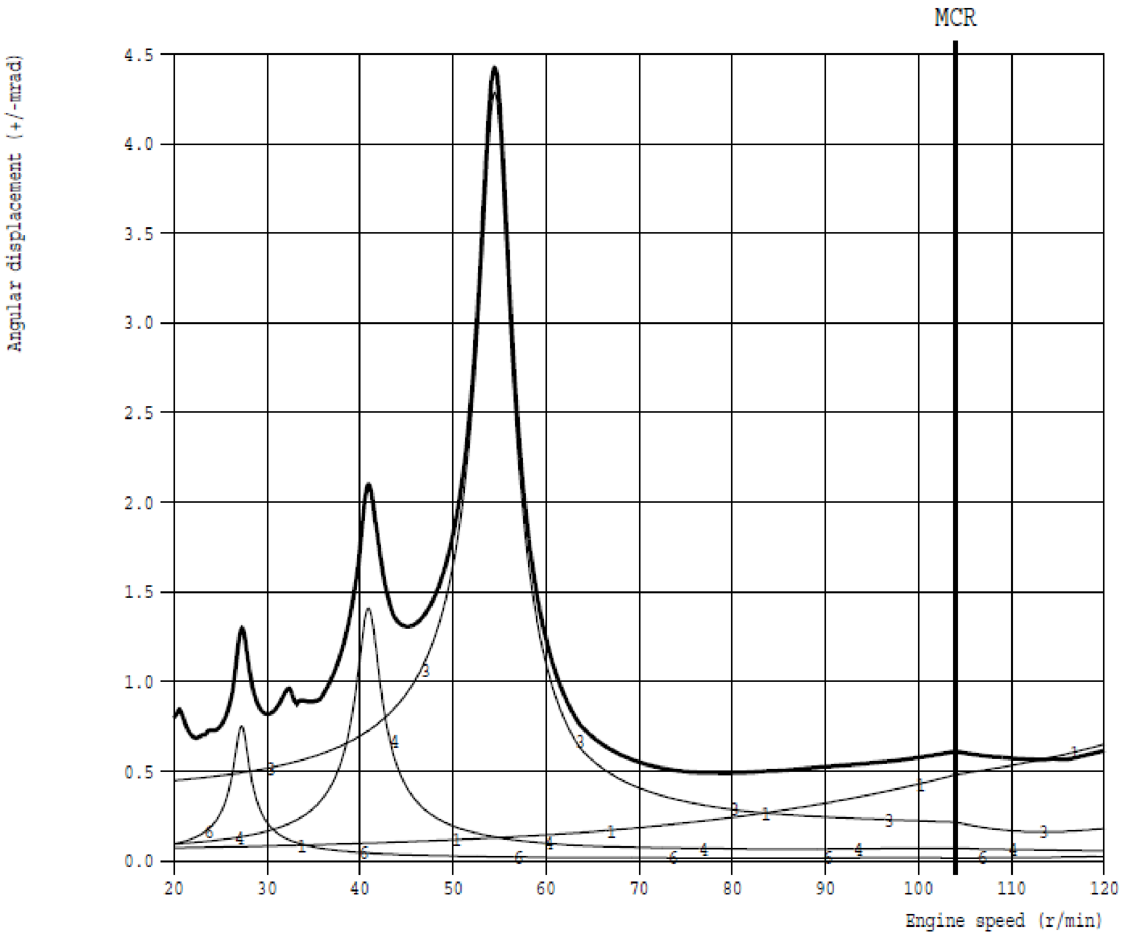

D.2. Misfiring condition

MAN Energy Solutions　　T O R S I O N A L　V I B R A T I O N　C A L C U L A T I O N　　Page 1
GTORSI 3.6.4/WIN32　　T A B L E　O F　I N F O R M A T I O N　　8 Aug 2024
Faculty of Maritime S　　09:50:31
Calculations made by anonymous user

12K98ME-C7, Mark VII,　　Hyundai Heavy Industrires
MCR 72240 kW @ 104 r/min　　1992

MISFIRING CYL 1, PROPELLER DAMPING 5.5% FLAT
Excitation: T243795

ENGINE LOAD : kW r/min
Propeller 72240 104

COMBUSTION CONDITION :
Misfiring cyl. 1

Gas harmonic components : 243795

Bore: 980　　Stroke: 2400　　Connecting rod: 3090　　R/L: 0.3883
Firing order: 1 8 12 4 2 9 10 5 3 7 11 6

Mass ID/Description	Tang. harmon ID	Firing angle (deg)	Osc. mass (kg)	Mom. of inertia (kgm^2)	Rot. speed (r/min)	Mass damping (Nms or %)	Tors. flex. (nrad/Nm)	Diameters outer/inner (mm)	Relative damping (Nms or %)
MAIN SHAFT									
61 Damper				9340	104.0	0.00%			
							17.544	0.0/ 0.0	210000
38 Flange				3444	104.0	0.00%			
							0.189	1061.0/150.0	0
1 Cylinder	243795	0.0	18756	36824	104.0	0.85%			
							0.237	1062.0/150.0	0.50%
2 Cylinder	243795	120.0	18756	36824	104.0	0.85%			
							0.230	1062.0/150.0	0.50%
3 Cylinder	243795	240.0	18756	36824	104.0	0.85%			
							0.229	1062.0/150.0	0.50%
4 Cylinder	243795	90.0	18756	36824	104.0	0.85%			
							0.231	1062.0/150.0	0.50%
5 Cylinder	243795	210.0	18756	36824	104.0	0.85%			
							0.234	1062.0/150.0	0.50%
6 Cylinder	243795	330.0	18756	36824	104.0	0.85%			
							0.173	1061.0/150.0	0.50%
23 Camshaft Drive				13223	104.0	0.85%			
							0.173	1061.0/150.0	0.50%
7 Cylinder	243795	270.0	18756	36824	104.0	0.85%			
							0.232	1062.0/150.0	0.50%
8 Cylinder	243795	30.0	18756	36824	104.0	0.85%			
							0.234	1062.0/150.0	0.50%
9 Cylinder	243795	150.0	18756	36824	104.0	0.85%			
							0.239	1062.0/150.0	0.50%
10 Cylinder	243795	180.0	18756	36824	104.0	0.85%			
							0.234	1062.0/150.0	0.50%
11 Cylinder	243795	300.0	18756	36824	104.0	0.85%			
							0.227	1062.0/150.0	0.50%
12 Cylinder	243795	60.0	18756	36824	104.0	0.85%			
							0.158	1061.0/150.0	0.50%
30 Thrst B/Ch driv				10600	104.0	0.00%			
							0.106	1062.0/150.0	0
32 Turning Wheel				20398	104.0	0.50%			
							3.251	805.0/ 0.0	0
43 Flange				4214	104.0	0.00%			
							3.274	805.0/ 0.0	0
44 Flange				4528	104.0	0.00%			
							3.781	805.0/ 0.0	0
45 Flange				6689	104.0	0.00%			

12K98ME-C7, Mark VII, Hyundai Heavy Industrires
MCR 72240 kW @ 104 r/min 1992

Mass ID/Description	Tang. harmon ID	Firing angle (deg)	Osc. mass (kg)	Mom. of inertia (kgm^2)	Rot. speed (r/min)	Mass damping (Nms or %)	Tors. flex. (nrad/Nm)	Diameters outer/inner (mm)	Relative damping (Nms or %)
							1.657	980.0/ 0.0	0
73 Main Propeller				540142	104.0	170.02% FLAT			

END OF MAIN SHAFT

PROPELLER DAMPING <-> RPM DEPENDENCY

ID 73 FLAT
rho= 5.5%
F1=170.02 cpm (estimated)

Speed (r/min)	Physical damping (kNms	, %critical)
10	1058	5.5
20	1058	5.5
30	1058	5.5
40	1058	5.5
50	1058	5.5
60	1058	5.5
70	1058	5.5
80	1058	5.5
90	1058	5.5
100	1058	5.5
110	1058	5.5

12K98ME-C7, Mark VII,
MCR 72240 kW @ 104 r/min
Bore 980 mm
Stroke 2400 mm
Conn rod 3090 mm
Osc mass 18756 kg
Firing order 1 8 12 4 2 9 10 5 3 7 11 6

ENGINE LOAD : kW r/min
Propeller 72240 104

Gas harmonic components : 243795

Hyundai Heavy Industrires

1992

MISFIRING CYL 1, PROPELLER DAMPING 5.5% FLAT
Excitation: T243795

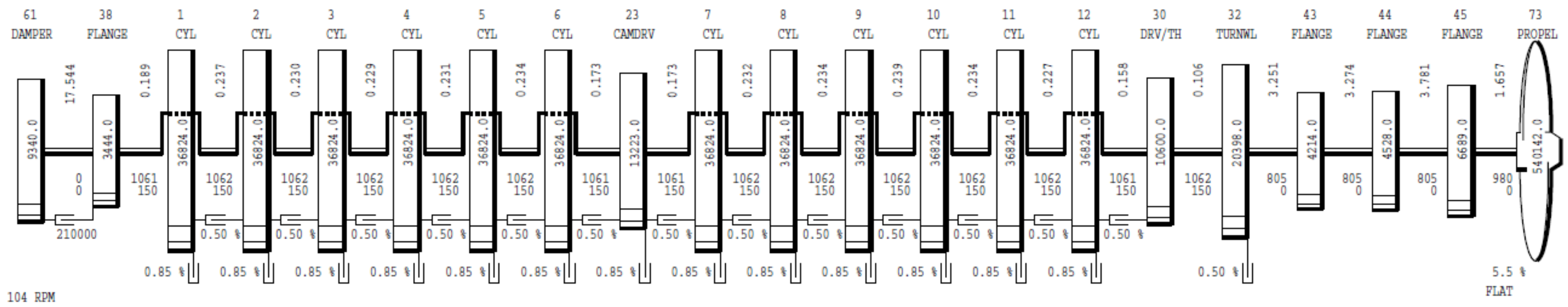

Units: Inertia kgm2
Diameter mm
Flexibility nanorad/Nm
Damping Nms/rad or % of critical

CALCULATION MODEL FOR TORSIONAL VIBRATIONS

MAN Energy Solutions
GTORSI 3.6.4/WIN32
8 Aug 2024 09:50:31
Page 3

MAN Energy Solutions GTORSI 3.6.4/WIN32 Faculty of Maritime S	TORSIONAL VIBRATION CALCULATION Hyundai Heavy Industrires	Page 4 8 Aug 2024 09:50:31
12K98ME-C7, Mark VII,	MCR 72240 kW @ 104 r/min	1992

MISFIRING CYL 1, PROPELLER DAMPING 5.5% FLAT
Excitation: T243795

ENGINE LOAD : kW r/min
Propeller 72240 104

Gas harmonic components : 243795

COMBUSTION CONDITION :
Misfiring cyl. 1

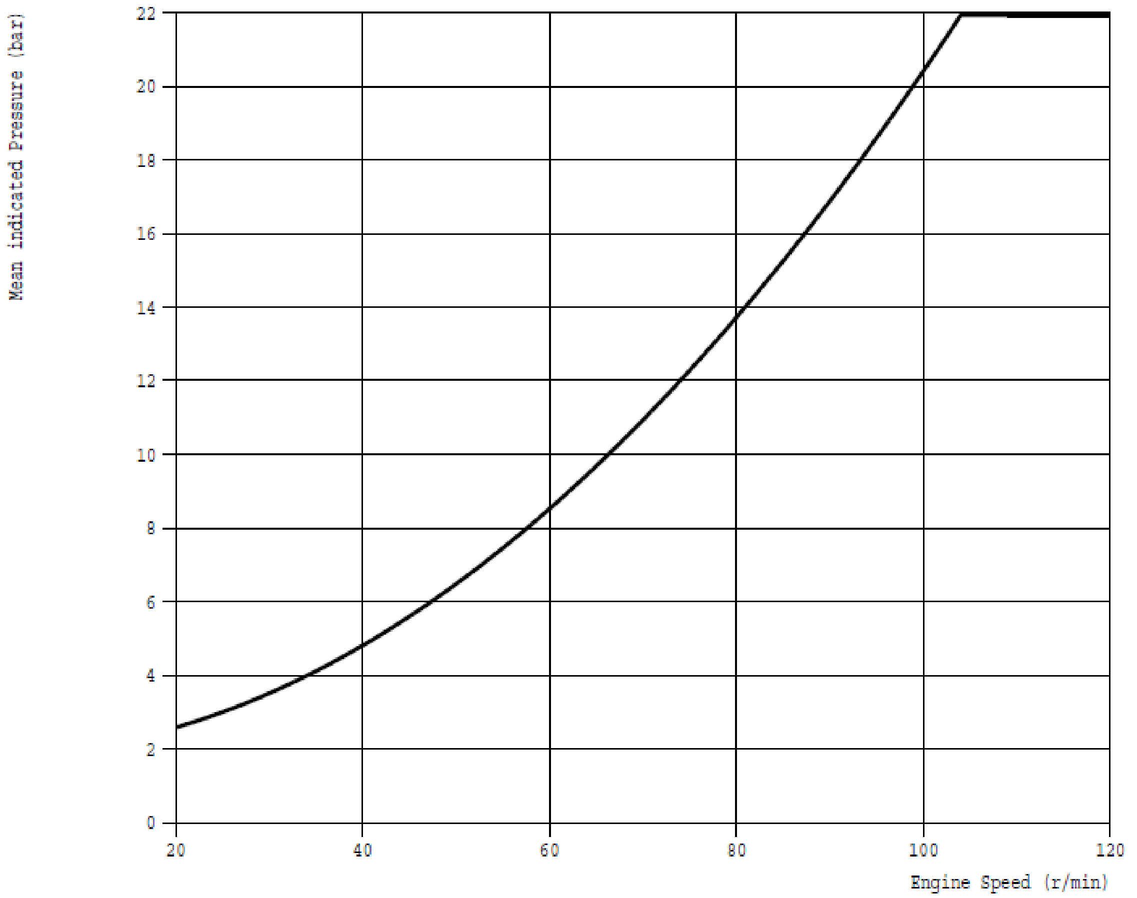

MAN Energy Solutions GTORSI 3.6.4/WIN32 Faculty of Maritime S	TORSIONAL VIBRATION CALCULATION Hyundai Heavy Industrires	Page 5 8 Aug 2024 09:50:31
12K98ME-C7, Mark VII,	MCR 72240 kW @ 104 r/min	1992

MISFIRING CYL 1, PROPELLER DAMPING 5.5% FLAT
Excitation: T243795

ENGINE LOAD :	kW	r/min
Propeller	72240	104

Gas harmonic components : 243795

COMBUSTION CONDITION :
Misfiring cyl. 1

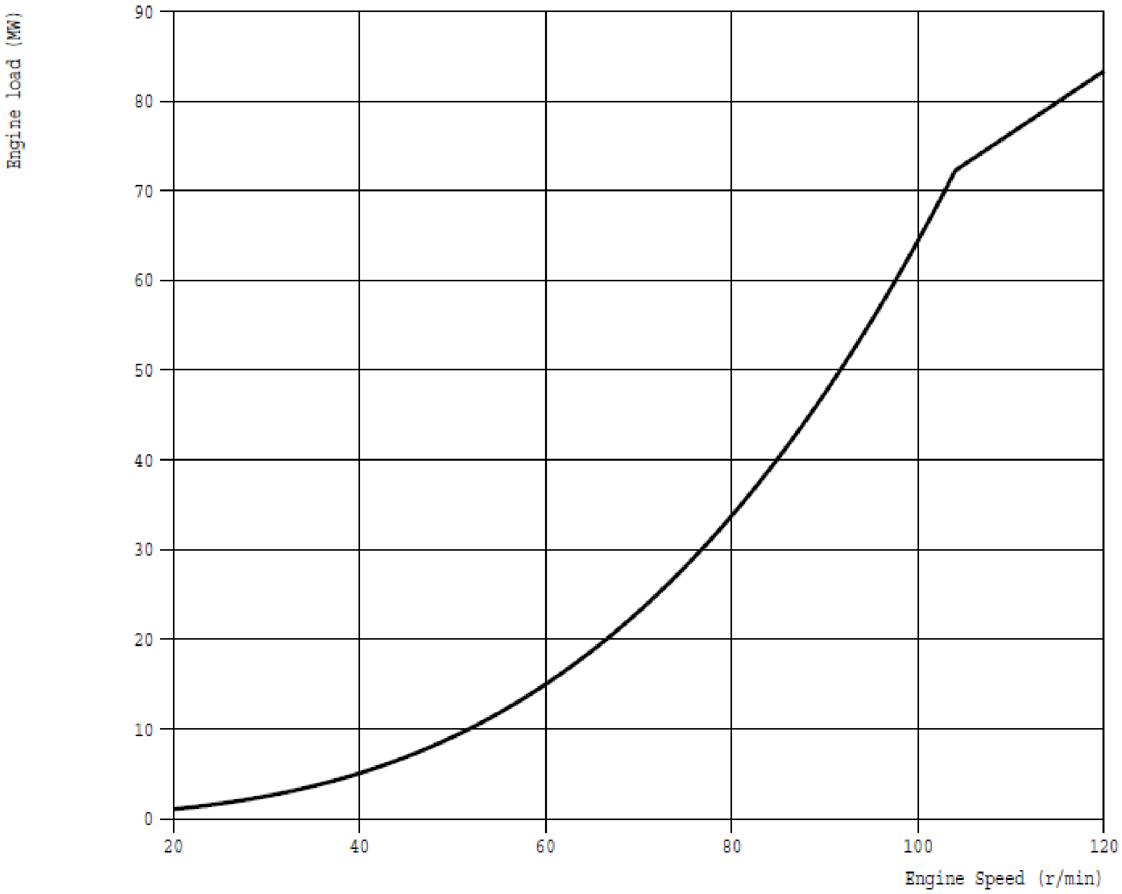

12K98ME-C7, Mark VII, Hyundai Heavy Industrires
MCR 72240 kW @ 104 r/min 1992

Modal form no. 1, Cyclic frequency = 17.178 rad/s , = 2.734 Hz , = 164.04 CPM

ID no	Mass name	Angular deflection (rad)	Shaft torque (kNm)	Torsional stress (MPa)	Kinetic energy (kNm)	Strain energy (kNm)	Damping loss per cycle external (kNm)	internal (kNm)
61	Damper	1.0516E+00			1.5239E+03		0.0000E+00	
38	Flange	1.0007E+00	-2.8983E+03	NaN	5.0890E+02	7.3686E+01	0.0000E+00	2.9301E+01
1	Cylinder	1.0000E+00	-3.9153E+03	-1.6702E+01	5.4332E+03	1.4487E+00	5.8034E+02	0.0000E+00
2	Cylinder	9.9650E-01	-1.4782E+04	-6.2877E+01	5.3952E+03	2.5892E+01	5.7628E+02	1.6268E+00
3	Cylinder	9.9061E-01	-2.5610E+04	-1.0894E+02	5.3316E+03	7.5425E+01	5.6949E+02	4.7391E+00
4	Cylinder	9.8228E-01	-3.6374E+04	-1.5473E+02	5.2423E+03	1.5149E+02	5.5995E+02	9.5186E+00
5	Cylinder	9.7141E-01	-4.7048E+04	-2.0013E+02	5.1269E+03	2.5566E+02	5.4763E+02	1.6064E+01
6	Cylinder	9.5793E-01	-5.7604E+04	-2.4503E+02	4.9856E+03	3.8823E+02	5.3254E+02	2.4393E+01
23	Camshaft Drive	9.4616E-01	-6.8013E+04	-2.9013E+02	1.7466E+03	4.0013E+02	1.8656E+02	2.5141E+01
7	Cylinder	9.3376E-01	-7.1705E+04	-3.0588E+02	4.7372E+03	4.4475E+02	5.0600E+02	2.7944E+01
8	Cylinder	9.1477E-01	-8.1851E+04	-3.4817E+02	4.5465E+03	7.7716E+02	4.8563E+02	4.8830E+01
9	Cylinder	8.9329E-01	-9.1792E+04	-3.9046E+02	4.3355E+03	9.8581E+02	4.6309E+02	6.1940E+01
10	Cylinder	8.6903E-01	-1.0150E+05	-4.3175E+02	4.1032E+03	1.2311E+03	4.3828E+02	7.7351E+01
11	Cylinder	8.4307E-01	-1.1094E+05	-4.7191E+02	3.8617E+03	1.4400E+03	4.1249E+02	9.0480E+01
12	Cylinder	8.1581E-01	-1.2010E+05	-5.1088E+02	3.6160E+03	1.6372E+03	3.8624E+02	1.0287E+02
30	Thrst B/Ch driv	7.9543E-01	-1.2897E+05	-5.5015E+02	9.8954E+02	1.3140E+03	0.0000E+00	8.2560E+01
32	Turning Wheel	7.8150E-01	-1.3146E+05	-5.5918E+02	1.8381E+03	9.1587E+02	1.1549E+02	0.0000E+00
43	Flange	3.3886E-01	-1.3616E+05	-1.3293E+03	7.1392E+01	3.0135E+04	0.0000E+00	0.0000E+00
44	Flange	-1.0837E-01	-1.3658E+05	-1.3334E+03	7.8453E+00	3.0541E+04	0.0000E+00	0.0000E+00
45	Flange	-6.2419E-01	-1.3644E+05	-1.3320E+03	3.8452E+02	3.5189E+04	0.0000E+00	0.0000E+00
73	Main Propeller	-8.4826E-01	-1.3520E+05	-7.3161E+02	5.7344E+04	1.5148E+04	0.0388*Cprop	0.0000E+00
				Total :	1.2113E+05	1.2113E+05	6.9628E+03 + prop.	(ext.+int.)

Resonances with vibration mode no. 1, natural frequency 164.04 c/min in the revolution range 26 - 130 r/min

Order	Critical speed (r/min)	Modal damping (%)	Vector sum normal	Vector sum misfiring	Indicated pressure (bar)	Harmonic components Total (bar)	Harmonic components Mass (bar)	Static amplitude cyl. 1 (mrad)
1	164.0	3.1562	0.0403	0.4247	21.9291	30.1796	11.3352	4.7894
2	82.0	3.1562	0.0020	3.7061	14.3337	1.5776	-10.5318	2.1845
3	54.7	3.1562	0.4896	0.5625	7.3912	1.8649	-3.0259	0.3920
4	41.0	3.1562	0.1104	0.2504	4.9613	2.5337	-0.2345	0.2371
5	32.8	3.1562	0.0406	0.3614	3.8366	1.7757	0.0374	0.2398
6	27.3	3.1562	0.1384	0.4153	3.2257	1.0595	0.0064	0.1644
7	23.4	3.1562	0.0406	0.3541	2.8573	0.6777	-0.0008	0.0896

Modal form no. 2, Cyclic frequency = 72.386 rad/s , = 11.521 Hz , = 691.24 CPM

ID no	Mass name	Angular deflection (rad)	Shaft torque (kNm)	Torsional stress (MPa)	Kinetic energy (kNm)	Strain energy (kNm)	Damping loss per cycle external (kNm)	Damping loss per cycle internal (kNm)
61	Damper	7.5937E+00			1.4110E+06		0.0000E+00	
38	Flange	1.0739E+00	-3.7163E+05	NaN	1.0406E+04	1.2115E+06	0.0000E+00	2.0300E+06
1	Cylinder	1.0000E+00	-3.9101E+05	-1.6680E+03	9.6474E+04	1.4448E+04	1.0305E+04	0.0000E+00
2	Cylinder	8.6160E-01	-5.8396E+05	-2.4840E+03	7.1618E+04	4.0409E+04	7.6498E+03	2.5390E+03
3	Cylinder	6.8906E-01	-7.5020E+05	-3.1911E+03	4.5806E+04	6.4722E+04	4.8927E+03	4.0666E+03
4	Cylinder	4.8681E-01	-8.8315E+05	-3.7567E+03	2.2863E+04	8.9305E+04	2.4421E+03	5.6112E+03
5	Cylinder	2.6111E-01	-9.7708E+05	-4.1562E+03	6.5773E+03	1.1027E+05	7.0255E+02	6.9283E+03
6	Cylinder	2.0682E-02	-1.0275E+06	-4.3705E+03	4.1265E+01	1.2351E+05	4.4077E+00	7.7606E+03
23	Camshaft Drive	-1.5776E-01	-1.0315E+06	-4.3999E+03	8.6219E+02	9.2027E+04	9.2094E+01	5.7822E+03
7	Cylinder	-3.3431E-01	-1.0205E+06	-4.3533E+03	1.0782E+04	9.0087E+04	1.1517E+03	5.6603E+03
8	Cylinder	-5.5611E-01	-9.5602E+05	-4.0666E+03	2.9835E+04	1.0602E+05	3.1868E+03	6.6615E+03
9	Cylinder	-7.5471E-01	-8.4872E+05	-3.6102E+03	5.4950E+04	8.4278E+04	5.8694E+03	5.2953E+03
10	Cylinder	-9.2275E-01	-7.0310E+05	-2.9908E+03	8.2144E+04	5.9075E+04	8.7741E+03	3.7118E+03
11	Cylinder	-1.0456E+00	-5.2506E+05	-2.2335E+03	1.0548E+05	3.2255E+04	1.1266E+04	2.0267E+03
12	Cylinder	-1.1190E+00	-3.2331E+05	-1.3753E+03	1.2080E+05	1.1864E+04	1.2903E+04	7.4544E+02
30	Thrst B/Ch driv	-1.1360E+00	-1.0740E+05	-4.5814E+02	3.5836E+04	9.1125E+02	0.0000E+00	5.7256E+01
32	Turning Wheel	-1.1407E+00	-4.4307E+04	-1.8847E+02	6.9532E+04	1.0405E+02	4.3688E+03	0.0000E+00
43	Flange	-8.8837E-01	7.7608E+04	7.5768E+02	8.7129E+03	9.7900E+03	0.0000E+00	0.0000E+00
44	Flange	-5.7003E-01	9.7223E+04	9.4919E+02	3.8546E+03	1.5475E+04	0.0000E+00	0.0000E+00
45	Flange	-1.5132E-01	1.1075E+05	1.0812E+03	4.0129E+02	2.3185E+04	0.0000E+00	0.0000E+00
73	Main Propeller	4.1005E-02	1.1605E+05	6.2797E+02	2.3793E+03	1.1160E+04	0.0004*Cprop	0.0000E+00
				Total :	2.1904E+06	2.1904E+06	2.1604E+06 + prop.	(ext.+int.)

Resonances with vibration mode no. 2, natural frequency 691.24 c/min in the revolution range 26 - 130 r/min

Order	Critical speed (r/min)	Modal damping (%)	Vector sum normal	Vector sum misfiring	Indicated pressure (bar)	Harmonic components Total (bar)	Harmonic components Mass (bar)	Static amplitude cyl. 1 (mrad)
5	138.2	7.8505	0.1183	0.4456	21.9291	7.0204	0.6648	0.0646
6	115.2	7.8505	0.3398	0.5508	21.9291	3.8194	0.1088	0.0435
7	98.7	7.8505	0.1183	0.5813	19.9510	2.2923	-0.0146	0.0275
8	86.4	7.8505	1.2071	1.5415	15.7056	1.1466	-0.0033	0.0365
9	76.8	7.8505	6.1330	4.9099	12.7949	0.4903	0.0004	0.0497
10	69.1	7.8505	0.3285	2.0157	10.7129	0.2596	0.0001	0.0108
11	62.8	7.8505	0.1144	1.6612	9.1725	0.2081	0.0000	0.0071
12	57.6	7.8505	1.4132	3.0526	8.0009	0.1503	0.0000	0.0095
13	53.2	7.8505	0.1144	1.7424	7.0891	0.0950	0.0000	0.0034
14	49.4	7.8505	0.3285	1.7749	6.3656	0.0853	0.0000	0.0031
15	46.1	7.8505	6.1330	4.8807	5.7819	0.0765	0.0000	0.0077
16	43.2	7.8505	1.2071	0.6929	5.3043	0.0605	0.0000	0.0009
17	40.7	7.8505	0.1183	1.0022	4.9084	0.0537	0.0000	0.0011
18	38.4	7.8505	0.3398	0.5911	4.5766	0.0469	0.0000	0.0006
19	36.4	7.8505	0.1183	0.8200	4.2958	0.0386	0.0000	0.0007
20	34.6	7.8505	1.2071	1.2007	4.0561	0.0341	0.0000	0.0008

12K98ME-C7, Mark VII,　　Hyundai Heavy Industrires
MCR 72240 kW @ 104 r/min　　1992

Modal form no. 3, Cyclic frequency = 87.349 rad/s , = 13.902 Hz , = 834.12 CPM

ID no	Mass name	Angular deflection (rad)	Shaft torque (kNm)	Torsional stress (MPa)	Kinetic energy (kNm)	Strain energy (kNm)	Damping loss per cycle external (kNm)	Damping loss per cycle internal (kNm)
61	Damper	-3.8101E+00			5.1726E+05		0.0000E+00	
38	Flange	9.5342E-01	2.7152E+05	NaN	1.1943E+04	6.4670E+05	0.0000E+00	1.3076E+06
1	Cylinder	1.0000E+00	2.4647E+05	1.0514E+03	1.4048E+05	5.7405E+03	1.5005E+04	0.0000E+00
2	Cylinder	9.9182E-01	-3.4497E+04	-1.4674E+02	1.3819E+05	1.4102E+02	1.4761E+04	8.8604E+00
3	Cylinder	9.1980E-01	-3.1316E+05	-1.3321E+03	1.1885E+05	1.1278E+04	1.2695E+04	7.0863E+02
4	Cylinder	7.8890E-01	-5.7159E+05	-2.4314E+03	8.7431E+04	3.7409E+04	9.3389E+03	2.3505E+03
5	Cylinder	6.0566E-01	-7.9325E+05	-3.3742E+03	5.1532E+04	7.2677E+04	5.5044E+03	4.5664E+03
6	Cylinder	3.8022E-01	-9.6341E+05	-4.0981E+03	2.0309E+04	1.0860E+05	2.1693E+03	6.8233E+03
23	Camshaft Drive	1.9507E-01	-1.0702E+06	-4.5654E+03	1.9196E+03	9.9079E+04	2.0504E+02	6.2253E+03
7	Cylinder	6.5139E-03	-1.0899E+06	-4.6494E+03	5.9607E+00	1.0276E+05	6.3669E-01	6.4564E+03
8	Cylinder	-2.4677E-01	-1.0918E+06	-4.6440E+03	8.5549E+03	1.3826E+05	9.1379E+02	8.6874E+03
9	Cylinder	-4.8602E-01	-1.0224E+06	-4.3491E+03	3.3184E+04	1.2231E+05	3.5445E+03	7.6847E+03
10	Cylinder	-6.9774E-01	-8.8587E+05	-3.7682E+03	6.8393E+04	9.3779E+04	7.3053E+03	5.8923E+03
11	Cylinder	-8.5916E-01	-6.8983E+05	-2.9343E+03	1.0370E+05	5.5676E+04	1.1076E+04	3.4982E+03
12	Cylinder	-9.6096E-01	-4.4843E+05	-1.9075E+03	1.2973E+05	2.2824E+04	1.3857E+04	1.4341E+03
30	Thrst B/Ch driv	-9.8915E-01	-1.7844E+05	-7.6118E+02	3.9566E+04	2.5154E+03	0.0000E+00	1.5805E+02
32	Turning Wheel	-9.9958E-01	-9.8440E+04	-4.1874E+02	7.7753E+04	5.1359E+02	4.8853E+03	0.0000E+00
43	Flange	-8.1386E-01	5.7130E+04	5.5776E+02	1.0648E+04	5.3052E+03	0.0000E+00	0.0000E+00
44	Flange	-5.4111E-01	8.3298E+04	8.1323E+02	5.0579E+03	1.1360E+04	0.0000E+00	0.0000E+00
45	Flange	-1.5551E-01	1.0199E+05	9.9575E+02	6.1711E+02	1.9664E+04	0.0000E+00	0.0000E+00
73	Main Propeller	2.6674E-02	1.0993E+05	5.9484E+02	1.4661E+03	1.0014E+04	0.0002*Cprop	0.0000E+00
				Total :	1.5666E+06	1.5666E+06	1.4634E+06 + prop.	(ext.+int.)

Resonances with vibration mode no. 3, natural frequency 834.12 c/min in the revolution range 26 - 130 r/min

Order	Critical speed (r/min)	Modal damping (%)	Vector sum normal	Vector sum misfiring	Indicated pressure (bar)	Harmonic components Total (bar)	Harmonic components Mass (bar)	Static amplitude cyl. 1 (mrad)
6	139.0	7.4345	0.6547	0.9814	21.9291	3.8611	0.1583	0.1095
7	119.2	7.4345	0.1872	0.6576	21.9291	2.3240	-0.0213	0.0441
8	104.3	7.4345	1.0780	1.6845	21.9291	1.3774	-0.0049	0.0670
9	92.7	7.4345	5.9778	5.0035	17.7934	0.6490	0.0006	0.0938
10	83.4	7.4345	0.4832	2.3956	14.7617	0.3051	0.0002	0.0211
11	75.8	7.4345	0.1869	2.0830	12.5186	0.2334	0.0000	0.0140
12	69.5	7.4345	1.4423	0.4064	10.8126	0.1873	0.0000	0.0022
13	64.2	7.4345	0.1869	1.8240	9.4848	0.1349	0.0000	0.0071
14	59.6	7.4345	0.4832	1.7697	8.4313	0.1247	0.0000	0.0064
15	55.6	7.4345	5.9778	4.8296	7.5814	0.1079	0.0000	0.0151
16	52.1	7.4345	1.0780	0.6351	6.8858	0.0836	0.0000	0.0015
17	49.1	7.4345	0.1872	1.2427	6.3093	0.0717	0.0000	0.0026
18	46.3	7.4345	0.6547	1.5568	5.8262	0.0612	0.0000	0.0028
19	43.9	7.4345	0.1872	1.0856	5.4174	0.0501	0.0000	0.0016
20	41.7	7.4345	1.0780	1.1350	5.0683	0.0433	0.0000	0.0014

MAN Energy Solutions GTORSI 3.6.4/WIN32 Faculty of Maritime S	TORSIONAL VIBRATION CALCULATION Hyundai Heavy Industrires	Page 9 8 Aug 2024 09:50:31
12K98ME-C7, Mark VII,	MCR 72240 kW @ 104 r/min	1992

Normal modes no. 1- 3 of main branch

Mode no 1, 164.04 cpm

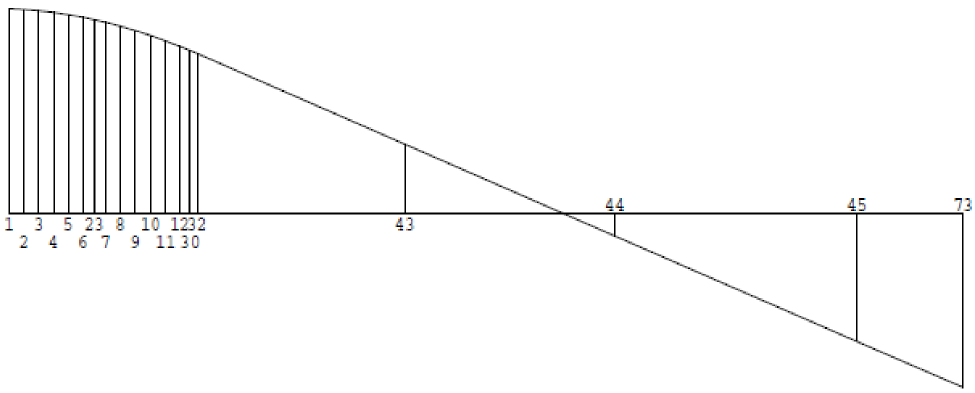

Mode no 2, 691.24 cpm

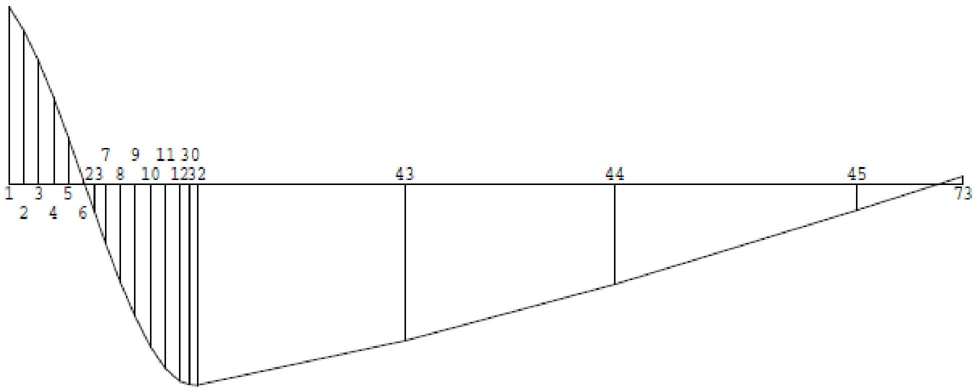

Mode no 3, 834.13 cpm

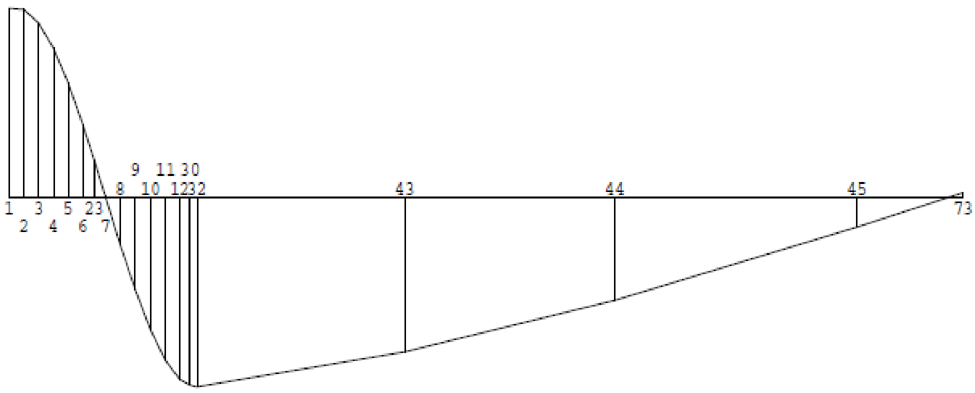

MAN Energy Solutions GTORSI 3.6.4/WIN32 Faculty of Maritime S	TORSIONAL VIBRATION CALCULATION Hyundai Heavy Industrires	Page 10 8 Aug 2024 09:50:31
12K98ME-C7, Mark VII,	MCR 72240 kW @ 104 r/min	1992

MISFIRING CYL 1, PROPELLER DAMPING 5.5% FLAT
Excitation: T243795

ENGINE LOAD : kW r/min
Propeller 72240 104

Gas harmonic components : 243795

COMBUSTION CONDITION :
Misfiring cyl. 1

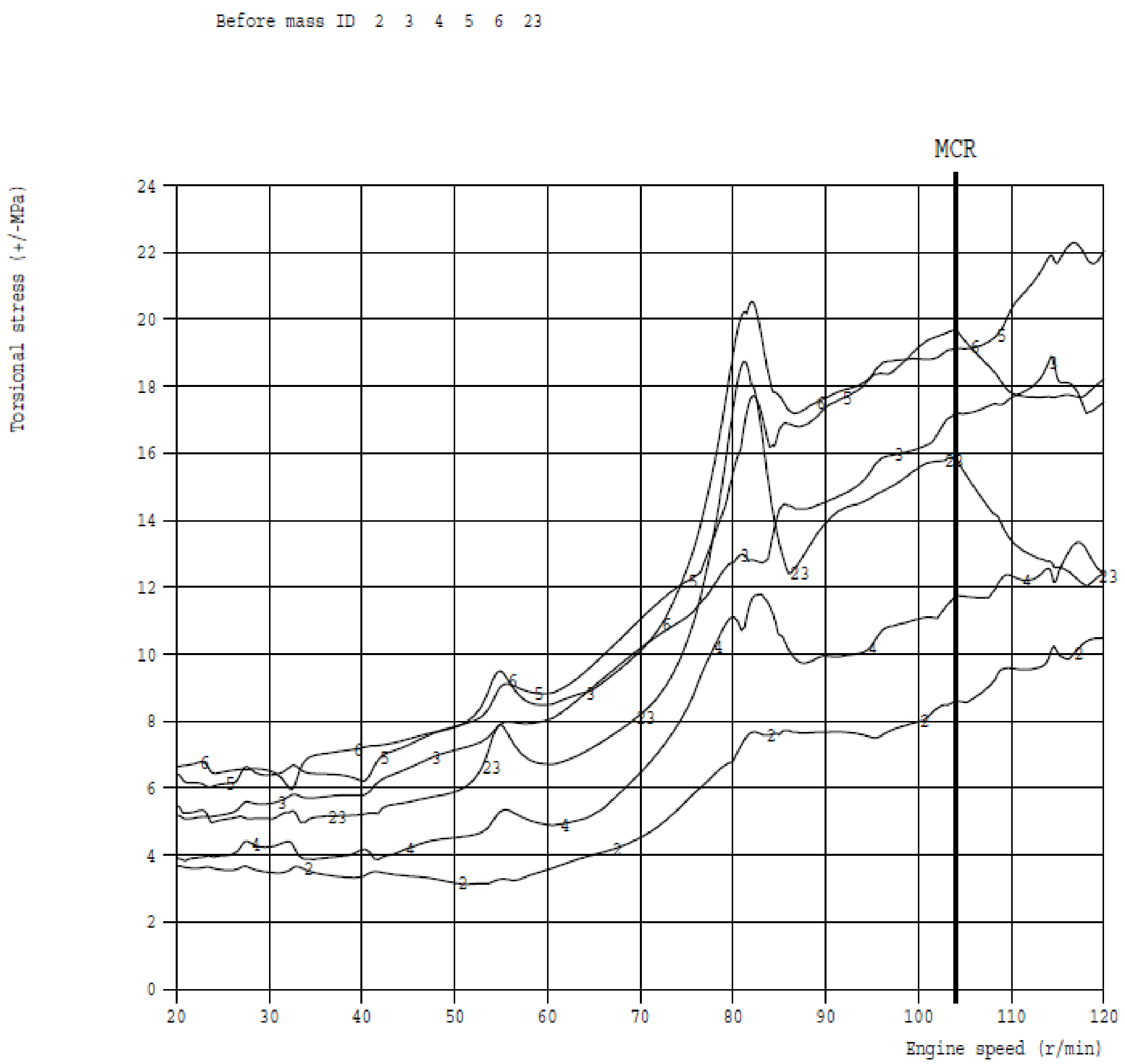

MAN Energy Solutions GTORSI 3.6.4/WIN32 Faculty of Maritime S	TORSIONAL VIBRATION CALCULATION Hyundai Heavy Industrires	Page 11 8 Aug 2024 09:50:31
12K98ME-C7, Mark VII,	MCR 72240 kW @ 104 r/min	1992

MISFIRING CYL 1, PROPELLER DAMPING 5.5% FLAT
Excitation: T243795

ENGINE LOAD :	kW	r/min
Propeller	72240	104

Gas harmonic components : 243795

COMBUSTION CONDITION :
Misfiring cyl. 1

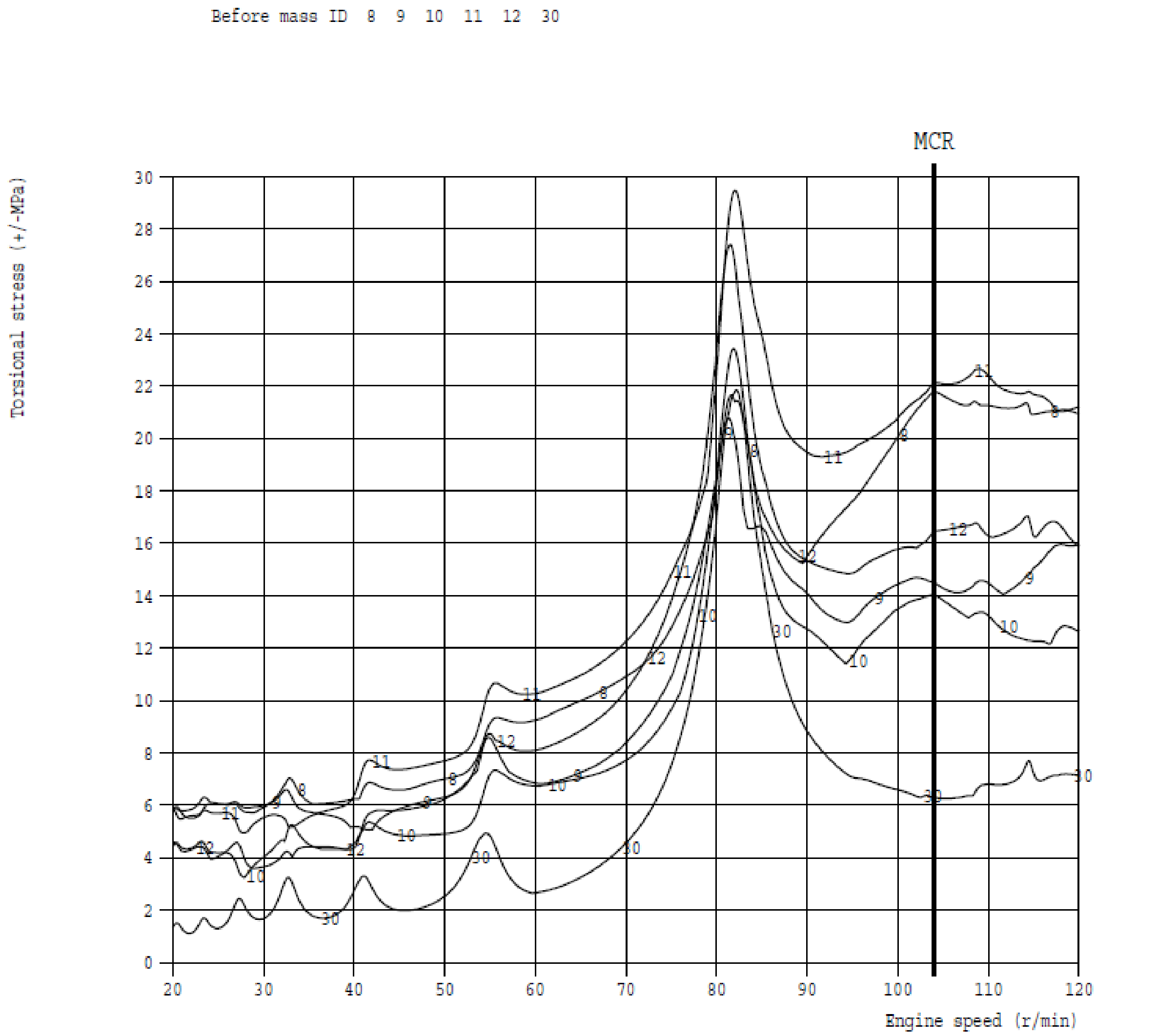

MAN Energy Solutions GTORSI 3.6.4/WIN32 Faculty of Maritime S	TORSIONAL VIBRATION CALCULATION Hyundai Heavy Industrires	Page 12 8 Aug 2024 09:50:31

12K98ME-C7, Mark VII,	MCR 72240 kW @ 104 r/min	1992

	MISFIRING CYL 1, PROPELLER DAMPING 5.5% FLAT Excitation: T243795
ENGINE LOAD : kW r/min Propeller 72240 104 Gas harmonic components : 243795	COMBUSTION CONDITION : Misfiring cyl. 1

CRANK_11 before mass ID 11 Cylinder

Order 1 2 3 4 5 6

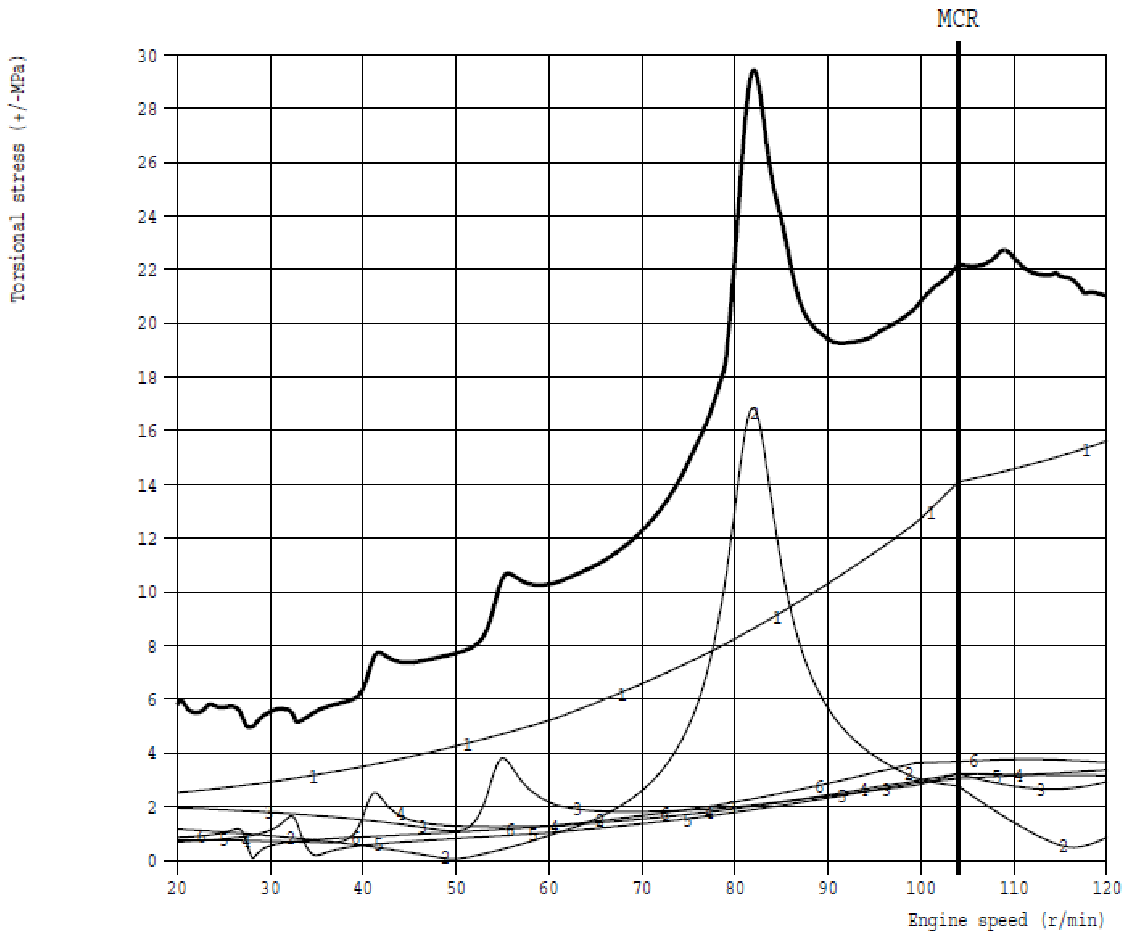

MAN Energy Solutions GTORSI 3.6.4/WIN32 Faculty of Maritime S	TORSIONAL VIBRATION CALCULATION Hyundai Heavy Industrires	Page 13 8 Aug 2024 09:50:31
12K98ME-C7, Mark VII,	MCR 72240 kW @ 104 r/min	1992

MISFIRING CYL 1, PROPELLER DAMPING 5.5% FLAT
Excitation: T243795

ENGINE LOAD : kW r/min
Propeller 72240 104

Gas harmonic components : 243795

COMBUSTION CONDITION :
Misfiring cyl. 1

CRANK_12 before mass ID 12 Cylinder

Order 1 2 3 4

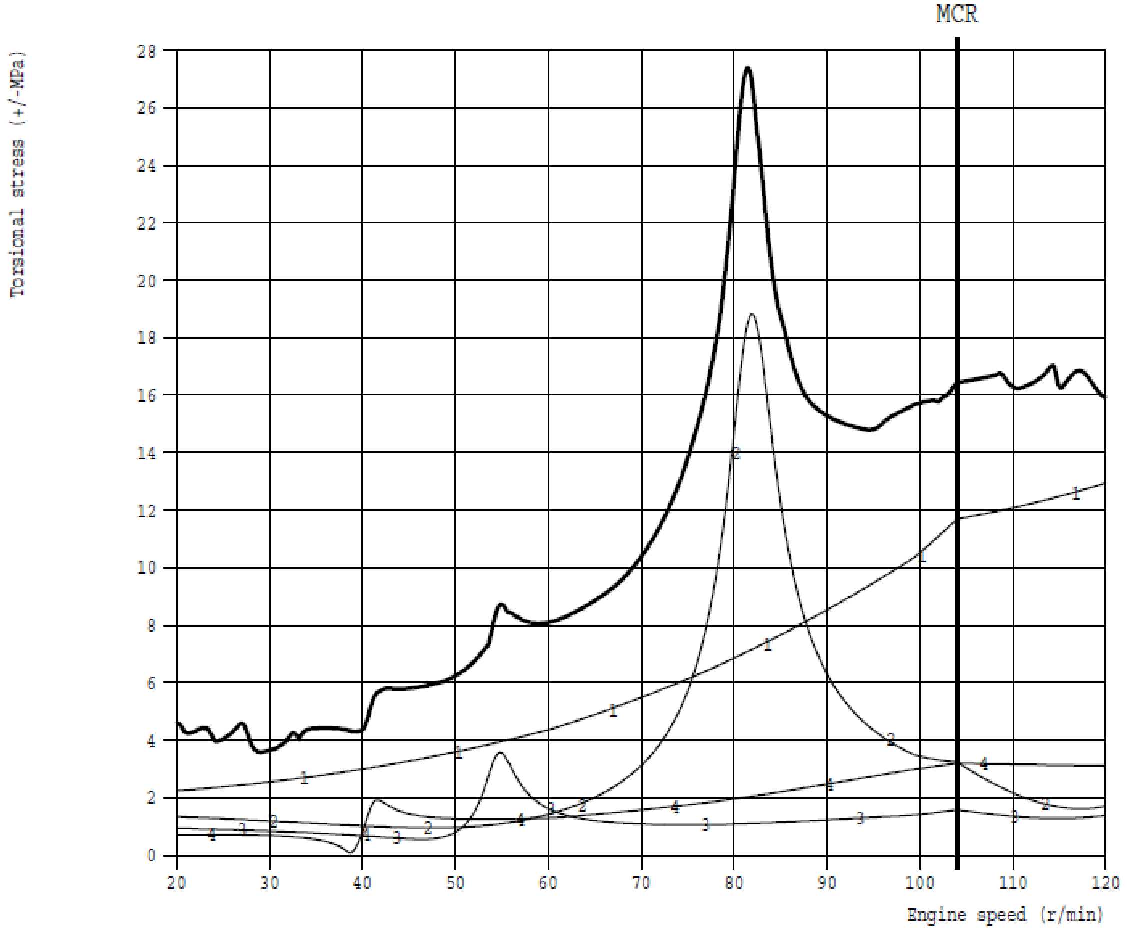

MAN Energy Solutions GTORSI 3.6.4/WIN32 Faculty of Maritime S	TORSIONAL VIBRATION CALCULATION Hyundai Heavy Industrires	Page 14 8 Aug 2024 09:50:31
12K98ME-C7, Mark VII,	MCR 72240 kW @ 104 r/min	1992

MISFIRING CYL 1, PROPELLER DAMPING 5.5% FLAT
Excitation: T243795

ENGINE LOAD : kW r/min
Propeller 72240 104

Gas harmonic components : 243795

COMBUSTION CONDITION :
Misfiring cyl. 1

FLANGE1 before mass ID 43 Flange

Order 1 2 3 4 5

Classification Society: IACS Rules

Dy= 805.0 mm Di= 0.0 mm SIGMAB= 800 MPa Ck= 1.00
Limits for synthesis:

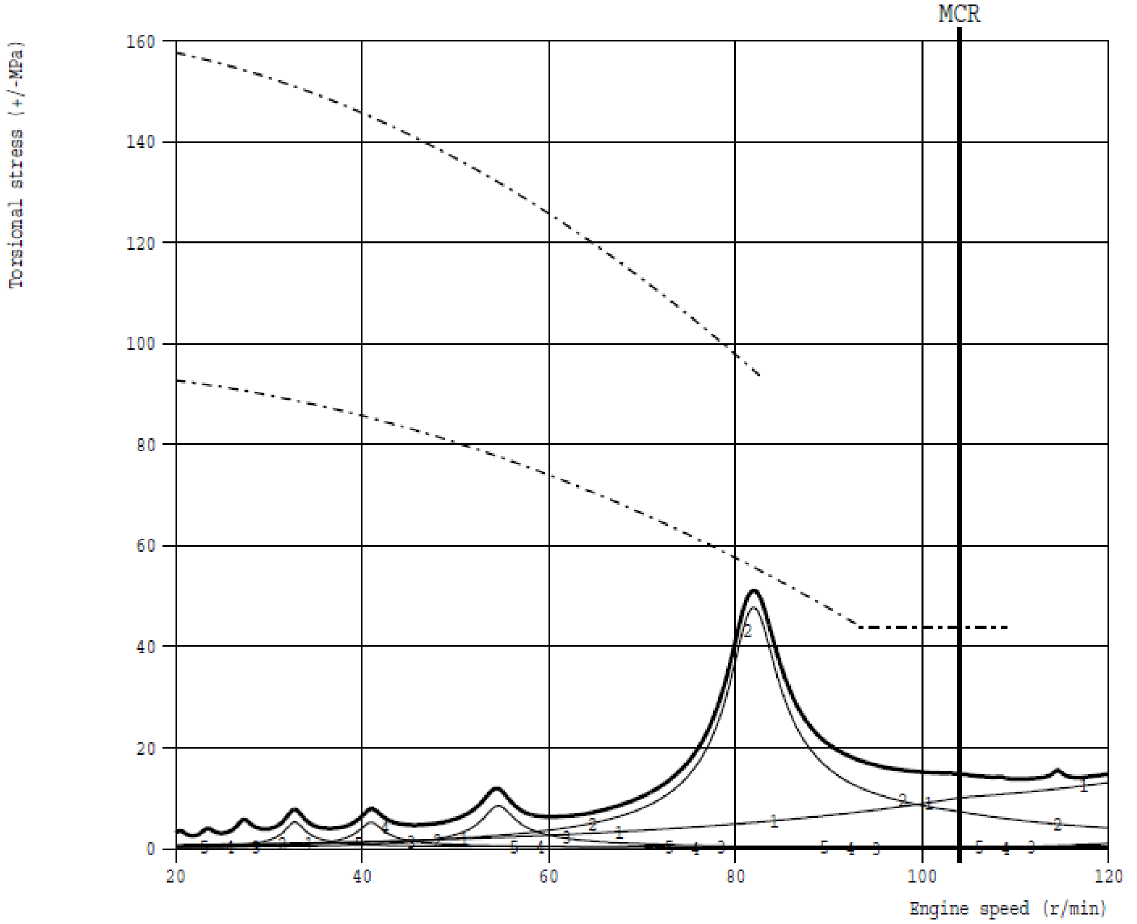

MAN Energy Solutions GTORSI 3.6.4/WIN32 Faculty of Maritime S	TORSIONAL VIBRATION CALCULATION Hyundai Heavy Industrires	Page 15 8 Aug 2024 09:50:31
12K98ME-C7, Mark VII,	MCR 72240 kW @ 104 r/min	1992

MISFIRING CYL 1, PROPELLER DAMPING 5.5% FLAT
Excitation: T243795

ENGINE LOAD : kW r/min
Propeller 72240 104

Gas harmonic components : 243795

COMBUSTION CONDITION :
Misfiring cyl. 1

PROPELLER before mass ID 73 Main Propeller

Order 1 2 3 4 5

Classification Society: IACS Rules

Dy= 980.0 mm Di= 0.0 mm SIGMAB= 600 MPa Ck= 0.55
Limits for synthesis:

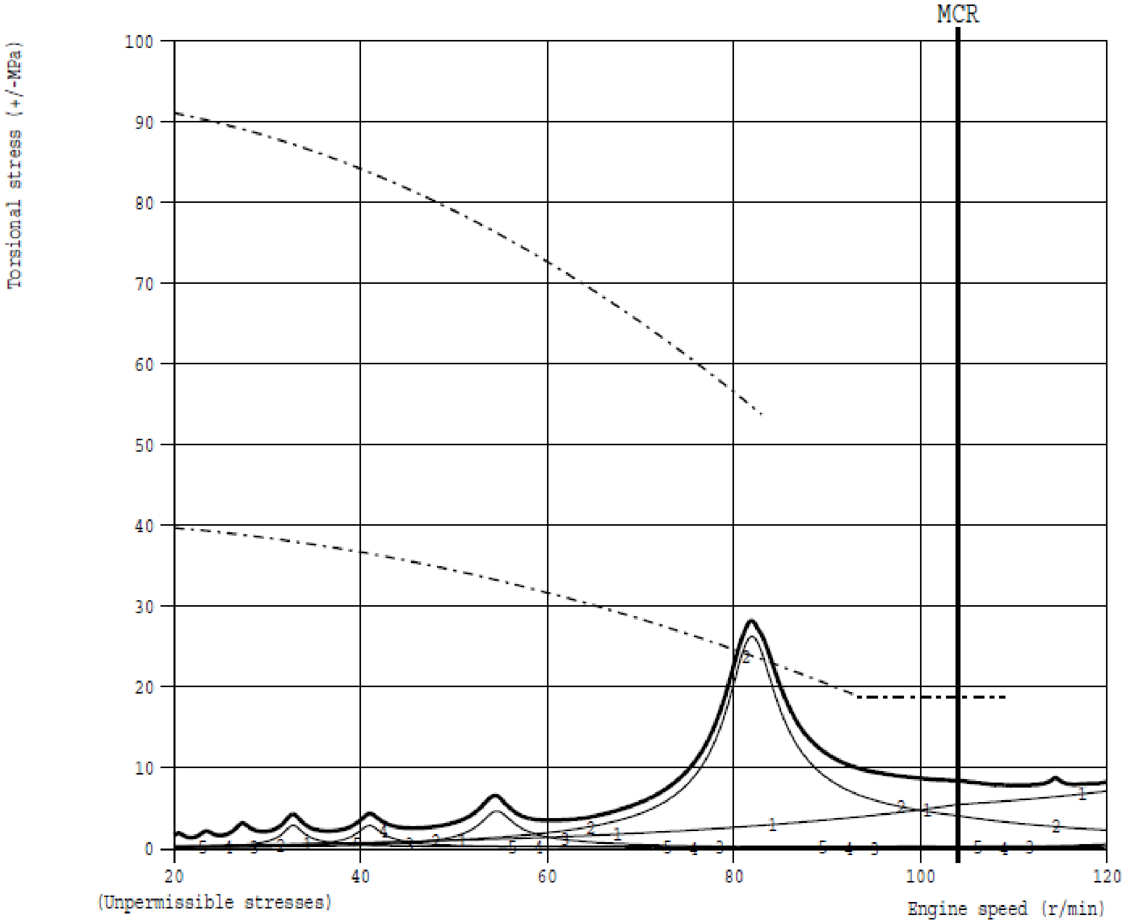

MAN Energy Solutions GTORSI 3.6.4/WIN32 Faculty of Maritime S	TORSIONAL VIBRATION CALCULATION Hyundai Heavy Industrires	Page 16 8 Aug 2024 09:50:31
12K98ME-C7, Mark VII,	MCR 72240 kW @ 104 r/min	1992

MISFIRING CYL 1, PROPELLER DAMPING 5.5% FLAT
Excitation: T243795

ENGINE LOAD :	kW	r/min
Propeller	72240	104

Gas harmonic components : 243795

COMBUSTION CONDITION :
Misfiring cyl. 1

D. INNER+FLG before mass ID 38 Flange

Order 2 6 7 8 9 10

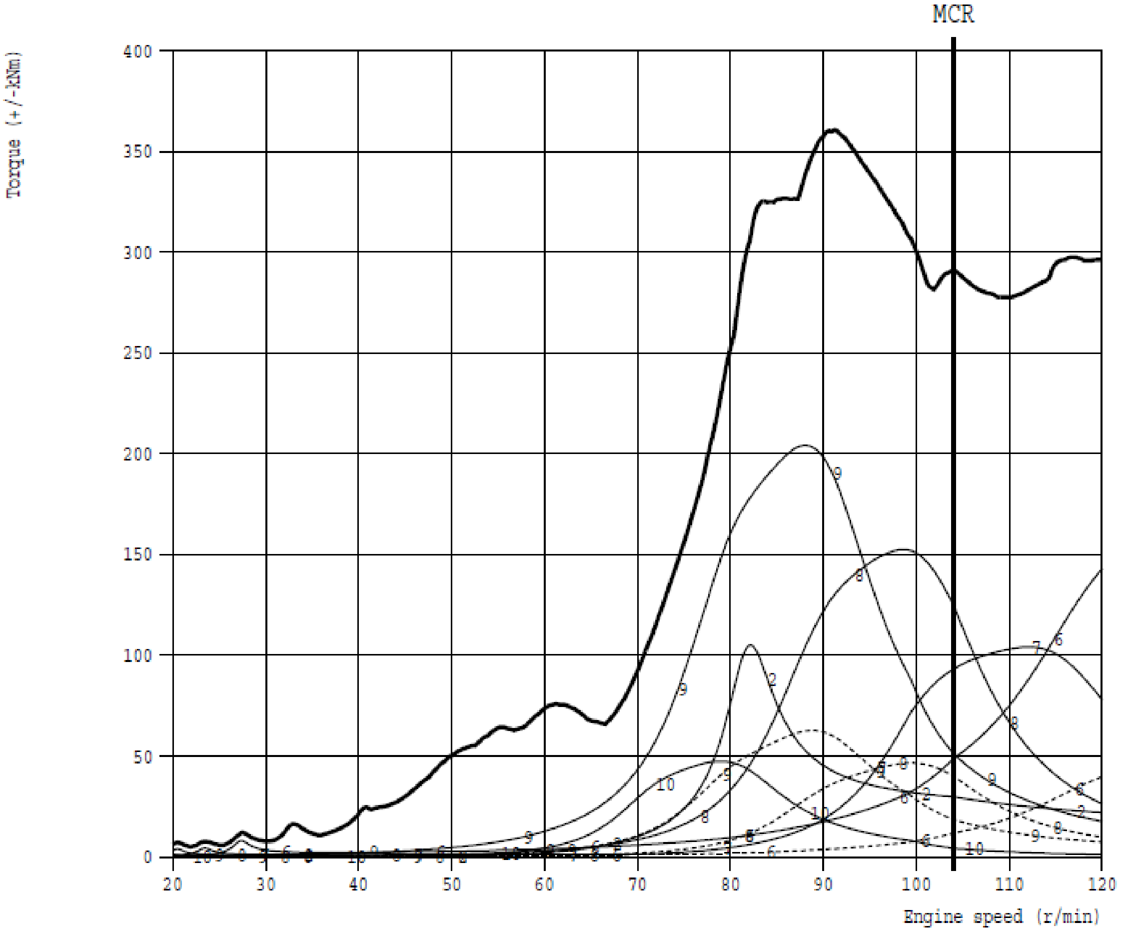

MAN Energy Solutions GTORSI 3.6.4/WIN32 Faculty of Maritime S	TORSIONAL VIBRATION CALCULATION Hyundai Heavy Industrires	Page 17 8 Aug 2024 09:50:31
12K98ME-C7, Mark VII,	MCR 72240 kW @ 104 r/min	1992

MISFIRING CYL 1, PROPELLER DAMPING 5.5% FLAT
Excitation: T243795

ENGINE LOAD :	kW	r/min
Propeller	72240	104

Gas harmonic components : 243795

COMBUSTION CONDITION :
Misfiring cyl. 1

D. INNER+FLG before mass ID 38 Flange

Order 6 7 8 9

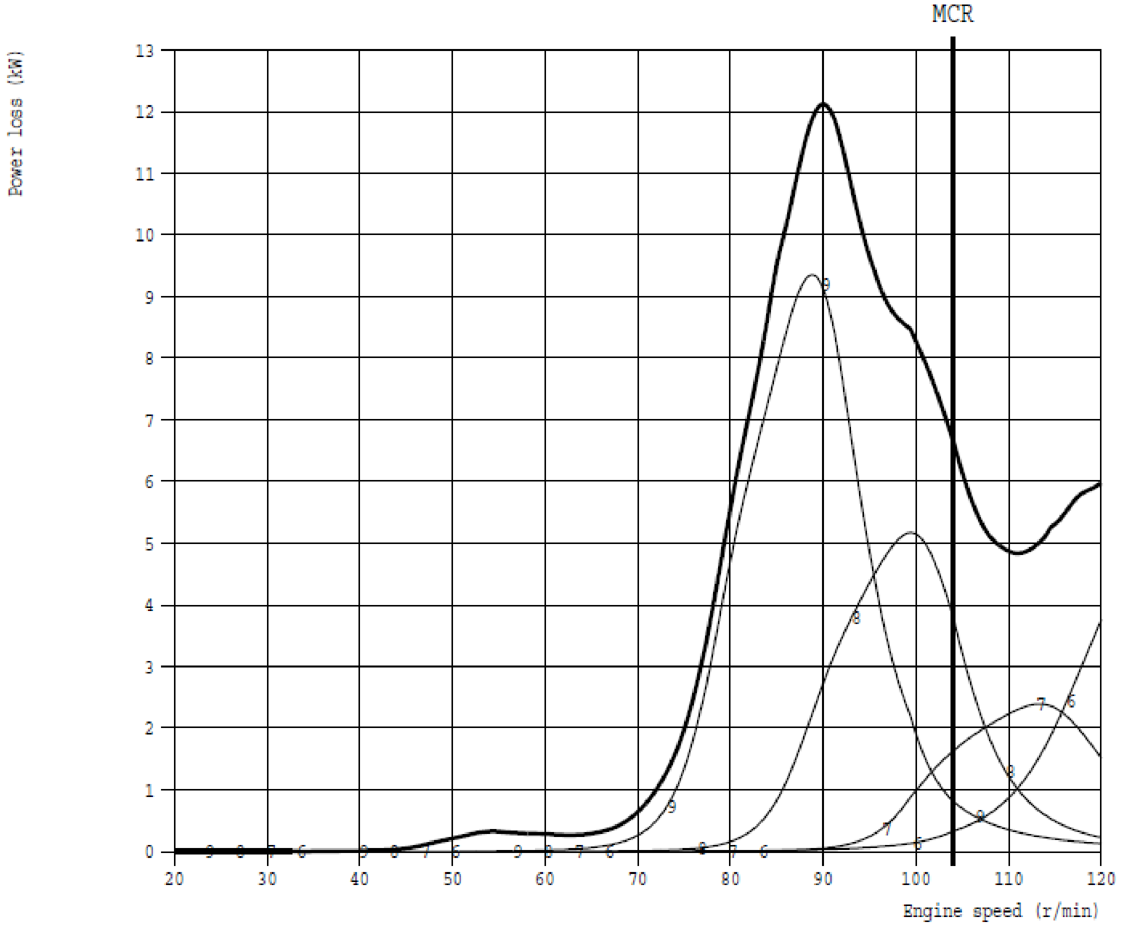

MAN Energy Solutions GTORSI 3.6.4/WIN32 Faculty of Maritime S	TORSIONAL VIBRATION CALCULATION Hyundai Heavy Industrires	Page 18 8 Aug 2024 09:50:31
12K98ME-C7, Mark VII,	MCR 72240 kW @ 104 r/min	1992

MISFIRING CYL 1, PROPELLER DAMPING 5.5% FLAT
Excitation: T243795

ENGINE LOAD : kW r/min
Propeller 72240 104

Gas harmonic components : 243795

COMBUSTION CONDITION :
Misfiring cyl. 1

Mass ID 1 Cylinder

Order 1 2 3 4 5

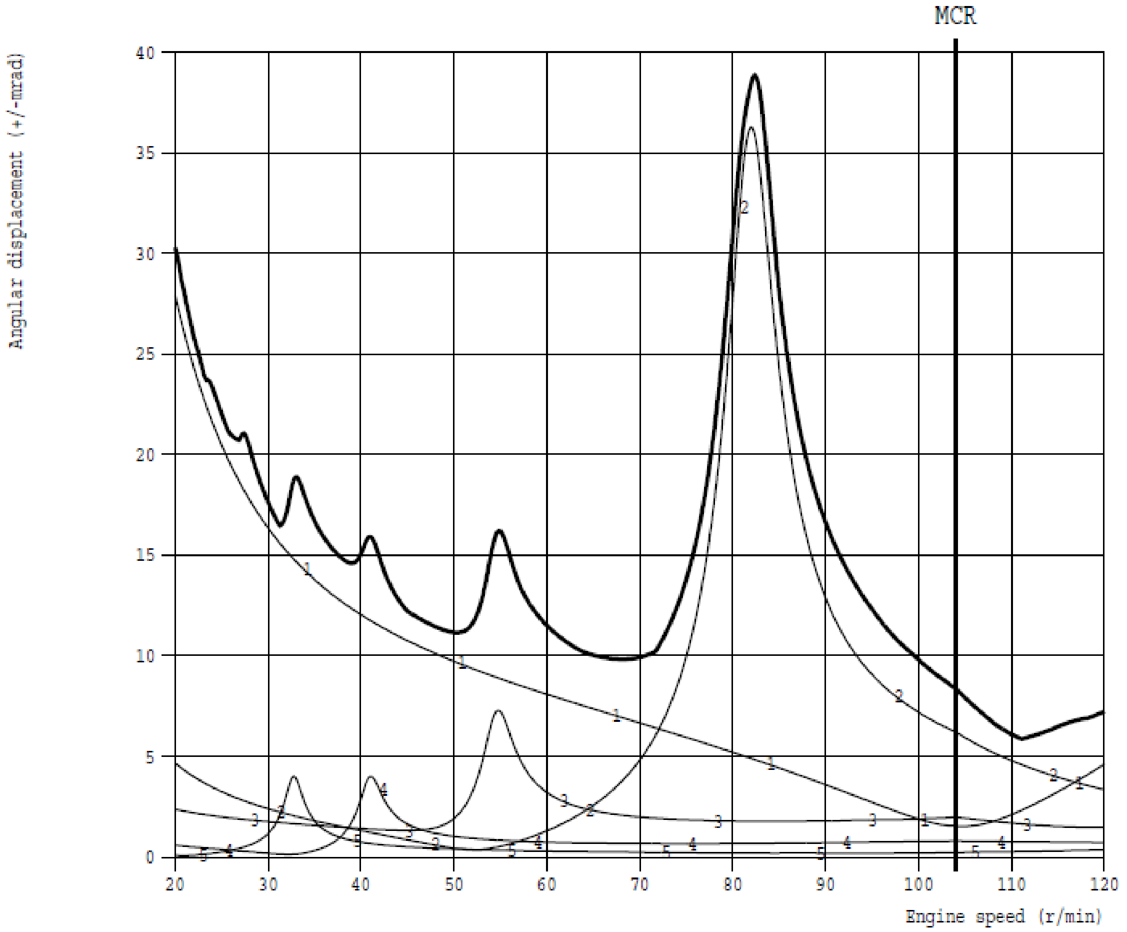

MAN Energy Solutions GTORSI 3.6.4/WIN32 Faculty of Maritime S	TORSIONAL VIBRATION CALCULATION Hyundai Heavy Industrires	Page 19 8 Aug 2024 09:50:31

12K98ME-C7, Mark VII,	MCR 72240 kW @ 104 r/min	1992

MISFIRING CYL 1, PROPELLER DAMPING 5.5% FLAT
Excitation: T243795

ENGINE LOAD : kW r/min
Propeller 72240 104

Gas harmonic components : 243795

COMBUSTION CONDITION :
Misfiring cyl. 1

Mass ID 73 Main Propeller

Order 1 2 3

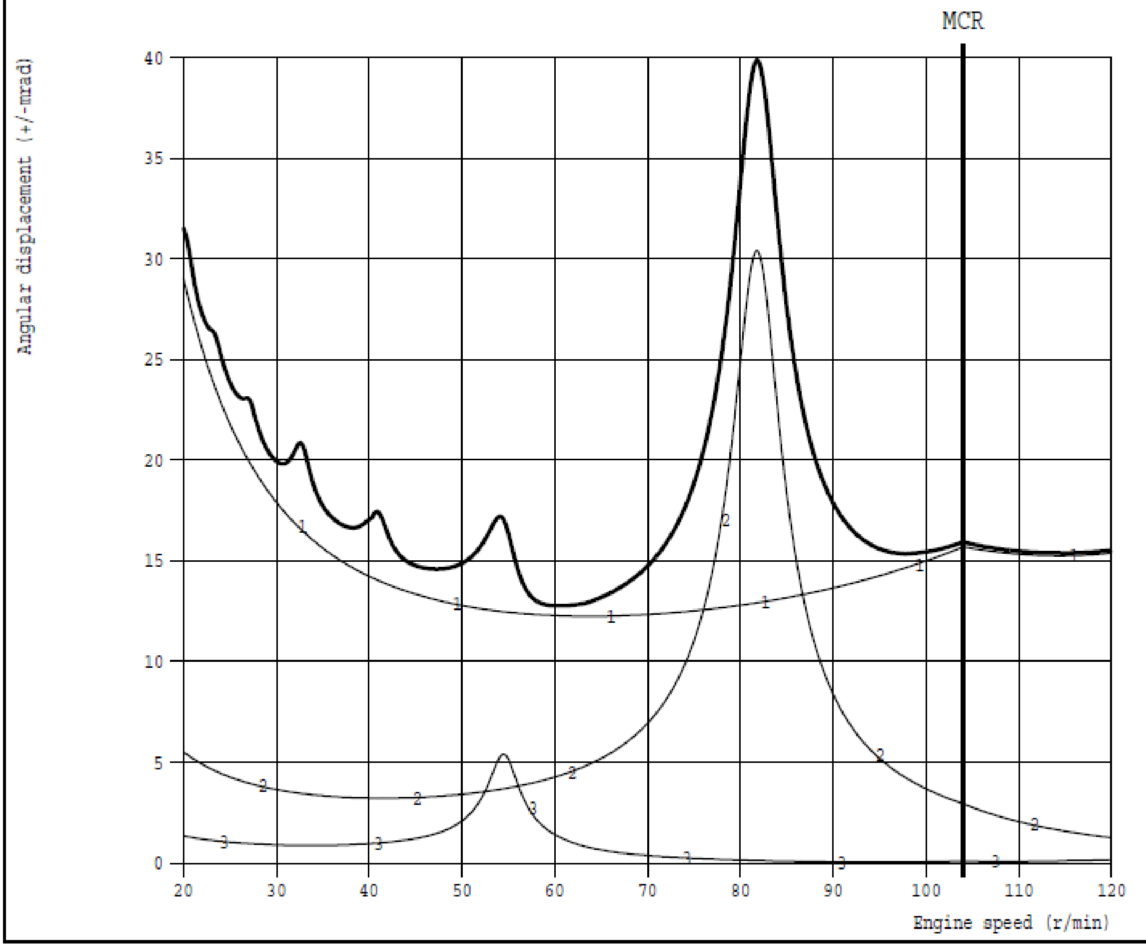

BIOGRAPHY

Karlo Bratić was born in Split in 1993. He earned a bachelor's degree in Naval Mechanical Engineering from the *Faculty of Maritime Studies in Split* in 2014. He went on to complete his master's degree at the same institution in 2016. Following his graduate studies, he briefly served as an engine apprentice with CMA CGM, after which he obtained his Certificate of Competency as an Officer in Charge of an Engineering Watch. In 2018, he commenced employment at *University of Split, Faculty of Maritime Studies*, as assistant at Department for Marine Engineering. During the same year, he enrolled in the doctoral program at the *University of Rijeka, Faculty of Maritime Studies*. In 2019, he transferred to the doctoral program at *University of Split, Faculty of Maritime Studies*.

Papers published in journals:

1. Pavlović, Igor; **Bratić, Karlo**; Kiciński, Radosław; Kluczyk, Marcin
   Testing and Modeling of Shaft Vibrations Due to Misalignment // Journal of marine science and engineering, 12 (2024), 12; 2284-2299. doi: 10.3390/jmse12122284
2. Martinić-Cezar, Siniša; **Bratić, Karlo**; Jurić, Zdeslav; Račić, Nikola
   Exhaust emissions reduction and fuel consumption from the LNG energy system depending on the ship operating modes // Pomorstvo: scientific journal of maritime research, 36(2022) (2022), 2; 338-346. doi: 10.31217/p.36.2.17
3. Perić, Tina; Stazić, Ladislav; **Bratić, Karlo**
   Potential Benefits of Electrically Driven Ferry, Case Study // Pedagogika (Sofia), 2021-7S (2021), 217-224. doi: 10.53656/ped21-7s.19pot
4. Jurić, Zdeslav; **Bratić, Karlo**; Dobrota, Đorđe; Štolfa, Ivan
   Influence of Cruise Ship Size on Length of Stay in Port // TransNav, 15 (2021), 2; 423-426. doi: 10.12716/1001.15.02.21
5. Vulić, Nenad; **Bratić, Karlo**; Lalić, Branko; Stazić, Ladislav
   Propeller Load Modelling in the Calculations of Marine Shafting Torsional Vibrations // Pedagogika (Sofia), 93 (2021), 6s; 204-216. doi: 10.53656/ped21-6s.18pro
6. Stanivuk, Tatjana; Stazić, Ladislav; Vidović, Frane; **Bratić, Karlo**
   Assessment of the Concept of the New Methodology for the Evaluation of Ship Planned Maintenance System // TransNav, 15 (2021), 4; 739-742. doi: 10.12716/1001.15.04.03
7. **Bratić, Karlo**; Stazić, Ladislav; Vukičević, Miroslav; Lalić, Branko
   Cruise Vessels Air Pollution Inventory for the Port of Kotor // Transactions on maritime science, 10 (2021), 1; 16, 8. doi: 10.7225/toms. v10.n01.016
8. Vulić, Nenad; **Bratić, Karlo**; Lalić, Branko; Stazić, Ladislav
   Implementing Simulation X in the modelling of marine shafting steady state torsional vibrations // Polish Maritime Research, 2 (110) 2021 (2021), Vol. 28; 63-71. doi: 10.2478/pomr-2021-0022
9. Mihanovic, Luka; Lalic, Branko; **Bratić, Karlo**; Stazic, Ladislav
   Distribution of the International Marine Traffic Air Pollutant Emissions in the Port of Split // TransNav, 15 (2021), 3; 611-614. doi: 10.12716/1001.15.03.15
10. Stazić, Ladislav; **Bratić, Karlo**; Dobrota, Đorđe; Lalić, Branko

Revisions of the SMS maintenance procedures based on computerized PMS data // Scientific Bulletin of Naval Academy, 23 (2020), 1; 166-170. doi: 10.21279/1454-864X-20-I1-021

11. **Bratić, Karlo**; Pavić, Ivan; Vukša, Srđan; Stazić, Ladislav
    Review of Autonomous and Remotely Controlled Ships in Maritime Sector // Transactions on maritime science, 8 (2019), 2; 253-265. doi: 10.7225/toms.v08.n02.011

Papers published in conference proceedings:

1. Pavlović, Igor; **Bratić, Karlo**; Vulić, Nenad; Roldo, Liane
   Principles of Torque Measurement in the PFST Instrumented Sliding Bearings Test Rig // 10th International Maritime Science Conference: Book of Proceedings / Vidan, Pero; Slišković, Merica; Katalinić, Marko (ur.). Split: Pomorski fakultet Sveučilišta u Splitu, 2023. str. 69-79
2. Radica, Gojmir; Vidović, Tino; Sumić, Tino; Mrakovčić, Tomislav; Račić, Nikola; Jelić, Maro; Lalić, Branko; **Bratić, Karlo**
   Maritime Alternative Fuels and Technologies for Sustainable Future // 10th International Maritime Science Conference: Book of Proceedings / Vidan, Pero; Slišković, Merica; Katalinić, Marko (ur.). Split: Pomorski fakultet Sveučilišta u Splitu, 2023. str. 348-356
3. Bukovac, Ozren; Pelić, Vladimir; Mrakovčić, Tomislav; Jelić, Maro; Radica, Gojmir; Vidović, Tino; Račić, Nikola; Lalić, Branko; **Bratić, Karlo**
   Remote expert system for diagnostics of propulsion engine // 2023 8th International Conference on Smart and Sustainable Technologies (SpliTech) 20.-23.06.2023
4. Stazić, Ladislav; **Bratić, Karlo**; Stanivuk, Tatjana; Vidović, Frane
   Student Advancement During Simulator Training // Časopis Pomorskog fakulteta Kotor, 2022. str. 44-51. doi: 10.56080/jms221104
5. Pelić, Vladimir; Radonja, Radoslav; Mrakovčić, Tomislav; **Bratić, Karlo**
   Natural gas as fuel for the COGES ship propulsion system // Proceedings of the 37th International Scientific & Expert Meeting of Gas Proffesionals. Zagreb: Hrvatska stručna udruga za plin (HSUP), 2022. str. 113-123
6. Stazić, Ladislav; Pavlović, Igor; Stanivuk, Tatjana; **Bratić, Karlo**
   Replacement of 2D simulator training with shorter 3D simulator training // 20th International Conference on Transport Science, ICTS 2022, 23. – 24. May 2022

Portoroz, Slovenia MARITIME, TRANSPORT AND LOGISTICS SCIENCE, CONFERENCE PROCEEDINGS. Portorož: Fakulteta za pomorstvo in promet Univerza v Ljubljani, 2022. str. 337-343

7. Radica, Gojmir; Mrakovčić, Tomislav; Račić, Nikola; Jelić, Maro; Lalić, Branko; Pelić, Vladimir; **Bratić, Karlo**; Kozina, Ante; Bulat, Domagoj
   Marine engines running on hydrogen additive in diesel fuel for emission reduction // Splitech 2021. Split, 2021, 2021137635, 3
8. Radica Gojmir, Mrakovčić Tomsilav, Račić Nikola, Jelić Maro, Lalić Branko, Pelić Vladimir, **Bratić Karlo**, Bulat Domagoj
   Analysis of two-stroke low speed marine engines operating on alternative fuels // 9th global conference on global warming gcgw 2021- conference proceedings. Zagreb, 2021. str. 279-282
9. Miroslav, Vukičević; Zorica, Đurović; Boris, Hrnčić; **Karlo Bratić**
   Optimization of Fuel Purifier Operation for More Efficient Elimination of Small Abrasive Impurities // Book of Abstracts. Kotor: Faculty of Maritime Studies Kotor, University of Montenegro, 2021.
10. Martinić, Siniša-Cezar; **Bratić, Karlo**; Slišković Merica; Račić Nikola
   Exhaust emissions from marine 4-stroke engine on the three fuel types // 2ND INTERNATIONAL CONFERENCE OF MARITIME SCIENCE & TECHNOLOGY NAŠE MORE 2021. Dubrovnik: Pomorski odjel Sveučilišta u Dubrovniku, 2021. str. 227-241. doi: 504.5:621.43.068
11. **Bratić, Karlo**; Vidović, Frane; Stazić, Ladislav
   Use of Merlin System and Recorded Instructions in Engine Room Simulator Training // Proceedings TIE 2020. 8th International Scientific Conference Technics and Informatics in Education. Čačak: Fakultet tehničkih nauka Univerziteta u Novom Sadu, 2020. str. 282-285
12. Stazić, Ladislav; **Bratić, Karlo**; Mihanović, Vice; Matjašić, Jure
   Maintenance process adjustment based on Computerized PMS data // 1st International Conference of Maritime Science & Technology Naše More 2019. Dubrovnik: Pomorski odjel Sveučilišta u Dubrovniku, 2019. str. 547-553
13. **Bratić, Karlo**; Stazić, Ladislav; Mišura, Antonija; Jurić, Zdeslav
   Spare Parts Optimization Using A Planned Maintenance System // Book of Proceedings, 8th International Maritime Science Conference. Kotor: CIP - Nacionalna biblioteka Crne Gore, 2019. str. 389-395